KAUNAS UNIVERSITY OF TECHNOLOGY PANEVEZYS INSTITUTE
WARSAW MOTOR TRANSPORT INSTITUTE
TALLINN UNIVERSITY OF TECHNOLOGY
RIGA TECHNICAL UNIVERSITY

INTELLIGENT TECHNOLOGIES IN LOGISTICS AND MECHATRONICS SYSTEMS

ITELMS'2008

PROCEEDINGS OF THE 3 RD INTERNATIONAL WORKSHOP

EDITED BY Ž.BAZARAS AND V.KLEIZA

May 22-23, 2008
Panevėžys, Lithuania

TECHNOLOGIJA
KAUNAS·2008

UDK 656.012(06)+621.382(06)

WORKSHOP IS ORGANIZED BY

Kaunas University of Technology Panevezys Institute
Warsaw Motor Transport Institute
Tallinn University of Technology
Riga Technical University

WORKSHOP IS SUPPORTED BY

State Fund of Science and Study of Lithuania

The proceedings of the 3rd International Workshop INTELLIGENT TECHNOLOGIES IN LOGISTICS AND MECHATRONICS SYSTEMS contain selected papers.

All papers were reviewed.

The style and language of authors were not corrected. Only minor editorial corrections have been carried out by the Publisher.

ISBN 978-9955-25-531-4

WORKSHOP SCIENTIFIC COMMITTEE

Chairman
Z. Bazaras, Kaunas University of Technology, Lithuania

Scientific Secretary
Prof. V. Kleiza, Kaunas University of Technology, Lithuania

Members
Dr. G. Badenes, Institute of Photonic Sciences, Spain
Prof. P. Balckars, Riga Technical University, Latvia
Prof. J. Bareišis, Kaunas University of Technology, Lithuania
Prof. P. Castro, Porto University, Portugal
Dr. J. Furch, Brno University of Defense, Czech Republic
Dr. V. Hutsaylyuk, Military University of Technology, Poland
Prof. J. Laugis, Tallinn University of Technology, Estonia
Prof. A. Levchenkov, Riga Technical University, Latvia
Dr. M. Litwin, Motor Transport Institute, Poland
Prof. Ribickis, Riga Technical University, Latvia
Prof. M. Sitarz, Silezian Technical University, TRANSMEC, Poland
Prof. A. Sladkowsky, Silezian Technical University, Poland
Dr. Ch. Tatkeu, Transport Electronics and Signal Processing Laboratory, France
Prof. V. Tilipalov, Kaliningrad State Technical University, Russia,
Prof. B. Timofeev, St. Petersburg State Polytechnic Institute, Russia
Dr. D. Vinnikov, Tallinn University of Technology, Estonia

LOCAL ORGANIZING COMMITTEE

R. Bukėnas
V. Narbutas
E. Patapienė
Dr. D. Susnienė
Dr. L. Šumskienė
Dr. A. Tautkus
Dr. D. Vaičiulis

PREFACE

The first (2006) and second International Workshops “Intelligent Technologies in Logistics and Mechatronics Systems ITELMS” were held at Riga Technical University. 3rd international workshop ITELMS'2008 continues two year tradition and takes place at Kaunas University of Technology Panevezys Institute on 22 - 23 May, 2008.

The aims of the Workshop are to share the latest topical information on the issues of intelligent technologies in logistics and mechatronics Systems. The papers in the Proceedings presented the following areas:

Intelligent Logistics Systems
Multi Criteria Decision Making
Composites in aviation and infrastructures
Automotive Transport
Intelligent applications of solid state physics
Intelligent Mechatronics Systems
Mechanisms of Transport Means and their Diagnostics
Railway Transport
Transport Technologies

In the invitations to Workshop, sent year before the Workshop starts, the instructions how to prepare reports and manuscripts provided as well as the deadlines for the reports are indicated.

A primary goal of Workshop is to present the highest quality research results. A key element in attiring goal is the evolution and selection procedure developed by the Workshop Scientific Committee.

All papers presented in Workshop and published in Proceedings undergo this procedure. Instruction for submitting proposals, including requirements and deadlines, are published in Call for Papers in the http://www.ktu.lt/lt/apie_renginius/konferencijos/2008/meniu.asp. Paper proposals must contain sufficient information for a trough review. All submissions to determine topic areas are directed to appropriate Topic Coordinators. The Topic Coordinators review the submissions much them to the expertise according to the interests and forward them to selected reviewers. At least two reviewers examine each submission in details.

Selection of papers for the Workshop is highly competitive, so authors should assure their submissions to meet all Workshop Scientific Committee’s requirements and to be of the highest possible quality.

All Workshop participants prepare manuscripts according to the requirements that make our Proceedings to be valuable recourse of new information which allows evaluating investigations of the scientists from different countries.

Prof. Ž. Bazaras
Prof. V. Kleiza

Contents

Proceedings of 3rd International Workshop ITELMS'2008

Theoretical Study on the Molecular Structures of Nitrophenols and Trinitrophenols

S. Bekešienė*, V. Kleiza, J. Tamulienė*****

* *Military Academy of Lithuania, Šilo 5A, LT-10322 Vilnius, Lithuania, E-mail: svajone.vosteriene@lka.lt*
** *Kaunas University of Technology, Panevėžys Institute, Klaipėdos st. 1, LT-35209 Panevėžys, Lithuania, E-mail: vytautas.kleiza@ktu.lt*
*** *Institute of Theoretical Physics and Astronomy, Goštauto str. 12, Vilnius, Lithuania, E-mail: gicevic@itpa.lt*

Abstract

Computational quantum chemistry is the ground of molecular modeling, on prediction the behavior of individual molecules within a chemical system. The basis of molecular modeling investigations is quantum mechanics, but in order to achieve quantitative results comparable with experimental we need supercomputer's power or parallel computers cluster. Such way is very useful with explosive materials that require exceptionally care in their handling.

The theoretical investigations of molecular electronic structure and geometrical data of 2, 4, 6-trinitrophenol and five positional nitro phenol isomers were performed applying of *ab initio* quantum mechanical methods using the GAMESS computer code integrated under the SCore type PC cluster TAURAS [1, 2]. Was used Hartree-Fock approximation with 6-31G* basis set (polarization ***d*** functions on second period elements; all in all 250 basis functions). Also 6-311G** basis set with two polarization ***d*** functions on second period elements, and plus one *f* function and diffuse *s* and *p* functions on second period atoms, and additionally diffuse functions on hydrogen atoms (all in all 770 basis functions). The basis functions used are necessary to achieve reliable results in such investigations. Calculated geometrical parameters were compared and found to be in good agreement with the data of X-ray diffraction. The nitro phenol molecular structure was affected by the position of the NO_2 group.

All calculations were made on the local area PC cluster TAURAS with the SCore cluster system software. Obtained results show that the cluster is good device for such tasks.

KEY WORDS: *nitro phenol, trinitrophenol, positioned isomer, parallel calculations, SCore cluster.*

1. Introduction

The analysis of explosives is of main significance in several analytical fields such as forensic identification of explosive residues in bombing investigations, detection of explosives hidden in airline baggage or mail, determination of purity assessment of explosives in storage, and environmental analysis of traces of explosives in seawater and industrial environments. Simultaneously, with the increase of analytical fields in which explosives are involved and the development of new types of explosives, the techniques used for the analysis of explosives have become more sophisticated.

Molecules having nitro groups are usually known as explosives. The thermal decomposition mechanisms and resultant products are important for any explosive, since they play a major role in predicting the feasibility of large-scale synthesis, the long-term stability for the purpose of storage and the sensitivity to various stimuli. Nitro phenols (Fig. 1) are a class of materials witch are classified as secondary explosives and is the one most frequently used in making ammunitions.

Only few of them molecular structures were examined experimentally. Hence it is necessary to find the geometric and electronic structure of the materials to know their properties that help us to create tools for explosive detection and more safe harmless.

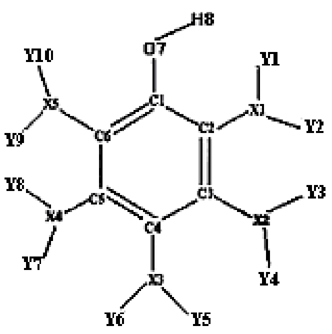

X=N or H atom, Y=O atom

2, 4, 6-trinitrophenol: $C_6H_4N_3O_7$
Molecular weight: 229.11
Color: yellow
State: crystals
Melting point: 122-123°C
Boiling point: 300°C
Solubility: water -12.82 g/L at 20-25°C: soluble in benzene, chloroform, ether, ethanol and acetone
Conversion factors: 1ppm = 9.37 mg/m^3; 1mg/m^3 = 0.107 ppm
Vapor pressure (at 25oC): 7.5x10-7mm Hg
Henry's Law constant(at 25°C): 1.7x10-8atm m3/mole

Fig. 1 The molecular structure of 2, 4, 6-trinitrophenol and characteristics

The vibrational spectra are the fingerprints for molecular species identification, so for detection explosives from spectral characteristics can be used Infrared (IR) and Raman spectroscopy methods. Raman spectroscopy is the study of a small portion of light scattered by a molecule, the light undergoing an exchange of energy with that molecule. Infrared spectroscopy is a technique based on the vibrations of the atoms in molecules. An infrared spectrum is commonly obtained by passing infrared radiation through a sample and determining what fraction of the incident radiation is absorbed at a particular energy. The energy at which any peak in an absorption spectrum appears corresponds to the frequency of a vibration of a part of a sample molecule. IR absorption information is generally presented in the form of a spectrum with wavelength or wave number as the x-axis and absorption intensity as the y-axis.

Vibrational frequencies depend on interactions between atoms and groups of atoms. They tell us about intra- and intermolecular interactions. Vibrational modes vary with the nature of atoms in the bond and chemical environment. They give us information about chemical bonding and the chemical environment. Many bond types exhibit characteristic (“fingerprint”) vibrational frequencies that allow us to establish the presence of certain functional groups, or products in a catalytic reaction.

In order to obtain the spectroscopic signature of the explosive molecules we performed frequency calculations for the different basis sets. The theoretical frequencies for 2, 4, 6-TNP was obtained. This work present the vibrational frequencies of the most stable geometry observed. These frequencies have to be real, or positive to consider that the geometry reach a minimum.

The SCore type cluster was applied to investigate vibrational spectra of 2, 4, 6-trinitrophenol molecules by means of *ab initio* quantum mechanical computational methods. The precise knowledge of vibrational spectra would allow detecting small amounts of these materials by means of spectroscopic methods. The purpose of our work was to investigate how strong calculated vibrational frequencies, infrared (IR) and Raman radiation intensities depend from the *ab initio* method used. We did not find in literature or in available databases the all results of analogous theoretical investigations for given molecules.

2. Investigation Methods for of 2, 4, 6-trinitrophenol Molecule

As was stated in the introduction the precise computations of 2, 4, 6-trinitrophenol molecule may be of interest for experimental spectroscopy. In this section we briefly describe the complexity of the investigation of electronic structure of molecules and present results and amount of necessary computational facilities in order to achieve reliable results for 2, 4, 6-trinitrophenol molecule.

The theoretical investigations of 2, 4, 6-trinitrophenol molecules need the supercomputer’s power and was performed by the SCore type cluster system of personal computers (PC). All calculations were performed by means of *ab initio* quantum mechanical methods using GAMESS computer code [2].

The basis of all such calculations is solving of multidimensional time independent Schrödinger equation.

$$\hat{H}\Psi_i = E_i \Psi_i \,, \tag{1}$$

here $\hat{H}$ – Hamilton operator of investigated quantum particle system; Ψ_i – wave function of the system; E_i – allowable energy value. Hamiltonian operator and wavefunction of the system depend on the coordinates of all particles (electrons and nucleus).

We use non relativistic Hamilton operator for electronic part of the problem

$$\hat{H}_e = \sum_{p=1}^{N} h_p + \sum_{p>q}^{N} g_{pq} \,, \tag{2}$$

here

$$h_p = \frac{1}{2}\nabla_p^2 - \sum_{m=1}^{M} \frac{Z_m}{r_{pm}} \tag{3}$$

is one electronic part of Hamiltonian operator; M is the number of nucleus; Z_m – the charge of m-th nuclei; r_{pm} – the distance between m-th nuclei and p-th electron;

$$g_{pq} = \frac{1}{r_{pq}} \tag{4}$$

is the two electronic part of Hamiltonian.

We use the atomic units system in all formulates. In one particle approximation the molecular wave function for closed shell electronic system (with odd number of electrons) is presented by Slater determinant

$$\Psi = \frac{1}{\sqrt{N!}} \det\left| \psi_1 \bar{\psi}_1 \psi_2 \bar{\psi}_2 \ldots \psi_{N/2} \bar{\psi}_{N/2} \right| , \tag{5}$$

where N is the total number of electrons:

$$y_i = j_i a \;\; ; \;\; \bar{y}_i = j_i b \; ; \tag{6}$$

y_i and $\bar{y}_i$ are one electron wave functions depending from ***i***-th electron coordinates: j_i – spatial part of electron wave function; a and b – spin orbitals. Molecular orbitals j_i are often expanded in the basis of Cartesian Gaussian atomic orbitals:

$$j_i = \sum_k c_k T_{ki} \, , \tag{7}$$

$$c_{\mathrm{GO}}(n,l,m) = N(a\,;l,m,n)x^l y^m z^n \mathrm{e}^{-a\,r^2} \, , \tag{8}$$

or in the matrix form

$$j = \chi \, \mathrm{T} \, , \tag{9}$$

here $N(a;\, l,\, m,\, n)$ – normalization coefficient; T is matrix with expansion coefficients for MO in the columns.

The first order variation of the full energy with additional requirement of orthogonality between MOs leads to matrix equation for MO coefficients matrix T and one elctronic energies matrix *e*.

$$\hat{H}^F \mathrm{T} = \mathrm{ST}\varepsilon \, , \tag{10}$$

where S is the matrix of overlap integrals between AO ($S_{ij} = \int c_i c_j \, dt$).

$$\hat{H}^F = \hat{h} + \sum_n (2\hat{J}_n - \hat{K}_n) \, , \tag{11}$$

Coulomb and exchange operators are defined accordingly

$$\hat{J}_n j_m(m) = \int \frac{\left| j_n(n) \right|^2}{r_{mn}} \, d\vec{r}_n \, j_m(m) \, ; \tag{12}$$

$$\hat{K}_n j_m(m) = \int \frac{j_n^*(n) j_m(n)}{r_{mn}} \, d\vec{r}_n \, j_m(m) \, . \tag{13}$$

As operators $\hat{J}$ and $\hat{K}$ depend themselves from MO j_i, equation (10) is usually solved by iteration so called self consistent field method (SCF). So all the problem is concerned with evaluation of great number of integrals with (11) operator and the use of linear algebra matrix computational methods. One of the methods to go beyond the one electron approximation during investigation of molecular electronic structure is use of multiconfigurational wave function of the form

$$y = \sum_I C_I f_I \, , \tag{14}$$

where f_I - one determinant function of the form (5). In that case during SCF procedure coefficients C_I from (14) and expansion coefficients from (7) are determined at the same time. It is very computational resources consuming methods, but when expansions in (7) and (14) are big enough it gives the results comparable with experimental ones.

Different basis sets were used during our computations: from 6-31 G* (with polarization ***d*** functions on second period elements; all in all 250 basis functions) to 6-311 G** (with two polarization ***d*** functions on second period elements) plus one ***f*** function and diffuse ***s*** and ***p*** functions on second period atoms and diffuse functions on hydrogen atoms (all in all 770 basis functions). The basis functions used are necessary in order to achieve reliable results in such investigations During multiconfigurational self consistent field (MCSCF) calculations performed for trinitrotoluene we left unfrozen 10 highest occupied MO and 10 lowest unoccupied MO from Hartree-Fock Slater determinant [4, 5]. All configurations generated from unfrozen MOs with spin projection zero were included in MCSCF procedure. We had more than 65000 configurations.

3. The Results of Investigations

Calculated bond lengths, bond angles, dipole moment and energy by HF/6-31* method are presented below, in Table 1 and Table 2. The molecular structure of 2, 4, 6-trinitrophenol molecule are shown in Fig. 1. The geometrical values of this molecule were optimized. All get results are compared with the experimental data.

With the available experimental geometrical data of 2, 4, 6-trinitrophenol, a comparison between the theoretical calculations and the experimental values can be made. The C- C bonds are dominated by the resonance and

Table 1

The 2, 4, 6-trinitrophenol molecule equilibrium bond lengths (Å) calculated in the HF approximation in the 6-31G* basis set on cluster TAURAS and experimental values[3]

Bound	Exp. [3]	HF/6-31G*
C1-C2	1.412	1.413
C2-C3	1.373	1.378
C3-C4	1.367	1.370
C4-C5	1.376	1.379
C5-C6	1.355	1.374
C1-C6	1.407	1.412
C1-O7	1.312	1.294
O7-H8	-	0.952
C2-X1	1.455	1.455
X1-Y1	1.227	1.200
X1-Y2	1.201	1.177
C3-X2	-	1.070
C4-X3	1.455	1.455
X3-Y5	1.214	1.186
X3-Y6	1.217	1.185
C5-X4	-	1.069
C6-X5	1.477	1.466
X5-Y9	1.183	1.189
X5-Y10	1.202	1.179
Y1-H8	1.680	1.750
Dipole moment	-	2.02
Energy	-	-916.08196

Table 2

The 2, 4, 6-trinitrophenol molecule equilibrium bond angles (^{o}) calculated in the HF approximation in the 6-31G* basis set on cluster TAURAS and experimental values[3]

Bond angles	Exp. [3]	HF/6-31G*
C1-C2-C3	123.2	122.6
C2-C3-C4	117.7	119.0
C3-C4-C5	122.1	122.1
C4-C5-C6	119.3	119.9
C1-C6-C5	122.4	121.7
C2-C1-C6	115.2	115.7
C2-C1-O7	124.5	123.5
C6-C1-O7	120.3	120.8
C1-O7-H8	-	110.3
C1-C2-X1	119.4	121.0
C2-X1-Y1	119.0	118.1
C2-X1-Y2	118.7	119.0
C2-C3-X2	-	120.1
C3-C4-X3	118.9	119.4
C4-X3-Y5	118.2	117.2
C4-X3-Y6	118.0	117.3
C4-C5-X4	-	120.6
C5-C6-X5	117.1	116.1
C6-X5-Y9	118.9	116.3
C6-X5-Y10	120.2	118.6

inductive effects. The bond lengths calculated by the HF/6-31G* method are close to the experimental values. For the C- NO_2 bonds, the HF/6.3l G* calculation tends to give shorted bonds than the experimental data. It is as expected that the C2- C1- C6 bond angle, which is attached by the hydroxyl group is smaller than 120^o and the C- C- C bond which is attached by the nitro group is larger than 120^o. The calculations on cluster TAURAS on the C- C-C bond angles give very close values similar to the X-ray data. By contrast, deviation of the C- O- H bond angle is more sensitive than that of other bond angles. The nitro group, linked to the hydroxyl group, of 2, 4, 6-trinitrophenol is found to be coplanar with the phenyl ring both experimentally and theoretically. For 2, 4, 6-trinitrophenol, the calculated twisted angles of the nitro group, which is attached to the opposite side of the hydroxyl group, are different from the experimental values.

It is predicted, that the above disagreement may be occurred due to bonding between the O atom of the nitro group and the O atom of the hydroxyl group. However, when closely examining non-bond O-O distance, the calculated value is found to be quite similar to the experimental one. On the other hand, the solvent influence to the structure of the investigated molecule is not searching, but this oxygen - solvent interaction may be the main reason of this C-N-O angle changes.

4. Vibrational Spectra Computations of 2, 4, 6-TNP

Theoretical investigations of 2, 4, 6-trinitrophenol molecule was performed by means of *ab initio* quantum mechanical methods using GAMESS computer code in Linux operating system [5]. Basis set 6-31 G* (with polarization d functions on second period elements) was used. All in all we had for 2, 4, 6-trinitrophenol 246 basis functions.

The calculations of harmonic vibrational spectra took about 40 minutes of clusters CPU time in *ab initio* method in HF approximation. For potential energy surface determination in Hartree-Fock (HF) approximation atomic orbital (AO) basis 6-31G* (total 250 basis functions) and the 6-311G* basis were used. Number of necessary to compute many center integrals was more than 10^9.

The calculated by cluster TAURAS neat infrared spectrum corresponding to 2, 4, 6-TNP was visualized by MOLDEN 4.6 (Fig.2). The bands that allow identifying the neat TNP were obtained in the range of 350-3350 cm $^{-1}$. The vibrational signatures observed in the region of 3269-3496 cm $^{-1}$ can be assigned to asymmetric and symmetric C-H stretch vibrations, respectively, belong to the alkyl CH_3 group and the aromatic ring. Other peaks of high intensity are 1885 cm $^{-1}$ (NO_2 symmetric stretching vibration), in the region of 1623-1639cm $^{-1}$ (Valence angle deformations in NO_2, CH_3 groups and benzene ring), 1306 cm $^{-1}$ (benzene ring in plane deformations).

Infrared spectrum of 2, 4, 6-trinitrophenol investigations after increasing basis set shows that few frequencies preserved the same form in Hartree-Fock approximation in the 6-311G* basis and in the 6-31G*basis. The two spectra (Fig. 2) are compare: 1562 cm^{-1} (a) and 1583 cm^{-1} (b) — benzene ring and NO_2 group deformations; 1817cm^{-1} (a) and 1743 cm^{-1} (b), 1922 cm^{-1} (a) and 1864 cm^{-1} (b) —all NO bond stretching vibrations.

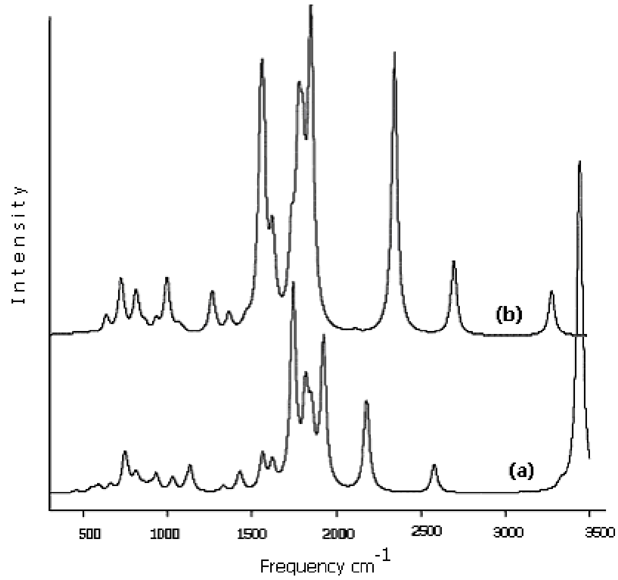

Fig.2 Infrared spectrum of neat 2, 4, 6-TNP in the range of 300-3500 cm^{-1}. IR vibrations calculated in the HF approximation: (a) in the 6-31G* basis; (b) in the 6-311G* basis

This means that quantitative investigation results with increasing the calculations can help us better understand for whom belongs: the benzene ring and NO_2 group deformations, the frequencies of NO group and CH bonds stretching vibrations. This information is important for detection.

5. Calculated Results of Positional Nitro Phenol Isomers

The 2-dinitrophenol (2-TNP), 3-nitrophenol (3-TNP), 4-nitrophenol (4-TNP), 5-nitrophenol (5-TNP) and 6-nitlrophenol (6-TNP) are the positional nitro phenol isomers, which were investigated by cluster TAURAS. Among them, only few of their molecular structures were examined experimentally.

Table 3

Calculated bound lengths (Å) of nitrophenols on PC cluster TAURAS

Bond	2-TNP	3-TNP	4-TNP	5-TNP	6-TNP
C1-C2	1.380	1.380	1.380	1.380	1.380
C2-C3	1.380	1.380	1.380	1.380	1.380
C3-C4	1.380	1.380	1.380	1.380	1.380
C4-C5	1.380	1.380	1.380	1.380	1.380
C5-C6	1.380	1.380	1.380	1.380	1.380
C1-C6	1.380	1.380	1.380	1.380	1.380
C1-O7	1.290	1.290	1.290	1.290	1.290
O7-H8	1.090	1.090	1.090	1.090	1.090
C2-X1	1.470	1.090	1.090	1.090	1.090
X1-Y1	1.380	-	-	-	-
X1-Y2	1.380	-	-	-	-
C3-X2	1.090	1.470	1.090	1.090	1.090
X2-Y3	-	1.380	-	-	-
X2-Y4	-	1.380	-	-	-
C4-X3	1.090	1.090	1.380	1.090	1.090
X3-Y5	-	-	1.380	-	-
X3-Y6	-	-	1.380	-	-
C5-X4	1.090	1.090	1.090	1.470	1.090
X4-Y7	-	-	-	1.380	-
X4-Y8	-	-	-	1.380	-
C6-X5	1.090	1.090	1.090	1.090	1.470
X5-Y9	-	-	-	-	1.380
X5-Y10	-	-	-	-	1.380
Y1-H8	1.57838	-	-	-	-
Y10-H8	-	-	-	-	3.43668
Dipole moment	3.852150	3.762023	5.348594	6.018802	6.236732
Energy	-509.1057	-509.1006	-509.1042	-509.0998	-509.0908

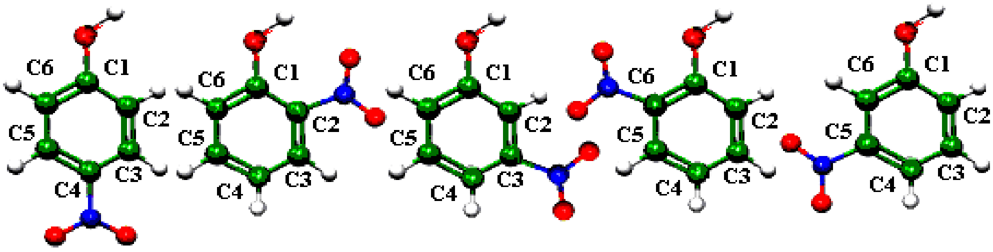

Fig.3 The NO_2 group positions on studied nitro phenol molecules

All calculations were performed by *ab initio* quantum mechanical methods using GAMESS computer code [2]. Their geometries and molecular structures are presented in Fig. 1 and Fig. 3. The bound lengths, angles, and dihedral angles of nitro phenols were calculated by cluster. The calculated bound lengths, dipole moments and energy are presented in Table 3. Previous calculations indicated that the geometries of some energetic materials calculated by *ab initio* methods are similar to that of the experimental data. From this, the *ab initio* approach can be applied to examine other explosives.

The performed theoretical analysis of the molecular structures of nitrophenols let to evaluate the stability of these molecules. The lowest energy was obtained for 2-nitrophenol.

6. Conclusions

Calculations of positional isomers of nitro phenol molecule at Hartree-Fock level show the influence of NO_2 groups to electronic structure and confirm the above theoretical prediction that the NO_2 groups influence the explosive molecule energy. The results of this study provide valuably information in the field of aromatic nitro compounds and let us foresee that cluster TAURAS allows solving of modern quantum chemical problems at necessary Hartree-Fock level.

Therefore, the calculations of 2, 4, 6-trinitrophenol molecule by HF/6-311G* showed significant change of vibrational spectrum characteristics from those calculated at HF/6-31G* level. Achieved results with increasing the calculations can help us better understand for whom belongs: the benzene ring and NO_2 group deformations, the frequencies of NO group and CH bonds stretching vibrations. This information is important for detection and allows more detail interpretation of experimental vibrational spectra of investigated molecules and more accurate investigation of thermo chemical reactions dynamics.

The electronic structure calculations provide useful estimates of the energetic properties of chemical systems, including preferred molecular structures, spectroscopic features and probable reaction paths. This review of some current electronic structure calculations has concentrated on discussion of *ab initio* techniques, as these are the most accurate and, in principle, universal methods.

Rapid advances in computer technology are making computationally expensive ab initio methods increasingly more practical for use with realistic chemical systems. In particular, cheaper methods such as density functional calculations and, layered models are continually being refined, and show promise of providing consistent and accurate chemical predictions for most complex systems.

References

1. Basis of PC clusters. Available at: http://clusters.top500.org/db.
2. **Alex A. Granovsky**. Available at: http://www.classic.chem.msu.su/gran/gamess/index.html.
3. **E. N. Duesler, J. H. Engelmann, D. Y. Curtin, I. C. Paul.** // Cryst. Strukt. Comm. 1978, Vol. 7, p. 449-461.
4. **H. Dorsett, A. White**, Overview of molecular modeling and *ab initio* molecular orbital methods suitable for use with energetic materials. DSTO, 2000, p. 1-35.
5. **M. W. Schmidt**, et al, J. Comput. Chem. 1993, Vol. 14, p. 1347.
6. **M. W. Schmidt, M. S. Gordon. //** Ann. Rev. Phys. Chem. 1998, Vol. 49, p. 233.
7. **Madejova J.** Review FT **-** IR techniques in Clay Minerals Studies // Vibrational Spectroscopy, 2003, 31, pp 1-10.
8. **Vošterienė** S., **Šulskus J**. GAMESS Calculations in Parallel Environment // Lithuanian Mathematical Journal. ISSN 0132-2818. 2005, 45 (spec. no.), p.190-193.
9. **S. Bekešienė, S. Sėrikovienė**. Quantum Chemical Calculations by Parallel Computer from Commodity PC Components // Nonlinear Analysis: Modelling and Control. ISSN 1392-5113. 2007, Vol. 12, No. 4, p. 461-468.
10. **R. J. Rakauskas, J. Šulskus, S .Vošterienė**. Simulation of Vibrational Spectra Peculiarities of Trinitrotoluene Molecule Using Parallel Calculations // Материалы XV международного семинара “Лазеры и оптическая нелинейность” 6-8 июня 2002 г., Минск, Беларусь. с. 162-168.
11. **Šulskus J., Rakauskas R. J, Vošterienė S.** PC Cluster Possibilities in Mathematical Modeling in Quantum Mechanical Molecular Computations // Nonlinear analysis: Modeling and Control. ISSN 1392-5113. 2002, Vol.7, No.2, p. 113-121.
12. **Ishikawa Y. et al. //** Proceedings of the 5th Annual Linux Expo.1999, p. 55-66.

Proceedings of 3rd International Workshop ITELMS'2008

Finding of hall parameters using by the magneto resistive method

J. Kleiza[*], V. Kleiza[**]

[*] *Vilnius Gediminas Technical University, Saulėtekio al. 11, LT-10223 Vilnius, E-mail: kleiza@mail.tele2.lt*
[**] *Kaunas University of Technology, Panevėžys Institute, Klaipėdos st. 1, LT-35209 Panevėžys, Lithuania, E-mail: vytautas.kleiza@ktu.lt*

Abstract

The problem of determining the product $\mu_H B$ of the Hall mobility and magnetic induction as well as specific resistivity ρ in the samples with two current contacts of nonzero length is considered. On the basis of the properties of conformal mappings, it is shown that when transmitting the current under the effect of a magnetic field or without it, there is a possibility to find the parameters in quest. Specials cases are examined where a sample has the form of a rectangle or circle.
KEY WORDS: *Hall mobility, tensor, specific conductivity, anisotropic, conformal mapping*

1. Introduction

Affecting an isotropically conductive plane sample of thickness h by a magnetic field whose vector $\mathbf{B}=\{0,0,B\}$ of magnetic induction is perpendicular to the plane of the sample, there emerges anisotropy of electric conductivity. In this case, the relation between the vectors of intensity $\mathbf{E}=\{E_x,E_y,0\}$ of the electric field and current density $\mathbf{J}=\{J_x,J_y,0\}$ can be expressed by the equality

$$\mathbf{E}=\mathbf{grad}\,\varphi=\rho\,\mathbf{J}+\mu_H\rho\,\mathbf{J}\times\mathbf{B},$$

therefore

$$\mathbf{J}=\boldsymbol{\sigma}\,\mathbf{grad}\,\varphi\ .$$

Here $\boldsymbol{\sigma}=\begin{pmatrix}\sigma_1 & -\sigma_2\\ \sigma_2 & \sigma_1\end{pmatrix}$ is Hall's electric conductivity tensor, ρ is specific resistivity of the sample, $\mu_H B=\tan\beta$, $\sigma_1=\sigma_0\cos^2\beta$, $\sigma_2=\sigma_0\sin\beta\cos\beta$.

In the physical sense, the problems of finding the product $\mu_H B$ of specific conductivity ρ of a sample and Hall mobility and magnetic induction are important. To solve them, we first formulate a boundary problem on distribution of the potential φ in any domain with two current contacts (Fig. 1a).

Within the domain the potential φ is harmonic function because

$$\operatorname{div}\mathbf{J}=\operatorname{div}\boldsymbol{\sigma}\,\mathbf{grad}\,\varphi=\sigma_1\left(\frac{\partial^2\varphi}{\partial x^2}+\frac{\partial^2\varphi}{\partial y^2}\right)=0\,. \tag{1}$$

In order to form boundary conditions, we will rely on the following property of the Hall tensor:

Theorem 1. Let Γ be a contour of the domain and $\mathbf{v_0}$ be unit vector of internal normal. Then, at all the points of the curve Γ

$$(\mathbf{J},\mathbf{v_0})=\frac{\partial\varphi}{\partial \mathbf{b}}\sigma_0\cos\beta\ ,$$

where $\frac{\partial\varphi}{\partial \mathbf{b}}$ is a derivative in the direction of the vector $\boldsymbol{b}$, and the vector $\boldsymbol{b}$ with the normal $\boldsymbol{\nu}_0$ forms a constant (independent of the curve Γ point) angle β (Fig. 1a).

Therefore, at the contour Γ points not coincident with the current contacts

$$\frac{\partial\varphi}{\partial \mathbf{b}}=0\,, \tag{2}$$

and at the remaining points

$$j = const\,. \tag{3}$$

To solve the boundary problem (1)-(3), we will conformally map the domain G into the upper half plane so that images of the boundary points g_0, g_1, g_∞ of current contacts were coincident with the points t =0, 1, ∞ of the real axis (Fig. 1b). Denote the image of point $g_{1/k}$ as t=1/k, where $k \in (0,1)$.

After mapping a half-plane by the integral

$$x + ih = \int_0^{t+iq} t^{\,b/p-0,5}(1-t)^{-b/p-0,5}(1-kt)^{b/p-0,5}\,dt$$

Into a parallelogram (Fig. 1c), we see that the potential linearly varies at its points and is equal to

$$j\,(x,h) = V\frac{h}{h_M}\,. \tag{4}$$

On the basis of expression (4) of the potential, we have proved

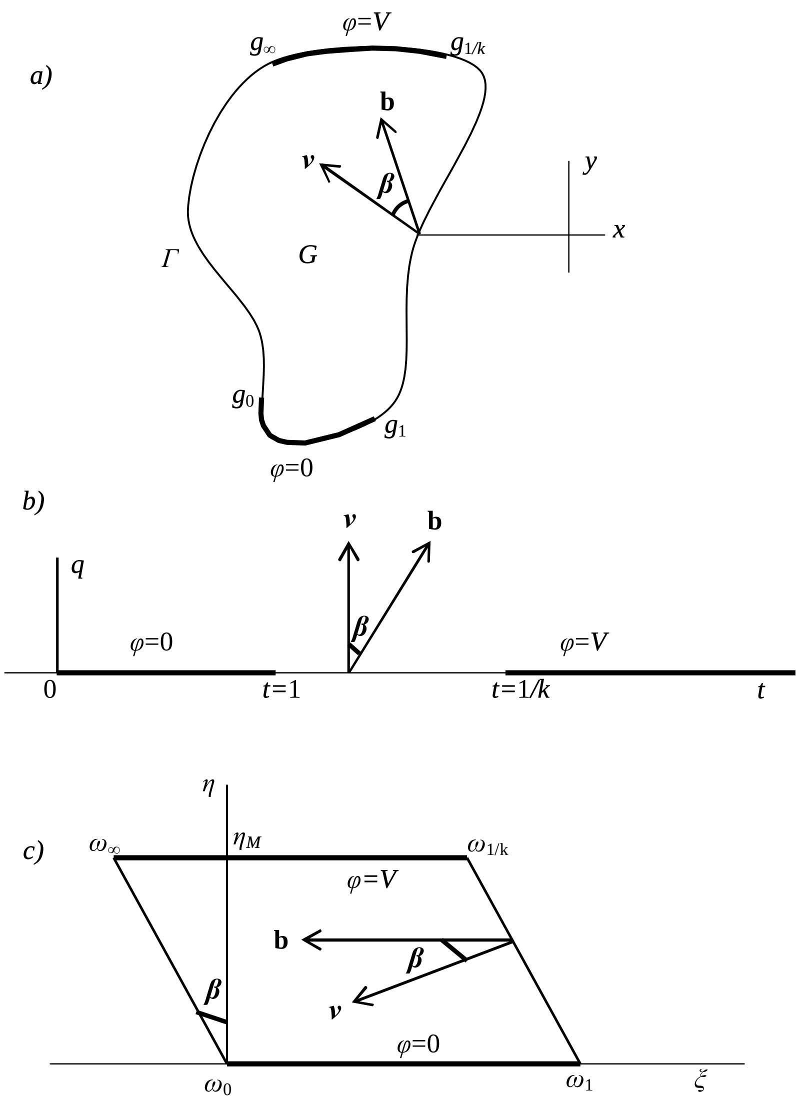

Fig. 1 Mapping of the domain of any form sample into a half plane and a parallelogram

Theorem 2. The intensity of current flowing via the sample is equal to

$$I_b = Vhs_0 \frac{A_{b,1-k}}{A_{b,k}} \cos b \ , \tag{5}$$

here *h* is height of the sample, s_0 is specific conductivity and

$$A_{b,k} = \int_1^{1/k} t^{\,b/p-0,5}(t-1)^{-b/p-0,5}(1-kt)^{b/p-0,5}\,dt \ .$$

2. Calculation of Hall Parameters

We present calculation formulas of the quantities s_0 and $m_H B$, where the domain *G* is a rectangle or a circle.

Let the current contacts in the rectangular shaped domain be arranged on two opposite sides (Fig. 2a). After measuring the current intensity under the effect of magnetic field I_β and without it, I_0 basing on (5) we build a system of equations to determine the specific conductivity s_0, parameter *k*, and angle *β*:

$$s_0 = \frac{I_0}{V}\frac{y_0}{h x_0},$$

$$k: \quad I_0 = Vhs_0 \frac{A_{0,1-k}}{A_{0,k}}, \tag{6}$$

$$b: \quad I_b = Vhs_0 \frac{A_{b,1-k}}{A_{b,k}} \cos b \ . \tag{7}$$

It has been proved that the right-hand sides of equations (6), (7) are monotone functions of the arguments *k* and of *β*, therefore the system (6)-(7) can be solved uniquely. Having solved it, we calculate the quantity $m_H B = \tan b$. It should be noted that if the domain *G* is a square, then conductivity s_0 and $m_H B$ are expressed by the elementary functions:

$$s_0 = \frac{I_0}{V} h, \quad m_H B = \frac{\sqrt{I_0^2 - I_b^2}}{I_0}, \quad (x_0 = y_0) \ .$$

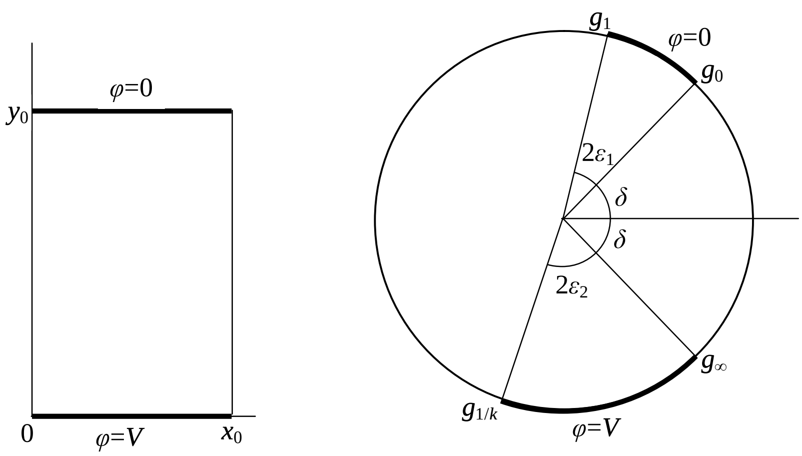

a) b)

Fig. 2 Arrangement of current contacts in the samples of the shape of a rectangle (*a*) and a circle shape (*b*)

If the sample is of a circle shape with arbitrarily arranged current contacts on its contour (Fig. 2b), then it suffices to solve only equation (7), because it is possible to calculate the parameter *k*, basing on the known geometry of contacts. Really, by conformally mapping the circle onto a half plane:

$$w = \frac{\sin(e_1 + d)}{\sin e_1} \frac{z - R\exp(id)}{z\exp(id) - R},$$

and observing that the image of the circle point $z = R\exp(-i(d + 2e_2))$ on the real axis is w=1/k, we obtain the expression of the parameter *k*:

$$k = \frac{\sin e_1 \sin e_2}{\sin(e_1 + d)\sin(e_2 + d)}.$$

Now, from (5) we derive the specific conductivity

$$s_0 = \frac{I_0}{Vh} \frac{A_{0,k}}{A_{0,1-k}},$$

and the angle β, by solving equation (6).

Apparently, even in the case of a circle shape sample we can do without solving equation (7), if the current contacts are arranged so that the relations: $e_1 = e_2 = e,\ d = \arccos\left(\sqrt{\cos 2e}\right) - e$ were valid, then

$$s_0 = \frac{I_0}{Vh}, \quad m_H B = \frac{\sqrt{I_0^2 - I_b^2}}{I_0}.$$

3. Conclusions

The new method for finding the specific conductivity s_0 of a plane sample and the product $m_H B$ using the sample of a rectangle or a circle shapes. An exceptional property of the method is that it suffices to have only two current contacts of any length and to measure flowing current intensities under the effect of a magnetic field and without it (compared with the classical methods, where four point contacts are fastened in the perimeter of a sample and three measurements of differences in currents and potentials are taken [1-3]). This, the Hall effect parameters have been successfully found on the basis of the magneto resistive effect only.

The equations obtained are easily solved with a high accuracy, because their coefficients are hypergeometric functions

$$A_{b,k} = \int_1^{1/k} t^{\,b/p-0,5}(t-1)^{-b/p-0,5}(1-kt)^{b/p-0,5}\,dt\ ,$$

those are implemented in any mathematical package. Therefore, in order to solve them, one can use standard procedures meant form solving equations.

On the other hand, based on the proved monotony of equations and approximation of hypergeometric functions by elementary functions [4-5], it is possible to compose algorithms, fast converting to solutions, in which only the elementary functions are used.

References

1. **Van der Pauw L. J.** A method of Measuring Specific Resistivity and Hall Effect of Discs of Arbitrary Shape // Philips Res. Repts. 1958, Vol. 13(1), p. 1-9.
2. **Kucys E.** Galvanomagnetic effects and investigation methods. Radio i sviaz, Moscow, 1992, [in Russian].
3. **J. F. Nye**. Physical properties of Crystals. Oxford University press, London, 1964.
4. **Abramowitz M., Stegun C. A.** Handbook of Mathematical Functions with Formulas, Graphs, and Mathematical Tables. New York: Dover, 1972.
5. **V. Kleiza, J. Kleiza.** Method of Calculation of Conductivity Tensor, DAN SSSR, 325(4), 1992, p. 711-715, [in Russian].

Proceedings of 3rd International Workshop ITELMS'2008

Design and Development Challenges of Power Electronics Converters for the Rolling Stock

T. Jalakas[*], D. Vinnikov[**], J. Laugis[***]

[*] *Tallinn University of Technology, Ehitajate tee 5, 19086, Tallinn, Estonia, E-mail: tjalakas@yahoo.com*
[**] *Tallinn University of Technology, Ehitajate tee 5, 19086, Tallinn, Estonia, E-mail: dm.vin@mail.ee*
[***] *Tallinn University of Technology, Ehitajate tee 5, 19086, Tallinn, Estonia, E-mail: laugis@cc.ttu.ee*

Abstract

In this article the design and development challenges of power electronics converters for rolling stock are analyzed. The main aim of this research was to investigate the main design criteria of a special type of switching-mode power supply for a rolling stock application. Results of the research can be used in development of high voltage auxiliary power supplies for railway use. The research contributes to advancement in converter techniques for railway rolling stock, enabling to optimize power circuit design and design new devices with higher power density and improved reliability.
KEY WORDS: *Rail vehicle, auxiliary power supply, rolling stock.*

1. Introduction

The aims of this research are most important problems related to the development of Auxiliary Power Supplies (APS) and traction converters for the rolling stock [1]:

1. A contradiction exists between the fast development of technology and long service time of rail vehicles (25-40 years). High-tech solutions become obsolete much faster than very costly mechanical parts are worn out. Due to this a need for reconstruction arises. The technical systems need to be reconstructed or modernized one to three times during a train's service time. Trains with reconstructed drives and other technical systems are in use in many countries.
2. Power characteristics of high-voltage power supply of train can be improved. This means an extended service life of an onboard battery and other low-voltage subsystems and devices. The efficiency of an APS of a train can be substantially improved by help of new semiconductor devices and control systems. New solutions require theoretical and experimental investigations, analysis and optimization.
3. Many technical problems related to the specific field of use – railway transport – need to be solved. The APS for the railway traction must remain stable during serious voltage fluctuations, bad line contact, and must have high immunity to electromagnetic interference. Additionally, it must be very powerful to provide stable output voltage in very high output current variations but the mechanical dimensions of it need to be as compact as possible. From another point of view, the APS must survive in different emergency situations, such as thunder, overvoltages, and short circuits in the overhead line and other circuits, etc.

Power electronics for railway transport is more complicated than for industrial uses because it is based on very strict specifications and requirements. To develop an optimal and successful voltage or traction converter for such applications, it is strongly recommended to define all the main criteria of planned device on the early stages of its development. Here all the criteria as well as specific railway considerations for the power electronic devices must be taken into account and analyzed precisely.

2. Main Criteria of the APS for Railway Applications

The auxiliary power supply converter and traction converter are one of the basic systems used in rolling stock. They power up the trains motors and provide power to every electrical system and equipment on a railway vehicle, including those that are critical to its safety and operability. A failure within those systems would render the whole vehicle non-operational, resulting in a financial loss, operational problems to the railway and discomfort to passengers.

The APS provides power to the onboard low-voltage auxiliary subsystems. To APS are connected: battery charging device, control and communication equipment, ventilation system, lights, compressors etc. [2] (Fig. 1.).

The ultimate suitability of any product depends to a substantial extent on the quality of the specification on which the product design is based. This is especially so within the highly specialized and environmentally demanding area of Rolling Stock. Prior to the development of any power electronic product for the rolling stock, all the major design requirements and specific considerations must be analyzed. Such APS design requirements need to be divided to two separate parts: factors related to the end-user and limitations concerning the specific area of use.

Factors which are becoming increasingly important to meet the aspirations of end-users are as follows:

- *Low cost of ownership.* Total life cycle costs mean that in addition to the initial price, maintenance and running costs must also be cut down. Failures and time for repairs must be minimized to provide the highest possible availability so that a given service can be provided with fewer vehicles [3].

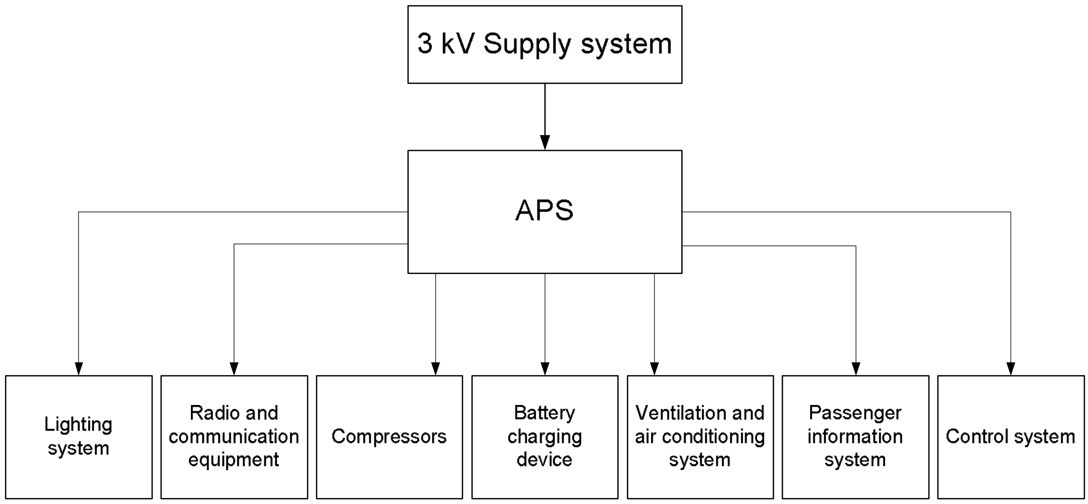

Fig. 1 Interaction of auxiliary power supply with onboard auxiliary devices

Table 1

List of European standards that are applied to railway application

EN50155	The main standard for railway systems
EN 50163	Defines supply voltages for traction systems
EN 60249-2-x	Specification for basic materials for PCBs and other assemblies
IEC 605	Test procedures and test equipment
EN 60068-2-x	Environmental testing procedures and equipment
EN 55022	Electromagnetic interference
IEC 801.3/4	Electrical noise immunity
EN 50126/8/9	Functional safety

- *Small overall dimensions.* Space on the vehicle is at a premium as more and more equipment has to be fitted to provide the onboard facilities of a modern railroad vehicle.
- *Low weight.* Minimizing vehicle weight reduces the track wear and tear lowers propulsion costs.
- *Low noise level.* Audible noise must be minimized to prevent annoyance to passengers. This applies to sound both inside and outside the vehicle.

It means that to meet the presented objectives, it is necessary to use the simplest circuits, consistent with achieving the required performance, thereby minimizing the cost and complexity. But another aspect is that technical and design issues crucial to the procurement of a reliable and maintainable product have to be considered and addressed within the main body by the reference to the main technical standards and specifications for the rolling stock. The main standard for power electronics for railway applications, EN50155, which has a local counterpart in many European countries, draws on requirements that are defined in approximately 50 other specifications and standards. Performance standards are defined for practically every facet of a railway's operational environment, including shock, vibration, extended temperature range, humidity, salt, fog, voltage fluctuations and many more (Table 1). The standard has been defined so that electronics in rail cars will be able to operate 24 hours a day for 30 years, or approximately 250,000 hours. Naturally, these stringent and comprehensive performance requirements are needed because the failure of an electronic assembly in a passenger train could jeopardize human lives.

Analyzing the standards and norms presented above, the main criteria influenced by the design of auxiliary power supply for the rolling stock may be determined:

- compliance with supply voltage requirements;
- compliance with a high variety of loads;
- compliance with electromagnetic interference requirements;
- compliance with electric safety requirements;
- compliance with physical requirements.

3. Analysis of Main Criteria of APS Based on Railway Standards and Norms

3.1 Compliance with Supply Voltage Requirements

For the optimization of the APS it is necessary to know the characteristics of the specific catenary supply system. The EN50163 standard requires that failure-free operation of electronics must be guaranteed with supply voltages between 70 and 120 percent of the nominal voltages defined in the specification (Table 2). Transient voltage fluctuations between 60 and 130 percent of nominal must not cause a fault [5]. Power interruptions cannot cause any malfunction of the equipment.

But the real situation is much more complex than it can be expected from the above definition. The first field questions are derived from its dynamic features, self-impedance, transients, noise, etc. Measurements of the catenary voltage waveform at the input of the old auxiliary power supply device were performed. The railway supply systems across Estonia are according to the old Soviet GOST standards (Table 2) that are setting much harder design criteria to the power electronics devices designed for railway use.

Table 2

Measured supply voltage fluctuations

Standard	Nominal voltage $U_{nom,}$ (VDC)	Continuous minimal voltage $U_{min,}$ (VDC)	Continuous maximal voltage $U_{max,}$ (VDC)
Former USSR standard *GOST*	3000 VDC	2400 VDC	4000 VDC
General European standard *EN 50163*	3000 VDC	2000 VDC	3900 VDC
Measurements	3341 VDC	2720 VDC	3835 VDC
Design requirements	3300 VDC	2000 VDC	4200 VDC

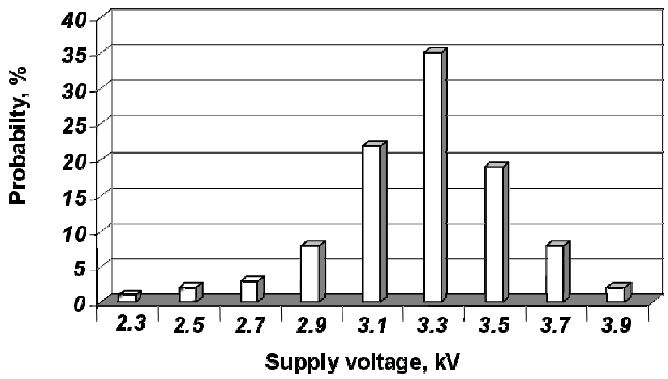

Fig. 2 Histogram of the measured supply voltage fluctuations

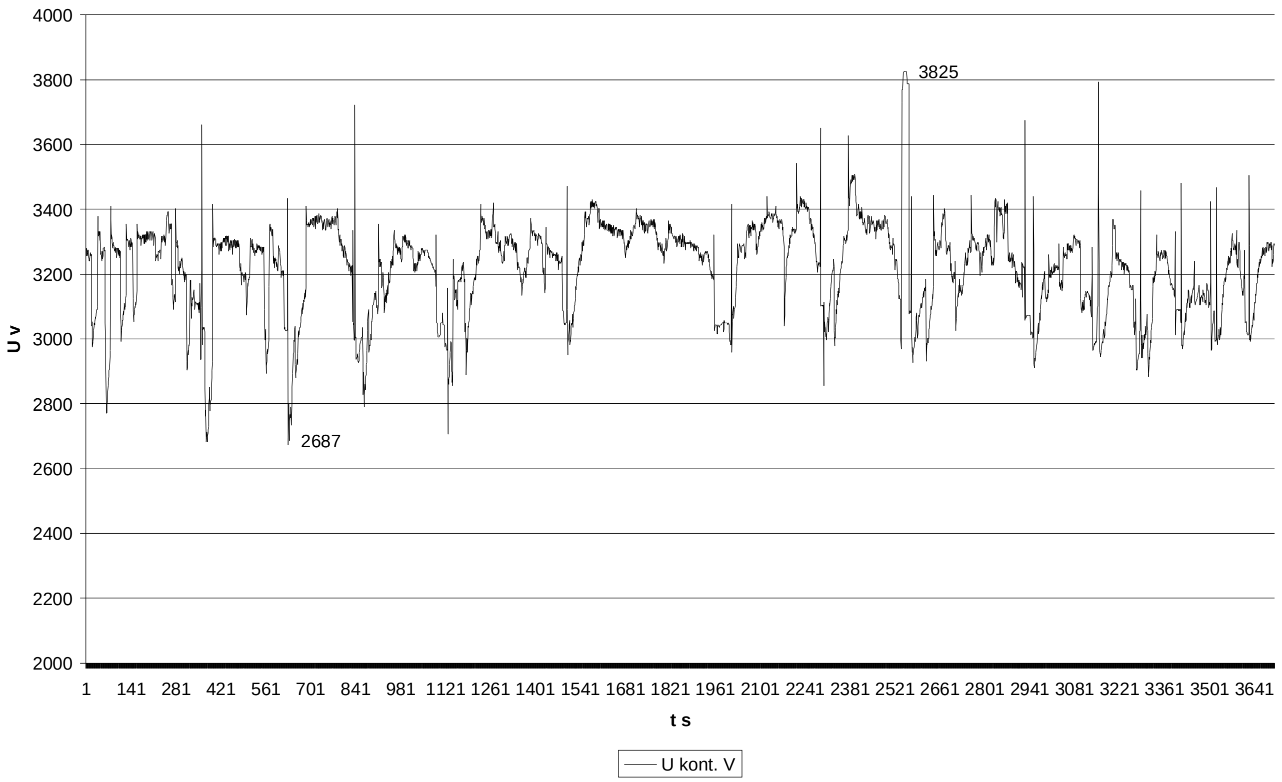

Fig. 3 Measured train catenary voltage profile

The measurements have shown that the catenary voltage changes between 2720 and 3835 volts (Fig. 3). The long-term measurements have shown that in some quite rare occasions the catenary voltage can change from 2536 to 3986 volts, exceeding standard maximal short-term catenary voltage limit. In the Table 2 are listed the standardized supply voltage fluctuations and measured values are compared.

The measured values show, that the catenary voltage is not according to the EN standards. The supply voltage fluctuations exceed the limiting values. Due the long supply lines, the voltage drop can be quite high, especially in winter, when the train's heating systems are operating at full capacity. The APS capable operating in those conditions must have input voltage range from 2000 V to 4200 V DC, the measured nominal voltage of the supply line is 3341 V DC; over 300 volts higher then standards allow, therefore the nominal input voltage of the APS must be 3300 V DC. On the Fig. 2 the appearance probabilities for different catenary supply voltages, in real traction conditions are presented.

3.2 Compliance with High Variations of Loads

The main objective of the APS is a stable operation despite voltage fluctuations on the primary side and variation of loads on its secondary side. To optimize the power characteristics of the developed APS it is necessary to analyze its loads in different operational conditions. APS has several types of loads: battery charging device, radio and communication equipment, lighting system, compressors, control system, ventilation and air conditioning system, passenger information system (Fig. 1).

Voltage fluctuations of the auxiliary low-voltage DC bus, such as may occur during the start-up of the auxiliary power supply apparatus, shall be limited to the range of –5% and +5% of the nominal APS output voltage found in Table 3. These fluctuations will not exceed 0.1 s in duration. This means that the APS needs a very short response time on variations of loads. Low-voltage DC power supply output overvoltages, such as may occur in the case of failure of the low-voltage power supply control systems, will be limited to 40% above the nominal Auxiliary DC-bus voltage of the APS (specified in Table 4), and will not exceed one second in duration [2].

Table 4

Allowed auxiliary DC-bus voltage fluctuations

Nominal APS output voltage, VDC	Minimal short-term voltage (at load), VDC	Maximal short-term voltage (at load), VDC
350	332.5	367.5

Load current of the auxiliary DC-bus is varying in a very wide range (up to 140 A) in different operation modes of a train. In an ideal case, the design of the APS must be coordinated such that peak loads can be supplied by the APS without reducing its output voltage below the minimum. Care must also be taken to ensure that the charging system will replenish the battery during normal operating runs of the vehicle.

Since all of the loads of the static inverter are car-borne, it is essentially a closed system. Therefore, the ultimate requirement of the static inverter is that it will deliver voltages with tolerances, transient capabilities, and harmonic content suitable to drive the car-borne devices. The static inverter will function to provide the specified outputs under the conditions of expected variations of both input voltages and output loads.

3.3 Compliance with EMC Requirements

With the increasing introduction of high-power electronic equipment, together with complex microcontrollers and a multitude of other electronic devices being installed on rail vehicles, electromagnetic compatibility within the rail environment has become a critical issue in every aspect of the design and implementation of rail vehicle and rail-associated apparatus. This has subsequently led to the mandatory requirement that all new railway applications must be tested for compliance with the European standard EN50121 [7]. The presented standard addresses some main aspects of the railway system that EMC concerns:

- •the effect of the railway system on the surrounding environment;
- •the effect of the railway system on signalling and communications equipment; and the ability of railway equipment and related apparatus to remain unaffected by the inherently severe environment within which it is intended to operate [8].

3.4 Compliance with Electric Safety Requirements

The main specific feature of the APS for the railway rolling stock is that the input and output sides of the developed APS need to be galvanically separated. The requirement for safety isolation depends on the integrity of the interconnections between the output of the power supply and the safety isolation provided by the load. Furthermore, it should be noted that voltages guaranteed to remain below 60 VDC are classed as safety extra low voltage (SELV) and precautions to protect the user are far less stringent. Reference should be made to the international standard IEC950 and

European norms EN60950 and EN50155. But if the load has inherent safety isolation, then the need to introduce a further safety isolation barrier at the power supply in question is not required [2].

There are very different voltage levels on the primary side (up to 4000 VDC) and on the secondary side (350 VDC) of the APS. Therefore, the input and output sides of the converter need to be galvanically isolated to meet the standards presented above. Usually to provide the necessary I/O galvanic separation power transformers are used. In view of all the requirements, a simplified block-diagram of a typical DC-DC auxiliary converter for railway rolling stock can be presented (Fig. 4).

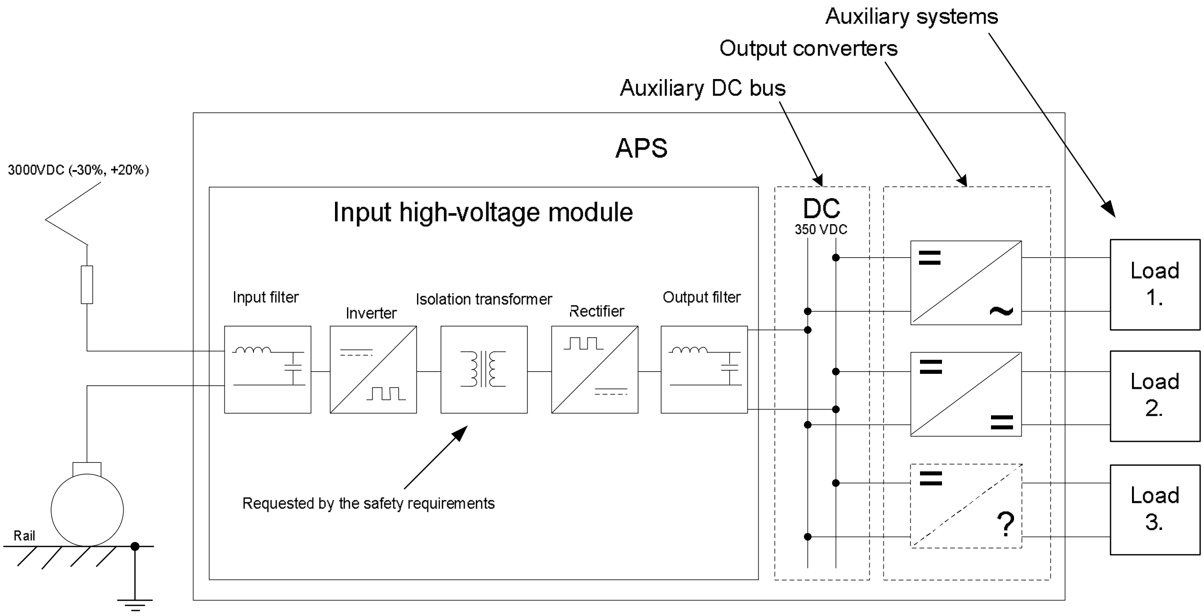

Fig. 4 Simplified block diagram of a typical auxiliary power supply for the 3.0 kV DC rolling stock

Since there is a need of the isolation transformer certain adjustments are to be made in the design of the power circuit of the APS. As mentioned above, one of the criteria of a successful APS is its compactness and small weight. However, it is a well known that the transformer is the main contributor in the size of any switching-mode power supply since it contributes about 25…30% of the overall volume and more than 30% of the overall weight [9]. In order to design small and compact electric power supplies, it is essential to reduce the size of the isolation transformer. The best way to achieve this is to employ high frequency excitation of transformer, although the used high-voltage semiconductors set limits to maximum switching frequency.

3.5 Compliance with Physical Requirements

3.5.1 Mechanical Considerations

Components used on rolling stock also must be qualified under the applicable mechanical standards. Moreover, they must be installed in such a way that ventilation is not obstructed and the mechanical mounting system must accommodate the shock and vibration inherent in rail cars. For mechanical reasons, printed circuit boards (PCBs) must have guides or rails on all four sides and must be locked in place when operational. Edge card connectors like those in PCs or so-called industrial PCs are not allowed. In addition to shock, the EN50155 railway standard also defines vibration for a specific frequency range. In particular, an electronic assembly or component must be tested at resonant frequency (if present) for a period of 15 minutes and additionally at 50 Hz for two minutes in all three directions [6].

3.5.2 Ambient Temperature and Humidity

The EN50155 standard defines different classes of operating temperatures, but railway systems typically require the complete industrial temperature range of -40°C to +85°C [6]. In many railway applications, fans, which are often prone to failure, are explicitly forbidden. Only passive heat sinks are allowed. To meet the temperature requirements of EN50155, tests are conducted for six hours at the highest temperature in the range and for two hours at the lowest point. Operation is also tested at points between either extreme. Humidity tests are similar to temperature tests. For example, electronics are subjected to 55°C at 95 to 100 percent humidity for 10 hours. Following those tests, the functioning and insulation strength of electronics is tested again.

4. Conclusions

A theoretical knowledge base related to the development of new converters techniques for the rail vehicles (electric trains) has been developed in the article. The practical part of this research based on the newly developed high-voltage auxiliary power supply. Also the results of this research can be used for development of modern traction converter for train. The research and development team has acquired valuable knowledge and skills.

Acknowledgement

Authors thank Estonian Science Foundation (Grant No. 7425 “Research of dynamic performance of high-voltage IGBTs”) for financial support of this study.

References

1. **Vinnikov D.**, **Lehtla T.** Influence of specific requirements on the design of auxiliary power supply for a light rail vehicle. 2nd International Symposium ”Topical Problems of Education in the Field of Electrical and Power Engineering“, Tallinn Technical University, 2005.
2. IEEE Standard for Passenger Train Auxiliary Power Systems Interfaces, IEEE Std 1476-2000, 2000.
3. **Vos P. G. E.** The auxiliary power supply system for double deck trains. IEE Colloquium on Auxiliary Power Supplies for Rolling Stock, 1992.
4. **Joosten, J.** Static converter technology [for railway applications]. IEE Colloquium on Auxiliary Power Supplies for Rolling Stock, 1992.
5. Standard EN 50163 “Railway applications - Supply voltages of traction systems”, 1996.
6. Standard EN 50155 “Railway applications - Electronic equipment used on rolling stock”, 2003.
7. **Hill R. J.** Electric railway traction. Part VII. Electromagnetic interference in traction systems. Power Engineering Journal, Volume: 11, Issue: 6, Dec. 1997.
8. Standard EN 50121 “Railway applications – Electromagnetic compatibility”, 2001.
9. **Marogy B. Y. M.** Specification of static auxiliary converters for rolling stock. IEE Colloquium on Auxiliary Power Supplies for Rolling Stock, 1992.
10. **Cann R. G.** The effect of output isolation requirements on traction converter design. IEE Colloquium on Auxiliary Power Supplies for Rolling Stock, 1992.
11. **Petkov R.** Design issues of the high-power high-frequency transformer. Proceedings of International Conference on Power Electronics and Drive Systems, 1995.

Proceedings of 3rd International Workshop ITELMS'2008

Development and Verification of Control and Protection Algorithms for the Special Purpose High Power Converters

I. Roasto*, D. Vinnikov, V. Vodovozov*****

* *Tallinn University of Technology, Ehitajate tee 5, 19086, Tallinn, Estonia, E-Mail: indrek.roasto@ttu.ee*
** *Tallinn University of Technology, Ehitajate tee 5, 19086, Tallinn, Estonia, E-Mail: dm.vin@mail.ee*
*** *Tallinn University of Technology, Ehitajate tee 5, 19086, Tallinn, Estonia, E-Mail: edrive@narod.ru*

Abstract

This paper describes the research, which mainly contributes to the study of specific requirements, which directly influence the design of special purpose high power converters. The main application field of these converters is rolling stock. It is well-known fact that power electronics for railway transport is more complicated than for industrial applications because it is based on very strict specifications and requirements. To develop an optimal and successful product (converter) for such applications, it is strongly recommended to define all the main criteria of the future power converter on the early stages of its development. In this paper the development and verification of control and protection algorithms for the rolling stock auxiliary power supply are discussed with the special emphasizes on railway standards EN50163 and EN50155.

KEY WORDS: *Control methods for electrical system, fault detection, protection algorithm, railway standards.*

1. Introduction

In Europe, the voltage levels and quality for railway applications are basically covered by two standards: EN 50155 and EN 50163. The first standard handles the performance of electrical and electronic equipment in railway. EN 50163 defines supply voltages for traction systems.

In this paper the fault detection and protection system of an auxiliary power supply (APS) is explained and shown how it complies with the railway standards EN 50155 and EN 50163. The APS is responsible for the conversion of high DC voltage from the catenary (3.0 kV) to some intermediate DC voltage level to supply secondary systems of a rail vehicle, such as lighting, braking, passenger announcement system etc. The APS is based on new generation HV IGBT transistors, which allow implementation of a half-bridge topology as shown in

Fig. 1 [1]. The benefits of a half-bridge topology-based APS are the increased reliability, simple maintenance and small running costs.

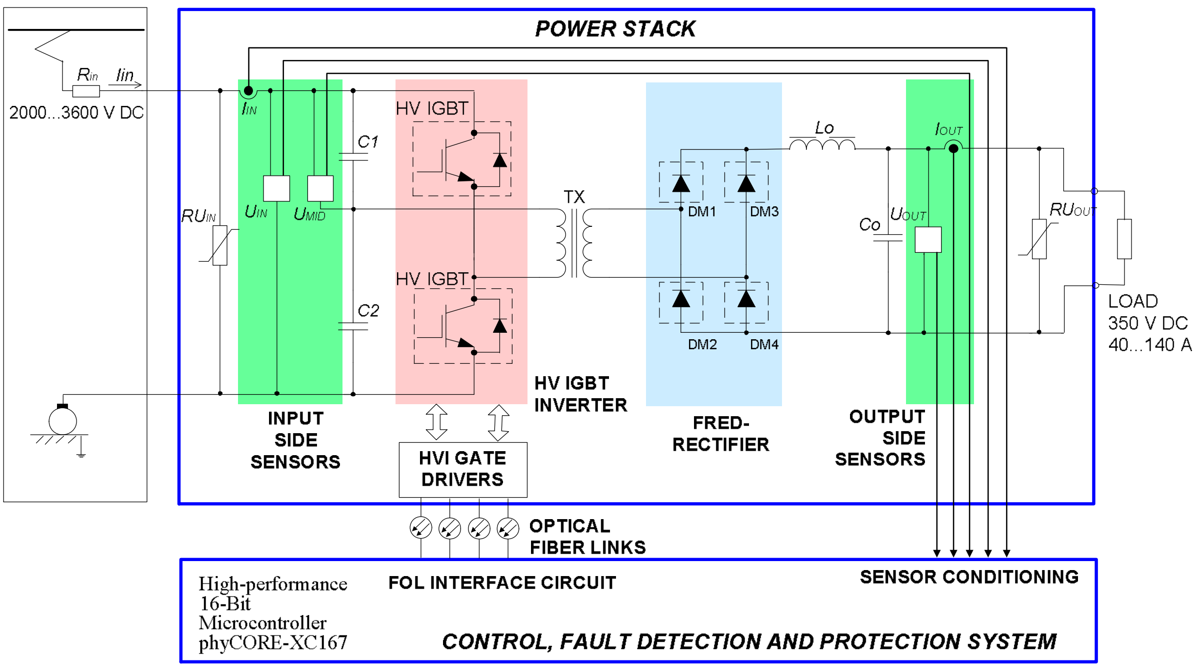

Fig. 1 Simple half-bridge isolated DC/DC converter topology for the rolling stock APS

2. The Standards

The standard EN 50155 determines operating voltage ranges for electrical devices in railway applications [2]. Equipment powered from static voltage converter must function properly with input voltages that range from 0.9 U_n to 1.1 U_n, where U_n is the nominal voltage. The equipment must also withstand input voltage fluctuations from 0.7 U_n to 1.25 U_n. The European standard EN 50163 determines the catenary voltage levels for traction systems [3]. In Estonia the nominal voltage is 3300 V, which differs slightly from the EU standard. According to standard EN 50163 the continuous maximal voltage value that may occur in this system is 3600 V. In a short time period (less than 5 min) up to 3900 V are allowed. The continuous minimal voltage value is 2000 V. The APS was build considering the two norms mentioned above: the input of the APS was designed according to EN 50163 and the output according to EN 50155 [4, 5].

3. Control System

The control system can be divided into three functional parts as shown in Fig 2:
- inverter control,
- protections,
- supervision and diagnostics.

Inverter control involves voltage regulator and pulse width modulation generator. Protection block consists of different kind of protection algorithms. The last part of the control system (Supervision block) contains logger and test functions and user interface.

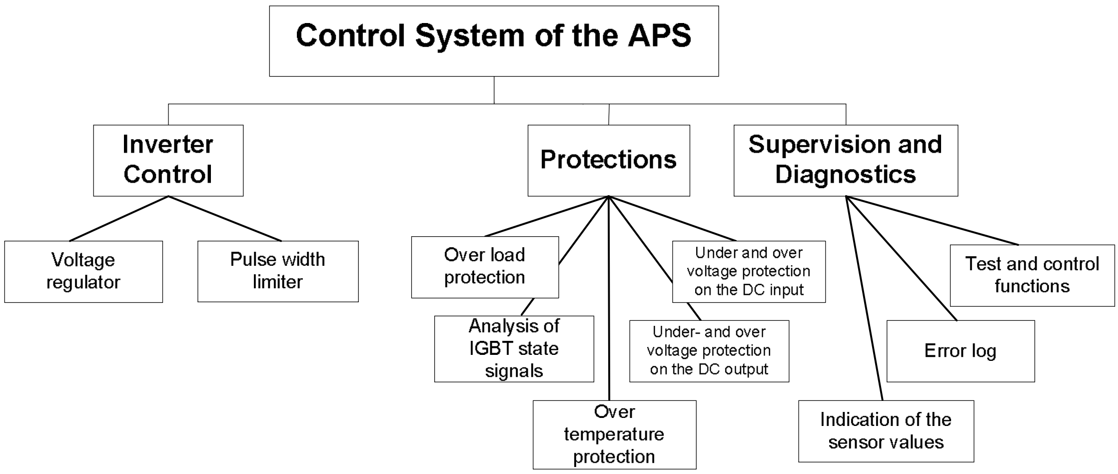

Fig. 2 Classification of functions of the control system

The APS is provided with three voltage and two current transducers as shown in Fig. 2: input voltage (U_{in}), input current (I_{in}), output voltage (U_{out}), output current (I_{out}), middle point (U_{mid}). Additionally the system has five temperature sensors. The following temperatures will be conditioned:
- transistor T1 – maximal allowed temperature 60 ºC,
- transistor T2 – maximal allowed temperature 60 ºC,
- rectifier – maximal allowed value 50 ºC,
- transformer – maximal allowed value 60 ºC,
- output filter inductor – maximal allowed value 60 ºC.

4. Control Algorithm

A general control algorithm is presented in Fig. 3. Starting the APS is an issue on each day when the train is driving and also after power interruptions and some faults, which require a microcontroller reset. To avoid dangerous current peaks in the output due to uncharged output capacitors, a soft start algorithm has been added to the control program as shown in Fig. 3. It gradually increases the pulse width of the IGBT transistors until the nominal voltage in the output has been reached. After that the main program starts. The main program consists of a loop, which constantly checks for errors. As long as there are no errors, the output voltage will be regulated. In case of an error the IGBTs will be blocked. The faults are divided into two groups. All faults that belong to the first Group are serious errors and need to be checked by humans. The recovery of the control program is only possible after microcontroller reset. The second group errors are less critical. The control program will not terminate. It will automatically recover if the error has past.

The fault detection and classification algorithm is shown in Fig. 4. It begins with the output voltage check. According to standard EN 50155 the allowed voltage range is 0.9 … 1.1 U_n (315…385 V). Any voltage value outside these limits creates a first group error, which results in control program termination as shown in Fig. 3.

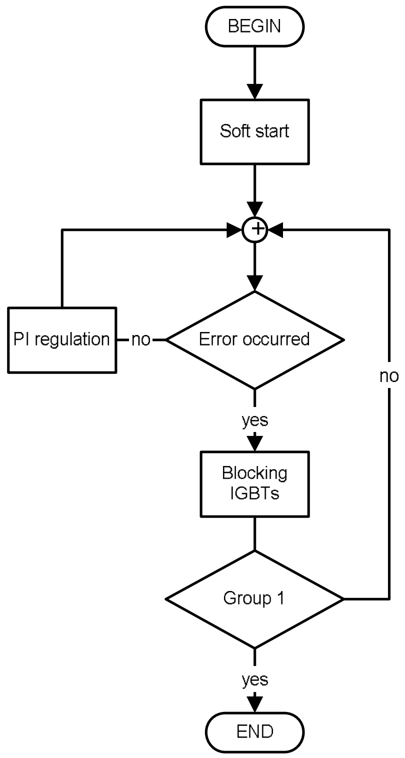

Fig. 3 The simplified control algorithm of the APS

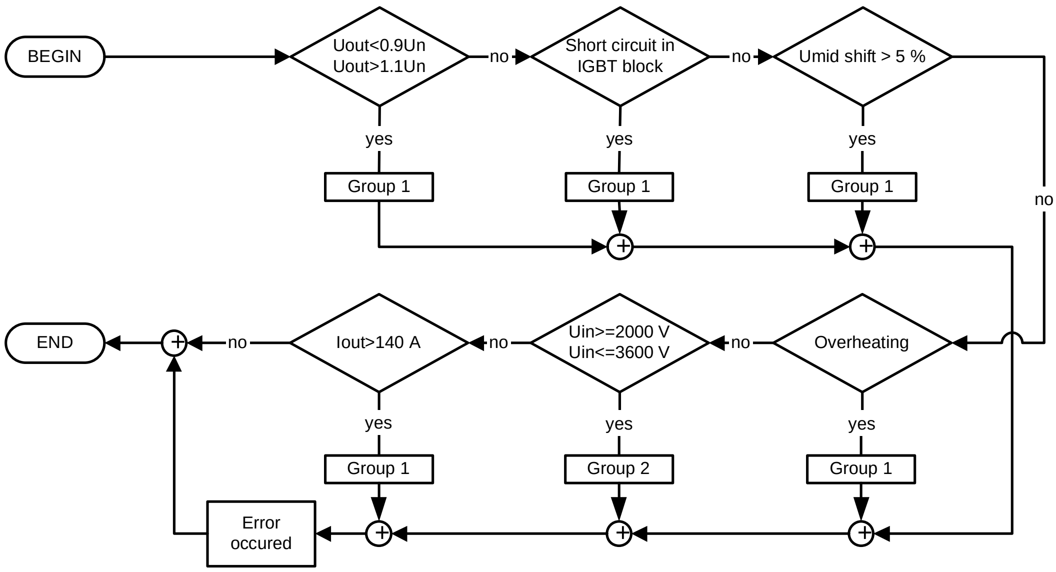

Fig. 4 Algorithm for fault detection and classification

The output voltage check is followed by short circuit detection block. In case of short circuit in the transistor, the IGBT driver will immediately block the transistor and send a signal to the microcontroller. This results in a first group error as shown in Fig. 4. The middle point voltage shift ($U_{mid} = U_{in} / 2$ see Fig. 1) is an important issue in the half-bridge converters. The middle point voltage shift can push the transformer core upon the saturation [6, 7]. Thus a voltage shift greater than 5% creates a first group error.

Since the thermal processes are slow and cooling down takes some time, also the overheating of a component causes first group error, which leads to a complete shut down of the power supply.

The standardized nominal value of the catenary voltage is 3000 V, thus according to standard EN50163 the minimal and maximal allowed values are 2000 and 3600 V respectively. If the voltage exceeds these values a second group error will be created. The IGBTs will be blocked. However, the control program keeps on running and after the error is resolved, the IGBTs will be switched on automatically.

The output power of the APS is 50 kW and maximal allowed output current is 140 A. Any higher current causes an overload error, which belongs to the first error group. The converter will be switched off.

5. Output Voltage Regulation

The voltage is regulated with PI regulator as shown in Fig. 3. The classical mathematical form of a digital PI regulator is presented in (1):

$$y_k = K_P e_k + K_I \sum_{i=1}^{k} e_i T_A , \tag{1}$$

where y_k is controlled variable, K_P is proportional gain constant, K_I is integral gain constant, T_A is integration time step, e_i is the sum of all errors in the regulator input. The disadvantage of this equation is the summation of the errors. In microcontrollers all the data is stored in variables, which size must be defined before compiling and running the program. Since the values and the number of errors in the regulator input are unknown, it is difficult to estimate the needed memory size. This can lead to unknown errors if the summation variable exceeds the predefined memory space.

$$y_{k-1} = K_P e_{k-1} + K_I T_A \sum_{i=1}^{k-1} e_i . \tag{2}$$

The (1) can be simplified. By subtracting (2) from (1) we will get the (3):

$$\Delta y = K_P \left(e_k - e_{k-1}\right) + K_I T_A e_k , \tag{3}$$

where Δy is a change in controlled variable. Taking into account that $y_k = y_{k-1} + \Delta y$ we get the (4)

$$y_k = y_{k-1} + K_P \left(e_k - e_{k-1}\right) + K_I T_A e_k , \tag{4}$$

where y_k is controlled variable at present moment, y_{k-1} is previous value of controlled variable, e_k is error at present moment, e_{k-1} is previous error. The regulator output can be calculated based on just two subsequent errors and the previous controlled variable value. There is no need to sum all the errors. Thus this algorithm is more reliable and simple than the classic equation of digital PI regulator.

6. Practical Results

The APS for the rolling stock has to fulfill the combined regulation requirements i.e. to provide a stable output voltage under the conditions of changing input voltage and load current. According to EN50155 the maximal allowed output voltage deviation is 10%. The simplified digital PI regulator algorithm was working effectively as shown in Fig. 5. The output voltage deviation was approximately 2%.

The control algorithm is provided with the soft start system, which prevents occurrence of large current peaks in the output. The soft start system gradually increases the pulse width signal of the IGBTs and the output voltage will grow smoothly.

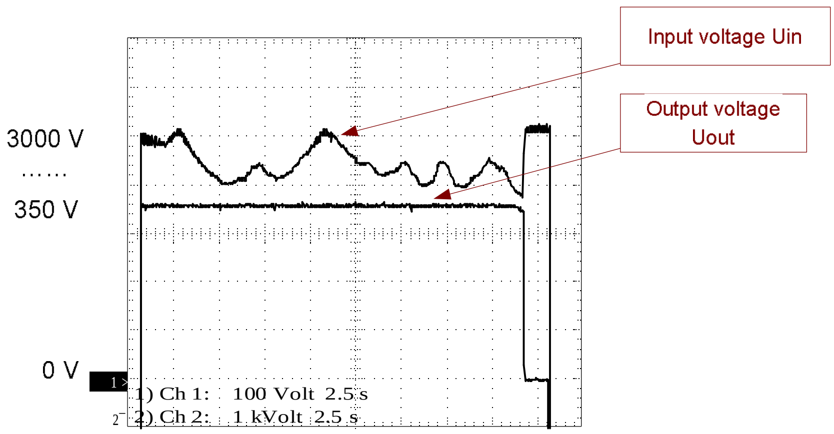

Fig. 5 The output voltage remains stable under conditions of changing input voltage and load current

The protection algorithms were also tested with positive results. As an example the reaction of the APS to the critical low input voltage is shown in Fig. 7. According to the standard EN50163 the minimum input voltage allowed is 2000 V. If the input voltage decreases below minimum value then the APS will be switched off as shown Fig. 7. If the input voltage grows bigger than 2000 V, the APS switches on again. Due to the soft start system the output starts to increase gradually. In the current case the reason for the input voltage peak after blocking IGBTs is the non stabilized high voltage power supply that was used in the laboratory

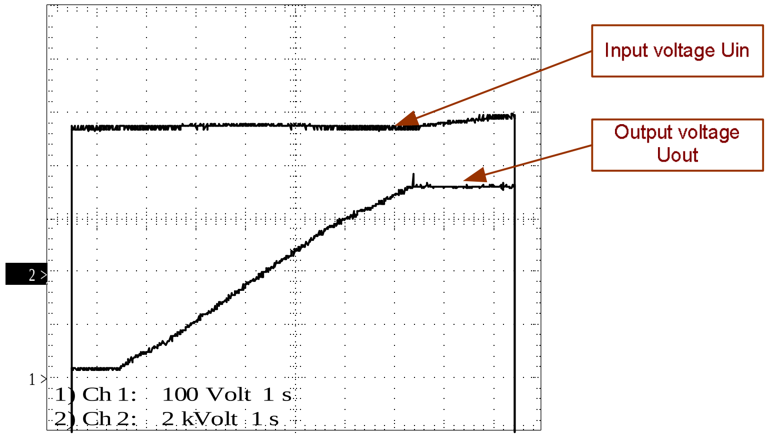

Fig. 6 Soft start during power up

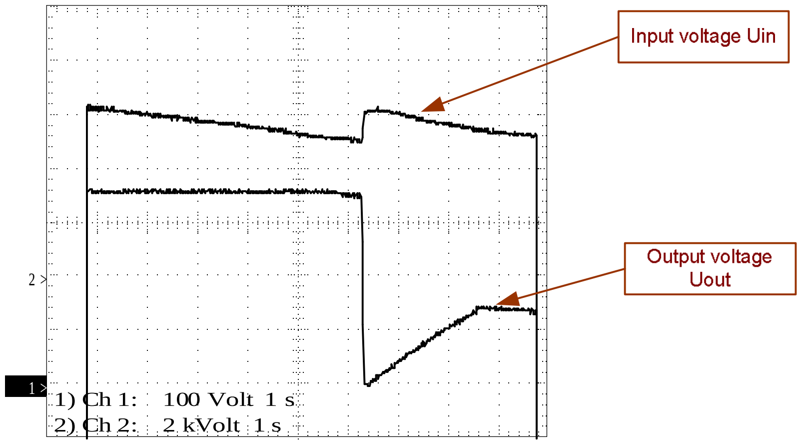

Fig. 7 The IGBTs will be temporarily blocked when the input voltage drops below 2000 V

7. Conclusion

New HV IGBTs on the market allowed constructing a HV APS using half-bridge topology, which simplified the control and the construction of the APS. The APS was designed according to EU railway standards EN 50155 and EN 50163. The following test results were received. The simplified PI regulator algorithm gave excellent results. The maximal output voltage deviation was only 2 %, which complies with the EU standard EN 50155. The protection system worked as expected. The input voltage range was chosen according to standard EN 50163. If the voltage exceeds these values, the APS blocks the IGBTs. The recovery follows automatically after the voltage is back within the standard determined range. The full-size converter's prototype has been elaborated and successfully tested in June 2007. The converter was tested in middle voltage as well as in high voltage range up to 4000 V.

Acknowledgement

Authors thank Estonian Science Foundation (Grant No. 7425 “Research of Dynamic Performance of High-Voltage IGBTs”) for financial support of this study.

References

1. www.eupec.com
2. EN 50155, “Railway applications. Electronic equipment used on rolling stock”.
3. EN 50163, “Railway applications. Supply voltages of traction systems”.
4. Using Modular DC-DC Converters to Meet European Standards for Railway Applications. VICOR Application Note, 2007.
5. **E. Godsey**. PE: “Rugged COTS Forged from European Railway Standards” // COTS journal. Feb. 2004.
6. **Redl R.**, **Sokal N. O.**, **Schaefer C. W.** Transformer saturation and unusual system oscillation in capacitively coupled half-bridge or full-bridge forward converters: causes, analyses, and cures // PESC ‘88, April 1988, Vol 2, p. 820-829.
7. **Srinivasan R.**, **Oruganti R.** A unity power factor converter using half-bridge boost topology // Power Electronics, IEEE Transactions, Vol 13, p. 487-500.

Proceedings of 3rd International Workshop ITELMS'2008

Head Injury Criteria *HIC* Dependence On Speed In Various Kinds Of Cars

L. Pelenytė–Vyšniauskienė

Kaunas University of Technology, Panevėžys Institute, Klaipėdos g. 1, LT-35209 Panevėžys, Lithuania,
E-mail: linapelenyte@gmail.com

Abstract

The largest number of car crashes happens at the moment of Frontal Crash. This article's aim is to analyse the types of Frontal Crashes and their repartition, to diagnose what part in occupant's safety the protection system's use takes, and also to analyse head injury coefficient dependence on car speed and show critical injuries and fatality limits in cases when driver is driving with no seat-belts in and while the car is without airbag. The research is done at the moment of ideal Frontal Crash by simulating distance from the occupant body to the wheel in different types of baskets.
KEY WORDS: *crash, occupants injuries, HIC, speed.*

1. Introduction

During car crashes injuries are usually dangerous. Up to 10 ... 12 % of injured occupants die during crash because of heavy injuries. Injury tolerance limits describe items such as fractures, injuries of organs, and other injuries. A classification is done via the Abbreviated Injury Scale (*AIS*) or Overall Abbreviated Injury Scale (*OAIS*). With the *AIS* or *OAIS*, the single or total injury is described. The data span within a range from 0 to 6.

The limits to the injury level depend on sex, anthropometrics, age, mass, mass distribution, and specific conditions [1]. The risk of head, thorax and abdominal injuries is significantly reduced in airbag–equipped cars compared to non–airbag cars. However, there is no concomitant reduction in the risk of upper and lower extremity injuries in airbag–equipped cars. In fact, the risk of lower extremity injuries (both KTH and below knee injuries) is higher among belted occupants in airbag – equipped cars than those with no airbag. This observation is similar to that found by Rupp et al. (2002). The risk of *AIS* 2+ injuries is highest to the lower extremities compared to any other body region in airbag–equipped cars. The risk of injury to the KTH (Knee – Thigh – Hip) complex is approximately the same as the risk of below knee injuries [2].

2. The Research on Head Injuries

Head movements in the car are not limited by any restriction systems. Therefore, at the moment of crash it hits various objects in the car (window, wheel, dashboard, etc.). The hit of the head can cause bruises, scrapes, wounds, contusion and commotion of cerebrum, cranium cracks, cerebral haemorrhage etc.

Encephalon injuries during motor transport accidents are mostly fatal for occupants up to 45 years old. When whole body injuries index $AIS = 5$, they reach even 84 % of whole body injuries [4].

According to the information of sixty researches there are many various criteria of injuries. Researches were lead by well–known scientists like Lissner, Lebow and Evans (1960), Ommaya and Hirsch (1971) and others. Classic *HIC* (Head Injury Criteria) were given in addition to Vienna institute‘s index, specified model of the brain and medium tension criteria. On recommended SAE (Safety of Automotive Engineers) basis head injury criteria were counted at every 3 *ms* time intervals. The criterion was specified by Versace in 1971 and described by equation [5]:

$$HIC = \left[\frac{1}{t_2 - t_1} \int_{t_1}^{t_2} a dt \right]^{2.5} (t_2 - t_1), \tag{1}$$

where t_1 and t_2 – any time moments during impact between the earlier mentioned t_{start} and end t_{end} times; a – acceleration in time interval $t_1 - t_2$.

Euro NCAP (European New Car Assessment Programme) has the highest reputation in analysing collisions. Through different tests it has set head, thorax and legs injuries, probability and extent in cases of frontal collisions.

Head injuries are assessed by *HIC* (Head Injury Criterion) coefficient Table 1.

According to *HIC* scale, when meanings are below 500, probability togged injured is very low. At 1000 approximately one out of six passengers might be in danger after skull fraction or brain damage. When HIC is above 2000 almost all the passengers get their heads injured. In such cases either death follows or long hospitalization.

HIC test is conducted using a 5 kg head model which is connected with a dummy. Impact speed meter is constructed into the 'head' and used to measure the impact velocity [1].

Table 1

Head injury coefficient meanings

HIC factor	
Meaning	Injury size
750	Low probability that brains will be injured
750 - 1250	Probable brains injury
1250	Brains injury

3. *HIC* Dependence on Speed in Various Kinds of Cars

The essence of this research is to find out occupant‘s minimum possible deceleration constants of the acceleration, using common occupant’s body forward movement [6]. It is known that occupant‘s deceleration of acceleration can be found out not only by taking measures or simulating the situation but using diagrams as well.

Calculating occupant‘s body movement at the moment of Frontal Crash, you need to pay attention to sequence of occupant‘s body movement. The car hits the obstruction. The bumper gets deformed while the power of hit exceeding several times the car weight, stop it.

Occupant starts moving in the same direction as car was going. His speed is equal to car speed before the hit. The car starts the backward movement, but occupant from inertia is still moving forward, when finally hits the parts of interior. Since the car moves backward after the hit, occupant‘s forward movement becomes shorter.

Parts of interior absorb part of occupant‘s kinetic energy and body starts moving backwards. Depending on the beginning of occupant‘s deceleration of acceleration and it growth, a part of car’s general deformation length is being used.

Simplified occupant’s body model centres of three masses are used for mathematical analysis. Supposing, that driver‘s height and weight are of average mean and he is not using any protection systems. Supposing, that head is going to hit the wheel in the direction B (Fig. 1) against no less than 25 % of its square.

The ideal Frontal Crash is being analysed, when car cabin remains undamaged and all-in-one occupant body is moving in rectilinear movement. Suppose, that occupant’s movement acceleration until the hit is constant.

Occupant having a certain mass is displaced (covers a certain distance):

$$s = s_{interiortotal} + s_{Fz}(t_{thoraxrebound}) - s_{thorax}(t_{start}), \tag{2}$$

where $s_{interiortotal}$ – obstacle, distance in a car from thorax (body) until the closest obstacle, where occupant can be displaced.; $s_{Fz}(t_{thoraxrebound})$ – distance, that the car covers, until the collision moment when thorax hits an obstacle; $s_{thorax}(t_{start})$ – distance that thorax (body) covers at the initial moment of collision.

Time, required to reach the final point and kinetic energy disappearance is equal [7] to:

$$t_{end} = t_{start} + \left(\frac{2s_{req}}{a_{const}}\right)^{0.5}, \tag{3}$$

where s_{req} is distance, required for the body not to be injured during the accident. It is calculated by the following formula:

$$s_{req} = \frac{1}{2}vt = \frac{1}{2}at^2 = \frac{E_{kin}}{m \cdot a_{const}}. \tag{4}$$

Time at the beginning of collision t_{start}, during which thorax (occupant) is displaced considering the distance $s_{thorax}(t_{start})$, acceleration function:

$$t_{start} = f(a_{thorax} = a_{const}). \tag{5}$$

Motion acceleration can be expressed by ratio $a = \frac{a_t}{g}$, then in a general case occupant motion during the accident is $s = s_0 + v_0 t + \frac{1}{2}at^2$, but as analysis shows, it is simplified (a = *const*), so $s = \frac{1}{2}at^2$. Occupant motion is $v = v_0 + at$. Having in mind a = *const*, so $v = at$. Occupant motion travel during the accident is $s = \frac{v^2}{2a}$.

However an occupant during the accident moves in the car interior, so his maximum travel is as long as up to the closest obstacle (windshield, panel, etc.). Time required to gain the initial acceleration equals the ratio of velocity and acceleration $t = v / a$. Since occupant is likely to move up to an obstacle, opposing system will start functioning when occupant moves in the distance s until the obstacle. According to formula (2) $t_2 = t_1 + \sqrt{2\,s/a}$, as t_1 = 0 so $t_2 = \sqrt{2\,s/a}$. Occupant's velocity on impact is $v = at_2$.

Using the formulas it is possible to calculate occupant motion accelerations, their duration, occupant motion during impact against opposing system and *HIC*. Since the acceleration is invariable so its volumes are selected.

Calculation in a few cases is given as a_1 = 10 g, 20 g, 30 g, 40 g, 50 g, 60 g. For the purpose of research 8 measures of different makes of cars and sizes were taken (Table 1). Measured distances from the outward man chest to the steering wheel are s_{max} and s_{min}. (Fig. 1 and Table 2).

According to the given procedure we will count all measured cars a (m/s^2), t_2, (s), v,(m/s) and *HIC*, when distance s between driver and steering wheel is minimal, medium and maximal.

The calculated head injuries coefficient *HIC* and its dependence on speed, are shown in Fig. 2 - 9. This is speed when body will get certain value of injury. In given figures two critical values of injuries can be seen: the first critical limit shows that when $HIC < 650$, head injuries are not fatal, brains are not damaged.

The second limit shows that when $HIC \geq 1000$, head injuries are possibly heavy: cracked cranium, bone breaks, heavy concussion and cerebral haemorrhage can be observed. One of six victims of the accident dies at the moment of crash [8].

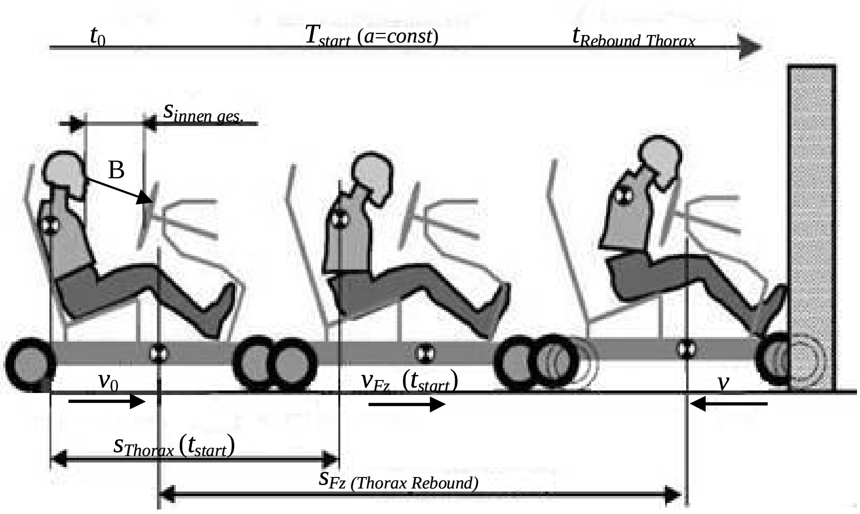

Fig. 1 Occupant motion until repercussion

Table 2

Measures of examined cars

Model	Year	Weight, *kg*	s_{max}	s_{min}	Model	Year	Weight, *kg*	s_{max}	s_{min}
Peugeot 605	1991	1460	65	40	Lancia Zeta	1997	690	43	22
VW Golf	1995	1120	55	34	BMW 524	1990	1500	48	26
Citroen C25	1990	2170	43	27	Opel Astra	1991	950	50	36
Mazda 323 F	1990	990	53	33	Audi A6	1996	1970	48	30

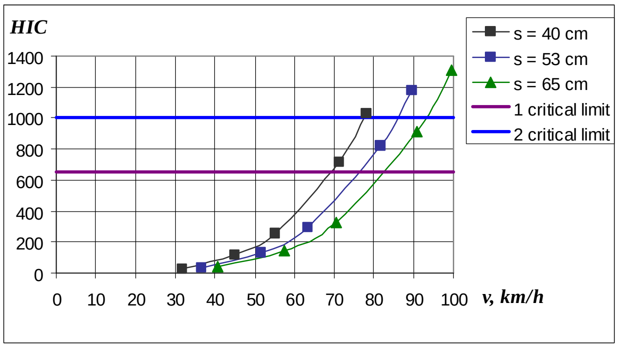

Fig. 2 *HIC* dependability on velocity (Peugeot 605)

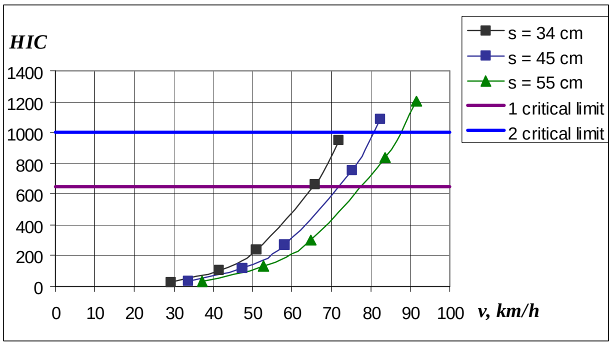

Fig. 3 *HIC* dependability on velocity (VW Golf)

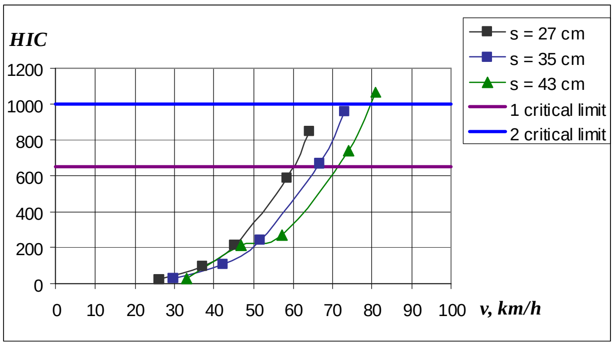

Fig. 4 *HIC* dependability on velocity (Citroen C25)

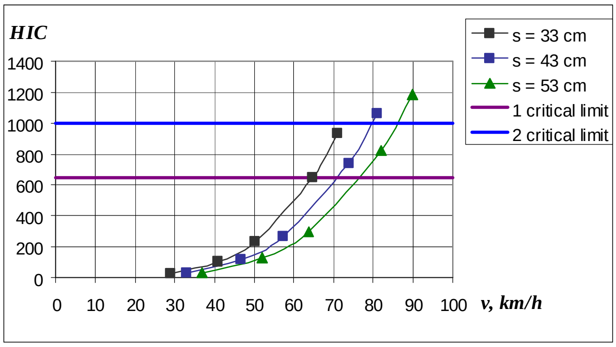

Fig. 5 *HIC* dependability on velocity (Mazda 323 F)

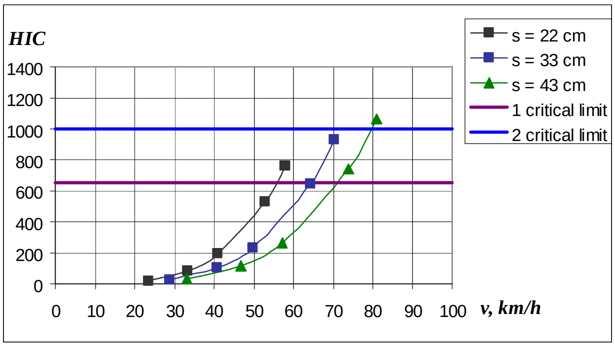

Fig. 6 *HIC* dependability on velocity (Lancia Zeta)

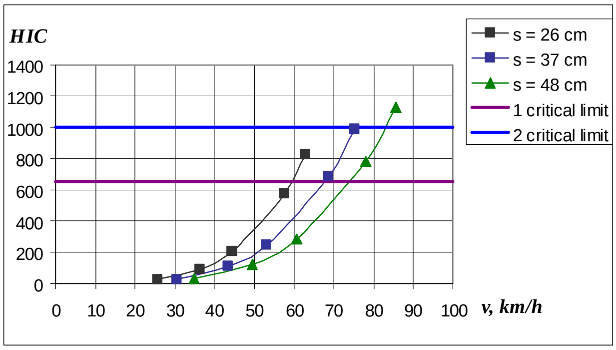

Fig. 7 *HIC* dependability on velocity (BMW 524)

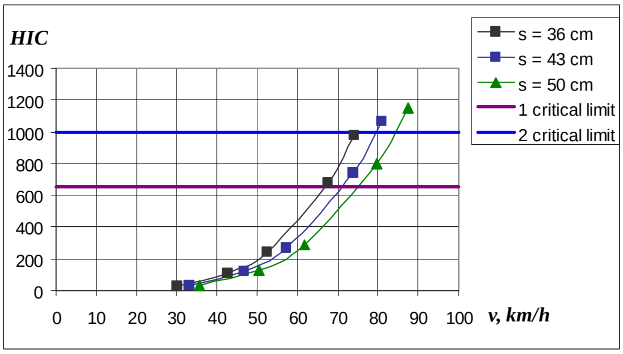

Fig. 8 *HIC* dependability on velocity (Opel Astra

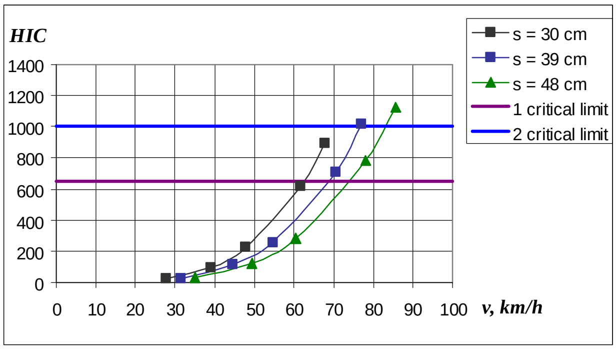

Fig. 9 *HIC* dependability on velocity (Audi A6)

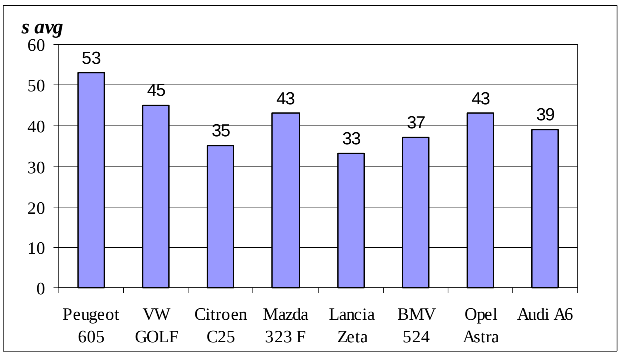

Fig. 10 Distribution of average distance *s*

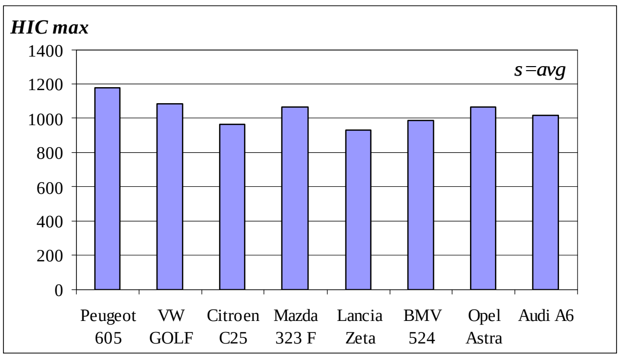

Fig. 11 Distribution of average distance *s* in the cars

While applying mathematical motion model it has become clear that after calculating occupant travel s and necessary body travel s_{reik}, the following versions are possible:

- $s > s_{req}$ – passenger suffers, safety increases, if s decreases;
- $s < s_{req}$ – passenger does not suffer, safety increase;
- $s \approx s_{req}$ – passenger does not suffer.

According to given figures, we can see that if the occupant until the resistance of protection systems goes undisturbed up to 60 – 80 km/h, in this case we get larger *HIC* values while *s* value is lower. Yet when speed is higher, the chance of injury also gets higher when we have s_{max}.

If after the crash, which matches the analysed ideal Frontal Crash case, there is a possibility to find out how far away the driver was sitting, so that having in mind his injuries value we can find out approximate car speed before the crash.

In Fig. 10 you can see average distances between the occupant and the wheel in the examined cars. It is clear that s_{max} is the highest in Peugeot 605 and the lowest in Lancia Zeta.

When occupants speed before hitting the wheel is over 80 *km/h* and the distance is medium, the highest *HIC* is observed in Peugeot: *HIC* = 1178 and VW Golf: *HIC* = 1084 (Fig. 11). The lowest possibility of injuries would be observed in Lancia Zeta: *HIC* = 927.

4. Conclusions

1. Having analyzed NHTSA database, such conclusions can be made: at the moment of crash, when *AIS* = 5 – 6, the head is injured in 53 % of cases and the chest is injured in 20 % of cases.
2. After measuring 8 cabins of cars, the biggest and the smallest distance between occupant and wheel was found out.
3. After calculating every car's *HIC* dependence on speed, when $s = s_{min}$, s_{vid} and s_{max}, we found out that the largest *HIC is* observed Peugeot 605 and the lowest in Lancia Zeta. It is found that only two cars (from 8 cars) don not reach the second critical fatal zone.

References

1. Association for the advancement of automotive medicine. The Abbreviated Injury Scale. Illinois: Revision Des Plaines. 1990, 80 p.
2. **Shashi K.** An overview of Knee – Thigh – Hip Injuries in Frontal crashes in the United States. National Highway Traffic Safety Administration. 2005, 416 p.
3. **Viano D.C.**, **Culver C.C.**, **Haut R.C.**, **Melvin J.W.**, **Bender M.**, **Culver R.H.**, **Levine R.S.** Bolster Impacts to the Knee and Tibia of Occupant Cadavers and an Anthropomorphic Dummy. Proceedings of the 22nd Stapp Car Crash Conference, SAE Technical Paper No. 7780896. 1994, p. 403–428.
4. **Daniel A.G.** Analysis of NASS Cases involving SUV Rollovers with Belted and Unbelted Occupants. Report of National Crash analysis Center (FHWA/NHTSA). May 2002, p. 1-15.
5. **Ommaya A.K.**, **Hirsch A.E.** Tolerances for Cerebral Concussion from Head Impact and Whiplash in Primates // Journal of Biomechanics. 1971, Vol. 4, p. 13–20.
6. **Kai I.** Innovative Energiemanagement Methoden zur Analyse und Verbesserung von Insassenschutzsystemen. Berlin: ISS – Fahzeugtechnik, 2000, p. 6–28.
7. **Pelenytė-Vyšniauskienė L.**, **Jurkauskas A.** Research into Occupant‘s motion in cars during crashes // Transport. Vilnius: Technika, 2004, Vol XIX, No 4. p. 184–190.
8. **Koshiro O.**, **Munekazu K.** Influences of the physical parameters on the risk to injuries in low impact speed // Accident Analysis & Prevention, 2004, Vol. 28, Issue 4, p. 265–271.

Proceedings of 3rd International Workshop ITELMS'2008

A method for FE analysis of wheel and rail interaction

D. Somov*, Ž. Bazaras**

* *Kaunas University of Technology, Kęstučio 27, LT-44025, Kaunas, Lithuania, E-mail: dmitrij@tkontaktai.lt*
** *Kaunas University of Technology, Klaipėdos 1, LT-35209, Panevėžys, Lithuania, E-mail: dekppf@ktu.lt*

Abstract

Two methods have traditionally been used to investigate the rail-wheel contact, that is the Hertz analytical method and simplified numerical methods based on the boundary element (BE) method. These methods rely on a half-space assumption and a linear material model. To overcome these limitations, a tool for FE-based quasi-static wheel-rail contact simulations has been developed. The modeling tool and a methodology are described in the presented paper. Simulation results are compared with Hertzian and BE solutions. Significant differences in the calculated state between the FE solution and the traditional approaches can be observed. These differences are most significant in situations with flange contact.
KEY WORDS: *wheel and rail interaction*.

1. Introduction

Most railway wheels are rigidly mounted on a steel shaft. A typical wheelset on a straight track is shown in Fig. 1. The axle load may be as high as 220 kN and the contact area between a wheel and the rail is roughly 1 cm^2. The contact region is thus very highly stressed. The interaction in the contact zone between wheel and rail is determined by the global dynamic behavior of the vehicle and by various physical phenomena that occur in the contact zone. The profiles of wheel treads and railheads are transformed by the wheel and rail interaction. This transformation, which may be severe in curves, has a significant effect on the contact state.

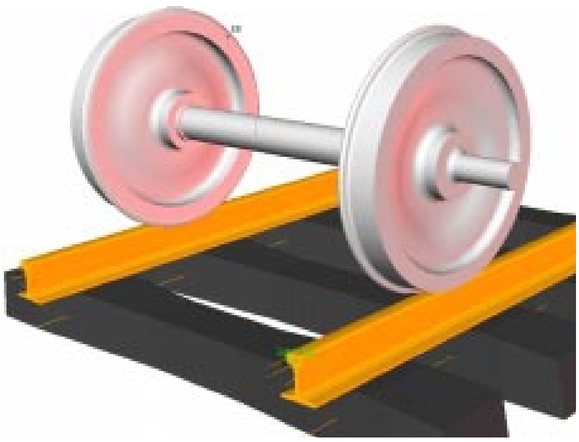

Fig. 1 Wheelset on a straight track

Software for vehicle motion simulations, are normally concerned with the orientation of each wheel relative to the track, and thus the pointof- contact between wheel tread an rail head and the contact forces that are caused by the dynamic interaction. The analysis was two dimensional and the exact solution was found. Carter showed that the difference between the circumferential velocity *VC* of a driven wheel and the translational velocity *VT* of the wheel has a nonzero value as soon as an accelerating or a braking couple is applied to the wheel.

2. FE Modeling of Wheel-Rail Interaction

A complete FE model of one wheel, a piece of rail, a set of contact elements and the quasi static loads on the wheel are interactively created with a library of Ansys macro routines that are accessed with the Ansys Graphical User Interface (GUI). Sets of keypoints that define the rail head and wheel tread profiles are assumed to exist as separate files. Keypoints that describe the shape of a profile are preferably generated with a standard Miniprof instrument. The two sets of keypoints are converted to 2-D spline curves by an Ansys macro routine.

The basic steps in the creation of a wheel-rail interaction model for an X1 motor coach in a curve with a radius of 303m and a standard UIC60 rail is presented below. The three-dimensional geometric model of the wheel is generated by revolving the two-dimensional spline curves that describe the profile of the wheel tread. The rail model is created by extruding railhead profile curves a distance of 600 mm, which is the distance between the sleepers. Two sets of curves for a new wheel and a new rail are shown in Fig. 2. The two solid bodies are shown in Fig. 3. To get a reasonable configure model, the wheel is spatially oriented relative to the rail according to the quasi-static state calculated by an MBS software, e.g. Gensys or Medyna. To aid an efficient discretization of the contact region, a measure of the expected contact length and the number of expected contact patches have to be supplied by the user.

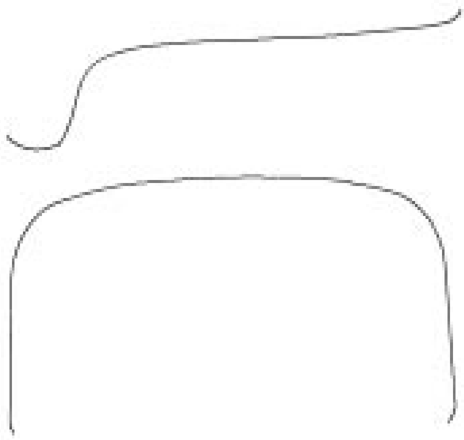

Fig. 2 Spline curves generated from measured point sets

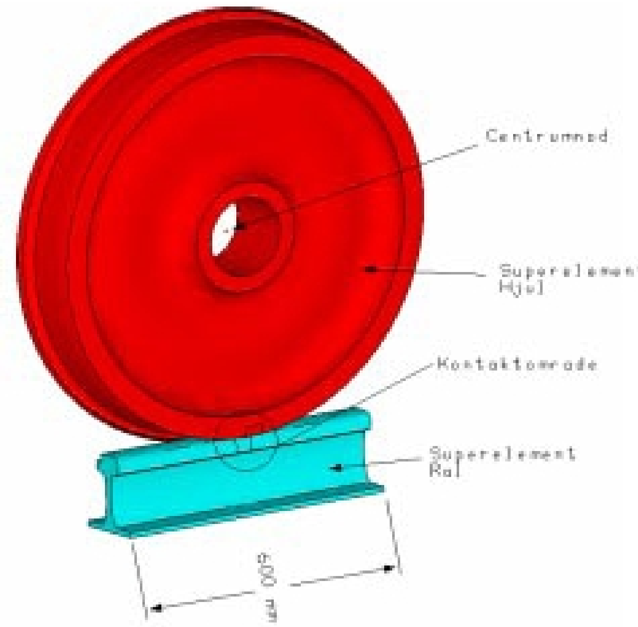

Fig. 3 Solid model generated from the profile curves

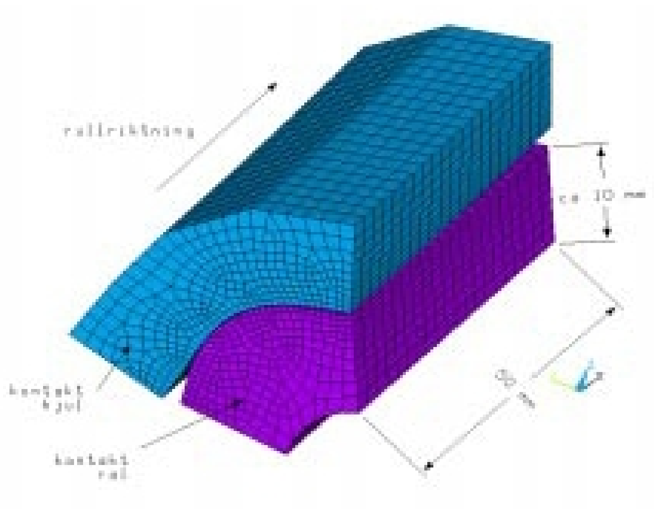

Fig. 4 The wheel-rail contact region

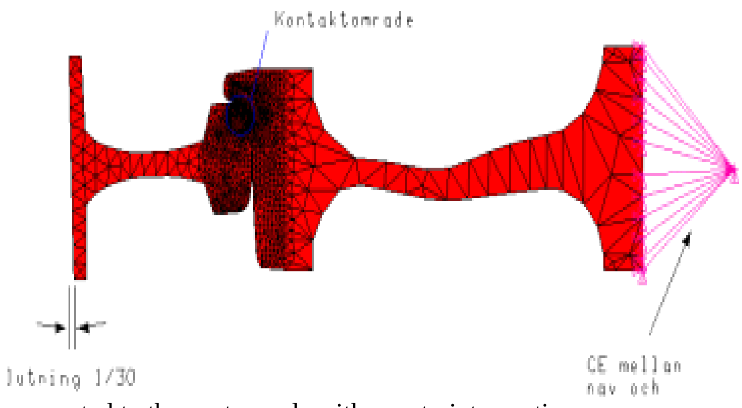

Fig. 5 The wheel hub is connected to the center node with constraint equations

The contact region, i.e. the small portion of the two bodies that are close to the anticipated contact patch, is meshed with the Ansys linear isoparametric element Solid45. For these elements, which almost exclusively are hexahedrons (see Fig. 4), an elastic-plastic material model with kinematic hardening is defined.

The size of the contact zone is approximately 30mm in the lateral direction of the rail, 50mm in the longitudinal direction, and 10mm in the normal direction. The size in the longitudinal direction is based on the size of the contact zone and the distance of rolling required for the simulation.

The main parts of the wheel and rail bodies are meshed with degenerated linear isoparametric elements. The hub surface is covered with shell elements. These two submodels are condensed to superelements. The nodes on the hub surface are connected to a center node with constraint equations (see Fig. 5).

3. Methodology

Here, the term methodology is used for a collection of methods and tools, the use of which is governed by a process superimposed on the whole. Generally, a method, which is an organized, single purpose discipline or practice, evolves as a distillation of the best-practices experience in a particular domain of cognitive or physical activity (IDEF4, 1995). A tool refers to a software system, such as a FE system, designed to support the method.

FE modeling of the wheel-rail interaction requires the shape of the geometric, domains, a material model, a value for the coefficient of friction, and knowledge about the contact forces. The material model is based on stress-strain curves supplied by the manufacturers of wheel and rail. The coefficient of friction is achieved from field instruments such as the Salient system tribometer. The profiles of railheads and wheel treads are measured with the Miniprof instrument. MBS-simulations provide contact point locations and quasi-static contact forces. These contact forces are transformed to global forces at the center node. With these data as input, the macro routines described above is capable of defining a complete FE model and the proper boundary conditions for a quasi-static simulation that capture the physical behavior that is caused by the combined rolling and sliding interaction. In a final step, the contact state history is extracted from the Ansys result database an exported in ASCIIformat for further analysis and manipulation.

4. Comparison with Traditional Methods

A sharp curve in a track trafficked by commuter trains serving the area is chosen for a comparison between the FE simulation results and results obtained with traditional methods. The chosen track carries almost exclusively unidirectional commuter trains with an average speed of 75 km/h. Two types of vehicles are used: the X1 and the X10 both operating in pairs with one powered unit and one trailing unit. This track and the rolling stock have been studied in a national Swedish program. Both rail and wheel profiles have been measured over a couple of years.

Two cases were used to study the model. Both cases were from simulation of the X1 powered unit and represent the first and second wheel set in the leading boogie. The coordinate system is chosen similar to the Deutche Industrial Norm (DIN) with positive vertical (z) co-ordinate upwards, y to left and x is positive to the train motion direction. Fig. 6 presents the contact points location on the wheel and the rail shows the forces in the center point of the wheel. From a geometrical perspective the two load cases represents the contact points with a large difference in the curvature of contacting bodies. In case 1, the minimum contact radius was about 300 mm and in case 2 it was about 20 mm. New rail profiles and a wheel profile from a X1 train that has been in traffic for two years were used in the two cases. In both cases, the normal force was 80377N. The tool for the FE analysis is made and the preliminary results along with the comparison to the main concurrently available methods is outlined. In the first stage the differences between the methods are presented (see Fig. 6).

The main scope for this work was to enhance the knowledge of the contact pressure and the maximum stresses in bulk material. This should give an appropriate basis to study the degradation mechanism along with the wear simulation. The results could not be compared with the Hertz method assuming one-point contact.

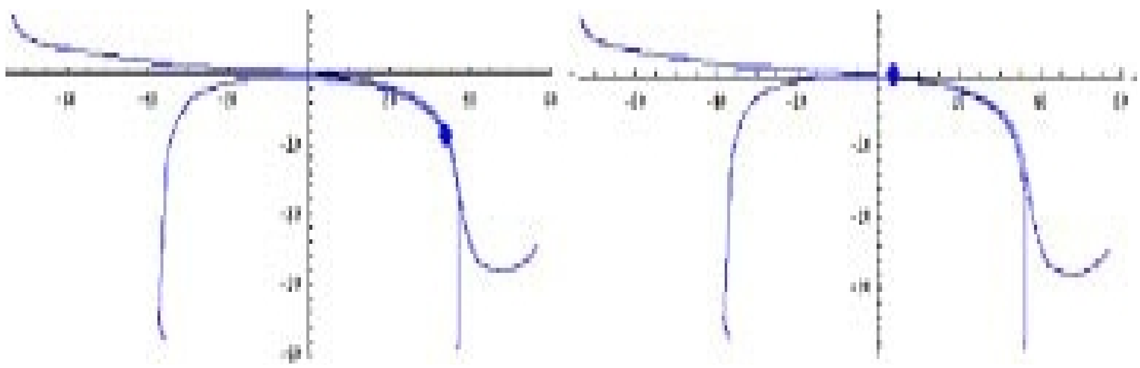

Fig. 6 Contact point location for the two test cases

Using the linear-elastic model the differences in results are significant in regards especially to the relatively new wheel and rail shapes. Significant flattening of the contact pressure profile was found with increasing plastic deformation. The maximum pressure and plastic work moved outward in the direction of the contact edge along with the increase of friction coefficient.

Experiments have shown that the losses in the rail crosssectional area remain approximately constant in time. Assuming a constant rate of degradation the relationship between the plastic flow and wear changes. In the initial phase, the plastic work is very large. The maximum equivalent von Mises stress exceeds even the ultimate stress limit which for the actual plasticity model was 606MPa. Thus, the material in this phase of the degradation process behaves perfectly plastic. The plastic flow hardens the material and makes the contact more conform. In the continuing process, other wear mechanisms will thus be significant.

5. Conclusions

A tool for contact mechanics modeling and simulation of the wheel rail contact has been developed. The geometry of the contact can easily be changed. The model can be generated from measured wheel and rail profiles. Traditional methods and computational tools are limited by an half space assumption and a linear material model.

The results from two test cases show that the difference in maximum equivalent stress between traditional methods and the FE model is small when the minimum contact radius is large compared to the significant dimensions of the contact area, i.e. when the half space assumptions is valid.

Reference

1. **Krauze H.**, **Poll G.** Wear of Wheel-Rail Surfaces, Wear 113 (1986), 103-122.
2. **Kapoor A.** et al. Surface Roughness and Plastic Flow in Rail Wheel Contact, Wear 253 (2002), 257-264.
3. **Engel P. A.**, **Yang Q.** General micro-hardness Indentation Theory for Multilayer contacts // J. Tribology. vol.119 1997, p. 1-7.
4. **Walthwer F.**, **Eifler D.** Local Cyclic Deformation Behavior and Microstructure of Railway Wheel Materials // Mat. Sc. and Eng. A387-389, 2004, p. 481-485.
5. **Maslukov V.**, **Suslov A.**, **Gorlenko A.**, **Inutin V.** and **Finatov D.** Technological Increase of Quality of Roll Surface and Durability of Railways Rails and Wheels. 9th International DAAAM Symposium-Cluj- Napoca, Romania 22-24 October, 1998.
6. **Ringsberg J. W.** Life Prediction of Rolling Contact Fatigue crack initation // Int. J. Fatigue. 23 2001, p. 575-586.
7. **Andersson E.**, **Berg M.** and **Stichel S**. Dynamics of rail vehicles Railway Technology, Dept. of Vehicle Engineering, Royal Institute of Technology, KTH, Stockholm, Sweden, 2000. [in Swedish].
8. **Shen, Z. Y., Hedrick, J. K., and Elkins, J. A.** A comparison of alternative creep-force models for rail vehicle dynamic analysis. The Dynamics of Vehicles, Proc. 8th IAVSD Symp., Hedrick,J:K: (ed.), Cambridge, MA, Swets and Zeitlinger, Lisse, 1984, p. 591-605.
9. **Vermeulen P. J.** and **Johnson K. L.** Contact of nonspherical bodies transmitting tangential forces // J. Appl. Mech. 1964, vol. 31, p. 338-340.

Proceedings of 3rd International Workshop ITELMS'2008

Modeling of Intelligent Agents and Neural Network Controller for Maritime Transport

M. Gorobetz*, A. Levchenkov, L. Ribickis*****

**Riga Technical University, Institute of Industrial Electronics and Electrical Engineering, Kalku str.1, Riga, LV-1658, Latvia. E-mail: mgorobetz@latnet.lv*
***Riga Technical University, Institute of Industrial Electronics and Electrical Engineering, Kalku str.1, Riga, LV-1658, Latvia. E-mail: levas@latnet.lv*
****Riga Technical University, Institute of Industrial Electronics and Electrical Engineering, Kalku str.1, Riga, LV-1658, Latvia. E-mail:leonids.ribickis@rtu.lv*

Abstract

The purpose of the research is to develop new mathematical models and new algorithms for intelligent agents with neural network controllers in maritime transport. Main goal of research is increasing of safety level of maritime transport. The research includes the analysis and modelling of intelligent electronics devices based on multi-agent approaches. Methodologies used in research are intelligent electronic devices and negotiations, artificial neural network controllers, bond graphing for mechatronic system analysis and control. The research proposes the solution for control task between intelligent maritime transport units and intelligent maritime control units with a purpose to prevent accidents. The model includes algorithms of intelligent ship mechatronic system control and intelligent schedule control.
KEY WORDS: *intelligent agents, artificial neural network, modelling.*

1. Introduction

The paper is based on authors' previous scientific work researching the intelligent agent systems and its' application in mechatronic systems.. Intelligent agents are computer modules, which work in global network and use methods of the artificial intelligence. Intelligent agents have possibility to negotiate with each other and cooperate their work to get better decision [1].

2. Problem Formulation

There are three main safety levels in transport systems. The first is the safety of mechatronics system of a vessel. That means, an intelligent diagnostic system for engine states is needed to separate dangerous situations by critical testimonies from sensors from the regular states of the system.

The second level is the safe control of mechatronics system in a ship. One of the primary tasks is an intelligent speed control of a ship, taking in account weather factors and schedule.

The third safety level includes an intelligent control of the whole maritime transport system. That is why the solution of coordination task between all maritime objects in the system is necessary.

3. Methods of Solution

Authors propose to use intelligent agents system [2, 3] for all three safety levels.

Intelligent agents for diagnostics system of ship engines, based on neural network and clustering, give possibility to detect and warn about changes in the engine, detect the problem immediately, and to fix it in some cases without human intervention.

Methodologies used for mechatronics system control in the research are bond graphing, expert systems and negotiations.

The research proposes the algorithm of intelligent speed control and the solution for coordination task between intelligent vessels with a purpose to prevent accidents using the algorithm of negotiation for intelligent agents.

4. Mathematical Models

Neural Networks. Clustering analysis is based on artificial neural network model. Each neuron has input data set, weight for each input data, activation function and output, which usually has binary value. Neural network consists of several layers. Each layer may have definite or indefinite number of neurons. Neural networks give possibility to analyze an object by input parameter set and to detect predefined class of the object on the output. That means, neural network should be trained to detect classes and classes are predefined.

1. Input data set: $X = \{x_1, x_2, \ldots, x_n\}$

2. Weights: $W = \{w_1, w_2, \ldots, w_n, w_{n+1}\}$
3. Transfer function: $F = x_1*w_1 + x_2*w_2 + \ldots + x_n*w_n + w_{n+1}$
4. Result classes: $C = \{c_1, c_2, \ldots, c_m\}$

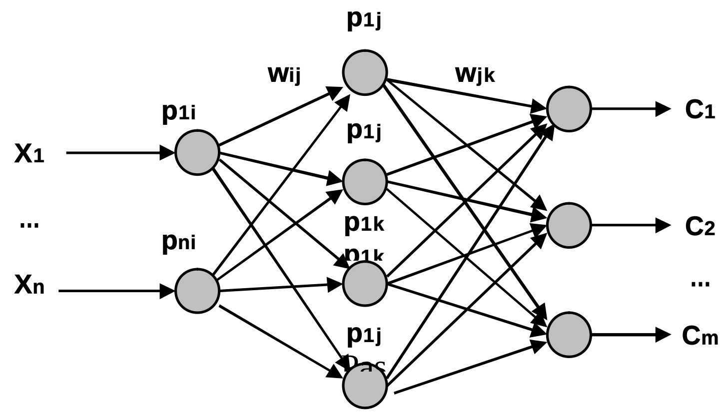

Fig. 1 Neural Network structure

Clustering Analysis. Clustering is one of adaptation methods [4]. It gives self-training possibilities to the intelligent agents and allows to classify unorganized input data. This way, clustering give possibility to create new neurons on the output layer of the neural network. Clustering analysis is used when output classes are not predefined. Mathematical model for clustering consists of following elements: set of input objects; set of attribute vectors for each object; dynamic set of clusters with variable size – at the beginning of analysis it is empty; dynamic set of prototype vectors for each cluster – attribute vector, which defines the class; set of cluster members for each cluster; set of sum vectors for each member – defines the correspondence of each member to prototype vector of the cluster; parameter of attentiveness – affects the precision of clustering analysis.

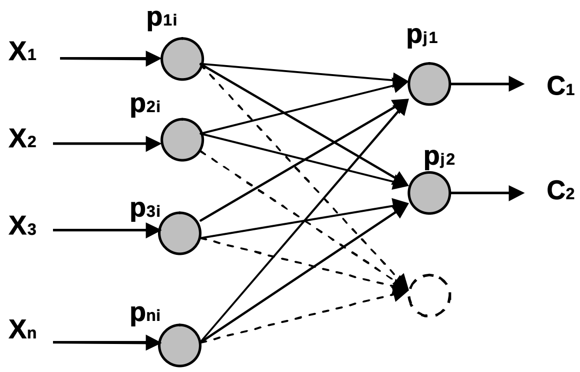

Fig. 2. Neural Network creation by clustering

Diagnostic System of Ship Engine

Set of states of an engine – $I^e = \{i_1^e, i_2^e, \ldots\}$

Set of properties of an engine – $X_i^e = \{x_{i1}^e, \ldots, x_{in}^e\}$

Set of clusters of engine states – $C^e = \{c_1^e, c_2^e, \ldots\}$

Engine states, members of cluster $M_c^e = \{m_{c1}^e, m_{c2}^e \ldots\}$

Prototype-vectors of clusters - $P_c^e = \{p_{c1}^e, \ldots, p_{cn}^e\}$

Sum vector of engine state - $S_m^e = P_c^e \cap M_c^e = \left\{s_{m1}^e, \ldots, s_{mn}^e\right\}$

Vigilance of agent – ρ^a $(0 < \rho^a \leq 1)$.

Mechatronics System Parameters for Vessel [5]

1. Vessel's motor excitation current I^t_e
2. Vessel's motor armature current I^t
3. Vessel's motor magnetic flux c^t_f
4. Vessel's motor torque constant c^t_m
5. Vessel's motor rotation speed n^t

6. Vessel's motor voltage U^t_m
7. Duty ratio of pulse regulation g^t

Coordination System between Maritime objects

1. A set of processors P – ports and other stationary points, where $P = \{P^1, P^2\}$, P Î N, ports: $P^1 = \{p_1^1, p_2^1, ..., p_s^1\} \subset P$
   Other points: $P^2 = \{p_1^2, p_2^2, ..., p_c^2\} \subset P$
2. A set of jobs V – vessels, where $V = \{v_1, v_2, ..., vu_m\}$
3. Vessel's schedule: $s_v : P^1 \to \{t_{v1}, t_{v2}, ..., t_{vs}\} \subset \Re$
4. Port's schedule: $s_{p^1} : V \to \{t_{p1}, t_{p2}, ..., t_{pm}\} \subset \Re$
5. Additional payments matrix A with criterions r, where A = $\{a_{1,1}, a_{1,2}, \dots, a_{r,n\times t}\}$, $r \in Z$, n=|S|, t=|U|;
6. A negotiation set B, where B = Ç$\sigma_k \to \varnothing$; Element conflicting objects and time to negotiate.
7. A set of time crossings $C \subset B$
8. A set of directive terms infringements $E \subset B$.

5. Algorithms for Intelligent Agent System

Clustering Algorithm for Engine Diagnostic. There are many algorithms for clustering analysis. On the current step of research authors propose to use one of the adaptive resonance theory (ART) algorithms for intelligent agents. General algorithm consists of four main steps. The first step the creation of the first prototype vector from the first input attribute vector. The second step is the beginning of the cycle, where a number of iterations depend on a number of objects. If this number is limited the number of iterations is finite. If objects are states of the process in mechatronic system, this number is unlimited, and clustering analysis is infinite. On the second step the next object is checked for membership of already created clusters. The step consists of three tests: test for attentiveness; comparing of attribute vector with prototype vector and attentiveness parameter; test for identity. If one of this tests failed new cluster is created, otherwise the object gets membership in already existed clusters. Authors propose to use the clustering algorithm for state analysis of complicated processes in the mechatronic systems obtaining information from sensors.

Step 1. The first prototype vector creation from the first property vector – $P_{c1}^e = X_{i1}^e$

Step 2. Cycle. Next object $i \in I$ is checked to be assigned to cluster from *C*.

Step 2.1. Check for vigilance: $|P_c^e \cap X_i^e| / (b + |P_c^e|) > |X_i^e| / (b + n)$; No – Step 4.

Step 2.2. Compare of with vigilance parameter: $|P_c^e \cap X_i^e| / |X_i^e| < r^a$; No - Step 4

Step 2.3. Check for identity: $|P_c^e| = |X_i^e|$? ; No - Step 4

Step 3. Assign current object *i* to cluster members $M_c^e (i = m \in M_c^e)$ .Go to Step 2

Step 4. Create new prototype vector. Go to. Step 2.

Algorithm of Intelligent Speed Control of a Vessel

Step 1. Detect next checkpoint - *chp*
Step 2. Calculate breaking point and breaking time: *brp = chp_dist – breaking_way(vmin ® 0)*
brt = breaking_time(vmin ® 0)
Step 3. Calculating rolling way and rolling time: *rw = rolling_way(v ® vmin)*
rt = rolling_time (v ® vmin)
Step 4. Evaluating the rolling way: *brp = s + rw* ? Yes – Step 5; No – Step 3
Step 5. If checkpoint type is a point: type[chp]="X"? Yes– Step 6; No – Step
Step 6. Start negotiations with point agent;
Step 7. Signal = green ? Yes – Step 1; No – *acceleration = false*
Step 8. If checkpoint type is port: type[chp]="S"? Yes – Step 9 No – *acceleration = false*
Step 9. Start negotiations with port's agent;
Step 10. Satisfies directive term *rt + brt £ t(chp)* ? Yes – *acceleration = false;* No – Step 3

Algorithm of Negotiations between Maritime Objects

Step 1. Getting input data from all jobs and processors about current situation in a zone;
Step 2. Negotiation Set B creating for all vessels coming to the port
Step 3. Crossing time set C calculating;
Step 4. Directive term checking - set E;
Step 5. CONFLICT ? Yes - New restriction in B, Step 2; No – Step 6;
Step 6. Creating new schedules;
Step 7. Sending acceptation messages to participants;

6. Computer Experiment

Neural Network Controller. DC drives are used in maritime transport for mechanisms, where uninterruptible rotation frequency control is necessary [6]. The model of DC drive neural network speed controller is created. General schema is presented on Fig. 3.

Neural network gets signal about rotation speed from engine sensor and also analyze own control signal, so feedback is realized.

General structure of neural network is following. Neural network consists of 1 input layer 1 hidden layer and 1 output layer. Each layer has set of weights and bias. Linear transfer function is used. Weighted inputs and bias are summarized. Weights of each layer are multiplied with input signals in each neuron. Output layer has only one neuron, because we need the only signal to control switching on a DC drive.

After neural network training by Levenberg-Marquardt algorithm to maintain speed in interval between 40 rad/s and 60 rad/s. These values are abstract and taken for demonstration of neural network control of DC drive with torque load.

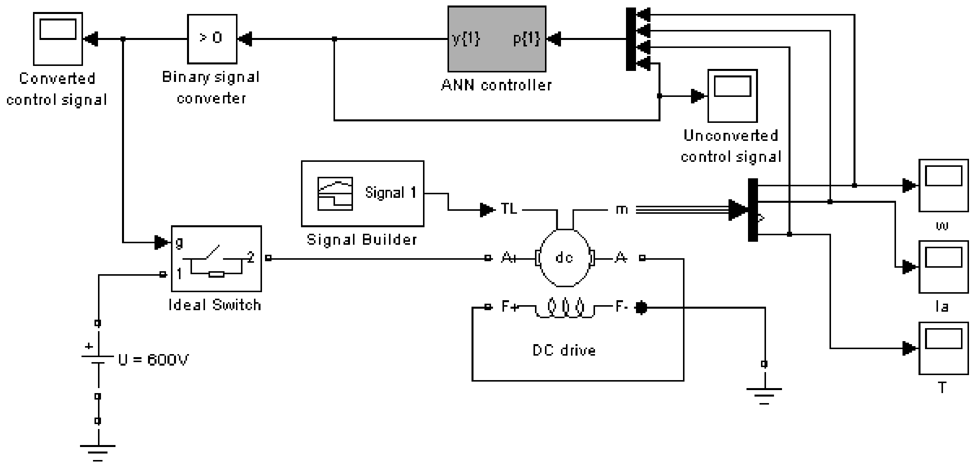

Fig. 3 Model of DC drives with ANN controller and load generator

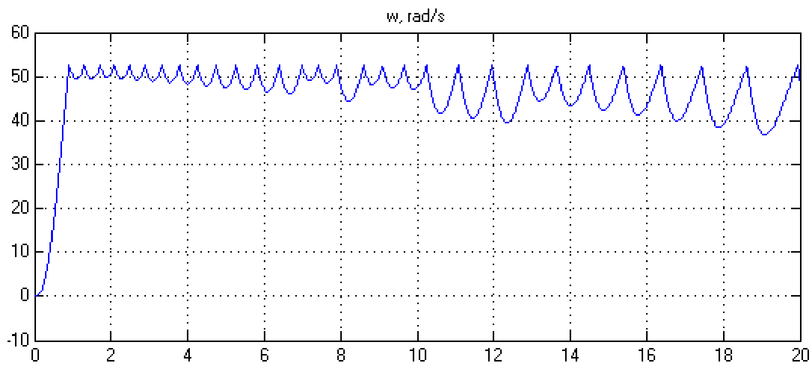

Fig. 4 Rotation speed controlled by neural network

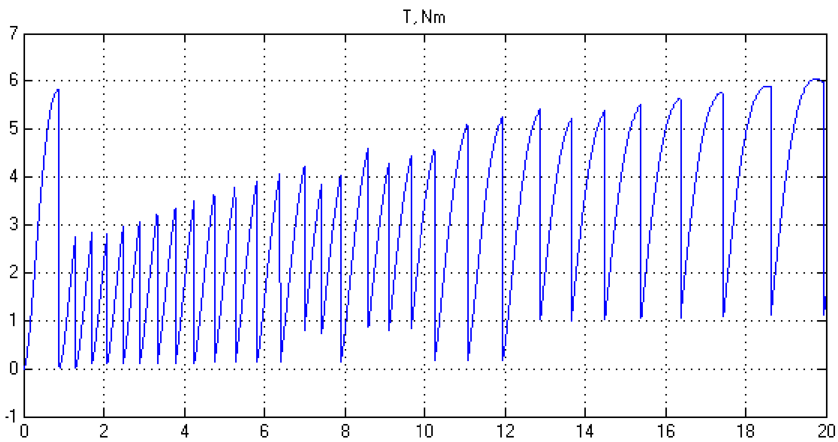

Fig. 5. Torque of an engine controlled by neural network

Modelling of Coordination and Scheduling. The specific environment is developed by authors for the dynamic modelling of intelligent agents for safety improving algorithms. The interface is presented on Fig.6 and Fig.7.

Model on Fig. 6 is presenting stream control algorithm. The algorithm controls only speed and movement direction without any coordination with other. It shows realization of second level of safety task.

Model on Fig. 7 presents realization of negotiation between intelligent agents of vessels. The situation shows that one of the vessels should wait before another one will free the way.

Both vessels have schedules and directive time. It is also controlled by this algorithm.

The results of using algorithms of artificial intelligence in maritime transport systems show the possibility to avoid crashes and detect dangerous points on the way. Algorithms advance safety improvement, optimization of energy usage, profit increasing, idle time minimization, coordination and schedule control.

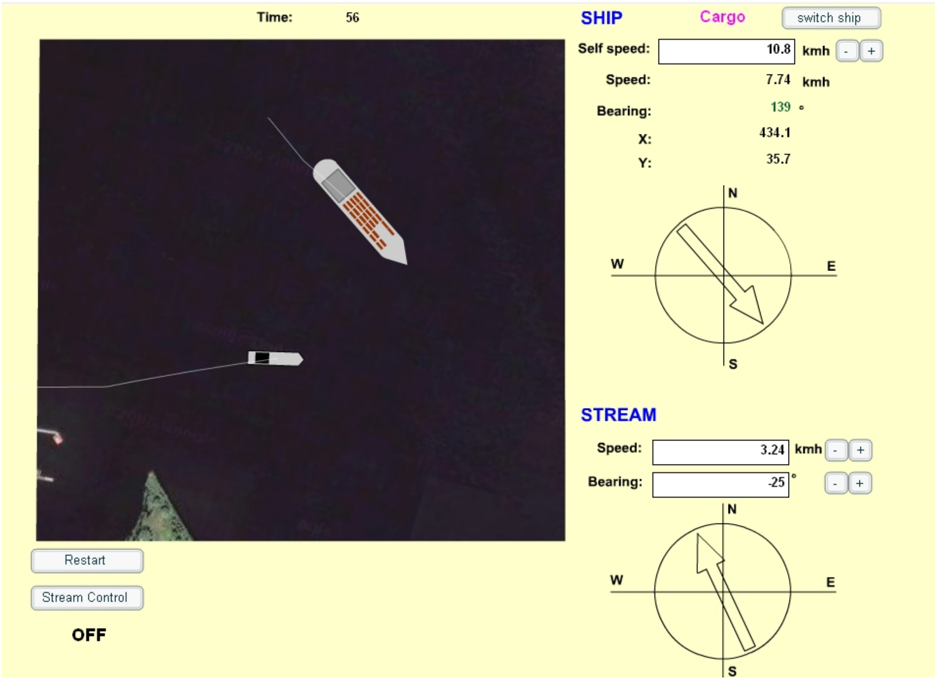

Fig. 6 Stream control algorithm

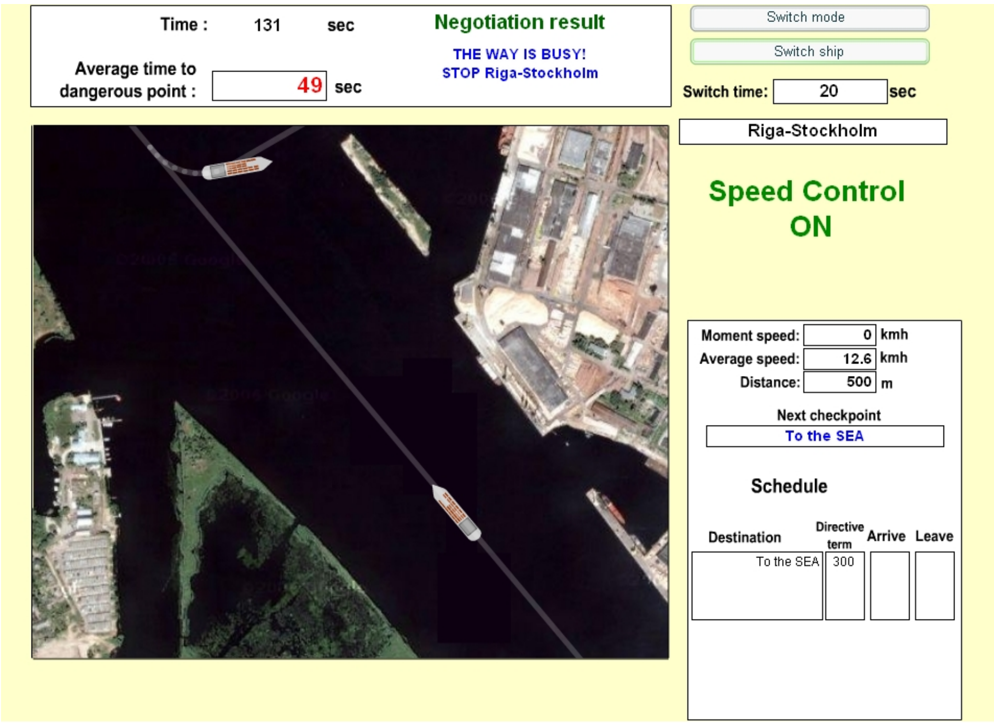

Fig. 7 Negotiations between vessels

7. Conclusions

Modeling results show the possibility to control speed of DC drive using trained neural network controller. It is very important to create as more as possible samples as possible for more precise training. Also selection of transfer function depends on task.

Neural network allow producing not only signal but set of control signals. Also input signals are not limited. Neural network controller may be used as for control as for forecasting and warning about dangerous situation. It may prevent breakdowns and accidents and may be used for optimal speed control of transport units.

Main advantage of using negotiations in intelligent agent systems is the possibility to coordinate actions of all participants in transport systems and to realize control, diagnostic and scheduling for transport. The additional value is the possibility of the developed systems to prevent accidents and to avoid different problems by intelligent diagnostic and coordination devices.

Acknowledgement

This work has been partly supported by European Social Fund within the National Programme "Support for carrying out doctoral study program's and post-doctoral researches" project "Support for the development of doctoral studies at Riga Technical University" (grant Nr. 2004/0002/VPD1/ESF/PIAA/04/NP//3.2.3.1/0002/0007).

References

1. **Luger G. F.** Artificial Intelligence. Structures and Strategies for Complex Problem Solving, Williams, 2003, 863. p
2. **Russel S. J.**, **Norvig P.** Artificial Intelligence. A Modern Approach, 2nd edition. Prentice Hall, 2006, 1408 p.
3. **Gorobetz M.**, **Levchenkov A.** Modelling Of Intelligent Agents For Scheduling In Maritime Transport Task. // Proceedings of 8th International Conference on Maritime Transport and Infrastructure, Riga, Latvia, 2006, p. 195-203.
4. **Greivulis J.**, **Levchenkov A.**, **Gorobetz M.** Modelling of Clustering Analysis with Special Grid Function in Mechatronics Systems for Safety Tasks. // Proceedings of 6th International Conference on Engineering for Rural Development, Jelgava, Latvia, 2007, p. 56-63.
5. **Rankis I.**, **Gorobetz M.**, **Levchenkov A.** Optimal Electric Vehicle Speed Control by Intelligent Devices. Rīgas Tehniskās universitātes raksti. Enerģētika un Elektrotehnika. Sērija 4, sējums 16. 2006. p. 127-137.
6. **Dirba J.**, **Ketners K.**, **Levins N.**, **Pugačevs V.** Transporta elektriskās mašīnas – Rīga: Jumava, 2002, 342 p.

Proceedings of 3rd International Workshop ITELMS'2008

Dynamic Modeling of Complex City Intersections for Transport Flow Problems

A. Levchenkov*, A. Mor-Yaroslavtsev**

* *Riga Technical University, 1, Kalku str 1., LV-1058 Riga, Latvia, E-mail: levas@latnet.lv*
** *Riga International School of Economics and Business Administration, Meza str.3, LV-1048 Riga, Latvia E-mail: andrew_my@riseba.lv*

Abstract

The purpose of this paper is to develop and study algorithms for interaction of Software Agents in group decision making support systems intended for logistic problems of control of transport flows on complex city intersections.

The paper regards the problem of modeling and solution of the problem of minimization of transportation costs and idle time of vehicles for the chosen version of the route and schedule at multiple intersections.

The authors offer a generalized algorithm for solution of the problem of drawing up an optimum schedule for traffic through multiple city intersections with the use of Software Agents and dynamic computer models of transport flows. It is also supposed that modeling software can detect formation of problematic situations, change the duration of one-type operations on separate processors and interact in search of the best solution.

The modeling program is controlling intersections under consideration, while the data collection and analysis program interacts with relational database and makes the optimum processors' operating schedule with the help of a group decision making support system. The processor is the traffic lights of the intersection, and the operation is handling of a transport flow to an assigned direction and time.

KEY WORDS: *Software Agent, Logistics.*

1. Introduction

With the help of the developed algorithm from a set of cars for particular intersection applying the Monte-Carlo method we select a certain vehicle. Its parameters are specified in the model: intersection, flow, vehicle ID, its velocity, acceleration, distance to the traffic lights and nearby obstacles, estimated braking distance and the time left until a prohibiting signal of the traffic lights. On the basis of the distance to the traffic lights and obstacles and the braking distance a conclusion on possibility to stop before or on a line at the signal of the traffic lights can be made.

Optimum data about the intersection processors' operating schedule received from the model are passed on by the Software Agents interacting with the database management system, recorded in previously prepared database table and displayed on the screen for users of a group decision making support system.

2. Mathematical Statement of the Research Problem

The following variables will be introduced:

$C = (c_1, c_2, \ldots, c_j, \ldots, c_m)$ – set of considered crossroads; where $c \in C$, i is an index of a crossroad;
$H = (h_1, h_2, \ldots, h_i, \ldots, h_k)$ – set of the given *vehicles* flow; where $h \in H$, i is an index of a car;
$R = (r_1, r_2, \ldots, r_j, \ldots, r_m)$, $r \in R$ – the number of traffic lanes in one direction; where j is an index of a flow;
$v_{i(t)}$ – speed of i vehicle at the time moment t;
sl_i - distance of i vehicle till k-th traffic light at the time moment t;
a_i – acceleration of i vehicle at the time moment t;
t_i – time;
b_i – braking distance of I vehicle till k-th traffic light at the time moment t;
x_i, y_i – position data of i vehicle at time moment t;
sp_i – distance of i vehicle at the time moment t till a car behind;
sa_i – distance of i vehicle at the time moment t till a car nearby;
sn_i – distance of i vehicle at the time moment t till a car in front of it;
TLk_i – duration of operation of L section for k traffic light;
V_{max} – maximum permissible value of speed on j traffic lane for vehicles;
V_{min} – minimum permissible value of speed on j traffic lane for vehicles.

The elements of modern graph theory, maximum flow function, can be used in modelling of vehicles flows.

We will consider the function which is defined for oriented graph $G = (V, E)$ in the following way:

1. each curve $e \in E$ is confered with positive rational quantity $c(e) \geq 0$ — its carrying capacity,
2. there is one top point v_0 — source $G_{v0}^{-1} = \varnothing$,

3. there is one top point v_z — flow $G_{vz} = \varnothing$.

Then oriented graph G is called a transport network and marked as $G(T)$.

Let us define flow function $j(e)$ in transport network $G(T)$ as a curve function with the following features:

1. $y(e) \geq 0$,
2. $y(e) \leq c(e)$,
3. for all $e \in E$: $\sum_{e \in E_v^-} y(e) = \sum_{e \in E_v^+} y(e)$, where $v \neq V_0$; $v \neq v_z$; $v \in V$; E_v^- is at the top point v set of input curves and E_v^+ is set of output curves.

At each top point v the sum of input flows is equal to the sum of output flows.

We are interested in the maximum value of flow function

$$\max \sum_{e \in E_v^-} y(e) = \max \sum_{e \in E_v^+} y(e) = y_z .$$

We will mark with A transport network's $G(T) = (V, E)$ set of top points $A \subset V$, which contains top point v_z ($v_z \in A$), and does not contain top point v_0 ($v_0 \notin A$). As a section in transport network $G(T)$ we will call curve set E^-_A, which goes to set of top points A. This notion differs from the considered before notion of section in an oriented graph. The section in the previous meaning contains also curves, which go from set of top points A.

The sum of all section curves carrying capacity is called carrying capacity $c(E_A^-)$ of section E_A^-, e.g.,

$$c\left(E_A^-\right) = \sum_{e \in E_A^-} c(e).$$

In the same way we can define also the value of flow $y(E_A^-)$ in section E_A^-:

$$y\left(E_A^-\right) = \sum_{e \in E_A^-} y(e).$$

As flow y in each curve e does not exceed its carrying capacity $y(e) \leq c(e)$, then there the following dependence is valid

$$y\left(E_A^-\right) \leq c\left(E_A^-\right).$$

The let us consider Ford (L. R.)–Fulkerson (D. R.) method for maximum flow defining $G(T)$. It was elaborated in the middle of 50s. The method consists of two parts: in the first part we will define the top points, in the second one we will increase flow function y, if top point v_z is defined. If top point v_z has not got a definition, then maximum flow y_z in the given transport network $G(T)$ is obtained.

The top point definition is a pair, where the first element is top point, from which the first element gets its definition, and the second one indicates its increasing (at the beginning it is 0).

The defining of top points is made in two ways. The top point v_0 is defined $(-, e(v_0) = \infty)$, which is not changed. We will choose top point v_i defined as $(v, e(v_i))$, then all top points $v_{j1}, v_{j2}, \ldots, v_{je}$, which correspond to the restrictions

$$y(v_{jk}) = \min\left[e(v_i); c(v_i, v_{jk}) - y(v_i, v_{jk})\right].$$

The second way to define top points $v_{j1}, v_{j2}, \ldots, v_{jl}$, which correspond to the restrictions $y(v_{jk}, v_i) > 0$, is the following: choose designation

$$(v_i^-, e(v_{jk})),\ k = 1, 2, \ldots, l;$$

where

$$e(v_{jk}) = \min\left[e(v_i); y(v_{jk}, v_i)\right].$$

If top point v_z is defined as $(v^+_{i1}, e(v_z))$ and flow $y(v_{i1}, v_z)$, then curve of a new flow (v_{i1}, v_z) is $y(v_{i1}, v_z) + e(v_z)$ and transition to other curve flows is changed.

If top point v_{i1} is defined as $(v^+_{i2}, e(v_{i1}))$, then curve (v_{i2}, v_{i1}) with flow $y(v_{i2}, v_{i1})$ is increased for $e(v_z)$ and new flow is

$$y(v_{i2}, v_{i1}) + e(v_z).$$

If top point v_{i1} is defined as $(v^{-}_{i2}, e(v_{i1}))$, then curve (v_{i2}, v_{i1}) flow is decreased for $e(v_z)$ and new flow is

$$y(v_{i2}, v_{i1}) - e(v_z).$$

It is continued while top point v_0 is reached, then flow function y is increased for value $e(v_z)$. The definings of all top points are canceled except v_0, and top point are started to be confered with new definitions. If we can not confer top point v_z with a definition then flow function can not be increased.

The first value $v^{\pm}$ of definition pair shows the shorten curve way from top point v_z to v_0. The second value ε shows possible flow increasing. Let us start with flow $y = 0$ for all $G(T)$ curves.

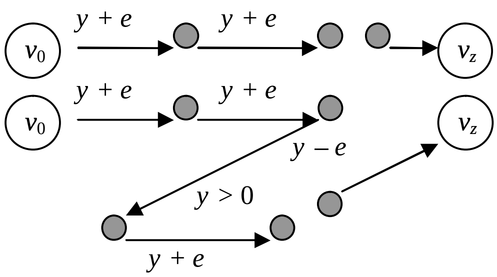

Fig. 1 Both cases of flow increasing

The considered graph theory method is applied in this article to solve the task of transport flow modelling.

It is considering the task of such t, lk, V_{max}, V_{min} defining, when H is maximum. The following algorithm is offered to solve this task.

3. Algorithm of Problem Solution

Step 1. Traffic Department Manager on the client-side (K) enters an inquiry for solution of this complicated problem, using interface (Wr) and information function f Kr:

Step 2. Supra program agent divides this problem into several subproblems

Step 3. To solve multi-criteria assignment problem, when the client has to choose the roads, and the criteria are both quality and quantity criteria, using the server (Fig. 1).

Step 4. Supra agent starts inquiry processing with interface (Wr) using information function (procedure) f Kr: If it receives the answer from server it can move to the next step. If the answer is not received, it has to search it in other server; otherwise the solution does not exist.

Step 5. Server (Wd) starts receiving an answer from data base (Dp) using function (procedure) $f$dp.

Step 6. Server (Wd) starts receiving client's task solution (Pd) using function $f$pd.

Step 7. Server (Wd) starts sending client's task solution to the server (Wr) using function $f$dr.

Step 8. Server (Wr) starts sending client's task solution to Supra program agent ***SPa*** that makes solution (s) analysis.

Step 9. To make up a schedule, Algorithm Steps analogue 3-8 are carried out.

Step 10. To analyze and evaluate made up traffic lights' work schedule.

Step 11. Server (Wr) starts sending client's task solution to Supra program agent ***SPa*** that makes solution (s) analysis to offer the client only the best task solution using function frSPa.

Supra agent (*SPa*) offers to the client (K) the best solution using function fSPaK.

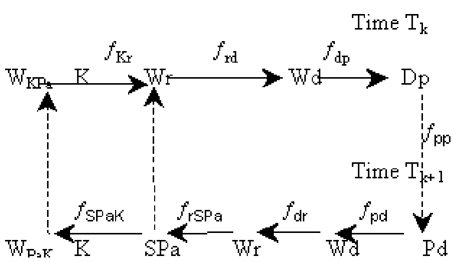

Fig. 2 Fragment of task solution algorithm

4. Role of Supra Agent

After solving one logistics task it is necessary to solve a new one. Supra agent coordinates the task of program agent that has to find an optimal solution for all sub problems.

5. Supra Agent Algorithm for Fixing on Data About Flow in Database

Step 1. Supra agent connects to the database of crossroad *Dp*.
Step 2. All variables of the flow for i = 1 till N about vehicles are set to the the current values.
Step 3. Preparation of SQL query.
Step 4. Execution of the query, writing into data base for the further calculations.

6. Results of Experimental Approbation of the Model

This part considers the results of the experimental approbation of the model. Fig. 3 demonstrates a moment of transport flow in the crossroads area. The main goal of the experiment was to check whether it is possible for vehicles data (speed, acceleration, braking distance and time and possibility to stop it in front of the crossroad) to be put into a specially developed data base.

Later on, the captured data can be applied in the mentioned above mathematic models of transport flows as well as for evaluation of different variants of possible urban transport flow organization, for example public transport zone, arrangement of new traffic lights and highway striping and consequence of these measures.

Fig. 3 There is participants of the flow: two cars, which have reached the traffic lights at the intermediary moment of time

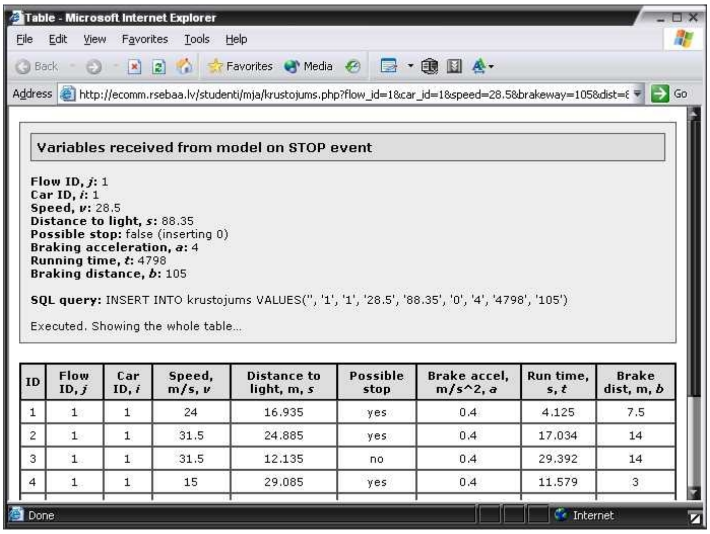
Table - Microsoft Internet Explorer

Address http://ecomm.rsebaa.lv/studenti/mja/krustojums.php?flow_id=1&car_id=1&speed=28.5&brakeway=105&dist=8

Variables received from model on STOP event

Flow ID, *j*: 1
Car ID, *i*: 1
Speed, *v*: 28.5
Distance to light, *s*: 88.35
Possible stop: false (inserting 0)
Braking acceleration, *a*: 4
Running time, *t*: 4798
Braking distance, *b*: 105

SQL query: INSERT INTO krustojums VALUES('', '1', '1', '28.5', '88.35', '0', '4', '4798', '105')

Executed. Showing the whole table...

ID	Flow ID, *j*	Car ID, *i*	Speed, m/s, *v*	Distance to light, m, *s*	Possible stop	Brake accel, m/s^2, *a*	Run time, s, *t*	Brake dist, m, *b*
1	1	1	24	16.935	yes	0.4	4.125	7.5
2	1	1	31.5	24.885	yes	0.4	17.034	14
3	1	1	31.5	12.135	no	0.4	29.392	14
4	1	1	15	29.085	yes	0.4	11.579	3

Done Internet

Fig. 4 Fragment of a specially developed data base, which keeps necessary data on vehicles participating in the flow. These data are input with pushing the button "Save current data in DB"

7. Conclusion

The problem of transport flow in modern cities under the condition of hard crossroads is becoming more important taking into account the increasing density transport flow and limited carrying capacity of the streets.

As this work demonstrates the mathematical and real transport flow modeling results do not correspond enough to the real situation because of quite many assumptions and restrictions, thus the transport flow control finds its application quite seldom.

Some progress in this field could be achieved applying the program of visual dynamic modeling of transport flow developed in this work. The program can be input with parameters of transport flows and crossroads characteristics, which allow bringing the developed model near the real situation of a hard crossroad zone.

One of the possible variants to apply data base is using of the algorithm published before [4].

The work demonstrates the principal possibility for visual modeling of transport and pedestrians flow at crossroads and urban transport stops, that proves the validity of the model.

We assume that after some improvement it could be successfully applied for automatization of urban transport or in automatically regulated systems with a correspondent material and technical basis and crossroads accessories.

References

1. **Ashton W. D.** The Theory of Road Traffic Flow. Methuen, London, 1966.
2. **Jonson J.**, **Wood D.**, **Wardlow D.**, **Murphy P.** Contemporary Logistics. Prentice Hall. NJ, 2002.
3. **Russell S.**, **Norvig P.** Artificial Intelligence:a modern approach. Prentice-Hall Canada, Inc., Toronto, 1995.
4. **Levchenkov A.**, **Smyshlaev I.** Algorithm for program agents in e-learning for solving logistics supply chains problems, ICS-2003 Proceedings, Valencia, 2003.
5. **Levchenkov A.**, **Mor-Yaroslavtsev A.** Visual dynamic modeling of transport flows for electronic business problems, ESM‘2004 Proceedings, Paris, 2004.
6. **Levchenkov A.**, **Kunicina N.**, **Mor-Yaroslavtsev A.**, **Dolganov A.** Modeling of Intelligent Intersections in Complex Mechatronic Systems, IESM ‘2007 Proceedings, Beijing, 2007.

The Clustering Analysis for Evaluating State of the Isulation for Intelligent Electrical Networks

A. Levchenkov[*], I. Uteshevs[**], M. Gorobetz[***]

**Riga Technical University, Institute of Industrial Electronics and Electrical Engineering, Kalku str.1, Riga, LV-1658, Latvia. E-mail: levas@latnet.lv*
***Riga Technical University, Institute of Industrial Electronics and Electrical Engineering, Kalku str.1, Riga, LV-1658, Latvia. E-mail: igors.utesevs@gmail.com*
****Riga Technical University, Institute of Industrial Electronics and Electrical Engineering, Kalku str.1, Riga, LV-1658, Latvia. E-mail: mgorobetz@latnet.lv*

Abstract

In this work is proposed the method of cluster analysis for evaluating the state of the insulation of electrical devices. With the work of electrical devices on its insulation influence the diverse factors: high or low the rate of temperatures, high voltage, vibration, radiation, chemical materials and yets. The action of all these factors must not to the premature failure of insulation, since this can lead to the emergencies. Thus, reliability of electrical devices work depend on the quality of insulation.

This problem it is especial for the electrical devices, which worked out its period or period of service of which it approaches final.

In the work it is proposed to use a method of continuous control of the state of the insulation of high-voltage devices. The method of the combination acoustic and electromagnetic signals is used. Processing the measurements of signals is performed in the neuron networks. This gives the possibility to self-learning neuron network.

Authors propose to use the algorithm for state insulation analysis in electrical devices obtaining information from acoustic and electromagnetic sensors.

Intelligent agents can separate dangerous situations by critical testimonies of sensors from the regular states of the system, detect and warn about changes in the system and to prevent emergencies, using the intelligent electrical network.
KEY WORDS: *intelligent electrical network, neural networks, clustering, insulation.*

1. Introduction

By the basic reason for aging isolation under the influence of strong electrical pour on they appear the so-called partial discharges. They are local breakdowns it weakened the

Feudatory sections of high voltage isolation. By such it is weakened or defective sections they are gas inclusions. In the process of operation gas inclusions can arise as a result of splitting or stratification of isolation from mechanical loads and vibration or during the decomposition of dielectric to input of gases, for example with the strong heating.

This leads to fact that in the gas inclusions with a certain value voltages go on breakdown. This breakdown is not complete, since the sizes of gas inclusions compose small part of the total thickness of isolation, and the remained isolation serves as the barrier, connected in series with the gas-filled gap. Therefore such breakdowns are called not complete, but partial breakdowns or partial discharges. The rate of destruction depends on that how they are frequently repeated and what energy is scattered in each single partial discharge.

This process leads to worsening in a quality of isolation and to damage its. Therefore it is important to carry out continuous control of state of isolation by electrical devices. The authors in this work propose the method of continuous control of insulation state, using neuron networks.

2. Problem Definition

In this work authors present the method of continuous control of state of isolation by different electrical devices. This method will make possible to detect possible damages for isolation. The system of acoustic and induction sensors is used. Electromagnetic signal enters more rapidly than acoustic and in neuron network input signal about a partial discharge. Neuron network compares the indications of insulation resistance with that minimally permitted and signals, if the value of insulation resistance approaches dangerous. Insulation state is classified with the aid of the cluster analysis.

3. Method of Solution

For solution of diagnostics problem of insulation state authors propose the method of partial discharges. The number of partial discharges is determined per unit time:

$$n_f = 4\, f \left(\frac{U - h\, U_{pd}}{U_{cd}\ (1-h)} \right), \tag{1}$$

where U – external voltage; U_{pd} – voltage of appearance partial discharges; f – frequency; h – relations coefficient:

$$h = \frac{U_B}{U_{pd}}\ , \tag{2}$$

U_B – partial discharges voltages breakdown.

Measure of intensity of the single partial discharge is:

$$q = \Delta U\ C_x\ , \tag{3}$$

where C_x – complex capacity of isolation.

The intensity of partial discharges is determined by the average current:

$$I_{pd} = n_f q\ . \tag{4}$$

Intensity of repeated partial discharges

$$I_{pd_i} = \sum_{i=1}^{k} (n_f q)_i\ . \tag{5}$$

With q=10^{-16}…10^{-14} Kl occurs aging isolation, while with q=10^{-9}…10^{-6} Kl isolation is destroyed in very short time. From equation (5) it is possible to determine the maximum permissible quantity of partial discharges:

$$\sum_{i=1}^{k} n_f = \frac{I_{pd}}{q}\ . \tag{6}$$

For measurement of partial discharges intensity it is possible to use a device, shown in Fig. 1. For the isolation control of electrical devices uses combination of electrical and acoustic sensors. Device contains the subject of studies 1, electromagnetic sensors 2, acoustic sensors 3, recorders 4 and 5. Electromagnetic sensor records current pulse through the partial discharge. Acoustic sensor records the sound of partial discharge. The criterion of detecting the place of partial discharge is a time difference Δt between electromagnetic and acoustic signals from the place it arose of partial discharge to appropriate sensors.

The speed of electromagnetic impulse is more than speed from of sound impulse. Therefore the electromagnetic signal, caused by current pulse, first comes, and then through the time interval Δt comes audio signal. The further source of partial discharge is located, the greater time interval Δt. Consequently, knowing the speed of sound in the known medium and time Δt, it is possible to determine the place of partial discharge.

Uses sensors of signals from the front, on the side and above, is possible to determine all three X, Y, Z coordinates of the place of partial discharge. Output 7 gives signal to the entrance into the neuron network.

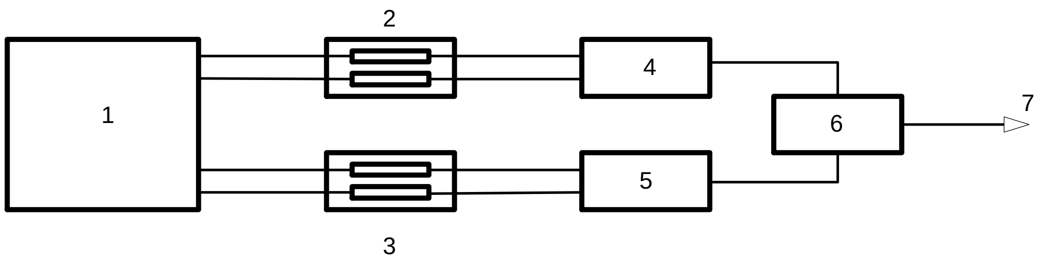

Fig. 1 Installation Diagram: 1 – research of object; 2, 3 – system of sensors; 4, 5 – the register system; 6 – summary system; 7 – output into the neuron network

4. Model of Neural Network for Task Solution

Authors propose to use Artificial Neural Networks to choose electric and electronic devices suitable in insulation control system. Neural Network should be trained to analyze the parameters of electronic device and detect the possibility of its usage in the specific task. Neural network mathematical model is based on perceptron structure, with 3 layers - input, hidden and output. Input will have electric and not electric parameters of electronic devices. Output layer classes are predefined electronic devices types. The class of analysed electronic device will be detected and the possibility to use it for insulation control

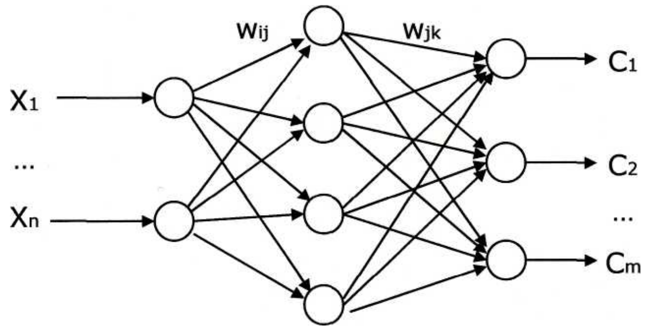

Input data set: $X = \{x_1, x_2, \ldots, x_n\}$
Weights: $W = \{w_1, w_2, \ldots, w_n, w_{n+i}\}$
Fitness function: $F = x_1 \cdot w_1 + x_2 \cdot w_2 + x_n \cdot w_n + w_{n+i}$
Result classes: $C = \{c_1, c_2, \ldots, c_m\}$

Fig. 2 Neural Network structure

5. Algorithm of Neural Network Training for Task Solution

Back-propagation is the basis for training a supervised neural network. Static back-propagation is used to produce an instantaneous mapping of a time independent input to a static output. These networks are used to solve classification problems. At the core of all back-propagation methods is an application of the chain rule for ordered partial derivatives to calculate the sensitivity that a cost function has with respect to the internal states and weights of a network. In other words, the term back-propagation is used to imply a backward pass of error to each internal node within the network, which is then used to calculate weight gradients for that node. Learning progresses by alternately propagating forward the activations and propagating backward the instantaneous errors.

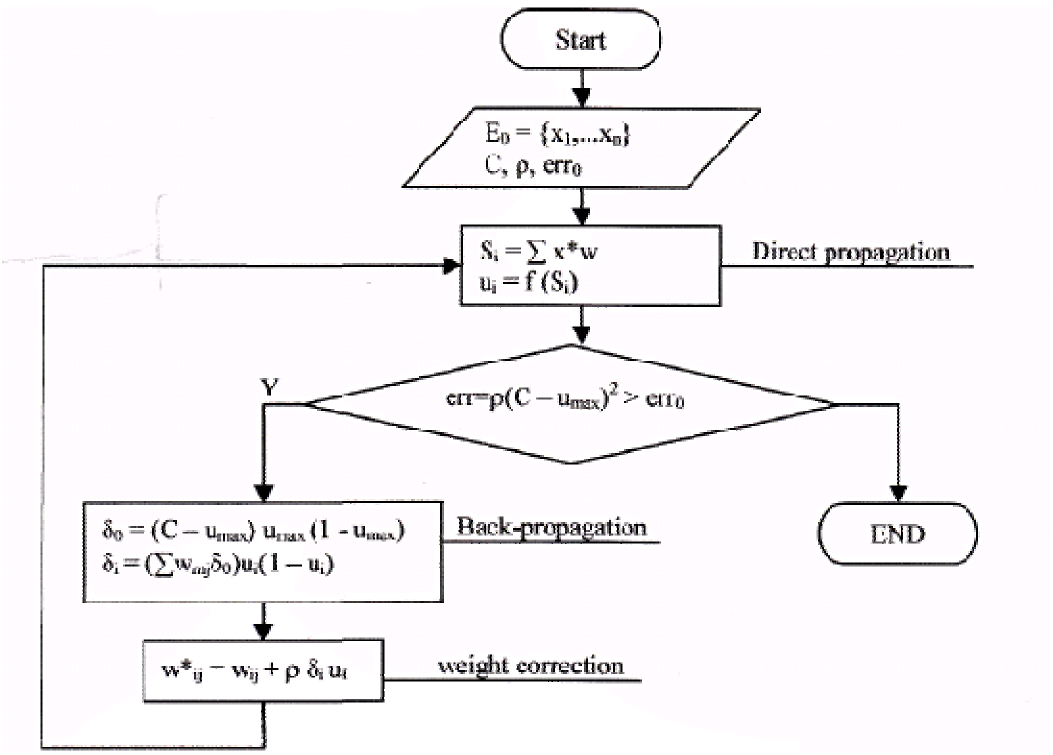

Fig. 3 Back-propagation algorithm for Neural Network training

6. Conclusions

Authors propose the method of cluster analysis and the algorithm for state insulation analysis in electrical devices obtaining information from acoustic and electromagnetic sensors. Neural Network should be trained to analyze the parameters of electronic device and detect the possibility of its usage in the specific task. These networks are used to solve classification problems.

Intelligent agents can separate dangerous situations by critical testimonies of sensors from the regular states of the system, detect and warn about changes in the system and to prevent emergencies, using the intelligent electrical network.

Acknowledgment

This research was supported by Ministry of education and science republic of Latvia grants "Science Development in Universities" "Development of intelligent neural network based software for calculation of equipment". The This work has been partly supported by European Social Fund within the National Programme "Support for carrying out doctoral study programme's and post-doctoral researches" project "Support for the development of doctoral studies at Riga Technical University" (grant Nr.2004/0002/VPDl/ESF/PIAA/04/NP/3.2.3.1/0001/0002/0007).

References

7. **Luger G. F.** Artificial Intelligence. Structures and Strategies for Complex Problem Solving, Williams, 2003, 863 p.
8. **Russel S. J.**, **Norvig P.** Artificial Intelligence. A Modern Approach, 2nd edition. Prentice Hall, 2006, 1408 p.
9. **Greivulis J.**, **Gorobetz M.**, **Levchenkov A.** Modelling of Clustering Analysis with Special Grid Function in Mechatronics Systems for Safety Tasks. // Proceedings of 6th International Conference on Engineering for Rural Development, Jelgava, Latvia, 2007, p. 56-63.
10. **Reskó B.**, **Szemes P.T.**, **Korondi P.**, **Baranyi P.H.** Hashimoto. Camera Motion Control based on Ubiquitous Computing (Artificial Neural Network Based Adaptive Object Tracking in Intelligent Space) // EPE-PEMC2004, Riga, Latvia.
11. **Rosin A.**, **Lehtla M.**, **Möller T.** Intelligent Control and Diagnostics System for Tallinn Trams. // EPE-PEMC2004, Riga, Latvia.
12. **Серебряков А.С.** Электротехническое материаловедение // Электроизоляционные материалы. «маршрут», Москва, 2005, 278 с. [in Russian].
13. **Борисов А.Н.**, **Левченков А.С.** Методы интерактивной оценки решений, Зинатне, Рига, 1982, 139 с. [in Russian].

Proceedings of 3rd International Workshop ITELMS'2008

Relationship of Development of Surface Short Cracks and Fracture Micromechanisms of in Aluminum Alloy 2024-T3

D. Kocańda[*], V. Hutsaylyuk[**], V. Hlado[***]

[*] *Military University of Technology, Gen. S. Kaliskiego str 2, 00-908, Warsaw, Poland, d.kocanda@wme.wat.edu.pl*
[**] *Military University of Technology, Gen. S. Kaliskiego str 2, 00-908, Warsaw, Poland, E-mail: v.hutsaylyuk@wme.wat.edu.pl*
[***] *Ternopil State Ivan Pul'uj Technical University, Ruska str. 56, 46001, Ternopil, Ukraine, E-mail: kafmat@tu.edu.te.ua*

Abstract

Experimental results of fatigue short crack growth examination from a central hole for 2024-T3 Alclad aluminum alloy sheet under cyclic zero-to-bending (*R*=0.1) were performed in the paper. Microscopic analysis made by using SEM microscope revealed that crack emanates at the edge of the hole beneath thin Alclad layer, on the border between Alclad layer and the matrix material. The source of the crack is a brittle cracked precipitates existed in the matrix material. It was established that in the 3 mm thick aluminum alloy sheet the length of short crack does not exceed 0.5 mm. The period of short crack growth covers 25% of total lifetime of tested specimens. The diagrams of experimentally determined crack growth rates versus cycle ratio and against the range of stress intensity factor confirm great discrepancies of growth rates particularly in the range of short cracks.

KEY WORDS: *fracture mechanic, aluminum alloy sheet, fatigue short crack growths.*

1. Introduction

Is strong loaded the air elements, in the trouble spot is riveted joint of wings of the plane. Allowable length of propagation short fatigue cracks from riveted holes can be criterion of safe operation.

The excess of allowable length by a short crack or size of threshold stress intensity factor K_{th} indicate to the beginning exhaustion of a resource of safe operation riveted joint. In this connection the researches of mechanisms of initiations and propagation short fatigue of cracks from an riveted holes in aluminum sheets of an alloy 2024-T3 are necessary which is used in aircraft.

Last thirty years a lot of attention is given to a question of research of initiations and propagation short fatigue cracks [1-12]. By a base material for such researches in aircraft is the aluminum alloy 2024-T3. The authors were engaged in research of propagation fatigue short cracks in the given material under influence various cyclic loaded during 2003-2006 years. Some of those publications are given in the list of the literature [1-3]. Through electronic transmission and scanning microscopes is investigated influences of a spectrum loaded with numerous overloads on fracture velocity of an alloy and opportunity of reconstruction of a history of velocity of propagation of cracks on the basis of character of a microstructure of a surface fatigue failure of the destroyed element.

But these researches mainly concerned long cracks, or cracks which are distributed of above value of threshold stress intensity factor. The basic relationship, of propagation short cracks is described in works [4-6]. Mark, that the propagation of short cracks strongly is influenced by with structure of a material. It causes necessity of research of micromechanisms of propagation short cracks, which are propagation of below threshold value K_{th}.

2. Methods and Results

Experimentally investigated specimens from sheet double-sided, lamellar aluminum 2024-T3 by thickness of 3 mm. Chemical structure of an alloy and the mechanical characteristics are given in [1, 10]. Specimens of length 90 mm and width 32 mm are cut out from a sheet in a direction forge rolling (LT).

Let's note, that specimens are cut out in two directions in a direction forge rolling (LT) and perpendicular (TL) characterize by disorder of the mechanical characteristics in limits: R_m = 447 ... 466 MPa, R_e = 303 ... 325 MPa. The thickness of a layer lamellar made about 0.12 mm, and according to radiography measurements by a method the residual compressing stress in this layer make about 40 MPa.

At the center of a specimen the hole by a diameter 3mm is executed. Specimens tested at a unilateral simple bend with factor of asymmetry $R = 0.1$ on equipment designed in Department of Bases of Designing of Machines Military University of Technology. The value of a bending stress is accepted $s_{max} = 100$ MPa, that corresponds to average bending stress in the plating of a wing of the plane. The frequency of tests made 23.5 Hz.

Specimens were investigated in an initial status without use with what or processing of a surface. It created the certain difficulties for the analysis of propagation of superficial cracks at use of replicas because of huge number artifacts. On this for the adequate analysis of propagation of cracks on a surface and study of micromechanisms of failure all specimens were investigated through scanning electronic microscopes.

During the analysis of a surface of a specimen investigated outside and inside of the party of an holes. Besides investigated the form of crack front a on a surface of failure of a specimen at different amount of cycles loaded and different magnitude.

Analyzed area of short cracks which according to [6] concern to those for which use of the approaches of the linear mechanics of failure is supposed. The choice of this range is explained to that in it rather simply to supervise propagation of cracks through the modern measuring equipment with the subsequent account in engineering techniques of predicting of durability of a construction.

The researches of specimens through scanning electronic microscope are realized at the Ternopil state technical university.

The purpose of these researches was confirmation of preliminary results of the replicas, received by a method, and also definition of the center initiations of a crack, form and kind of front of a crack, microfailure mechanism.

For this purpose at first investigated specimens on the side of a working surface and inside of hole. Investigated specimens with different amount of cycles, and operating time and various length of a crack. In a Fig. 1 from the left party the crack which is submitted propagation in the field of border of an hole.

On a surface the seen traces of mechanical damages which most likely are a consequence of processes of transportation and performance of an hole, and also superficial crack. In area around of a crack on small distance from it seen local contraction, which differ from a base material more light by color. It indicates to presence of local areas plastic deformation which have arisen in consequences of propagation of a crack under a layer lamellar. The crack partially leaves on a surface by coalescence of the neighboring areas. On the other hand on the inside party of an hole the local plastic areas practically are absent, in the field of a crack small, cracks practically do not overstep the bounds.

Following fractographical of research are realized in a quarter of elliptic area on a surface of failure by the limited crack on a surface of a specimen and hole.

Fig. 1 Microcrack on a working surface of a specimen and on the inside of an hole

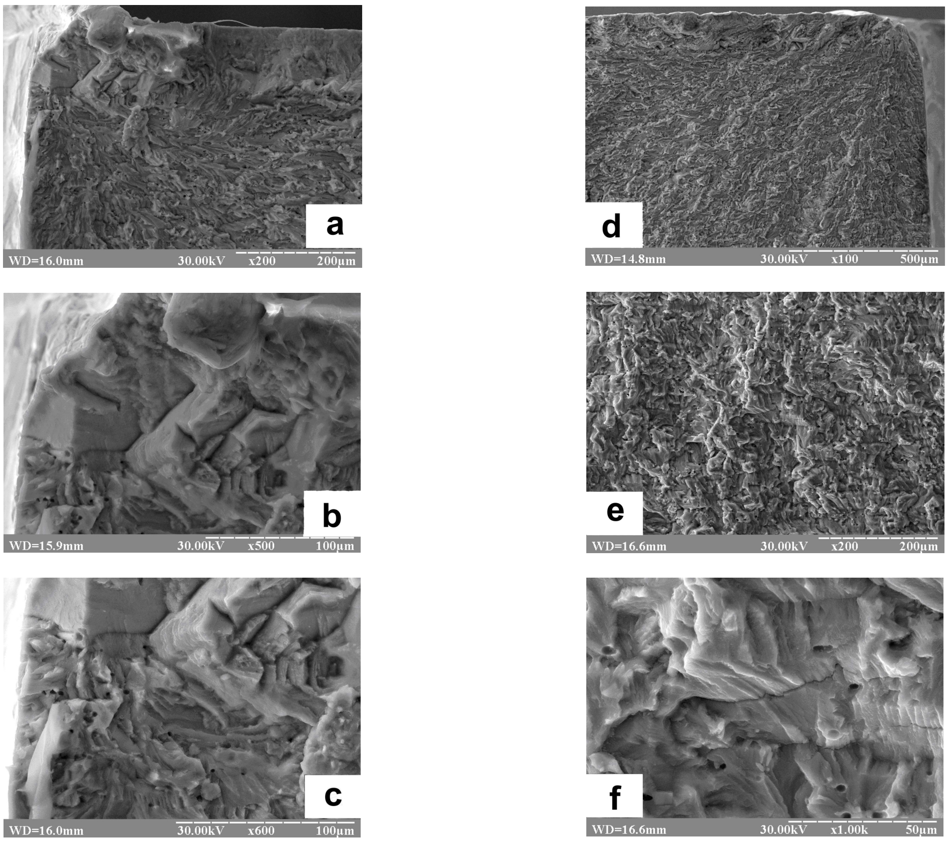

Fig. 2 Place of failure on a fracture surface and area propagations of a crack in its area

The next task was definition of the center initiations of a crack and micromechanism of fracture. On the basis of preliminary researches was determined, that the crack is initiated in near-surface region and is distributed in two directions with different velocity. On this for researches the area on border of a layer lamellar and inside party of an hole of a Fig. 2 is chosen.

As it is present from a Fig. 2a a place initiations of a crack localized under a surface lamellar nearby borders of an hole. At this place there is an area large local deformation which is a consequence of productions of an hole in a sheet. The summation of these deformations results that arise rather large in comparison with the size of a grain fracture facets which are under the platen of a material bulge during productions an hole. Common the character of failure these fracture facets typical cleavage about what indicates character of an inclination of sides facets also local cracks in their body (Fig. 2b). In comparison with fracture of a layer lamellar which type fracture facets there slightly another also is realized cleavage (Fig. 2a), it is probable is connected with preliminary deformation of a surface and direction of the application of loading.

At survey of area initiations of a crack under other corner (Fig. 2c) on a surface facets it is visible fatigue striations which have arisen in a consequence of irregular propagations of a short microstructural crack. It also indicates to failure quasi-cleavage in this area. The character is kept and in area around of a place initiations, but facets absolutely of other size and on their surface the small holes, practically correct circle of the form, fatigue striations are visible. The holes probably have appeared as a consequence of failure of impurity in a material, and facets create river line in a direction propagation of the major crack.

It is confirmed by a photo in a Fig. 2d on which the direction river line of propagation of a crack is precisely visible. At localization in a place initiations of a crack is noticed a local crack (Fig. 2d) which crosses a little facets. Also it is precisely visible in a Fig. 2e of failure is realized by a method quasi-cleavage.

Besides during researches initial and final length of a crack for the given material and such as loaded was determined. According to experimental data minimal length of a crack on a surface makes 0.1mm, on the inside party of an hole 0.06 mm. Maximal length for a short crack on a surface of a specimen was accepted on the basis of preliminary researches and literary data at a level of 3 mm, in too time length of a crack on the inside party of an hole on the basis of measurements is accepted as 1.8 mm.

The following task realized during researches this definition of the form of front of a crack. The example of propagation of a crack at different stages in specimens LT is submitted on a photo of a Fig. 3a and 3b. In a Fig. 3a the crack which is shown propagation on a surface from border of an hole (magnitude 20x). The same crack is submitted in the next figure under other corner. On a photo at magnitude 100x are observed propagation of a crack on a wall of an hole. Macro failure observed at magnitude 25x together with the form of front of a crack is shown on a photo of a Fig. 3c and 3d. On the initial stage of fracture the front of a crack a quarter elliptic with missing radial from place initiations by crests and hollows of fracture, observable on a surface, (Fig. 3c) was exemplary. Practically at the end of

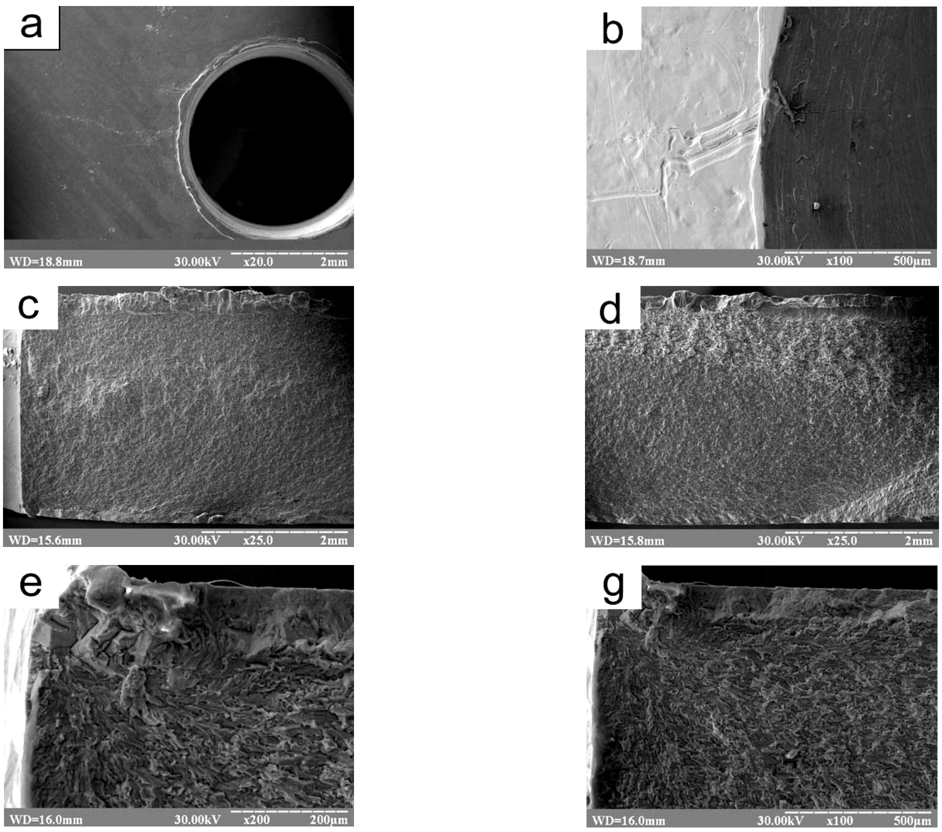

Fig 3 View of a crack on a fracture surface at different stages of his propagation

the term of operation the form of front of a crack becomes semi elliptical, that confirms the next photo in a Fig. 3d. The front of a crack covers a surface of a specimen and wall of an hole. On the basis of the analysis of these two photos it is possible to assert, that the crack in a sheet propagation simultaneously in two perpendicular directions in depth of a sheet lengthways at cross section and along a surface of a specimen. A photo of a fracture surface of connected with areas of increase short fatigue of cracks in a Fig. 3e and 3d.

In a Fig. 3e the area initiations of a crack under a layer lamellar placed between a surface of a specimen and walls of an hole is visible. The crack was propagation on border of an hole directly in a place of a base material and layer lamellar from failure cleavage of an impurity intermetallic of phases of iron and cuprum. (top left corner of a photo). Failure of these impurity which size makes from 2 up to 15 mm is not transferred instantly in the plastically deformed layer lamellar. This layer implicitly covers initiations of a crack, as in it the own residual compressing stress by size about 40 MPa work. On the basis of that in the initial period of fracture of a specimen the crack propagation in base a material along faster than wall of an hole and was then directed to the party of a surface of a sheet. Both these cracks had semi elliptical front (photo in a Fig. 3g). The crack which was distributed in a direction of a surface of a sheet tunneling a layer lamellar from below in a consequence that the fragile layer lamellar failure.

As the process of formation of front of a crack rather complex follows from the analysis of preliminary photos and for his description the additional explanations are required. On this in a Fig. 4 is given a photo with areas of cracks and scheme of propagation of a major crack.

Here by letters a and b is indicated near-surface region of area of cracks, which propagation at first along surfaces of a specimen and hole. The letter c corresponds to front of a crack, which already common for initial areas and actually is offered as front of a short crack for subsequent use in design models of predicting.

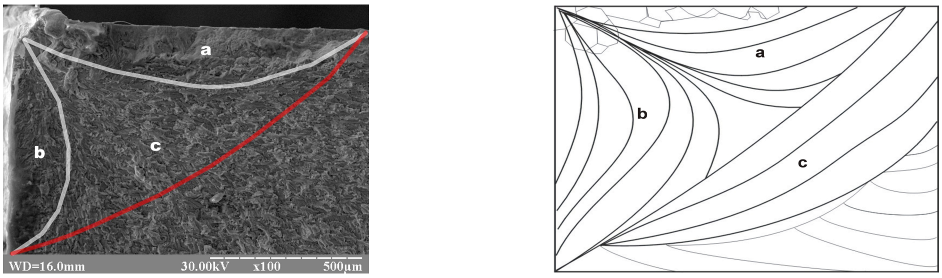

Fig. 4 View of a crack on a fracture surface at different stages of its propagation and his scheme

3. Conclusions

The mechanism initiations and propagation short fatigue of cracks from an hole in lamellar sheets an alloy and aluminum 2024-T3 is investigated. The analysis of a fracture surface of specimens at different stages of test is realized through scanning electronic microscopes has allowed to establish the complex mechanism of formation of front of a crack and micromechanisms of fracture on the initial stage of formation of a short crack.

References

1. **Kocanda D.**, **Kocanda S.**, **Torzewski J.** Velocity fatigue fracture in aluminum alloy 2024-T3 and possibility its reconstruction at programs spectrum loading. Bulletin MUT, 2-3: p. 69-83, 2003. [in Polish].
2. **Kocanda D.**, **Kocanda S.**, **Torzewski J.** Reconstruction of fatigue crack growth rate for 2024-T3 aluminum alloy sheet on the basis of fractographic analysis // Archive Mech. Engineering. LI, 3: p. 361-376, 2004.
3. **Kocanda D.**, **Kocanda S.**, **Torzewski J.** Velocity fatigue fracture in aluminum alloy 2024-T3 and possibility its reconstruction at different type loading. Materials XXI Symposium Experimental Solids Mechanics, Jachranka 2004, Official Publish Warsaw Polytechnic, 23-44, 2004. [n Polish].
4. **Miller K.J.**, **de los Rios E.R.** (Editors). Short fatigue cracks. ESIS Publication 13, Mechanical Engineering Publications, London, 1992.
5. **Miller K.J.** The two thresholds of fatigue behaviour // Fatigue Fract. Engng Mater. Struct. 18, (9) p. 931-939, 1993.
6. **Kocanda D.** Research schort fatigue crack. Experimental methods in fracture materials and construction. Basis research P. II, Handbook by editor J. Szala, ATR Bydgosch, p. 59-148, 2000.
7. **Wanhill R.J.H.** Flight simulation fatigue crack growth guidelines. Proc. 8th Int. Congress Fatigue 2002, 1/5, p. 573-584, Sweden, 2002.
8. **Halliday M. D.**, **Cooper C.**, **Poole P.**, **Bowen P.** On predicting small fatigue crack growth and fatigue life from long crack data in 2024 aluminium alloy // Int. J. of Fatigue. Vol. 25, p.709-718, 2003.
9. **Kocanda D.**, **Kocanda S.**, **Kulec P.** Short fatigue crack in avia aluminum alloy 2024-T3 // Science book Opole Polytechnic series Mechanics. No. 83, P.2, p.83-90, 2005 [in Polish].
10. **Li X.D.** Micromechanical model of stage I to stage II crack growth transition for aluminium alloys // Theoretical and Applied Fracture Mechanics. Vol. 24, p. 217-231, 1996.

Assessment of Preventive Maintenance Interval for Vehicles

I. J. Furch

University of Defence, Faculty of military technologies, Kounicova str. 65, Brno, Czech Republic, E-mail: jan.furch@unob.cz

Abstract

The paper deals with the problem of determination of the optimal vehicle service maintenance interval of operation. The Weibull progression is the possible method for determination of the optimal interval of the vehicle service maintenance. The Nelson method was used for the determination of parameters of the Weibull progression and specification of confidence intervals.
KEY WORDS: *interval service maintenance vehicles, Weibull progression, Nelson method.*

Abstract

The initial programme of the vehicle maintenance is often developed in cooperation with a supplier and a user. However, the initial maintenance programme does not have to be optimal. That is why it is desirable to initialize data collection about real process of defect degradation and incidence immediately after the operation start. If these data are available, their analysis can be carried out and on the basis of the analysis the contents of the initial maintenance programme can be changed to better meet the requirements of the user.

1. Introduction

For determination of the optimal interval of the vehicle service maintenance it is necessary [1]:

- to divide the defects which occurred at the vehicles, into the groups according to the defect seriousness,
- to choose an adequate division type of continuous accidental quantity,
- to define parameters of this division,
- to calculate a middle period between individual defect groups according to the defect seriousness,
- to calculate middle period between defects not divided into groups,
- to determine confidential intervals according to [5],
- to carry out both comparison of the results for the calculation of the middle period between defects,
- to determine the interval for vehicle service maintenance,
- to verify the calculated interval for service maintenance in practice and carry out the subsequent correction, which will contribute to determination of the optimal interval of vehicle service maintenance.

2. Defects Classification

The significant step when reliability is analysed is defining and classification of the term **defect**. The defect is such a change of the normal state of the object, which causes either complete interruption of object functions (failure) or decrease its functional abilities under the defined limit (fault). That is why, the defect and a correct function as well as its negation belong to the main subjects of reliability study.

Defects can be divided into the groups according to many points of view, for example according to [2]:

- speed of origin,
- extent,
- causality,
- consequence seriousness.

In this case it is best to use the defect division according to defect consequence seriousness, which is mentioned in the following part.

Categories of the defect consequence seriousness [2]:

- MINOR consequence is not caused by the defect which decreases nor influences function abilities, efficiency and object performance under the defined limit and acceptable limit values.
- MAJOR consequence is caused by the defect which could initiate decrease of the object function abilities under the acceptable limit value but whose consequence is manageable by the crew during the operation.
- CRITICAL consequence is caused by the defect which could decrease function abilities of the object that could increase the risk of the defect which could lead to a catastrophic defect, unless adequate remedial measures are taken immediately or in a stated time.

- CATASTROPHIC consequence is caused by such a defect which could result in such serious object damage that safe end of object functions would be impossible or it could also lead to the health damage, life danger or casualties or huge material or other damage.

3. Choice of an Adequate Division Type of Continuous Accidental Quantity

Among the most important divisions of continuous accidental quantity used in the sphere of reliability can be included exponential, normal, logarithmically-normal, Weibull etc. divisions. Each of these divisions can be applied in different areas of machinery, under specific conditions. The easiest calculation of the reliability characteristics is enabled by the exponential division, however, its occurrence in the branch of vehicle reliability is limited.

3.1. Determination of the Continuous Division Type

For further work it is necessary to determine continuous division type which will describe best the indicator of the vehicle reliability. Verification of the behaviour of the defect intensity or stream of defects in time [3] will be carried out. This specified test is determined to testing whether the periods of time till the objects defect are exponentially divided; it means whether the defect intensity is constant.

To make the process valid, it is necessary to meet the following requirement which is to have at least ten periods of time till the defect occurs. Then according to the number of selection of n samples either numeral process or graphic method for small amount of samples are used. In the article there is shown a calculation with the help of numeral method. Next another condition must be met and that is that for all test samples there must be the same operating environment. At the end of the test period not all the samples must have a defect. In that time there will exist on the whole r noted valid periods of time till the defect occurs. The periods of time till the defect occurs will be arranged in an ascending value order and the arranged selection will be marked t_1 , t_2 , ..., t_r .

Accumulated period of time till i defect will be calculated as [3]:

$$T_i = \sum_{k=1}^{i} t_k \ . \tag{1}$$

Procedure for lection range bigger than 40 samples**.** Time interval between zero and total accumulated exam time T is divided into m same intervals of the length of w. The expected number of defects in each interval is:

$$E = w \frac{d}{T^*} \ , \tag{2}$$

where m must be chosen in such a way so that E was equal or bigger than 5.

Test statistics will be calculated:

$$c^2 = \sum_{i=1}^{m} \frac{(O_i - E)^2}{E} \ . \tag{3}$$

The calculated value c^2 will be compared with the theoretical value $c^2(n)$ given in the table A1 [3], $n = m - 1$.

One-sided test will be carried out on the level of significance 10% using the table A1 [3] in this way:

- if $c^2 > c^2_{0.90}(n)$, then the precondition of the constancy of the defect intensity is rejected,
- during this procedure it is not possible to assess whether the defect intensity increases or decreases,
- otherwise the precondition of the constancy of the defect intensity is rejected.

From the above mentioned information and individual division procedure knowledge we can assume that Weibull division corresponds best with defect occurrence in vehicles.

3.2. Weibull’s Division

Weibull’s division is used for many pieces of machinery and other equipment which cannot use the exponential division, especially for such pieces of machinery which show mechanical depreciation and material fatigue. This division best matches the stated requirements and therefore will be used in calculations. The following part states relations for the calculation of spot estimates of the most important indexes of Weibull’s division valid both for restored and unrestored products. In case of zero threshold value (c = 0) division $W(a, b)$ has only two parameters:

- parameter a is the so-called parameter of position,
- parameter b is the so-called parameter of shape.

For the distributive function of division $W(a, b)$ applies:

$$F(x) = 1 - \exp\left[-\left(\frac{x}{a}\right)^b\right], \quad x > 0. \tag{4}$$

Average value of function $E(x)$ of Weibull's division:

$$E(x) = a \cdot \Gamma\left(1 + \frac{1}{b}\right), \tag{5}$$

where Γ denotes gamma function; its value is tabulated [4].

3.3. Determination of Parameters α and β of Weibull's Division Using Nelson's Method

Nelson's method is suitable for the processing of generally censored files. Formulation of the problem: when observing a group of objects for a longer time, a situation can arise for individual elements when the total observed interval of the period of operation splits up into two characteristic intervals I and II (see Fig. 3.1.):

Type I: These are intervals of the period of operation, limited at both ends by the failure of the observed element. According to the definition they are intervals of the period before defect (in restored elements the period between defects). These intervals will be further referred to as "finished".

Type II: These are intervals of the period of operation, limited at one end by the defect of the observed element and at the second end by a differently determined moment in which the observation (test) will be ended by reaching T_s^* without coming to the defect. These intervals will be further referred to as "unfinished".

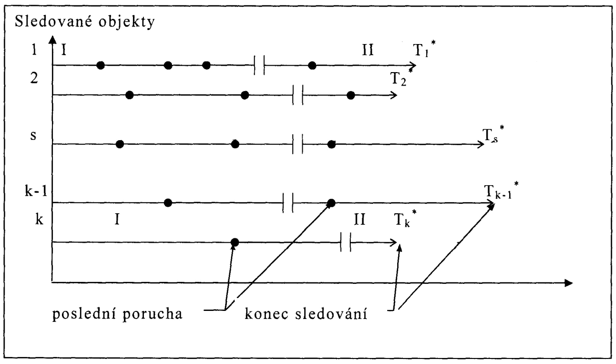

Fig. 1 Intervals of the time of operation

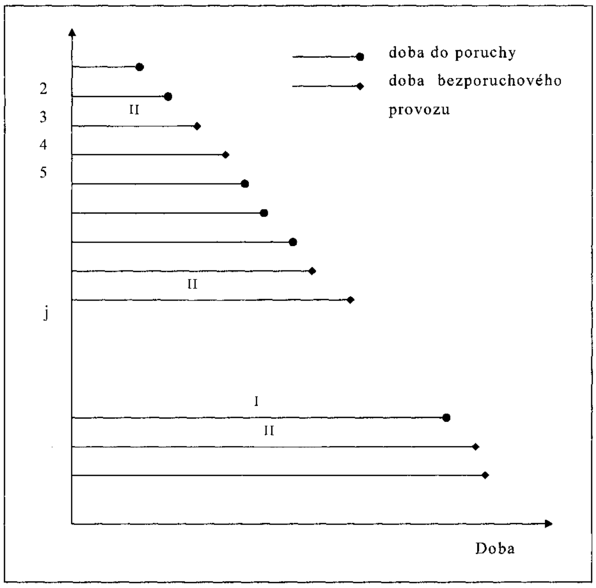

Fig. 2 Generally censored and classified file of data

Type II intervals cannot be neglected when guessing the parameters of division and they cannot be judged as equivalent to intervals I. For illustration, Fig. 3.2 shows a file of data filed according to the period of operation before defect or the period of operation before stopping the observation.

Estimation of parameters of Weibull's division is based on the linearization of the relation for cumulative intensity of defects $H(t)$.

$$H(t) = \left(\frac{t}{\alpha}\right)^{\beta}. \tag{6}$$

After taking the logarithms and modification the equation will get this form:

$$\ln H(t) = \beta \ln t - \beta \ln \alpha . \tag{7}$$

The above-stated relation is linear and can be solved in different ways:

a) graphically on logarithmic paper,

b) numerically (e.g. using the method of smallest squares).

To obtain the next calculation it is necessary to derive the relation for the estimation of cumulative intensity of defects $\hat{H}(t)$ in individual parts of the classified file of censored data.

3.4. Determination of Confidential Interval for Parameter *a* when Parameters *b* and *g* are Known

Bilateral confidential interval $< a_D, a_H >$ for parameter a when parameters b, g with confidential coefficient $1 - a$ are known, will be stated from the relations [5]:

$$a_D = \left(\frac{2.\sum_{i=1}^{n} (x_i - g)^b}{c^2_{1-\frac{a}{2}}\ (2n)} \right)^{\frac{1}{b}} \tag{8}$$

$$a_H = \left(\frac{2.\sum_{i=1}^{n} (x_i - g)^b}{c^2_{\frac{a}{2}}\ (2n)} \right)^{\frac{1}{b}} \tag{9}$$

where $c^2_q(n)$ is the value of quantile c^2-division with n degree of slackness, which is found in [5] in Table 6.

Unilateral confidential intervals with confidential coefficient $1 - a$ will be determined according to the relation for pro a_D, however, a instead of $a / 2$ will be used in the values of quantile.

4. Conclusion

The article gives an account of a possible approach to the determination of the optimal interval of service maintenance of vehicles in operation. For the determination of the interval of service maintenance it is necessary to gather and classify data about defect occurrence into groups according to the importance of defect consequences. It is also necessary to choose a suitable type of continuous division using the validity test of the presumption of constant intensity of defects or constant parameter of defect flow [3]. When the mechanism of defect occurrence and the dependence of vehicle depreciation are known, it is possible to use Weibull’s division, which seems to be the most suitable one. Parameters of presumed division were calculated using Nelson’s method for censored files. Relationships for the calculation of average period before defect for individual groups of defects according to the importance of the defect consequences have been mentioned. If need be, the same relation can be used for the calculation of average period before defect without the classification of defects according to the importance of the defect consequences using Weibull’s division. Following the analysis of calculated values and the originally stated interval of service maintenance for the given vehicle, on putting the vehicle into operation the determination of a new interval of vehicle service maintenance and its repeated inspection in practice is done according to the above-stated procedure. This process of approximation leads to the determination of optimal interval of service maintenance of vehicles.

References

1. **Furch J.** Rationalization of maintenance system of ground forces technology in the Army of the Czech Republic. PhD thesis. Brno: Military Academy. 2001.
2. ČSN 01 0602: Spolehlivost v technice. Hledisko třídění poruch a mezních stavů objektů. Praha: ÚNM. 1985. [in Czech].
3. ČSN IEC 60605-6: Zkoušení bezporuchovosti zařízení.Část 6: Testy platnosti předpokladu konstantní intenzity poruch nebo konstantního parametru proudu poruch. Praha: ČNI. 1998. [in Czech].
4. ČSN 01 0611: Pravidla pro stanovení bodových a intervalových odhadů ukazatelů spolehlivosti, parametrické metody. Praha: ÚNM. 1983. [in Czech].
5. ČSN 01 0224: Pravidla stanovení odhadů a konfidenčních mezí pro parametry Weibulova rozdělení. Praha: ÚNM. 1980. [in Czech].

Proceedings of 3rd International Workshop ITELMS'2008

The Investigation of Car Collision with the Road Restraint Systems

A. Tautkus

Kaunas University of Technology, Panevėžys Institute, Klaipedos str. 1, LT-35209 Panevėžys, Lithuania,
E-mail: arunas.tautkus@ktu.lt

Abstract

Collisions with immovable obstacles are pointed out while registering car collisions. One of the most frequent cases is sidelong collision with road fencings and kerbs. Such road accidents are caused by the wrong choice of speed on road turns, skidding due to road and weather conditions, etc. Certain issues occur while investigating such road accidents: the place of the collision, the speed before the accident, the car movement trajectory after the hit etc. These issues are dealt with in this article. With the help of computer software different car accidents with a stationary and energy absorbable barriers have been modeled and the trajectories of car movement are defined in this paper.
KEY WORDS: *collision, transport whecle, road restriction.*

1. Introduction

To increase safety in the city streets and country roads different stationary safety barriers and bollards have been framed in the roadsides and over bridge sides. Though they play safety function, but one type of collisions is car contacts with such elements. There are a lot of more stationary barriers: wayside trees, traffic stanchions, utility poles, bus-shelters, different structures etc. At the moment of a car collision with stationary obstacles hard impact strain appears which determines serious injuries of people and big damages of cars. The reasons of such collisions are different: high speed, bad driving conditions, construction rigidity of safety barriers.

In Lithuania such collisions make about 12-13 per cent of all road accidents [1]. Information to investigate the reasons and mechanisms of car collisions can be gathered analyzing real happened accidents or modeling different probable situations. The last-mentioned way is becoming more and more popular, because it allows forming the conclusions and predictions [2, 3].

The author of this paper has created the methodology to model car collisions with different stationary safety barriers. This methodology allows to estimate the collision with barriers made from different material and to model different situations as well as to define the trajectory of car movement after the collision [2]. The paper deals with two cases of car collision with a safety barrier: collision with a stiff barrier and collision with energy absorbable barrier.

1. The Roadside Hazards and Restraint Systems

The growing number of cars in the roads influences on the changes of road and street infrastructure. Different kinds of elements appear in the streets (viaducts, tunnels, bridges and etc.), which endanger road safety. Such stationary road elements or objects can be classified into the following groups:

- Rigid objects: trees, lighting poles, signal supports, utility poles and plants;
- Buildings (living and industrial facilities);
- Bridge piers;
- Abutments and tunnel entrances;
- Drainage features;
- Agresyve and treatment of safety barriers;
- Intersections;
- Ditches;
- Slopes (fill slopes and cut slopes);
- Gradient: blunt slopes;
- Rock face cuttings;
- Kerbs;
- Central reservations (medians);
- Others ways (roadways, railway, waterways).

This classification is shown in Fig.1.

Road restrain systems are classified according to the construction type, upbuild way, used materials. According to the safety purpose restrain systems are grouped into transport and pedestrian. According to the construction type there are single-sided and double-sided. According to used materials they can be combined, strainable and unstrainable. According to the upbuild way they can be grouped into permanent and temporary. According to the used materials they are ferroconcrete, metallic, plastic and combined. Some of them are shown in Fig.2-5.

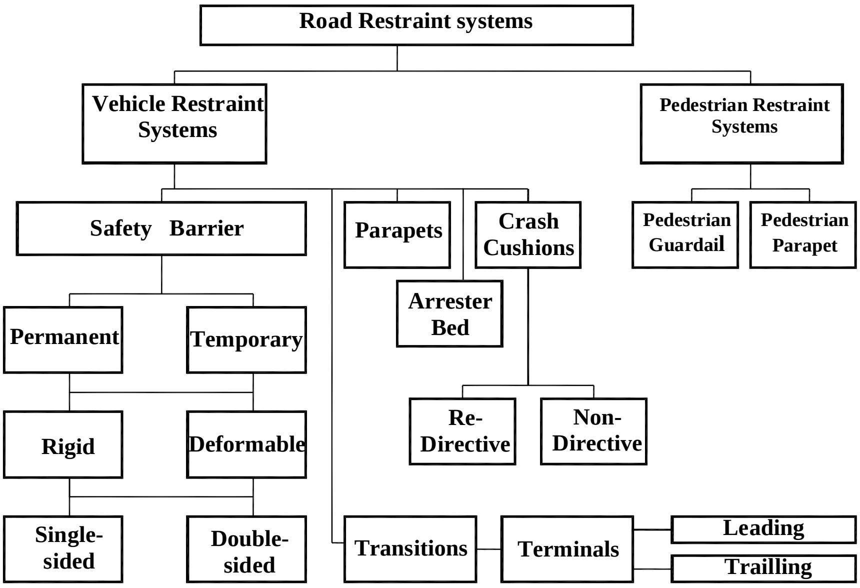

Fig. 1 The clasification of road restraint systems

Permanents safety barriers

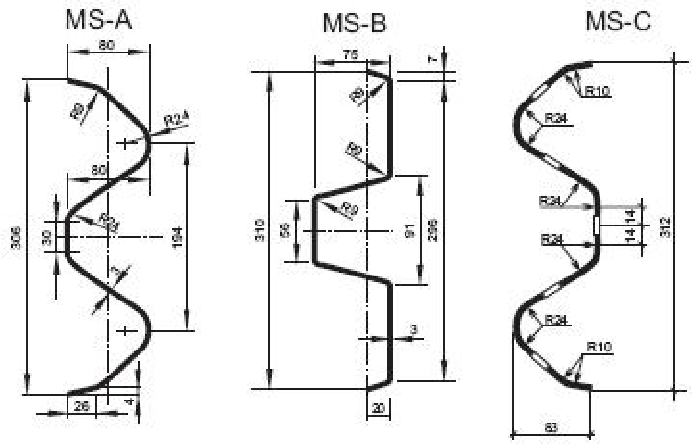

Fig. 2 Metallic safety barriers

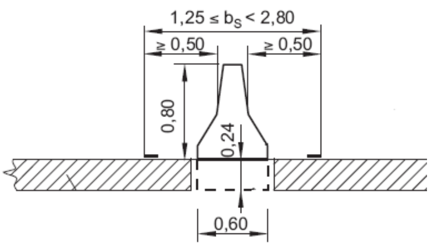

Fig. 3 Ferroconcrete safety barriers

Fig. 4 Energy absorbable safety barriers

Temporary safety barriers

Fig. 5 Plastic temporary road and pedestrian safety barriers

In Lithuania today the main types of safety barriers are these: ferroconcrete safety barriers; cable safety barriers with ferroconcrete bollards (these are not built any more and older are being changed, because they do not meet the requirements of passive traffic safety); metallic safety barriers. Chosen type of safety barriers can vary according to the road or street situation – allowable speed, transport type, riskiness (pedestrian and bicycle paths, pavement, high slopes, road turns, bridges, viaducts, water ways, buildings and other constructions, tress etc.).

Safety barriers are tested and certified in accredited testing laboratories. Every type gets a certificate with described impact of transport means on safety barriers and their "behaviour" during collision as well as the impact of safety barriers on the passengers. During the test the safety barriers are tested with cars, moving in different speed and angle to the construction, with sensors, video cameras and other equipments, fixing deformations during the collisions and after it, as well as the effects of the collision on transport means and passengers. Having assessed the results of the tests, the safety barriers are classified, the safety barriers and their constructions are certified determining the choice of its type for each particular situation.

2. Modeling and Investigation of Collisions and Their Movement Trajectories with Different Safety Barriers

The evaluation of car movement trajectories after contact is a very important factor for the road accident investigation. The evidence of the accident lets estimate the positions of vehicles before hit and after hit, which helps define car speed before hitting. The computer modeling of collisions is performed for evaluation of the car movement trajectories after hit. The modeling is performed with the help of software. It was noticed that the trajectory of a car after contact depends on its speed and on the collision angles. Because of that, collisions were modeled with different car speeds: 36 km/h, 50 km/h and 90 km/h, as well as collision angles: 10°, 20°, 30°, 45°.

2.1. Investigation of Car Movement Trajectories after Contact in Case of Collision with Stationary ferroconcrete safety barriers

Traffic accidents are modeled at a low collision speed – 36 km/h, at an allowed speed in towns – 50 km/h and at a higher speed – 90 km/h. The car movement trajectories after the accident are presented in Fig. 6-8.

The starting conditions were created as close as possible to the real traffic accidents. The speed of the car until hitting the obstacle was: v = 36 km/h; 50 km/h; 90 km/h;

- Car mass: m =1300 kg;
- Collision angles: 10°, 20°, 30°, 45°;
- Time of modulation: 2 s;
- Car width: H_g = 1,8 m;
- Car length: L_g = 5 m;
- diameter of round obstacle d = 0.45 m;
- Aerodynamic coefficient: c_w = 0.4;
- Road conditions – dry asphalt;
- Impedance of rolling: f = 0,015;
- Cohesion coefficient f_x = 0,4 [4];
- Longitudinal road slope $a_{lon.} = 0^0$;
- Latitudinal road slope $a_{lat.} = 0^0$;
- Hit recovery coefficient k = 0.3 [5].

Having analyzed the results it is obvious that the loss of speed after hit depends on the initial speed of a car and the angle of collision. The bigger collision angles the higher speed loss is after the hit. From the car movement trajectories after the modeled accident is obvious that the character of the trajectory depends on: the angle of collision, the car speed before hit. The bigger angle between the movement direction and road fencing is the bigger deflection of the trajectory appears. This is noticed at all analyzed cases when the collision speed was 36 km/h, 50 km/h and 90 km/h. The smaller contact angle the more time a car is skidding along the side surface of the road fencing. When the collision speed is low (36 km/h) and the contact angle is 10° the car is skidding along the side surface of the road railing and stops without moving away from it.

As it has been mentioned before, the location of the vehicle after hit does not depend on the angle of collision but also on its speed. The diagrams demonstrate that when the speed increases almost 3 times deflection to the side increases almost twice. This fact is observed in all cases analyzed when the collision angles with a stationary road element was equal to: 1 - 10°, 2 - 20°, 3 - 30°, 4 - 45°.

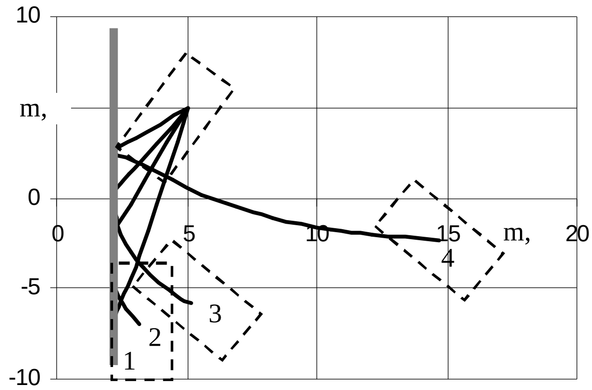

Fig. 6 Trajectories drawn by car centers of gravity at the moment of collision with a stationary obstacle, when the speed before the contact 36 km/h and collision angles equal: 1 - 10°, 2 - 20°, 3 - 30°, 4 – 45.°

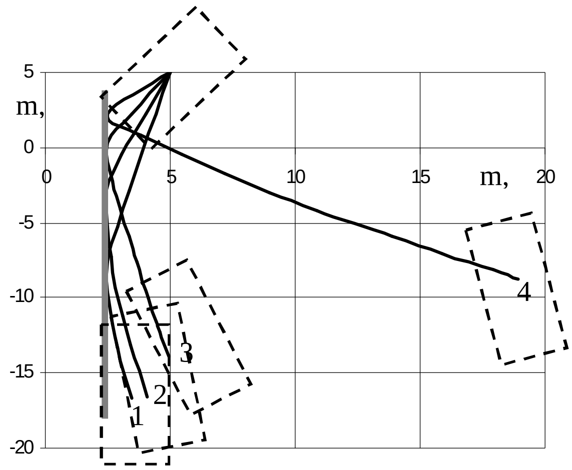

Fig. 7 Trajectories drawn by car centers of gravity at the moment of collision with a stationary obstacle, when the speed before the contact 50 km/h and collision angles equal: 1 - 10°, 2 - 20°, 3 - 30°, 4 – 45.°

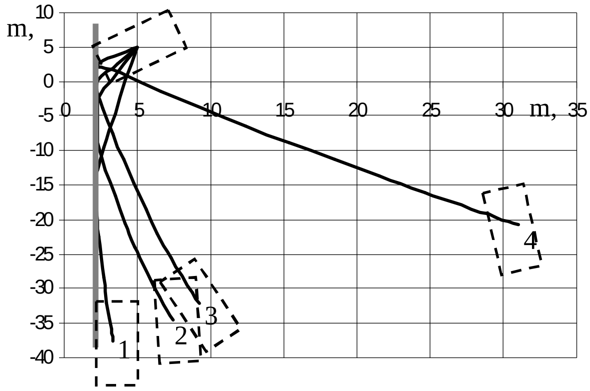

Fig. 8 Trajectories drawn by car centers of gravity at the moment of collision with a stationary obstacle, when the speed before the contact 90 km/h and collision angles equal: 1 - 10°, 2 - 20°, 3 - 30°, 4 – 45.°

2.2. Investigation of Car Movement Trajectories after Contact in Case of Collision with energy absorbable safety barriers

Car collisions with energy absorbable safety barriers are modeled the same as with stiff safety barriers. The speed of the car before collision is: v = 36 km/h; 50 km/h; 90 km/h and angles are: 10°, 20°, 30°, 45°. The type of the barrier is shown in Fig. 2.

The car movement trajectories after the accident are presented in Fig. 9 ... 11.

Having analysed the collisions with energy absorbable safety barriers it can be claimed that these barriers are always strained during the collision. Their deformations depend on the car speed before the collision and the collision angle. The largest deformations have been fixed when the speed was 90 km/h and the angle was 45° (Fig. 11), and the least – when the speed was 36 km/h and the angle was 10°(Fig. 9). Therefore the energy absorbable safety barriers are better in the aspect of safety.

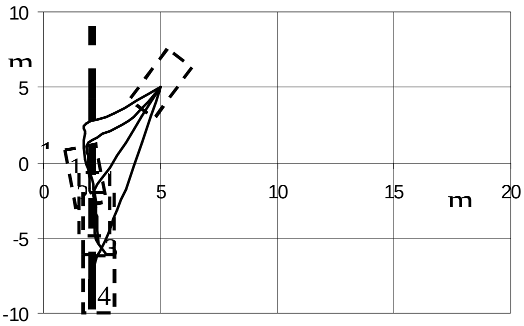

Fig. 9 Trajectories drawn by car centers of gravity at the moment of collision with energy absorbable safety barriers, when the speed before the contact 36 km/h and collision angles equal: 1 - 10°, 2 - 20°, 3 - 30°, 4 – 45.°

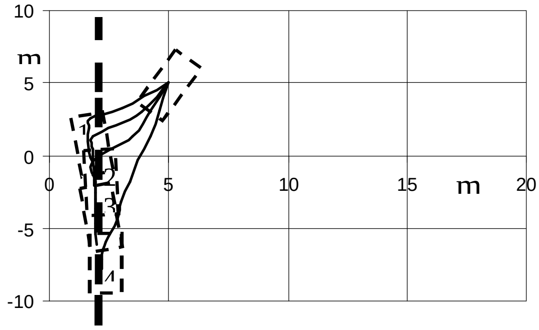

Fig. 10 Trajectories drawn by car centers of gravity at the moment of collision with energy absorbable safety barriers, when the speed before the contact 50 km/h and collision angles equal: 1 - 10°, 2 - 20°, 3 - 30°, 4 – 45°.

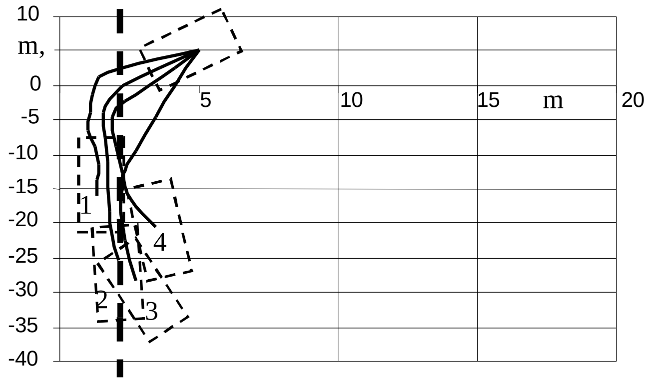

Fig. 11 Trajectories drew by car centers of gravity at the moment of collision with energy absorbable safety barriers, when the speed before the contact 90 km/h and collision angles equal: 1 - 10°, 2 - 20°, 3 - 30°, 4 – 45.

3. Conclusions

Having performed the modeling of the collision with a stationary ferroconcrete road element at certain conditions has been defined that the car movement trajectory depends mainly on the conditions of the collisions and the speed of a car before it contacts with the obstacle. The bigger the angle between the movement direction and road fencing, the bigger side deflection appears on the trajectory. The bigger the speed of the vehicle before the collision the longer its movement trajectory after it hits the obstacle.

During the collision with stiff barriers a car often meets the second knock with other road elements or transport means, but this phenomenon seldom happens during the collisions with energy absorbable safety barriers.

During the collisions with energy absorbable safety barriers less car deformations have been noticed on the cars and less injures have appeared. Energy absorbable safety barriers are more perfect in the aspect of safety.

References

1. **Tautkus A.**, **Jurkauskas A.** Evaluation of car crash parameters in the case of collision // TRANSPORT. Vilnius: Technika, 2002, XVII t., No. 3, p. 91–95.
2. **Tautkus A.**, **Bazaras Ž**. The investigation of car movement trajectories after contact in the case of collisions with stationary safety barriers // Urban Transport XIII: Urban Transport and the Environment in the 21st Century: 13th international conference on urban transport and the environment in the 21st Century, 3-5 September 2007, Coimbra, Portugal / Wessex Institute of Technology; editor C. A. Brebbia. Southampton: WIT Press, 2007. ISBN 978-1-84564-087-3. p. 557-565. (WIT Transactions on the Built Environment. ISSN 1746-4498; Vol. 96).
3. **Blundell M.** and **Harty D.** The Multibody systems approach to vehicle dynamics. Elsevier: Great Britain, 518 p.
4. **Shang Liu C., Peng H.** Road friction coefficient estimation for vehicle path prediction // Journal Vehicle System Dynamics. Vol. 25 Suppl., 1996, p. 413-425.
5. **J. A. Neptune**. Crush stiffness coefficients, restitution constants and a revision of CRASH 3 and SMAC. SAE Paper 98-0029.

Proceedings of 3rd International Workshop ITELMS'2008

Public Transport System and its Challenges for Sustainability

D. Susniene*, A. Jurkauskas, J. Prunskienė*****

**Kaunas University of Technology, Panevėžys Institute, Klaipedos str. 1, LT-35209 Panevezys, Lithuania,*
E-mail: dalia.susniene@ktu.lt
***Kaunas University of Technology, Panevėžys Institute, Klaipedos str. 1, LT-35209 Panevezys, Lithuania,*
E-mail: algis.jurkauskas@ktu.lt
****Kaunas University of Technology, Panevėžys Institute, Klaipedos str. 1, LT-35209 Panevezys, Lithuania,*
E-mail: jurgita.prunskiene@ktu.lt

Abstract

This paper deals with the quality of transportation services in public transport system. There is an overview of how to apply total quality management in this field. Looks at customer dissatisfaction by focusing on the events, which provide the source of the dissatisfaction and complaints. Uses data from research in public transport. Customer experience, customer dissatisfaction and customer complaints have not previously been studied to any greater extent in public transport research. Interest in this type of study has increased, however, perhaps as a result of customer focusing and increased attention to quality for passengers. Increased competition no doubt plays an important role as well. Quality improvement is a continuous process and providing public transportation services the key issues should be staff knowledge and understanding of customer needs, service provided, current possibilities and its limits. Only continuous focus on improvement of total quality will help the transport company to be the leader in a highly competitive market.

KEY WORDS: *public transport, quality, sustainability, customer expectations and satisfaction.*

1. Introduction

Public transport in Lithuania undergoes great changes and highly competitive environment makes a big influence to its activity. In order to survive and be the leaders in this field each company must focus on the provided customer service quality.

Recent changes in funding levels and structures combined with a changing market now require public transportation managers to become conscious of management philosophy, and to consider the need for changes if services are going to be effective [1, 12]. Service-sector organizations face a higher level of complexity than manufacturing firms, requiring management to consider a full range of management practices, including:

1. Best-practice analysis both within an organization, and comparisons among similar organizations (peer analysis) to avoid repeating mistakes and to identify management techniques and performance targets;
2. Process analysis to uncover the ways in which service workers interact with customers;
3. Continual application of quality-management techniques to improve key functions on an on-going basis.

Transport managers need to consider these issues as critical to the long-term survival of their organizations, even if day-to-day management issues could easily absorb most available management attention.

The purpose of this paper is to discuss possible aspects of sustainable public transport system development and to describe, analyze and interpret passengers' experience while traveling and especially critical incidents and their cause. With the help of passenger's experience of the journey, it is easier to:

- Identify weaknesses/advantages in the current service;
- Study the relationship between experience and service;
- Study how implementation of the service affects the passenger's behavior;
- Work out models in order to foresee more easily what effects various quality improvements have on traveling.

The object of the study is transportation companies in Lithuania and their provided services, social-economical factors influencing their activities.

The methods used in this study are critical incident method, questionnaires and interviews. A central part in the analysis and interpretation of data is the formation of categories. The categories should reflect the material, primarily the causes of the critical incidents and customer dissatisfaction.

2. The Use of Cars Should Pay for Better Public Transport

Thus the "traffic problem" is not a new problem–though its range, reach and impact on both urban and rural quality of life is now so pervasive as to demand solution. Its nature and extent was summarized by Transport 2000 in their Blueprint For Quality Public Transport [11, 13]. In many cities, the success of the car is now the most serious threat to the freedom and mobility the car gave us in the first place. Car traffic congestion is a growing problem due to the huge number of cars, and it leads to many other problems, for example environmental and aesthetic problems.

Recent years have seen a huge rise in levels of car ownership. In the 15 EU countries, the number of cars per 1000 people has risen from 184 in 1970 to 656 in 2006. This is a negative impact on the efficiency of public transport services as buses as they stuck in the middle of the congestion.

The car traffic involves problems:

- Longer traveling times for car drivers and public transport (congestion)
- Pollution (noise and air)
- Traffic safety (also for public transport)
- Much city space is occupied for car lanes and parking places
- Disturbance of outdoor activities.

The philosopher O. Thyssen has explained the car paradox extremely precisely: “When freedom of transport extends from being the privilege of the elite to becoming everybody’s right, the problem will be that everybody’s freedom undermines every-body’s freedom. It is a particular problem, which arises collectively and unintentionally. Nobody created it and nobody is able to solve it. One’s own contribution is just a single drop in the ocean. So we continue to supply each our own drop, and altogether they produce an ocean of problems.”

A variety of suggestions are made to improve transport; several of these relate to educing the reliance on cars as the mode of travel to work. The European Commission also focuses on the need to support the development of sustainable forms of transport [4, 5, 14]. The car traffic dilemma is that more success brings along larger problems for car travelers and other travelers. But increasing the capacity through widening of the roads does not solve the problem. No city has ever solved the traffic problem by giving more space to cars and parking. If instead we convert car traffic into public transport we shall experience a better service in public transport with higher traveling speed and higher reliability.

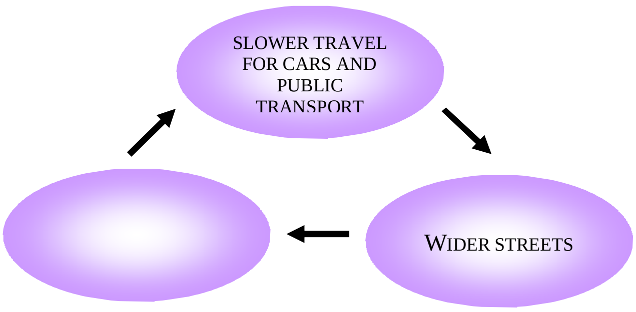

Fig.1 The bad cycle

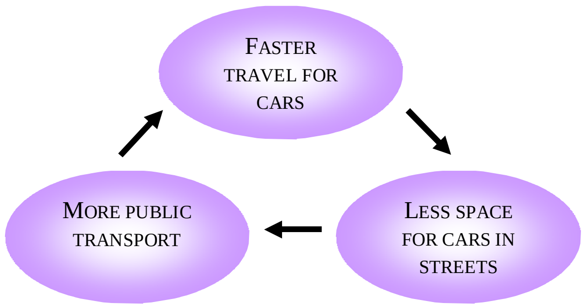

Fig.2 The good cycle

The explanation is simple. Car traffic means low capacity of infrastructure, since a single car requires 22.1 m^2 per traveler and a bus only 1.2 m^2 per traveler. Therefore, when a limited space is available and maximization of street capacity is wanted it requires a limitation of the car use and an intensification of the public transport. This is the way of maintaining maximum mobility.

Therefore, the conclusion is to obtain livable cities, car traffic must be limited, and at the same time public transport must be upgraded in order to obtain mobility.

3. Public Transport: the City’s Partner in the Service of Urban Accessibility

More than they ever did in the past, people now recognize public transport’s legitimacy in successfully producing healthy, safe, clean, efficient, pleasant and convivial cities – in short, dynamic cities that people like to live in.

The stakes for public transport are not just higher, but have also evolved. Originally earmarked from home – work journeys, public transport in future will play a broader, more varied role. The possibility to travel is being perceived more and more as a right and as a means for people to exercise their freedom.

It is up to public transport to become the instrument for this by facilitating access – within the meaning ascribed to the term “urban accessibility” – for the greatest number of people to all the diverse activities spread across a city’s territory [6, 8, 10].

The way the transport system functions in any large city brings into play a host of actors, while its efficiency depends on the quality of interactions between those same actors. As one of them, the public transport operator will have to forge partnerships with other actors if it intends to carry out its mission in an acceptable fashion. Notable actors include the local authorities, businesses, equipment manufacturers, fleet manages for individual vehicles, and other operators. Eventually, the ambitious target represented by urban accessibility in the city of tomorrow will call for a sharing of responsibility that binds policy officials and local politicians and the directors and staff of transport operators. There is no reason why the inhabitants of the city should not be involved too and perhaps consulted about choices that will affect their quality of life so close to home. Nothing less than new forms of urban governance need to be invented.

4. Quality in Public Transport

One of the reasons that quality has suddenly begun to evolve from a Cinderella aspect of operations into this strategic role is the realization that attention to quality is the most effective way of reducing costs and wasted time.

Another reason that quality is becoming the focal point of top management attention is the growing understanding of just what the costs of poor quality are. The costs of waste, rework, warranty, appraisal, prevention and lack of attention to detail may account for between 15% and 40% of turnover not only for manufacturing company but for service company as well [2, 3]. So what is quality?

5. Quality is a Continuous Interpretation, Understanding and Satisfaction of Customer Needs

A customer driven approach dictates that management activities are aimed at providing high-quality services to the transportation company's customers. The approach attempts to answer the question:" How can my transit system satisfy customer needs?" The answer to this question is that the transportation company needs to:

1. Provide reliable service – customers should have confidence that vehicles will come and transport them on time, or when promised.
2. Ensure that services are safe and secure – customer should feel safe and secure while using the system.
3. Provide convenient services – customers should be able to use transit to travel from residential areas to major destinations or activity centers at times/days they need to travel.
4. Provide clean and comfortable services – customers should find the vehicles and facilities clean and comfortable when riding or waiting.
5. Make services understandable – customers should understand easily how to use the services through effective user information and materials.
6. Make services affordable – customers should be able to afford to use the transit system.
7. Ensure that staff is empathetic and that customers know it – customers should feel that the transport system staff care about their needs.

It is not enough to implement these seven criteria in a transport company work [9]. Only total quality management (TQM) can be a turning point in organizing company's activity and focusing its attention to satisfying customer needs. What is total quality management?

Total quality management is involving every employee in quality assurance of company activity [1, 4].

Fig. 3 presents an overview of transport company functions with the focus on delivering high-quality customer service. As shown, the transportation managers need basic input of funds with which to procure vehicles and facilities and pay drivers and other staff. Such resources (vehicles, facilities, staff) are used to operate transportation service. If the resources are managed well, the system and its staff provide transportation services or output that meets the needs of their customers by being reliable, safe convenient, comfortable, understandable, affordable, and empathetic.

The following management functions/controls are required and must be well conceived and effective to allow transportation company to manage the system in a way that supports good customer service. It will need:

- Human relations program to recruit, hire, train, and motivate drivers and other staff;
- Vehicle planning, procurement, and maintenance program;
- Facilities maintenance program;
- Risk management program;
- Program to manage service contracts (operations and maintenance);
- Sound operating procedures for drivers, dispatchers, and customer service staff;
- Operations supervision program (on street and in-house) – operating and management processes and procedures needed to supervise and manage operations;
- Fare structure, fare media, and fare handling procedures;
- Service planning program;
- Communications program (customers to staff/drivers to base);
- Financial management – to make services affordable;
- Marketing and public input/outreach programs;

Table 1 presents the relationship between the specific functional activities and the achievement of customer-driven goals.

While it can be argued that all transportation functions affect service, some are more important than others in this regard.

6. Research into the Quality of Transportation Services

In order to check the transportation quality of transportation service we executed a research of customer experience. The empirical point of departure was studies of public transport in Vilnius and Panevezys.

We analyzed customer complaints in writing and interviews with passengers who experienced shortcomings in service quality using public transport. Comparative analysis was used to draw the conclusions and to assess the value of acquiring facts about customer-experienced quality and customer dissatisfaction through the front-line staff.

Analyzing and interpreting the data we form the categories and subcategories. In the formation of the categories of the present study, efforts have been made to proceed to the greatest possible extent from the respondents' own formulations and to use these as “labels” for the categories. We can notice that these seven categories easily comply with the seven criteria of satisfying customer needs.

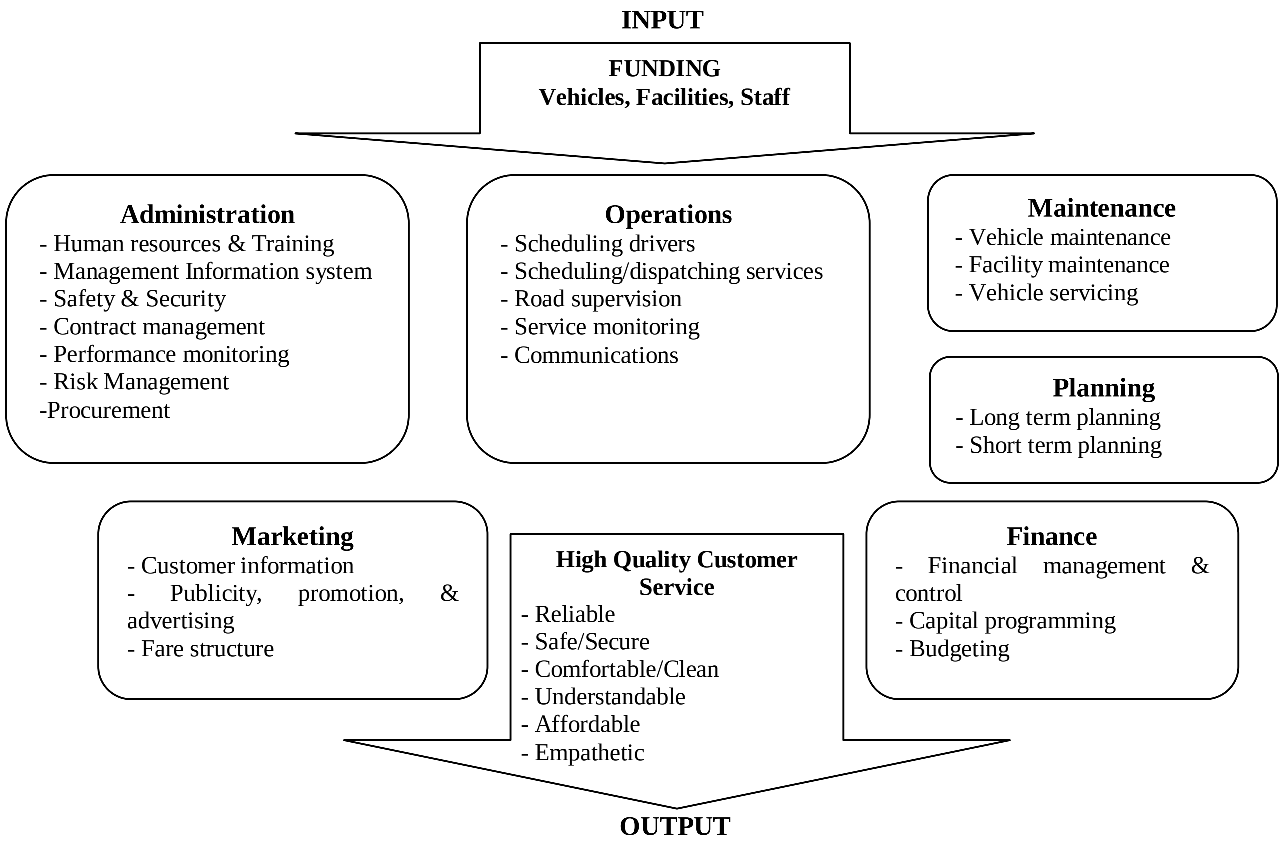

Fig. 3 Transportation management functions, focused on customer service

Table 1

Relationship of customer service attributes to transport company functions

Customer Service Attribute / Transport Company Functional Activities Critical to Customer Service	Reliable	Safe/Secure	Comfortable/ Clean	Convenient	Under-standable	Affordable	Empathetic
ADMINISTRATION							
Risk Management & Safety/Security	●	●					
Contract Management Program	●	●	●	●			●
Human Resources Program to Recruit, Hire, and Train Staff	●	●					●
OPERATIONS							
Operating Procedures for Drivers, Dispatchers, and Customer Service Staff	●	●					●
Operations Supervision and Service Monitoring	●	●					●
Service Operations Management	●	●		●			
Communications Program	●	●		●	●		●
MAINTENANCE							
Vehicle Maintenance and Servicing	●	●	●				
Facilities Maintenance		●	●				
PLANNING							
Planning	●			●	●	●	
MARKETING							
Fare Structure and Fare Media					●	●	
Marketing & Public Information Program					●		●

Most of all passengers were dissatisfied with the space and design of the vehicle 351 out of 810, i.e. uncomfortable and dirty busses, crowding, lack of space and seats, uncomfortable getting on and off. Another big category, which caused customer negative journey experience, was treatment and conduct. Passengers complained about rude and unpleasant behavior of the drivers and other front line staff that account for 12 %. The dominant cause of passenger dissatisfaction was problems with traffic planning: inconvenient departure and arrival times, problems with the timetables and information.

Distribution among categories of customer complaints Table 2

Main category	Sub-category	Total	%
Treatment / Conduct (Empathetic)	Driver	**(86)**	
	Unpleasant treatment	57	
	Way of driving	23	**9**
	Driving past	6	
	Other personnel	**(27)**	
	Unpleasant treatment	27	3
Punctuality (Reliable)		**(59)**	
	Too early	19	
	Too late	37	**7**
	Non-appearance	6	
Information (Understandable)		**(35)**	
	Journey times	13	**4**
	Timetables and changes	32	
Technical faults (Safe and Secure)		**(68)**	
	Car accidents	1	
	Injury during journey	1	**10**
	Fault in the vehicle	34	
	Faulty equipment	24	
	Old means of transport	8	
Space in / design of the vehicle (Clean and Comfortable)		**(372)**	
	Crowding	77	
	Lack of comfort	88	
	Lack of seats	63	**43**
	Getting on and off	51	
	Lack of cleanness	72	
Traffic planning (Convenient)		**(89)**	
	Setting of fares	52	
	Timetable coordination	11	**12**
	Departure times	26	
Miscellaneous (Affordable)		**(117)**	
	High fares	18	
	Waiting rooms and bus shelters	15	**12**
	Retailers	3	
	Uses other means of transport	81	
Total		**826**	**100**

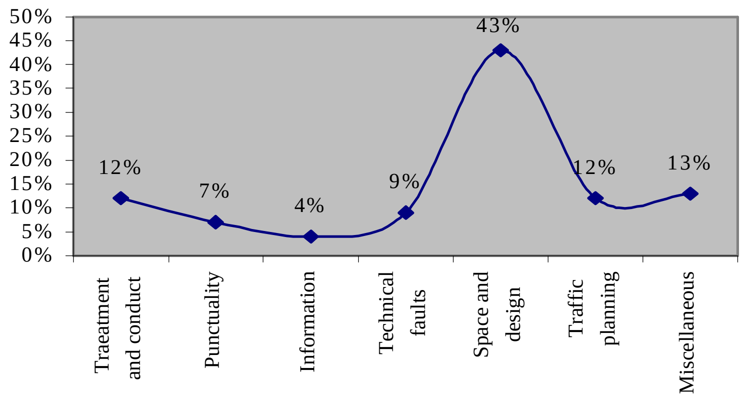

Fig. 4 Division of the groups according to the results

Drivers are not satisfied with the traffic planning, old busses and access to information. One interpretation of the results is that the front-line personnel have a poor conception of what creates customer dissatisfaction. We cannot gain a sufficiently good picture by interviewing the bus drivers of what really are customer-experienced shortcomings in quality that result in dissatisfaction. This may be due to the fact that the bus drivers have poor contact with and rarely conduct a conversation with their customers. It may even be the case that the bus drivers look primarily to their own interest and not to that of the customers. A third interpretation is that part of what the customers are dissatisfied with are in the bus driver's view somebody else's responsibility, for example timetables that are difficult to read or poor information in conjunction with changes in the timetable. It may even be the case that the driver sees his task to drive the bus from point A to point B. giving service to the customers does not seem to be as important a main task. This may depend on an unclearly defined role and unclear customer and service responsibility.

7. Conclusions

According to the results of the investigation we can conclude that the quality of transportation service is far from the customer expectations and needs. It is necessary for transportation companies to look for and implement the new management models in their system in order to survive in a very competitive market.

Many of the new TQM concepts have to be applied in service sector industries, including public sector organizations such as public transportation. TQM is a comprehensive and long-term transformation of the culture of the organization, focusing on people first – including passengers, employees, and the community. Public transportation should implement seven TQM principles:

- *Put customer first.* Every service should meet or exceed the expectations of the customer, and every member of the organization and every process should work toward this end.
- *Manage and improve processes*. "Process" describes how work activities are performed. Improvement of processes can both create a higher quality service, and increase efficiency. Support activities such as training, service planning, and maintenance are among the processes that can be managed and improved.
- *Manage by fact.* Facts and data are used in a quality organization to help managers set directions for strategic and short-range planning, and to evaluate progress on achieved goals and objectives.
- *Cultivate organizational learning.* Learning organizations are able to thrive in rapidly changing environments because they are objective in their decision-making, are open to internal communication, involve teamwork, create the useful tools needed for everyone to do the best job, and reward the desired behaviors.
- *Train, empower, and recognize employees*. Employees are the most important assets of a transportation system, and they need to be trained to be able to meet customer expectations, empowered to identify and solve problems, and satisfy customers. Finally, employee contributions to improved performance need to be recognized.
- *Improve labor-management teamwork.* Employees need to be involved in any quality effort, quality policy decision making.
- *Lead the change in organizational culture*. TQM is a long-term commitment to a fundamental change in the way an organization works. Leadership at all levels of the organization is required to make this kind of change.

The benefits of TQM can be seen in a variety of ways. Even a relatively small investment in TQM can lead to a dramatic effect. But the major benefits come from long-term strategic advantages the quality conscious company can build over its rivals. For example, there are clear marketing advantages to be gained from a reputation for across the board quality in service, especially if the competitive pricing that comes from cutting quality costs backs up that reputation. Quality builds a committed customer base and provides a common focus for the activities of everyone in the organization, from top to bottom.

References

1. **M. van Biema, B. Greenwald**. Managing Our Way to Higher Service Sector Productivity // Harvard Business Review. July-August 1997, p. 87-95.
2. **P. Senge**. The Fifth Discipline: The Art and Practice of the Learning Organization, Doubleday/Currency, 1990.
3. **M. G. Brown and Associates**. Defining customer requirements. 1994.
4. **P. K. Doran**. A Total Quality Improvement Programme, 1996.
5. **C. A**. **Kennedy**. A comparison of the sustainability of public transport and private transport systems // Transportation. 29 (4), 2002, p. 459-493.
6. **J.-P. Bailey**. Public transport in the face of more stringent demands // Public Transport International. 1, 2000, Special Millennium Report, p. 40-44.
7. MOTiF-Market Orientated Transport in Focus.Contract No.UR-97-SC.1149.Final Report for Publication 2000.
8. **S. Fujii, R. Kitamura**. What does a one-month free bus ticket do to habitual drivers? An experimental analysis of habit and attitude change \\ Transportation. 30 (1), 2003, p. 81-95.
9. http://www.sustainable_int.
10. http://www.uitp.com.
11. **Viegas, J. M**. Public transport in the sustainable urban transport policy package: taking an integral policy approach. ECMT/OECD Workshop on implementing strategies to improve public transport for sustainable urban travel. Athens, Greece, 1999.
12. **Hußmann H**. The Bus Transit System and its Contribution to Promoting Mobility and Quality of Life. Public transport '05. 61st International Congress Paris 2005.
13. **N. L. Robert.** Thoughts on sustainable mobility // Periodica Politech. ser. soc. Man.sci. vol. 10, 2002, p. 117-122.

Proceedings of 3rd International Workshop ITELMS'2008

Stress Strain State of Mechanically Heterogeneous Welded Joint with a Hard Interlayer at the Plane Deformation Subjected to Tension

A. Bražėnas*, D. Vaičiulis**

* *Kaunas University of Technology, Daukanto 12, LT – 35212, Panevėžys, Lithuania, E-mail: algis.brazenas@ktu.lt*
** *Kaunas University of Technology, Daukanto 12, LT – 35212, Panevėžys, Lithuania, E-mail: dainius.vaiciulis@ktu.lt*

Abstract

The paper presents results analytical investigations of mechanically heterogeneous butt welded joints with a hard interlayer at the plane deformation. There are presented dependencies for stress strain state components determination in welded joints with the hard interlayer subjected to static tension.
KEY WORDS: *welded joint, static tension, stress strain state, hard interlayer.*

1. Introduction

A great number of welded joints show higher or lower heterogeneity of mechanical properties of their separate zones. The mechanically heterogeneous welded joint zone which strength properties are higher than this of a base metal is called hard interlayer, in opposite case – mild interlayer. The welded joint with a hard weld is frequently used. During welding of hard steel at thermal effect zone, which strength is higher then base metal one, is set up. It caused heterogeneous stress state and non-uniform strains distribution in direct of welded joint longitudinal axis.

Strain state of welded joints with a hard interlayer is analysed in works [1, 2]. There is obtained that, when $g_e = s_e^H / s_e^M$ is small, before fracture of welded joint at the external point of contact plane of hard metal H and mild metal M (fusion line) elastic plastic straining in hard metal appears. When it relative thickness $\ae^H = h / d$ (h and d is thickness of weld and diameter of specimen respectively) is small elastic plastic straining begins in all volume of the hard interlayer. Fracture of this welded joint with a hard interlayer occurs in cross-section of mild metal M which is on relative distance larger or equal than $\bar{l}_1 \geq 2l_1 / d \geq 1.2$ from the contact plane. In this cross-section $s_r^M = 0$. Strength of a welded joint with a mild interlayer M analytically and experimentally is investigated in work [3]. Analytical investigation which are devoted to analysis stress strain state of welded joints with a hard interlayer are not known.

2. Analysis Stress Strain State of Welded Joint With a Hard Interlayer at Plane Deformation Subjected to Tension

The stress state of butt welded joint with a mild interlayer, subjected to tension (compression) at the plane deformation on dimensionless co-ordinates $x=x/l$, $h=y/l$ and relative thickness of a mild interlayer $\ae^M = 2h / 2l$ is analysed in work [3] ($2h$ is thickness of mild interlayer and $2l$ is thickness of welded plate). The problem was solved by using presumptions that the modules of elasticity of both materials are equal each to other ($E^H = E^M = E$), and Poisson's ratio $n=n^M=n^H=0.5$. The stress state components of a hard interlayer also is analysed on dimensionless co-ordinates $x=x / l$, $h^H=y^H / l$ with initial point is at the centre of hard interlayer (Fig. 1, a).

When $s_i \leq s_e^M$ and $v = v_p = 0.5$ in welded joint $s_x = t_{xy} = 0$ and at the plane deformation $s_y = p$, $s_z = 0.5\,p$ and $s_i = \sqrt{3}p/2$ (p is mean stress caused by external load). When $p > 2s_e^M / \sqrt{3}$ elastic plastic straining begins in all volume of the mild interlayer. But on the contact plane of metals M and H the mild metal strains are constrained by hard metal H. Due to interaction of metals H and M shear stress appears and near the contact plane there is a triaxial stress state. In the mild metal M tension stress s_x^M and in metal H compression stress s_x^H appears (Fig. 1, b). Analogical stress state near the contact plane of H and M metals appears in welded joint with a mild interlayer.

Equilibrium condition of element $x_i^H x_i^* 1^* 1^H$ of metal H (Fig. 1, b) makes it possible to calculate mean value of stress s_x^H on the thickness of interlayer

$$\sigma_{x\,m}^H = \frac{1}{\ae}\int_0^{\ae} \sigma_x^H \, d\eta^H = -\frac{1}{\ae}\int_{\xi}^{1} \tau_{xy}^{H*} \, d\xi \,. \qquad (1)$$

Stress s_x^H may be expressed from Eq.(1) by using function $f_2\,(h^H)$ it distribution in direct of axis h^H. Then $s_x^H = -f_2\left(h^H\right)\int\limits_x^1 t_{xy}^{H*}(x)\,\mathrm{d}x + C_1$ (constant $C_1 = 0$ because $s_{x|x=1}^H = s_{x1}^H = 0$).

When relative thickness of mild weld $æ^M = 1.2$ in according to Saint-Venant's principle stress s_{xc}^M at the centre of weld and stress in hard metal at the relative distance from the contact plane $d^H = 1.2$ approximately disappears ($s_{xc}^M \approx \left|s_{x|h^H=0}^H\right| \approx 0$). Therefore in work [3] is accepted that in welded joint with a mild interlayer functions of distribution stresses s_x^H at the distance d^H and stresses s_x^M at the relative thickness of mild weld $æ^M = 1.2$ are the same. Experimental investigations [1, 2] showed that stress $\left|s_x^H\right|$ increases analogically with decreasing distance's from the contact plane. Therefore is assumed that stress s_x distribution in relative thickness of interlayer $æ$ in welded joints with a mild and hard interlayer in range of variation $0 < æ \le 1.2$ is the same. Then function $f_2\,(h^H)$ may be obtained substituting h^H and $æ^H$ in expression of $f_2\,(h^M)$ [3] instead of h^M and $æ^M$

$$f_2\left(h^H\right) = 3 - 3\left[1 - \frac{1}{F\left(æ^H\right)}\right]\left[1 - \left(\frac{h^H}{æ^H}\right)^2\right] \Big/ æ^H\left[1 + \frac{2}{F\left(æ^H\right)}\right], \tag{2}$$

where $F\left(æ^H\right) = 1 + M_1\left(æ^H\right)^{n_1}$; $M_1 = 6.23 + 0.758\left(g_N - 1\right)$; $n_1 = 2.53 - 0.15\left(g_N - 1\right)$.

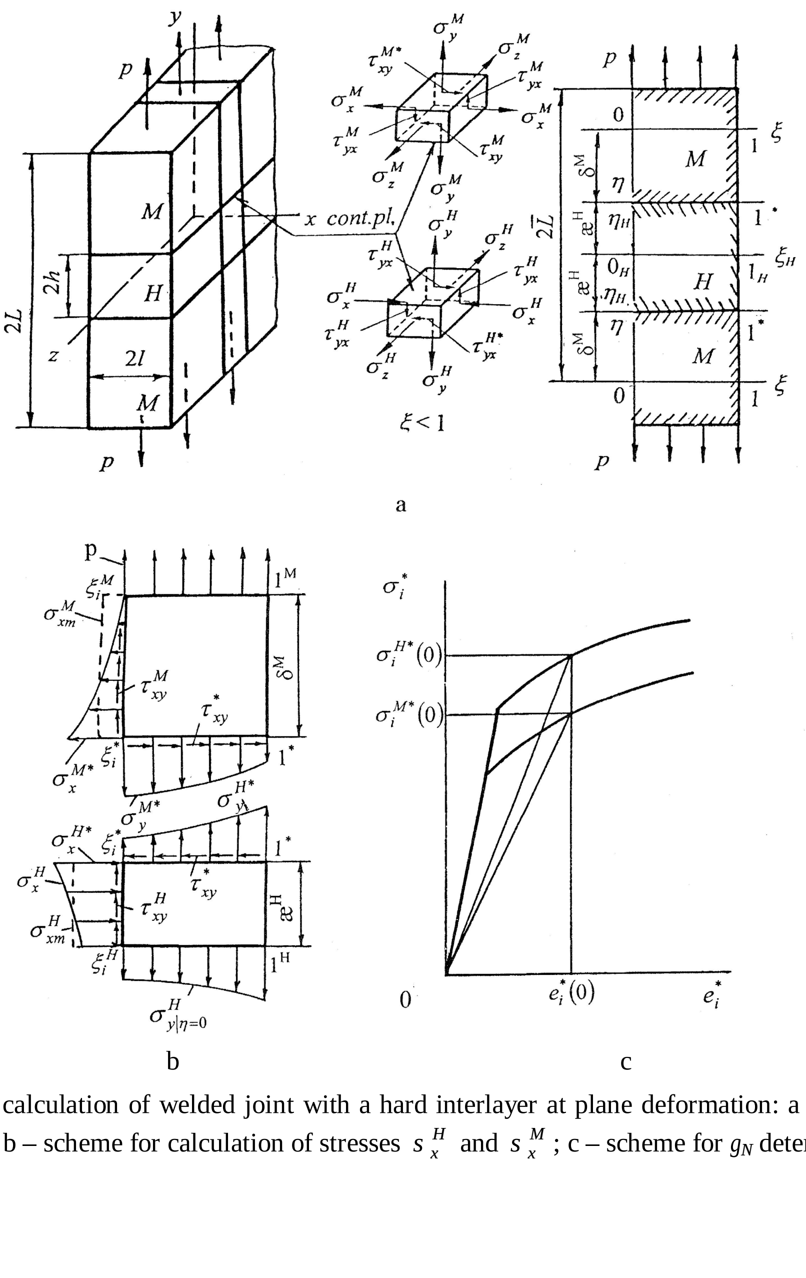

Fig. 1 Scheme for the calculation of welded joint with a hard interlayer at plane deformation: a – welded joint with a hard interlayer; b – scheme for calculation of stresses s_x^H and s_x^M; c – scheme for g_N determination

Shear stress t_{xy}^{H} in cross-section $h^{H} = const$ may be calculated from equilibrium condition

$$t_{xy}^{H} = -\int_{0}^{h^{H}} \frac{\P s_{x}^{H}}{\P x} dh^{H} + C_{2}\,, \tag{3}$$

where $C_2 = 0$ because $t_{xy\,|h^{H}=0}^{H} = t_{xy\,c}^{H} = 0$. After designating

$$\Phi\left(\eta^{H}\right) = \int_{0}^{\eta H} f_{2}\left(\eta^{H}\right) d\eta^{H} = 3\frac{\eta^{H}}{æ^{H}} \frac{1-\left[1-\frac{1}{F\left(æ^{H}\right)}\right]\left[1-\frac{1}{3}\left(\frac{\eta^{H}}{æ^{H}}\right)^{2}\right]}{1+\frac{2}{F\left(æ^{H}\right)}} \tag{4}$$

and from Eqs.(2) – (4) is calculated shear stress

$$t_{xy}^{H} = F\left(h^{H}\right) t_{xy}^{H*}(x) = pC_{p}^{*}x\,, \tag{5}$$

where pC_{p}^{*} is parameter of shear stress.

Expression of s_{x}^{H} is obtained from Eq.(1)

$$s_{x}^{H} = -\frac{1}{2} f_{2}\left(h^{H}\right) pC_{p}^{*}\left(1-x^{2}\right). \tag{6}$$

From the hypothesis of flat sections when $n = 0.5$ and metal H is deformed elastically follows that on the contact plane at plane deformation stress intensity at the point of contact plane $x^* = 0$ by estimating that $s_{i} = \sqrt{\frac{3}{4}\left(s_{y}-s_{x}\right)^{2}+3t_{xy}^{2}}$ and $t_{xy|x=0} = t_{xy}(0)$[(1)] stress s_{y}^{H*} at the contact plane, when $s_{i1}^{H*} \le s_{e}^{H}$ [(2)]

$$s_{y}^{H*} = \frac{2}{\sqrt{3}} s_{i}^{H*}(0) + s_{x}^{H*}\,. \tag{7}$$

In this case stress intensity of metals H and M at the contact plane

$$s_{i}^{*} = \sqrt{\left[s_{i}^{*}(0)\right]^{2} + 3\left(pC_{p}^{*}x\right)^{2}}\,. \tag{8}$$

Stress intensity of metals H and M at the contact plane centre, when strain intensity $e_{i}^{*}(0)$ is known, may be determined by dependence

$$\left.\begin{aligned} &s_{i}^{*}(0) = E\, e_{i}^{*}(0), && \text{when } s_{i}^{*}(0) \le e_{e}\,, \\ &s_{i}^{*}(0) = s_{e}\left(e_{i}(0)/e_{e}\right)^{m_{0}}, && \text{when } s_{i}^{*}(0) > s_{e}\,, \end{aligned}\right\} \tag{9}$$

where m_0 is characteristic of material hardening at elastic plastic zone when it tension diagram $s_i / s_e - e_i / e_e$ is approximated by power function.

When $s_{i1}^{H*} > s_{e}^{H}$ stress

$$s_{y}^{H*} = s_{x}^{H*} + \frac{2}{\sqrt{3}} s_{i}^{H*}(0) - D^{H} pC_{p}^{*}x^{2} \tag{10}$$

and stress intensity

$$s_{i}^{H*} = \sqrt{\left[s_{i}^{H*}(0) - \sqrt{3}pC_{p}^{*}D^{H}x^{2}/2\right]^{2} + 3\left(pC_{p}^{*}x\right)^{2}}\,. \tag{11}$$

---

* denotes values on the contact plane

[(1)] index (0) denotes stress strain state components when $x = 0$

[(2)] lower index 1 denotes values at the external contact plane point $x^* = 1$

When $s_{i1}^{H*} \le s_e^H$ coefficient $D^H = 0$.

Stress strain state components of metal M is calculation by dependencies presented in work [3]:

$$t_{xy}^M = F\left(h^M\right)pC_p^* x \ ; \quad s_x^M = f_2\left(h^M\right)pC_p^*\left(1-x^2\right)/2\,, \tag{12}$$

$$s_y^M = s_x^M + 2s_i^M(0)/\sqrt{3} - D^M F\left(h^M\right)pC_p^* x^2\,, \tag{13}$$

where D^M is coefficient determined from the condition $e_{y1}^{H*} = e_{y1}^{M*}$ at an external point of the contact plane x^*=1 by approaching method.

Longitudinal strain

$$\left.\begin{aligned} e_y &= \sqrt{3}\, s_i/2E, && \text{when } s_i \le e_e\,, \\ e_y &= \sqrt{3}\, s_i/2E', && \text{when } s_i > s_e\,, \end{aligned}\right\} \tag{14}$$

where $E' = E\left(s_i/s_e\right)^{(m_0-1)/m_0}$ is secant modulus of material tension curve.

The parameter of shear stresses is calculated from integral equilibrium condition

$$p = \int_0^1 s_y\, dx \tag{15}$$

written for Eqs.(10) and (12) when $h^H = æ^H$ and $h^M = d^M$. Then

$$pC_p^* = \frac{2\sqrt{3}\left(g_N - 1\right)s_i^{M*}(0)}{f_2\left(d_H\right) + f_2(æ) - \left(D^M - D^H\right)}, \tag{16}$$

where $g_N = s_i^{H*}(0)/s_i^{M*}(0)$ is coefficient of mechanical heterogeneity (Fig. 1, c); coefficient D^H = 0 when $s_{i1}^{H*} \le s_e^H$.

When $s_{i1}^{H*} > s_e^H$ coefficient

$$D^H = \left(2s_i^{H*}(0)\sqrt{\left(s_{i1}^{H*}\right)^2 - 3\left(pC_p^*\right)^2}\right)\Big/\sqrt{3}pC_p^*\,. \tag{17}$$

In this case s_{i1}^{H*} is calculated by the presumption, that potential energy of material H at point x^* = 1 under elastic and elastic plastic loading is the same. Then $s_{i1}^{H*} = s_e^{H*}\left(\overline{s}_{i\,f1}^{H*}\right)^{\frac{2m_0^H}{m_0^H+1}}$. Intensity of fictitious elastic stress $s_{i\,f1}^{H*}$, which corresponds to $e_i^*(0)$ when material H is absolutely elastic at the point and x^* = 1

$$s_{i\,f1}^{H*} = \sqrt{s_i^{H*}(0)_f^2 + 3\left(p_f C_{p\,f}^*\right)^2}\,, \tag{18}$$

where $s_i^{H*}(0)_f = g_{N\,f}\, s_i^{M*}(0)$ is intensity of fictitious elastic stress on the centre of contact plane.

Fictitious coefficient of mechanical heterogeneity $g_{N\,f} = g_e$, when $e_i^{H*}(0) \le e_e^H$ and $g_{Nf} = \left(e_i^{M*}(0)/e_e^M\right)$ when $e_i^{H*}(0) > e_e^H$. Parameter $p_f C_{p\,f}^*$ is calculated from formula (16) by substituting $g_{N\,f}$ instead of g_N.

From Eqs.(1) – (18) follows that most convenient stress components to calculation by choosing strain intensity value $e_i^*(0)$. Then parameters $s_i^{H*}(0)$, $s_i^{M*}(0)$, g_N, pC_p^*, e_{i1}^{H*} are determined by Eqs.(1) – (18) respectively. In this case mean stress p may be calculated from condition (15) by estimating Eq.(10) written to contact plane when $h^H = æ^H$. Then

$$p = \frac{2}{\sqrt{3}}s_i^{H*}(0) - \frac{1}{3}pC_p^*\left[f_2\left(æ^H\right) + D^H\right]. \tag{19}$$

Because pC_p^* depends on g_N, D^M and D^H, stress strain state components are calculated by approaching method. The determination stress and strain distribution in welded joint with a hard square simplified weld (weld without reinforcements) was chosen. It is a welded joint of steel 15Cr2MoVTi welded by automatic submerge-arc welding with the wire Sv-10CrMoVTi under the layer of flux AN-42. Mechanical characteristics of welded joints separate zones are presented in Table 1.

Stresses distribution on the contact plane of it welded joint is showed in Fig. 2 and strain e_y distribution – in Fig. 4. From Fig. 2 follows that with increasing of $\ae^H$ stress $\left| s_x^{H*}(0) \right|$ decreases and $s_x^{M*}(0)$ increases.

Table 1

Mechanical properties of investigated weld joint with a hard interlayer

Zone of welded joint		Base metal M	Weld metal H
		Steel 15Cr2MoVA	Sv-10CrMoVTi
E	MPa	$1.96 \cdot 10^5$ ($1.98 \cdot 10^5$)	$2 \cdot 10^5$ ($1.98 \cdot 10^5$)
s_e	MPa	490	550
$s_{0.2}$	MPa	534	685
s_{ut}	MPa	720	765
s_K	MPa	1510	1500
y	%	73.8	69.5
m_0	-	0.129	0.095

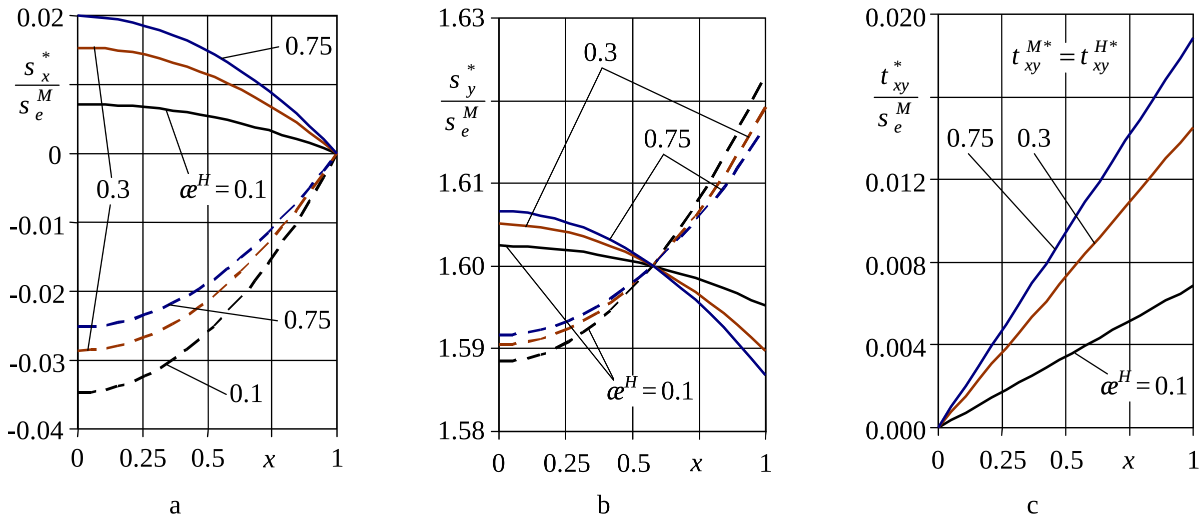

Fig. 2 Stresses distribution on the contact plane of welded joint with a hard interlayer, when $\bar{L} = 2.2$, $p = s_e^H = 785$ MPa, $g_e = 1.122$, $m_0^H = 0.095$: (———) – stresses in base mild metal; (– –) – in hard interlayer

3. Determination of a Mean Longitudinal Strain e_{ym} in Base of Deforming $\bar{L}$

The mean longitudinal strain e_{ym} in base of deforming $\bar{L} = L / l$ may be calculated from strain e_y distribution in direct of longitudinal axis (Fig. 3).

The maximum value of mild metal $e^M_{y\max}$ at strain loading (e_{ym} = const) increases with decreasing of relative base of deforming $\bar{L}$ and increasing g_N. Because solution of strain distribution on the contact plane is approximate, mean longitudinal strain e_{ym} at the base of deforming $\bar{L}$ is calculated at the longitudinal section $x = x_c = 0.5$. For longitudinal strain e_{ym} determination $\bar{L} \geq \ae^H + d^M$ of welded joint with a hard interlayer (Fig. 3, a) values of stresses $s^H_{yx_c}\big|_{h^H=0}$, $s^H_{xx_c}\big|_{h^H=0}$, $s^{H*}_{yx_c} = s^{H*}_{y|x=0.5}$, $s^{H*}_{xx_c} = s^{H*}_{x|x=0.5}$ and strains $e^H_{yc} = 3\left(s^H_{yx_c}\big|_{h^H=0} - s^H_{xx_c}\big|_{h^H=0}\right)/4E$; $e^{H*}_{yx_c} = 3\left(s^{H*}_{yx_c} - s^{H*}_{xx_c}\right)/4E$; $e^M_{yl} = e^M_{y}\big|_{h^M=0} = 3p/4E'^M\big|_{h^M=0}$ must be calculated. When $s_i^H > s_e^H$, Young's modulus E must be substituted by E'^H.

In the other cross-sections of weld joint strain e_y may be calculated from presumption that in intervals $\ae^H$ and d^M (Fig. 3, a) and $\bar{L} - h_s$ (Fig. 3, b) strain e_y is distributed by square parabola law. Then a mean longitudinal strain when $\bar{L} \geq 1.2 + \ae^H$ and $\bar{l}^M = \bar{L} - \left(1.2 + \ae^H\right)$ (Fig. 3, a)

$$e_{ym} = \frac{1}{\bar{L}}\left[e^M_{yl}\left(\bar{L} - \ae^H - \frac{1}{3}\bar{l}^M\right) + \frac{2}{3}e^H_{yc} + \frac{1}{3}e^{H*}_{yx_c}\left(\bar{l}^M + \ae^H\right)\right] \tag{20}$$

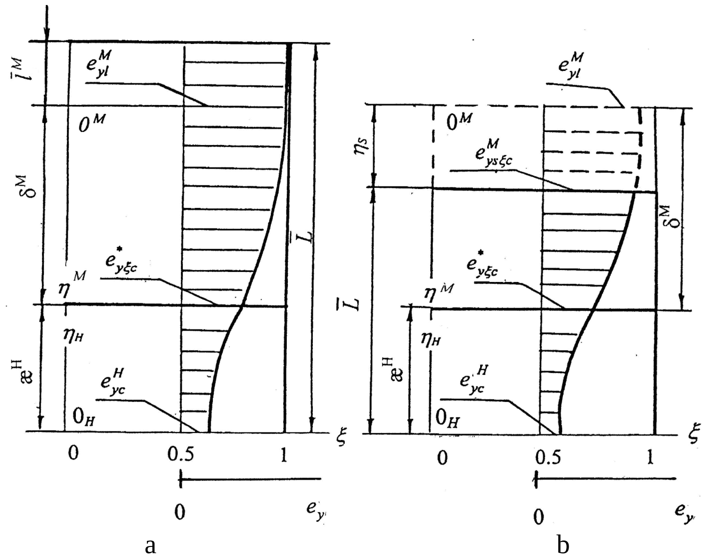

Fig. 3 Scheme for calculation of mean longitudinal strain e_{ym} in base of deforming $\bar{L}$: a – $\bar{L} = \ae^H + d^M$; b – $\bar{L} < \ae^H + d^M$

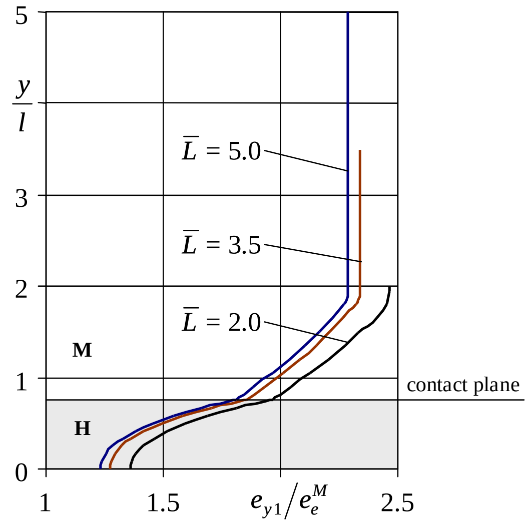

Fig. 4 Dependence of strain e_{y1} distribution on the surface of welded joint on $\bar{L}$, when $\ae^H = 0.75$, $e_{ym}/e_e^M = 2.0$

and when $\bar{L} < 1.2 + \ae^H$, $h_s = \ae^H + 1.2 - \bar{L}$

$$e_{y\,m} = \frac{1}{\bar{L}}\left[\frac{1.2-h_s}{3}\left(2e^M_{ysx_c} + e^{H*}_{yx_c}\right) + \frac{\ae^H}{3}\left(2e^H_{yc} + e^{H*}_{yx_c}\right)\right]. \qquad (21)$$

When $\bar{L} < \ae^H + d^M$ (Fig. 3, b) at the cross-section $h^M = h_s$ strain value $e^M_{ysx_c} = 3\left(s^{\,M}_{ysx_c} - s^{\,M}_{xsx_c}\right)/4E'^M_{ysx_c}$ must be determined.

Dependence of strain e_y distribution in direction of y axis in welded joint with a hard interlayer on $\bar{L}$ is showed in Fig. 4. From Fig. 4 follows that maximum values e_y appears in mild metal M at the distance from contact plane $\bar{L} - \ae^H$. Value of this strain increases with decreasing $\bar{L}$ and increasing g_N.

4. Conclusions

The most heavily loaded zones of welded joint with a hard interlayer are external point of contact plane metals H and M for a hard metal and for a mild metal at relative distance from the contact plane d^M, in which stress $s^{\,M}_{x}$ disappears. Fracture of welded joints occurs in this zone of mild metal.

Strength of welded joint with a hard interlayer subjected to tension at plane deformation is equal $p_{ut} = 1.1547 s^{\,M}_{ut}$.

Strain $e^M_{y\,max}$ at strain loading increases with increasing base of deformation $\bar{L}$.

References

1. **Бакши О. А., Шрон Р. З.** Прочность при статическом растяжении сварных соединении с мягкой прослойкой.– Сварочное производство. 1962, No.5, c.6-10. [in Russian].
2. **Шатов А. А.** О вовлечении твердой прослойки в пластическую деформацию.– Вопросы сварочного производства. – Труды Челябинского полит. ин-та, Челябинск: Изд-во Челябинского полит. ин-та, 1968, No.63, c.102-108. [in Russian].
3. **Bražėnas A., Daunys M.** The stress strain state and plasticity of mechanically heterogeneous welded joints with a flat interlayer subjected to tension (compression) // Mechanika. Kaunas: Technologija, 1995, Nr.1, p.67-75.

Methodology of Operation Multifaceted Efficiency Prognosis

A. Dervinienė

Kaunas University of Technology, Studentų st. 48-324, LT-51367 Kaunas, Lithuania, E-mail: alma.derviniene@ktu.lt

Abstract

The methodology of operation multifaceted efficiency prognosis performed by group expert is discussed in this article. The main attention is paid to the estimation of an expert decisions risk level. This rate is usable for aggregation estimations results (according many rates) performed by group expert.

The expert's decision risk level is based on consistency and transitivity of estimations (according to the type of expert subjective heuristics). Our improved methodology of identification expert subjective heuristics type is discussed in this paper.

KEY WORDS: *expert estimation, risk level, methodology.*

1. Introduction

For the estimation of any aim consummation level, for prognosis of receivable solution results and etc., not always we can find and use the analytical methods and optimisation methods based on its. Often methods based on expert estimations are used, that is, human intellect is being used as a measuring instrument. The two typical cases are possible:

1. The experts group is *large enough*.
2. The experts group consists from 2-7 persons (very frequent situation in practise).

The robust algorithms [1, 2] for data processing based on defiance of "marginal" estimations are applicable in the first case.

To apply the robust algorithms for data processing is too risky in the second case (the "marginal" estimations is not necessarily are less reliable). To know the single expert estimations risk level (the expert‘s weight [3] or competence [4, 5] coefficient) it is desirable in this case.

For estimation of expert facilities the following criterions are offered [6]:

1) *consistency* of estimation;
2) *transitivity* of estimation;
3) *availability of complex strategies.*

These criterions applicable if the excess of expert's data is obtainable. The first (consistency) criterion is usable if the expert gives the repeated estimation of the same object. Very important, that the second estimation shouldn't be under influence of the first estimation (this is requirement to methodology of the experts' data collection).

2. Estimation of Expert Decisions Consistency

The **consistency** (n) (subject to usable data) is rateable such:

1. When the expert refers tolerant intervals in $[a,b]$: first (x_{j1},x_{j2}) and repeated (y_{j1},y_{j2}) (see Fig. 1).

In that case the consistency rate is presented:

$$v_j = b_j \cdot g_j = \frac{2\left|(x_{j1},x_{j2}) \cap (y_{j1},y_{j2})\right|}{(x_{j2}-x_{j1})+(y_{j2}-y_{j1})} \times \left[1 - \frac{(x_{j2}-x_{j1})+(y_{j2}-y_{j1})}{2(b-a)}\right], \tag{1}$$

where $b_j = \dfrac{2\left|(x_{j1},x_{j2}) \cap (y_{j1},y_{j2})\right|}{(x_{j2}-x_{j1})+(y_{j2}-y_{j1})}$ is estimations conjunction rate (it is equals 1 if (x_{j1},x_{j2}) and (y_{j1},y_{j2}) are fully conjunct, or 0 – if not crossed); $g_j = 1 - \left[(x_{j2}-x_{j1})+(y_{j2}-y_{j1})\right] / \left[2\,(b-a)\right]$ show the relative precision (distinctness) of j–th expert's estimations; $|(x, y)|$ – the potency of set (x, y) (when Lebeg measure is usable $|(x, y)| = y - x$); $\cap$ – symbol of sets crossing.

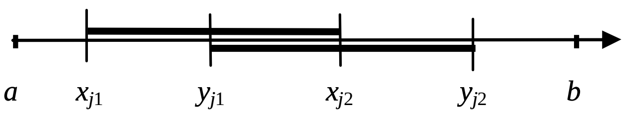

Fig. 1 Expert's referred intervals

2. When the expert refers “pessimistic”, “most reliable” and “optimistic” estimations from interval $[a,b]$. In fact, the expert gives first and repeated estimations submitted in a “triangle” membership function: $m_{j1}(x)\big|_{x\in[a,b]}$ and $m_{j2}(x)\big|_{x\in[a,b]}$.

In that case the consistency rate is presented:

$$v_j = b_j g_j = \max_{a\in[0,1]}[a \,\|(H_a(m_{j1}(x)) \cap H_a(m_{j2}(x)) \neq \varnothing] \times \left[1 - \frac{|H_0(m_{j1}(x))| + |H_0(m_{j2}(x))|}{4(b-a)}\right], \tag{2}$$

where $H_a(m_j(x))$ – a-level set of fuzzy number $m_j(x)$; $H_0(m_j(x))$ – 0–level set of fuzzy number $m_j(x)$.

3. When the expert gives fuzzy numbers submitted in a “trapezoid” membership function.
Sometimes indication of the “pessimistic”, “most reliable” and “optimistic” estimations can put a strain on expert. From psychological point of view a more convenient way is where an expert is asked to point out [3]:
1) interval (x_1, x_2), where the most typical value of the criterion is, by the opinion of an expert (Fig. 2);
2) subjective probability p, under which the expert is right.

In that case the estimation is presented:

$$X_i = ((x_1, x_2), p). \tag{3}$$

Estimation equation (3) can be changed with a trapezoid type membership function (see Fig. 2):

$$m(g) = \begin{cases} 1 + (x - x_1)\dfrac{p}{(x_2 - x_1)(1-p)}, & \text{if} \quad x \in [c, x_1], \\ 1, & \text{if} \quad x \in [x_1, x_2], \\ 1 - (x - x_2)\dfrac{p}{(x_2 - x_1)(1-p)}, & \text{if} \quad x \in [x_2, d], \end{cases} \tag{4, a}$$

$$c = x_1 - (x_2 - x_1)\frac{1-p}{p}, \qquad d = x_2 + (x_2 - x_1)\frac{1-p}{p}. \tag{4, b}$$

We can easily notice, that formula (4) is valid only if $c \geq a$ and $d \leq b$. Or else formula (4) has to be modified (see [3]).

In that case the consistency rate is presented:

$$v_j = b_j g_j = \left(\frac{2\int\limits_X (m_{j1}(x) \wedge m_{j2}(x))dx}{\int\limits_X m_{j1}(x)dx + \int\limits_X m_{j2}(x)dx} \right)^{0,5} \times \left[1 - \frac{\int\limits_X m_{j1}(x)dx + \int\limits_X m_{j2}(x)dx}{2(b-a)}\right]. \tag{5}$$

where „$\wedge$“ – membership function’s „intersection“.

3. Estimation of Expert Competence

For estimation of expert facilities the criterion of **availability of complex strategies** (that is expresses expert’s ability to generalize and aggregate available information) is very important.

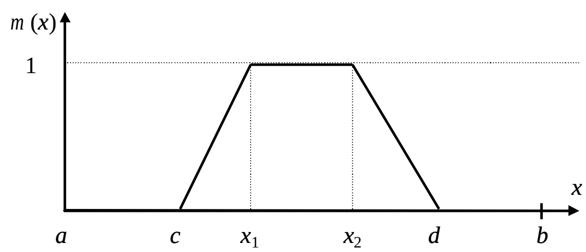

Fig. 2 Estimation submitted in a “trapezoid” membership function

This criterion is in use with **transitivity** criterion [5]. The value of complex expert's **competence criterion** (weight coefficient) is founded according to scheme (algorithm):

The set $S_i | i=\overline{1,n}$ of an object, action or process A goals is formed. The set S has to be full, but minimal; it is desirable that the goals shouldn't be overlap [7].

After interviewing of each expert such information is obtainable:

a) for estimation of each A (there A – object, action or process) goal S_i its subjective ***importance rate*** $g_i \in [0,1]$ is suggested;
b) the ***consummation rate*** h_{s_i} (further h_i) of each goal S_i is prognosticated;
c) the system (heuristics) of complex rate (criterion) e_A for aggregation of each A goal importance's and consummation's estimations is offered;
d) the e_A value by intuition (but not calculated), what further is called h_A, is proposed.

Rates $h_i|_{i=\overline{1,n}}$ and e_A have to be quantitative, that is, measurable, calculable or subjectively rateable. They mostly are presented in normal numbers, that is e_A, $h_i \in [0, 1]$.

Estimation of expert competence (availability of complex strategies and transitivity of offered estimations) is called a_j (j – it is index (name) of the expert). The expert's competence rate a_j (subject to usable data) is founded the same as consistency rate (according formulas (1) – (2), (5)) where h_A is usable instead primary estimation, e_A – instead repeated estimation. The values of h_A and e_A is available operating with data in points a), b) and c).

If the estimations of goals importance (g_i) and consummation (h_i) rates don't cause the some problems, the formalization of expert heuristics (as the way of decision search) is especially complicated task. The solution of this task in any general way should matter the formalization of human thought.

The experimentation to formalize heuristics is founded in literature (for example [8]). That is usually associated with solution of concrete problem. This also involves in the expert researches.

Such schemes of g_i and h_i estimations aggregation are mostly met [5]:

1) the expert tries to estimate average e_A of goals $S_i | i=\overline{1,n}$ consummation rate h_i;
2) for data aggregation (the evaluation of e_A value) the expert underlines the goals with high consummation rate h_i;
3) for data aggregation the expert underlines the goals with high product of importance and consummation rates $g_i\, h_i$;
4) for data aggregation the expert underline the goals with low consummation rate h_i;
5) for data aggregation the expert underline the goals with low product of importance and consummation rates $g_i\, h_i$.

Sometimes an expert can himself suggest the scheme (heuristics type) of importance and consummation rates aggregation into one complex rate (criterion) e_A. The additional test of the heuristics type identification is suggested [9].

The first scheme of estimations aggregation is mostly met and best researched. In fact – it is result of formula calculating h_i medium value:

$$e_A = \sum_{i=1}^{n} g_i h_i \,//\, \sum_{i=1}^{n} g_i \,. \tag{6}$$

Symbol "//" is sign of division. If fuzzy numbers are dividend, then instead ordinary division its adjective division is executed.

$$(GH)_a \,//\, G_a = (a_1, a_2)//(b_1, b_2) = ((a_1 : a_2),(b_1 : b_2)),\; a_1 > 0\,, b_1 > 0, \tag{7}$$

where $(GH)_a$ and G_a – a-level sets of fuzzy numbers (GH) and G that is expressed by $\sum_{i=1}^{n} g_i h_i$ and $\sum_{i=1}^{n} g_i$.

Formula (6) are applied when the goals $S_i | i=\overline{1,n}$ of A (there A – object, action or process) are independent and theirs consummation h_i estimations – additive.

Applying to this low indistinct Choquet integral, the more universal form (tolerant to interdependence of goals) can be got [10]:

$$C = \sum_{i=1}^{n} (h_i \times [\, f(S_i, \mathbf{K}, S_n) - f(S_{i+1}, \mathbf{K} S_n)]) \,, \tag{8}$$

$$f(0) = f(S_{n+1}) = 0\,; \qquad f(S_i, \mathbf{K} S_n) = 1\,; \qquad f(S_i, \mathbf{K} S_n) \geq f(S_j, \mathbf{K} S_n),\ \text{jei}\ \ j > i\,, \tag{9}$$

where $f(S_i, ..., S_n)$ – indistinct measure of goals ($S_i, S_{i+1}, ..., S_n$) importance, when conditions (9) is supplied.

The expert has to form estimations $f(S_i, ..., S_n)$ according to test values g_i. In the simple case

$$f(S_i, \mathbf{K}, S_n) = \frac{1}{\sum_{z=1}^{n} g_z} \sum_{z=i}^{n} g_z. \tag{10}$$

Formula (8) is other notation of formula (6). For description (formalisation) all others schemes of an expert estimations g_i and h_i aggregation into one complex rate e_A is recommendable to apply parameter g_l and Sugeno integral based on it [9, 10].

The point of method is such when fuzzy set is given:

$$B = h_1 / g_1 + h_2 / g_2 + \mathbf{K} + h_n / g_n, \tag{11}$$

where $0 \le g_i \le 1$, it is possible to define for it (for set B) parameter g_l, whose rating parameter l must supply condition

$$-1 < l < \infty \tag{12}$$

and can be finding as follows:

$$\frac{1}{l}\left[\prod_{i=1}^{n}(1 + l g_i) - 1\right] = 1 \tag{13, a}$$

(in the case of second aggregation scheme) or

$$\frac{1}{l}\left[\prod_{i=1}^{n}(1 + l g_i h_i) - 1\right] = 1 \tag{13, b}$$

(in the case of third aggregation scheme).

The Sugeno integral of discreet fuzzy set (11) is expressed:

$$S = \sup_{a \in [0,1]} \min\{a; g_a) . \tag{14}$$

Using parameter g_l, g_a in (14) is as follows:

$$g_a = \frac{1}{l}\left[\prod_{i|h_i \ge a}^{n}(1 + l g_i) - 1\right] \tag{15, a}$$

(in the case of second aggregation scheme) or

$$g_a = \frac{1}{l}\left[\prod_{i|g_i h_i \ge a}^{n}(1 + l g_i h_i) - 1\right] \tag{15, b}$$

(in the case of third aggregation scheme).

In all cases the complex rate e_A is expressed:

$$e_A \rightarrow S. \tag{16}$$

If goals with low consummation rate h are meaning (fourth and fifth aggregation schemes), then accented not goal consummation but its *unconsummation level.* So instead estimations $h_{i\,|\,i=\overline{1,n}}$ in formulas (15, a) and (15, b) we need to use theirs inversion $1 - h_{i\,|\,i=\overline{1,n}}$, g_a is as follows:

$$g_a = \frac{1}{l}\left[\prod_{i|(1-h_i) \ge a}^{n}(1 + l g_i) - 1\right] \tag{17, a}$$

(in the case of fourth aggregation scheme) or

$$g_a = \frac{1}{l}\left[\prod_{i|(1-g_i h_i)\geq a}^{n}(1+l g_i h_i)-1\right] \tag{17, b}$$

(in the case of fifth aggregation scheme).

Integral (14) express the complex right estimation of goals *unconsummation* (e_A inversion), applying formulas (17). To get the estimation of complex rate (criterion) e_A, enough to have inversion value of formulas (17) and (14):

$$e_A \to S = 1 - \sup_{a\in[0,1]} \min\{a\,; g_a\,). \tag{18}$$

As we have already mentioned, the expert's competence rate a_j (subject to usable data) is founded the same as consistency rate (according formulas (1) – (2), (5)) where h_A is usable instead primary estimation, e_A – instead repeated estimation.

When the expert refers h_A and e_A as tolerant intervals in [a, b], so:

$$a_j = b_j g_j = \frac{2\left|(h_{j1},h_{j2})\cap(e_{j1},e_{j2})\right|}{(x_{j2}-x_{j1})+(y_{j2}-y_{j1})}\times\left[1-\frac{(h_{j2}-h_{j1})+(e_{j2}-e_{j1})}{2(b-a)}\right]. \tag{19}$$

When the expert refers h_A and e_A "pessimistic", "most reliable" and "optimistic" estimations from interval [a, b], so:

$$a_j = b_j g_j = \max_{a\in[0,1]}[a\,\|(H_a(h_j(x))\cap H_a(e_j(x))\neq\varnothing]\times\left[1-\frac{\left|H_0(h_j(x))\right|+\left|H_0(e_j(x))\right|}{4(b-a)}\right]. \tag{20}$$

When the expert gives h_A and e_A submitted in a "trapezoid" membership function, so

$$a_j = b_j g_j = \left(\frac{2\int_X (h_j(x)\wedge e_j(x))dx}{\int_X h_j(x)dx+\int_X e_j(x)dx}\right)^{0,5}\times\left[1-\frac{\int_X h_j(x)dx+\int_X e_j(x)dx}{2(b-a)}\right]. \tag{21}$$

The formulas (19) ... (21) are „compatible", i.e. estimations from different experts can be comparable or otherwise processing (for example, searching of its average) even if experts operate different types of data (estimations in the real numbers intervals, estimations submitted in a "triangle" membership function, estimations submitted in a "trapezoid" membership function). Because estimation in the real numbers intervals can be interpreted as a "rectangular" membership function of estimations (as an instance of estimations submitted in a "trapezoid" membership function). The "triangle" membership function is the partial case off "trapezoid" membership function.

4. Generalization of Group Experts' Estimations

The complex indistinct group expert estimation of an object, process or action A is characterized by:

$$H_{A1}(x) = \frac{1}{\sum_{j=1}^{k} a_j}\sum_{j=1}^{k} a_j h_{jA}(x) \tag{22, a}$$

or

$$H_{A2}(x) = \frac{1}{\sum_{j=1}^{k} a_j}\sum_{j=1}^{k} a_j e_{jA}(x) \tag{22, b}$$

or (on purpose to use all available information)

$$H_A(x) = \frac{H_{A1}(x)+H_{A2}(x)}{2}\,. \tag{23}$$

The consistency rate v_j of expert opinion instead of his competence rate a_j can be applied.

6. Conclusions

For the decision-making based on expert researches the risk level dependent on expert's facilities (defined with the consistency and competence criterions) must be known.

To get the upper reliability of operation prognosis it is desirable to use the group expert researches based on single expert facilities evaluation.

The classical method of robust decisions search based on elimination of "extreme" estimations is too risky when number of experts is not enough big.

The expert's competence rate can be founded applying excess of the experts offered information.

For estimation of an expert competence rate, identification of the right scheme (heuristics) of this expert subjective partial estimations aggregation into one complex rate (criterion) is very important.

The mostly met schemes of partial estimations aggregation into one complex rate (criterion) can be described with fuzzy integrals.

References

1. **Shrestha G. B.**, **Rahman S.** A Method to Estimate the Reliability of Expert Judgement. // Southeastcon '89. Proceedings of IEEE Conference "Energy and Information Technologies in …" 9-12 April 1989. – p. 152-157.
2. http://ieeexplore.ieee.org/iel2/804/3643/00132348.pdf
3. **Puškorius S.** Risk Assessment of Decisions Making // Public policy and Administration. Kaunas: Technologija, 2006. No 16. p. 46-52.
4. **Švėgžda O.**, **Magyla T.** Trapezoid Membership Functions in Inference Mechanizm // Electronics and Electrical Engineering. Kaunas: Technologija, 2002.- No 4(39). p. 66-69.
5. **Voloshin A.F.**, **Antosiak P.P.** Problems of corporate socially essential decision making (Проблемы принятия коллективных социально-значимых решений) // Proceedings of XII-th International Conference „Knowledge-Dialogue-Solution", Varna (Bulgaria), 20-25 June 2006.- P. 153-157.
6. **Bagdonas V.**, **Daunoras J.**, **Dervinienė A.** Methodology of Operation Efficiency Prognosis // Electronics and Electrical Engineering. Kaunas: Technologija, 2006. No 5(69).- p. 95-98.
7. **Larichev O.I.** Decision Making as a Research Branch: Methodological Problems, 7 p.
8. http://www.raai.org/library/papers/Larichev/Larichev_1985b.pdf
9. **Keeney R.**, **Raifa H.** Decisions with Multiple Objectives: Preferences and Value Tradeoffs. New York:Wiley, 1976. 600 p.
10. **Tsarkov D.**, **Horrocks I.** Ordering Heuristics for Description Logic Reasoning // Proceedings of International Joint Conference of Artificial Intelligence 2005", Edinburg, Scotland, 30 July – 5 August 2005. p. 609-614.
11. http://www.ijcai.org/papers/1352.pdf
12. **Dubois D.**, **Marichal J. L.**, **Prade H.**, **Roubens M.**, **Sabbadin R.** The Use of the discrete Sugeno integral in Decision Making: A Survey // International Journal of Uncertainty Fuzziness and knowledge-based systems. 2001. Vol. 9. p. 539-561.
13. **Grabisch M.** The application of fuzzy integrals in multicriteria decision making // European J. of Operational Research. 1996, vol. 89, p. 445-456.

Proceedings of 3rd international Workshop ITELMS'2008

Detection of the Flying Objects and Radar System Modeling

A. Pincevičius*, V. Kleiza**

* *Military Akademy of Lithuania, Šilo str. 5a, LT-10322 Vilnius, E-mail: pincev@cablenet.lt*
** *Institute of Mathematics and Informatics, Akademijos st. 4, LT-08663 Vilnius, Lithuania, E-mail: vytautas.kleiza@ktl.mii.lt*

Abstract

The scheme of the dislocation of 3D radars is proposed and detection process of a flaying object is discussed in this paper. The formulae for the evaluation of the probability of detection of a flaying object in case of surveillance by one radar or radar system proposed. The cases, when the probabilistic density of the detection of a flaying object expressed by normal distribution or Relay distribution (in case of bad meteorological conditions) are discussed. The quantitative estimation of the detection system with concrete parameters carried. The results of the calculation allow estimate efficiency of the surveillance system. Method of calculations can bee used for study process or for the estimation of the systems of detection of a flying object.
KEY WORDS: *radar system, Poisson process, probability of the detection.*

1. The process of the detection of flying object

In order to ensure the reliability of the surveillance of some airspace zone, we suggest dislocating the 3D radar stations following the scheme indicated in Fig. l. We will investigate the most unfavorable case for the detection system that is the case when we have the least time for the detection of a flying object. In this case we must choose the parameters of the radar station in such a manner that the object be detected with the desirable probability within a definite distance. The possibility of the detection of the object depends not only on the properties of the radar. It depends on the meteorological conditions, the parameters of the object, properties of the reflection and on possible hindrances.

In practice radar activity is characterized by the momentary probability of the detection of a flying object (that is the probability of detection during one observation) [1]:

$$g = \frac{1}{\overline{n}(r)}, \tag{1}$$

here $\overline{n}(r)$ is the mean number of the observations necessary for detecting an object within a certain distance (evidently under certain meteorological conditions and with standard properties of flying objects). This quantity may be determined by experiment in each specific case.

The Queuing Theory will be utilized for the theoretical evaluation of this probability. During the process of the detection of a flying object all conditions of Poisson process are satisfied: stationarity, ordinariness and independence of events. In this case the probability of the "capture" at least one object may be written so:

$$P(t) = 1 - e^{-lt}, \tag{2}$$

here l is intensity of the flow (the number of demands during the unit of time).

One of the most important factors determining the probability of detection is the distance to the flying object. The probability $P(r)$ that is the probability of the "capture" of a flying object in the distance r may be presented by the formula [1]:

$$P(r) = 1 - e^{-j(r)}, \tag{3}$$

where $j(r)$ is the so-called "potential of detection". The variable g is connected with the derivative of the potential of detection $f(r) = \frac{dj(r)}{dr}$, that describes the intensity of the detection of the objects [1]:

$$g = 1 - e^{-f(r)v\Delta T}, \tag{4}$$

We denominate v as velocity of the flying object, ΔT as period of observation, because flying objects are most frequently observed by the instrument working in an impulse regime and within periods of certain duration.

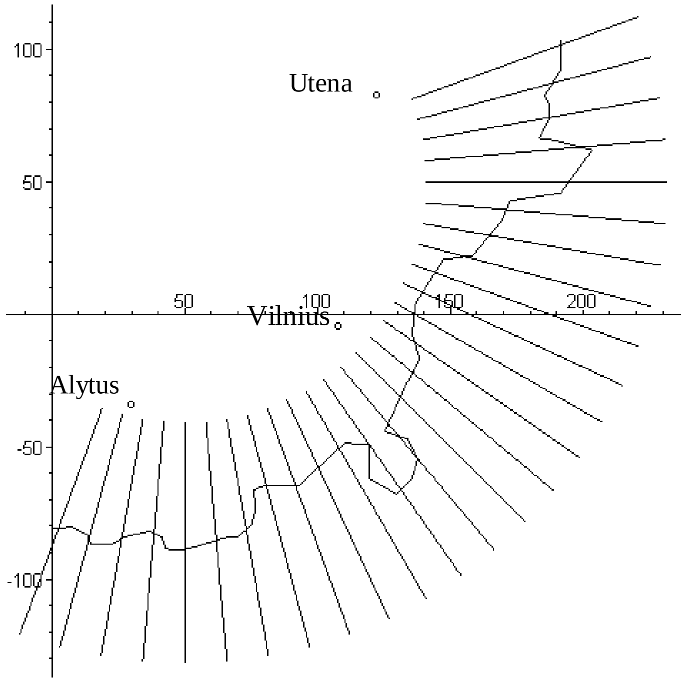

Fig. 1 Chosen paths of the moving object

2. Estimation of probability of the detection of a flying object

In many cases the probability of the detection of a flying object may be expressed by normal distribution:

$$P(r) = \int_0^r p(r)dr = \frac{1}{\sqrt{2p}\, s_r} \int_0^r e^{-\frac{(r-r_a)^2}{2s_r^2}} dr\,, \tag{5}$$

where $p(r)$ is a probabilistic density of the flying object detection, r_a is mean distance within which a flying object is detected, s_r is mean square deviation (the error of r_a).

We get from (3):

$$j\,(r) = -\ln(1 - P(r))$$

and

$$f(r) = \frac{P^{/}(r)}{1-P(r)} = \frac{p(r)}{1-P(r)}. \tag{6}$$

In case when the efficiency of the radar station is low, for example due to bad meteorological conditions, Relay distribution can be applied. In this case the density of the probability distribution is written:

$$p(r) = \frac{r}{s_r^2} e^{-\frac{r^2}{2s_r^2}}. \tag{7}$$

For the numerical evaluation of the radar surveillance system it is necessary to know some principal parameters of radar station and the flying object. For example [2, 3]:

- mean distance of the detection of the object - r_a=150 km,
- the rate of the turn of the antenna - 6 times per minute,
- distinguishing might to the azimuth - $\Delta a = 3^0$,
- the speed of the flying object v = 330 m.

The mean square deviation may be estimated by the formula (see [1]):

$$s_r = \frac{1}{6}(k_1^{/} k_2^{/} k_3^{/} - k_1^{//} k_2^{//} k_3^{//}) r_a, \tag{8}$$

here coefficients $k_i^{/}$ and $k_i^{//}$ enable us to take meteorological conditions, properties of the radar and character of the target into account.

Coefficients $k_i^{/}$ correspond to the best estimations (from 1 to 1.5) and $k_i^{//}$ - to the worst ones (from 0.5 to l). If we appreciate the activity of radar under normal conditions, we apply normal distribution and we take such mean values of coefficients:

$$k_1^{/} = 1.1 \div 1.2\,,\ k_2^{/} = 1.1 \div 1.2\,,\ k_3^{/} = 1.1 \div 1.2\,,\ k_1^{//} = 0.8 \div 0.9\,,\ k_2^{//} = 0.8 \div 0.9\,,\ k_3^{//} = 0.8 \div 0.9\,.$$

We obtain the mean quadratic deviation in interval $0.1\, r_a \leq s_r \leq 0.2\, r_a$, therefore in further calculus in case of normal distribution we shall take the value of mean quadratic deviation s_r^{n} equal to $s_r^{n} = 0{,}1\, r_a$.

In case of very bad meteorological conditions, it is necessary to apply the Relay distribution and evaluate the activity of the radar station using boundary scale numbers:

$$k_1^{//} = 0.5\,,\ k_2^{//} = 0.5\,,\ k_3^{//} = 0.5\,.$$

In this case the mean quadratic deviation will be: $s_r^{R} = 0.25\, r_a$.

Keeping in mind that the radar antenna turns round in about 10 s, in every rotation each angle of observation $\Delta a = 3^0$ can be "seen" during $\frac{1}{12} \approx 0.083$ s, that is the period of observation $\Delta T \approx 0.083$ s. During this time the observed object with the velocity of movement v = 330 m/s flies no more than 28 m. We can consider its distance from the radar during the period of observation equal to constant because that distance is not less than 50 km and. error is negligible.

The flying object may be observed within the distance r about 50 - 200 km from the radar station and can be "seen" $n = 150/(0.33 \times 10) \approx 46$ times (antenna turn around within 10 s).

If the probability of the detection of flying object in one observation is equal to g, then the probability for one radar to detect the object within the interval of observation $\Delta r \approx 150$ km, that is to detect at least once in n experiments may be written so (every "capture" is an independent event and the probability of an opposite event is equal to $1 - g_i$:

$$P_n = 1 - (1 - g_1^1)(1 - g_2^1)...(1 - g_n^1). \tag{9}$$

In the case a few radar stations try to "capture" the flying object, the exact formula of detecting the object is equal to:

$$g = g^1 + g^2 + .. , \tag{10}$$

where g^i stands for the probability of detecting the object by one radar. Now we will carry out the numerical evaluation of the investigated surveillance system.

3. The results and discussion

We shall evaluate the probability of the detection of a flying object in case the air space surveillance system consists of three uniform radar stations which schema is represented in Fig. 1. The graphs of probabilistic density of the detection of a flying object are presented in Fig. 2. In Fig. 3 one can see the dependence of instantaneous detection probabilities on the distance.

The graph visually shows that the probability of the detection of a flying object very strongly depends on meteorological conditions. Further, by using formulae (9) and (10) detection probabilities when the object moves along the trajectories indicated in Fig. 1 and all three radars are in action can be found. The results of this calculus (probabilistic fields) are exposed in Fig. 3 (normal distribution) and Fig. 4 (Relay distribution). We see that in case of Relay distribution the probability of the detection of a flying object is less by one order comparing with normal distribution case. For practical use we recommend the figures where the equipotential lines of the probabilities of detection are represented. (see Fig. 5).

We observe that in case of favorable air conditions the probability of detection amounts to 45%. The dislocation of equipotential lines is also usable, that is the dislocation of radar stations is usable. In order to achieve better parameters of the detection system more radar are necessary, especially under poor meteorological conditions.

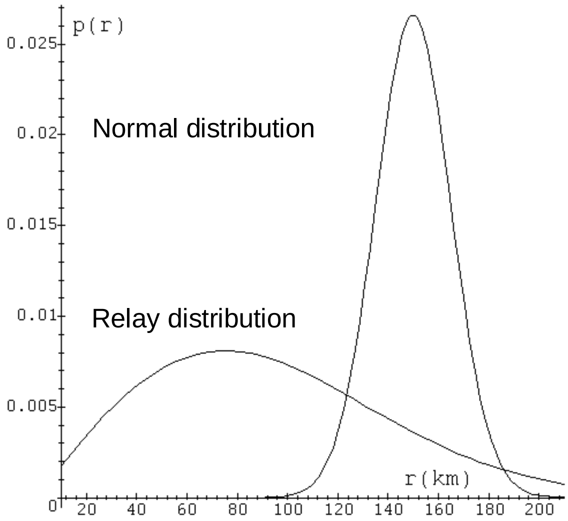

Fig. 2 Dependence of the probability density of the detection of a flying object on its distance from the radar: normal distribution $s_r^n = 0.1\, r_a$, Relay distribution $s_r^R = 0.25\, r_a$

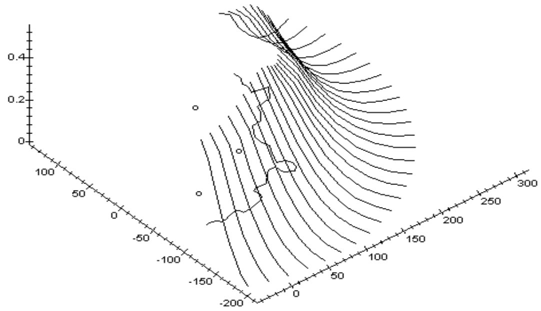

Fig. 3 The probability of detecting a flying object. normal distribution in this case: r_a=150 km, $s_r = 0.1 \cdot r_a = 15$ km

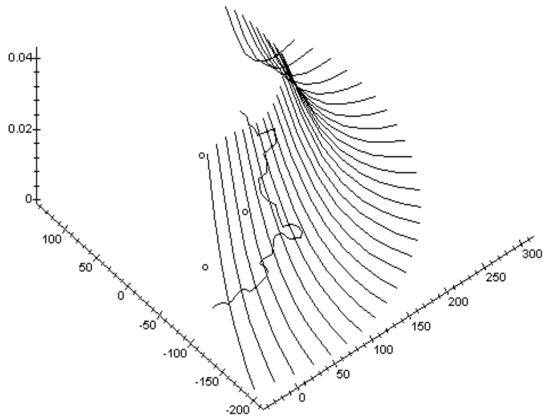

Fig. 4 Probability of detecting of the flying object by a radar system. Relay distribution in this case: r_a=150 km, $s_r = 75$ km

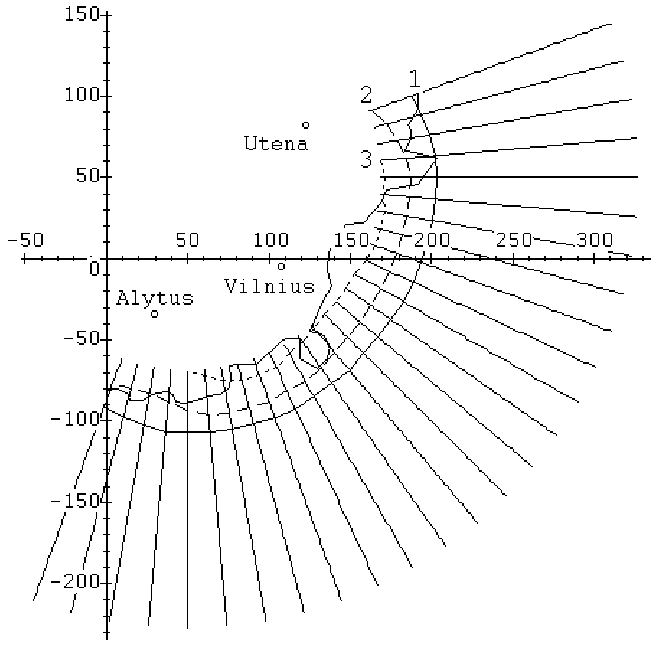

Fig. 5 Probability of detecting a flying object by a system of radars (normal distribution). Equipotential lines: P = 0.25 (curve 1), P = 0.35 (curve 2), P = 0.45 (curve 3)

4. Conclusions

Detection process of a flaying object is discussed and the scheme of the dislocation of 3D radars is proposed in this paper. Quantitative estimation of such a system is carried out by taking technical characteristics of radars and meteorological conditions into account. The probability of the detection of flying object in some fixed distance by radars system is calculated and diagrams of probabilistic fields are drawn.

The created programs may be applied for the estimation of detection systems of flying objects, selection of radar parameters, their quantity and dislocation. They are usable for designing of such systems. Method of calculations can bee used for study process.

References

1. **Горбунов В. А.** Эффективность обнаружения целей.-Москва: Воениздат, 1979.- 160 с., [in Rusian].
2. Encyclopedia of Modern U.S. Military Weapons /Ed. By W.J.Boyne. The Army Times publishing Company, 1995. 499 p.
3. **Schlesinges R. J.** Principles of Electronic Warfare, Prentice **-** Hall, Inc., New Jersey, 1961. 315 p.
4. **Pincevichius A.**, **Rakauskas R. J.** Skraidančio objekto geografinės padėties nustatymo radiolokacijos priemonėmis optimizavimas, Aviacija, Nr. 6, 2002, p. 74 – 78, [in Lithuanian].

Proceedings of 3rd International Workshop ITELMS'2008

Correlation Between Cleavage Stress of the Heat – Resistant Steel and Type Preliminary Plastic Deformation

P. Yasniy*, I. Okipny, V. Hutsaylyuk*****

* *Ternopil State Technical University, Ruska str. 56, 46001, Ternopil, Ukraine, E-mail: yasniy@networkacad.net*
** *Ternopil State Technical University, Ruska str. 56, 46001, Ternopil, Ukraine, E-mail: kafmat@tu.edu.te.ua*
*** *Military University of Technology, Gen. S. Kaliskiego str. 2, 00-908, Warsaw, Poland, E-mail: v.hutsaylyuk@wme.wat.edu.pl*

Abstract

The effect of the preliminary plastic and cyclic elasto – plastic deformation on the heat – resistance 15Cr2MFA steel cleavage stress in two structural states, which simulate the radiation embrittlements, in the middle and at the end of the operating time of the WWER – type nuclear reactor body. Steel preliminary plastically deformed by the static and combined tension in both structural statuses.. The dependences of a cleavage stress and character of its change from a type preliminary deformation. In a case combined deformation is show decrease of magnitude of cleavage stress.

1. Introduction

Preliminary elasto – plastic deformation causes not only the change of the materials mechanical properties, but effects greatly the brittle fracture resistance [1, 2], impact strength [3], ductile-brittle transition [4]. Fracture toughness under static loading after preliminary elasto - plastic loading can be increased, decreased or changed non – linear depending on the temperature, preliminary elasto - plastic deformation (PPD) range, etc. As the brittle fracture resistance depending on the PPD and the temperature is described due to the local fracture criteria, cleavage stress σ_{cl} can be used as this criterion. In papers [5-7] the analyses of results testify that PPD can increase or decrease the cleavage stress depending on the type of loading (quasi - static, cyclic) and the kind of deformation (tension, pressing).

But the problem of effect of the preliminary combined deformation containing static and cyclic component on the cleavage stress is not studied good enough.

The objective of the work is to investigate the effect of the preliminary deformation type on the cleavage stress σ_{cl} of the 15Cr2MFA heat - resistant steel, which simulates the radiation embrittlements in the middle and at the end operating time of the nuclear reactor body.

2. Testing Procedures

Investigations were carried out at the servo - hydraulic testing machine STM-100 controlled by the personal computer. Characteristics of the mechanical properties and cleavage stress were found under single tension of smooth cylinder specimens. To investigate the effect of the cyclic elasto – plastic deformation on the cleavage stress 5 mm and 20 mm diameter working area specimens were used. 8 mm and 5 mm diameter working area specimens with the 20 mm working part length were used for the investigation of the preliminary plastic deformation effect.

The specimens were tested is two structural states which simulate the radiation embrittleness in the middle and at the end of the operating time of the WWER – type nuclear reactor body.

Chemical composition as well as the mechanical properties characteristics of the tested steels are presented on the Table 1 [8].

One series of specimens made of 15Cr2MFA(III) and 15Cr2MFA(II) steel was preliminaries plastically deformed under tensile stress and combined tensile stress (unaxial tension with low-amplitude cyclic component) up to

Table 1

Chemical composition, mechanical properties of the 15Cr2MFA steel

Material, composition, %	*T*, K	s_y	s_u	*d*	*y*
		MPa		%	
Steel 15Cr2MFA(II) 0.18C; 0.62Mo; 0.27Si; 0.29V; 0.48Mn; 2.58Cr; 0.019S; 0.16Ni; 0.013P; 0.011Ti	293	900	1000	15.8	39.2
	453	750	826	8.5	23.0
	573	653	694	11.7	36.0
Steel 15Cr2MFA(III) Chemical composition the same	293	1100	1160	16.6	67.2
	473	956	1016	15.6	67.2
	623	880	970	15.2	54.0

the plastic deformation e_{pr} = 0.5%; 1.0%; 3.0% with 423…623 K temperature range. stress range under combined tension of 15Cr2MFA(III) steel was Ds = 90 MPa at the temperature 423 K and Ds = 110 MPa at the temperature 623 K with the loading frequency f = 25 Hz. Specimens made of 15Cr2MFA(II) steel were preliminary deformed up to the plastic deformation e_{pr} = 1.0% and 3.0% at the temperature 623 K under the tensile and combined tensile stress, stress range being Ds = 110 MPa and 220 MPa, loading frequency f = 25 Hz. To localize the fracture zone on the specimens made by 15Cr2MFA(II) steel 0.5 mm radius concentrator was cut after plastic deformation.

Another series of specimens made of 15Cr2MFA(III) steel was cyclically elasto – plastically deformations at the room temperature. Under the cyclic loading the range of the elasto – plastic deformation was: e_a = 0.46%; 0.6%; 0.8% under the relative operating time $\overline{N} = N/N_T$ = 0.25 … 0.75; $e_a = e_{max} - e_{min}$ correspondingly N_T is number of cycles before crack initiation.

In Fig. 1 the schemes of the preliminary plastic and cyclic elasto – plastic deformation of specimens are presented.

Investigation of the cyclic elasto – plastic deformation regularities was carried out under the strong loading cycle in the symmetric cycle $R_e = e_{min} / e_{max} = -1$. Here e_{min}, e_{max} – the smallest and the largest elasto – plastic cycle deformation correspondingly. Loading frequency was chosen when self – heating was not available and equaled 0.25 Hz.

The strength and linear strain was controlled while testing. Investigation results were tape – recorder and processed with the help of programs realized in MathCAD. Simultaneously for visual control diagrams registration on the double – axis automatic recorder in the coordinated “strength – linear deformation”.

Cleavage stress s_{cl} of the original and deformed material was found at the temperature 77 K. With this purpose the specimens were located into the thermoisolated champers filled with the liquid nitrogen [9]. During the testing the current value of P and the rod displacement Dl was registered on the tape – recorder and on the double – axis automatic potentiometer of the H110 type. In all cases the diagrams P - Dl were of the linear character before fracture. Cross, residual macroscopic deformation was not available.

It should be stressed, that the testing results were considered to be correct when they were obtained on the specimens the brittle fracture of which was on the specimen working area within the measuring base.

Fig. 2 shows dependence of the cleavage stress s_{cl} on the preliminary plastic deformation under tension and combined tension at the deformation temperature 423 K and 623 K.

Fig. 2 testifies that at the temperature 423 K under the preliminary plastic strain up to 0.5% the cleavage stress s_{cl} is being decreased as compared with the virgin material. Further increase of the plastic strain up to 3.0% causes the increase of the cleavage stress of the 15Cr2MFA(III) steel for both kinds of temperature. It should be noted, that the value of the cleavage stress is greater at the deformation temperature 623 K both under tension and combined tension as compared with that of deformation temperature 423 K. For both temperatures greater values of cleavage stress s_{cl} as compared with the combined preliminary plastic strain under the preliminary plastic tensile deformation were obtained.

Fig. 3 shows the dependence of the effect of the PPD under tension and combined tension on the cleavage stress s_{cl} of 15Cr2MFA(III) steel.

When stress range under the combined tension and similar preliminary plastic strain increases, the cleavage stress s_{cl} increases insufficiently as compared with that of the virgin material, it being more sufficient when e_{pr} = 1.0% (Fig. 3). Further increases of PPD causes some decrease of cleavage stress, but it remains to be greaten than that in the virgin material. It should be taken into account that cleavage stress at PPD 3.0% under tension is greater than that under the combined tension.

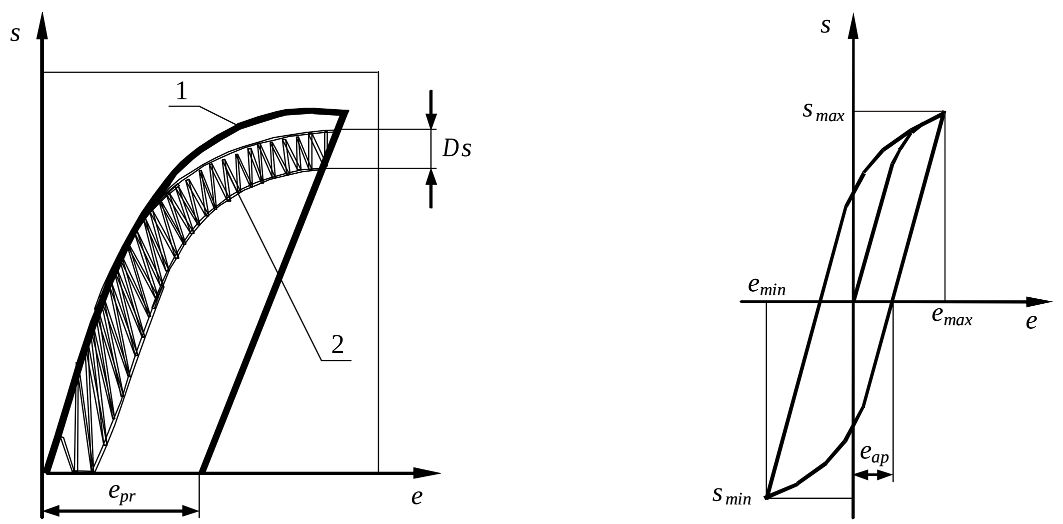

a b

Fig. 1 Schemes of the preliminary plastic deformation: a – tension (1) and combine tensile (2); b – cyclic elasto-plastic deformation

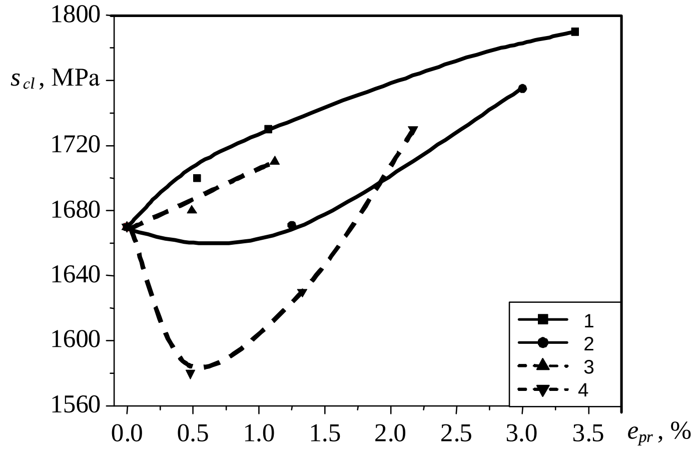

Fig. 2 Dependence of cleavage stress s_{cl} of 15Cr2MFA(III) steel from the preliminary plastic strain under tension (1, 3) and combined tension (2, 4) at 623 K (1, 2) and 423 K (3, 4) and Ds = 110 MPa (1, 2), Ds = 90 MPa (3, 4)

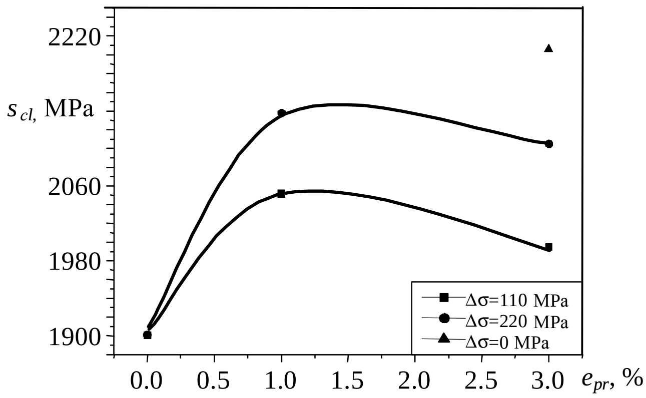

Fig. 3 Dependence of the 15Cr2MFA(II) steel cleavage stress s_{cl} on the level of the preliminary plastic strain under tension or combined tension at 623 K

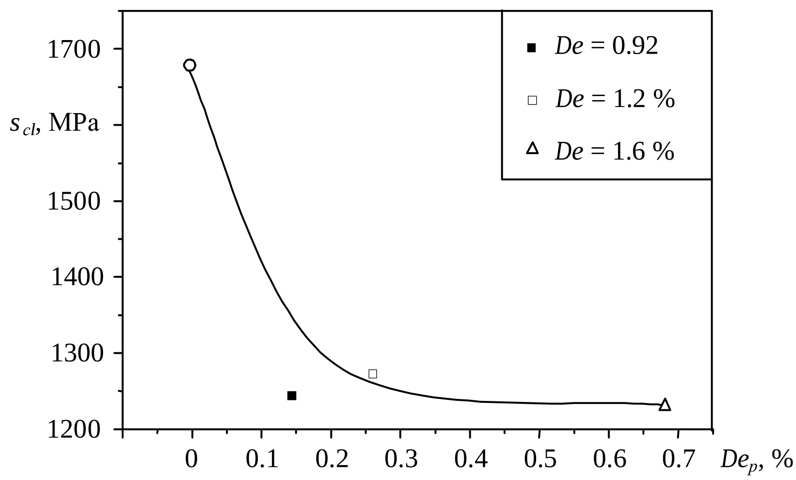

Fig. 4 Dependence of 15Cr2MFA(III) steel cleavage stress on the strain range

In Fig. 4 dependence of stress range effect on the cleavage stress under cyclic elasto-plastic strain in 15Cr2MFA(III) steel is presented.

The greater stress range under the cyclic elasto-plastic strain, the less is the cleavage stress of 15Cr2MFA(III) steel (Fig. 4).

3. Conclusion

Increase of the preliminary plastic strain at 423 K and 623 K causes the increase of the 15Cr2MFA(III) steel cleavage stress. Under both preliminary tension and combined tension the cleavage stress increases more sufficiently after deformation at 623 K than that at 623 K.

Under the combined tension up to the plastic strain 0.5% at 423 K, the cleavage stress decreases as compared with that of the virgin material. But the further increase of the 15Cr2MFA(III) steel preliminary plastic deformation causes the increase of the cleavage stress as compared with the virgin material. But in all cases the cleavage stress under the combined tension is less than that after the preliminary tensile deformation.

The increase of the preliminary plastic strain under both tension and the combined tension was found to cause the increase of the 15Cr2MFA(II) steel cleavage stress as compared with the virgin material. It should be pointed out that cleavage stress under tension are higher than those under the combined tension.

The increase of the strain range under the cyclic elasto-plastic deformation causes the increase of the 15Cr2MFA(III) steel cleavage stress.

References

1. **Troshchenko V.T.**, **Krasovsky A.Y.**, **Synyavsky D.P.** The effect of the loading cycle deformation and asymmetry history on the VT9 alloy cyclic fracture toughness characteristics // Problems of strength. 1982. No. 12. p.3-6. [in Russian].
2. **Troshchenko V. T.**, **Krasovsky A. Y.**, **Synyavsky D. P.** The effect of the fracture history on the VT9 alloy cyclic fracture toughness characteristics // Problems of strength. 1982. No. 4. – p. 28-32. [in Russian].
3. **Paris P.C.**, **Gomez M.P.**, **Anderson W.E.** A ration analytic theory of fatigue // The Trend in Engineering the University of Washington. 1961.vol. 13, No. 1 p. 9-14.
4. **Troshchenko V. T.**, **Pokrovsky V. V.** The effect of the loading cyclisity on the steels crack resistance characteristics. Report 2 // Problem of strength. 1980. No. 12. p.14-17. [in Russian].
5. **Karzov G. P.**, **Margolin B.Z.**, **Shvetsova V. A.** Physical-mechanical modeling of the fracture processes. St-Peterburg: Politechnika, 1993. 391 p. [in Russian].
6. **Troshchenko V. T.**, **Pokrovsky V. V.** and **Kaplunenko V. C.** The prediction of the crack fracture toughness of thermostable steels with allowance for effect of the specimens sizes. Communication 1. The outcomes of experimental investigation // Problem of strength. 1997. No. 1. p. 5-20. [In Russian].
7. **Roman I.**, **Ono Kanji.** Model for fracture toughness alteration due to cyclic loading // Int. J. of Fract. 1982. No. 19. p. 67-80.
8. **Pokrovsky V. V.**, **Ivanchenko A. Y.** The effect of the preliminary thermo – mechanical loading regimes on the increase of the brittle fracture resistance of the heat – resistant steels // Problems of strength. 1999. No. 2. p.126-128. [in Russian].
9. **Yasniy P. V.**, **Hutsaylyuk V. B.** The effect of the cyclic elasto – plastic deformation on the fracture mechanism and the cleavage stress of the heat – resistant steel // Visnyk of the Zhytomyr engineering – technological university. 2001. Issue 16. p. 8-18. [in Ukrainian.

Proceedings of 3rd International Workshop ITELMS'2008

Engineering Basics of Multilayer Structural Element Design

J. Bareišis[*], V. Kleiza[**]

[*] *Kaunas University of Technology, Panevėžys Institute, Daukanto str. 12, LT-35212 Panevėžys, Lithuania, E-mail: jonas.bareisis@ktu.lt*
[**] *Kaunas University of Technology, Panevėžys Institute, Klaipėdos str. 1, LT-35209 Panevėžys, Lithuania, E-mail: vytautas.kleiza@ktu.lt*

Abstract

The paper proposes an original method of multilayer structural element designing. It is a result of work of multiple years carried out by the author of the paper and his colleagues. One of the key advantages of this method is its simplicity. It is easy to understand for anyone with the engineering background. Calculations for multilayer beams, columns or other structural elements can be even further facilitated using computer equipment. This paper discusses the qualities of application of multilayer structural elements and provides formulae for the calculation of stress and stiffness in such elements.
KEY WORDS: *multilayer structural elements.*

1. Introduction

Most of the modern structural materials consist of composites that give the product a certain set of properties. In all cases, it is a system of different materials where each component has a specific purpose. Combined performance of different materials in the composite is equivalent to developing a new material with properties different from those of its components both quantitatively and qualitatively. These are multi-component structural elements that can be developed using polymer and composite materials, steel, concrete, wood, etc. Most widespread of these are multilayer structures commonly made of composite materials. Structural systems that include elements of various geometrical shapes made of different materials are usually called hybrid systems.

Multi-component structural elements are used for many different purposes, from domestic electric appliances and cars to structures used in construction and planes. Multilayer structures are particularly widespread in the production of gliders and lightweight planes [1, 2], isothermal bodies [3], construction [4-8], etc. Layering of materials can produce structures of desired properties in required directions with regard to all loads, their directions, anisotropicity of employed materials and other relevant requirements.

Where material of only one type is used, in most cases its strength properties may not meet the mass, price and other requirements set for a given structure. Optimal parameters of constructional elements can only be achieved through the use of different materials of different strength as well as other physical and mechanical properties. Optimal structure of the product may be obtained by matching anisotropic properties of mechanically strong materials with their comparative mass or price.

2. Application and Efficiency of Multilayer Structural Elements

Multilayer structures were first applied in the production of thin-walled structures of lightweight materials. When producing big thin-walled structures, often their bending resistance has to be increased. Increasing the wall thickness would be economically inefficient and would in turn increase the weight of the structure. Meanwhile, if a porous plastic or honeycomb core is inserted between the composite, aluminium or steel sheets, the strength of the slab may become equal to that of reinforced concrete, only 20 times lighter, while its thermal conductivity will be more than 20 times lower. Porous and honeycomb inserts not only improve the mechanical properties of the product, but also decrease its thermal conductivity and increase fire resistance and acoustic opacity [8, 9].

Multilayer structures are most widely applied in the production of gliders [1], [2], [10]. Three-layer structure of fibreglass and filler was first used by Richard Eppler and Hermann Naegele in the construction of “Phoenix” sport gliders in 1956. In Lithuania, the first glider - BK-7 - made solely of composite materials was constructed in Prienai sports aviation factory in 1972.

Multilayer hybrid structures composed of hot and cold hardened glass-reinforced plastic or carbon fibre reinforced plastic of various grades featuring very different strength and stiffness parameters were used in subsequent models of Lithuanian gliders – LAK-12, LAK-17 “Lietuva” and other [10], [11]. This allowed the development of structures that provided these glides with excellent aerodynamic characteristics. Today, Lithuanian gliders LAK-19, LAK-19T and LAK-20 meet global standards and are in great demand all over the world. This was possible only through proper use of materials and structure elements. One of the key structural elements is the cantilever wing braced inside the fuselage. It consists of a spar and a three-layer skin shaping the profile of the wing (Fig. 1, a). The cross-section of the spar has an I-beam profile (Fig. 1, b) inserted in a box with filler at the root chord (Fig. 1, c).

Composites penetrate into all fields of engineering including construction industry [4-8]. Polymer composite materials (PCM) can be used for roof structures, roof and floor coating materials, interior and exterior decorative wall panels, ducting components, pipelines and even all bearing elements and structures in small buildings, thus entirely replacing conventional construction technologies. These materials are convenient in construction because they don't need finishing, additional anticorrosive priming and painting or decorative coating. This significantly cuts the construction costs as well as speeds up and facilitates assembling works.

PCM rods and solid PCM grids for concrete reinforcement replacing the currently used metal reinforcement will lighten and reduce the cost of concrete span slabs as well as other construction elements and structures, and will allow the improvement of their assembling procedures and development of new construction technologies.

When composite materials and structures made of such materials – including multilayer structures – are used in construction, the following goals can be achieved:

1. Increase of strength, stability and stiffness at reduced amounts of materials in use;
2. Reduction of weight of individual building elements and the entire building as well as the dimensions of the structure cross-section;
3. Improvement of thermal insulation and acoustical properties;
4. Maximum exploitation of all material properties through appropriate distribution of structure layers;
5. Reduction of weight and dimensions of structures bearing composite elements with thermal insulation layers;
6. Reduction of energy costs of structure production, transportation and assembling.

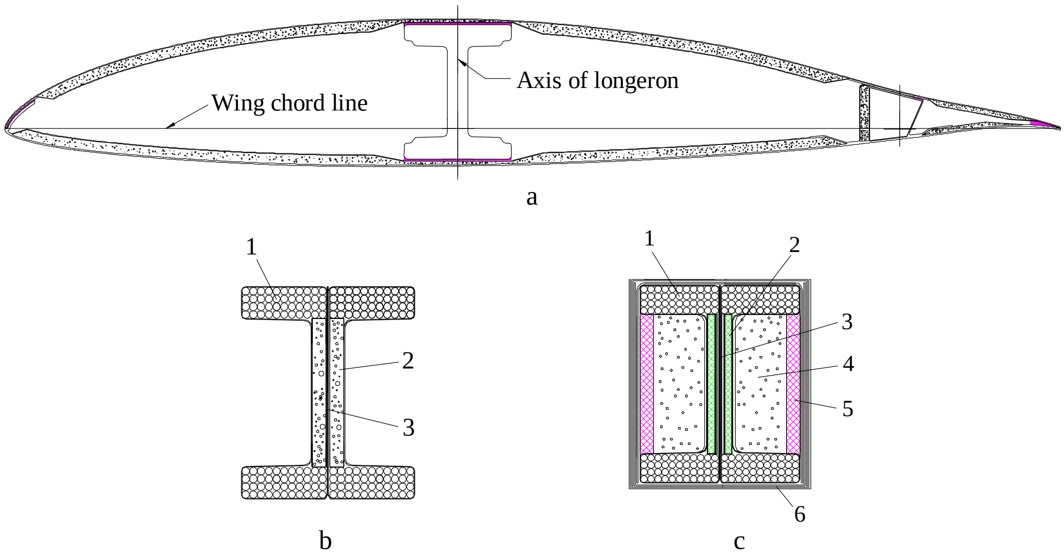

Fig. 1 Cross-section of a glider wing

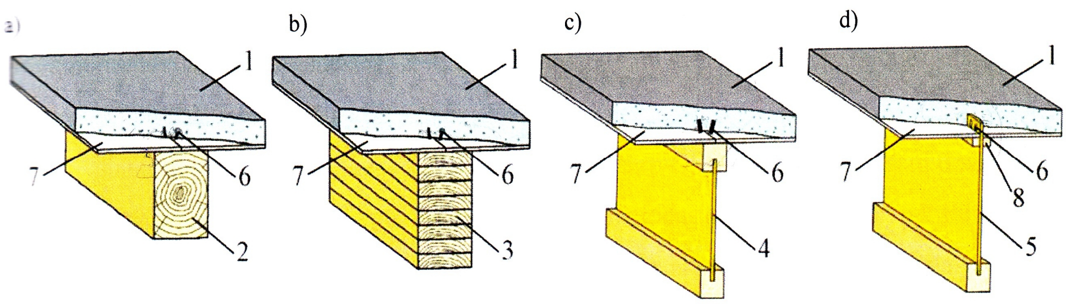

Fig. 2 Composite wood-concrete beam span structures [5]

With the help of multilayer composite structures, the weight of building span structures and especially roofing can be reduced by 3 to 4 times, while the weight of the foundation can drop by as much as 4 to 10 times. This can dramatically cut the costs of construction especially when the building has to be build on weak soils or the height of the building has to be raised [8, 11].

Today, composite cast in situ steel and concrete span structures reinforced with moulded metal sheets are increasingly often used in construction. Such sheets are used as permanent formwork during the concreting of structures and act as external reinforcement under the effect of loads during the use of the structures. Where moulded sheets are employed, the combined performance of the concrete layer and the sheets is much better and the use of the height of such slab is more efficient.

The use of composite wood-concrete structures is also expanding [5]. Compared to wood structures, wood-concrete systems are twice more strong, while the stiffness of their plane is 3 to 4 times higher. Wood components of the beams are most often made of solid timbers of rectangular cross-section when the span of the composite span structure is up to 6 m (Fig. 2, a), or of glued timber of rectangular cross-section when the distance between the supports is 6 to 10 m (Fig. 2, b). Thin-walled profiles can also be used as wooden span beams (Fig. 2, c, d), especially those made of oriented particle boards that are jointed with the concrete slab using different methods [5].

The use of composite structures in construction industry is stimulated by two major considerations: significantly lower cost of production and reduced energy cost of building maintenance together with structure lightness while retaining the same technical properties.

3. Basic Premises of Multilayer Structural Element Design

In general, a multilayer structural element (Fig. 3) consists of *n* layers of different thickness d_i and width b_i, that have different elasticity characteristics E_i, n_i, strength and fracture stresses and deformations. The state of a multilayer structure is analysed at small linear deformations with respect to lateral shear deformations. Deformation values have to be equal across the layer contact surface, i.e. there should be no creep of the layers. In case of creep, the composite element would loose its integrity.

The method of multilayer structural element calculation proposed by the authors of this paper is based on the following premises [11]:

1. In the structural composite element under deformation, the cross-sections remain flat and perpendicular to the longitudinal layer of the beam in spite of whether the material of the layer is linearly elastic.
2. Linear longitudinal deformations at the level of the structural element are distributed according to the linear law.
3. Mechanical characteristics of the layer depend on the experimentally determined properties of the reinforcing and binding material of the composite as a whole.
4. There is no creep at the joints of the layers.
5. Poisson’s ratios of materials comprising the layers are equal$n = n_i$.

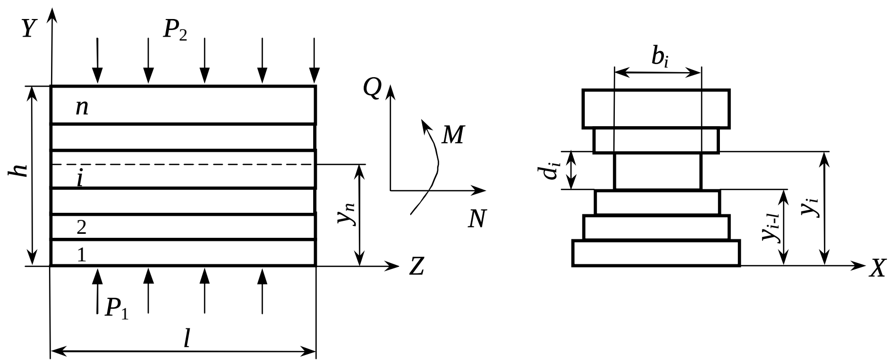

Fig. 3 Multilayer structural element

When applying this method it is important to know the characteristics of the material in the direction of the load. Structure of desired stiffness and strength is easy to design by changing the materials comprising the structural element and geometrical parameters of the layers. The method described herein has been acknowledged and tested using other methods [11]–[13].

4. Design of Multilayer Beams

When examining the strength and stiffness problems of multilayer structural elements, it is necessary to know the coordinates of the element cross-section stiffness centre and the directions of the principal axes of inertia going through this centre. In general, the centre of stiffness of the cross-section of a multilayer structural element does not match the geometrical centre. Of course, in order to find the axial load, the point of effect of the resultant of external forces has to be in the stiffness centre of the cross-section. When bending, temporary bending moment are usually placed in the planes that are perpendicular to the cross-section plane and that cross the principal axes of inertia, while the crossing point of the latter is in the stiffness centre of the cross-section. In case of such bending, the planes of the bending moment match the neutral layers, therefore we will call the principal axes of inertia the directions of the neutral layers. Often, the analysis is applied to structural elements that have one or two geometrical and/or stiffness symmetry axes. In such case, it suffices to calculate the ordinate of the neutral layer:

$$y_E = \left[\sum_{i=1}^{n} B_{yi} d_i + 2\sum_{i=2}^{n} B_{yi} \sum_{j=1}^{i-1} d_j \right] \Big/ 2\sum_{i=1}^{n} B_{yi} \,. \tag{1}$$

Often, we have to deal with asymmetric multilayer structures. In such cases, we have to know how to calculate the position of the neutral axis in respect of both axes, the crossing point of which is the centre of stiffness of the multilayer structural element. It has been found that after a proper transformation, the formula (1) can be used for the calculation of x_E coordinate:

$$x_E = \left[\sum_{i=1}^{n} B_{xi} c_i + 2 \sum_{i=2}^{n} B_{xi} \sum_{j=1}^{i-1} c_j \right] \Big/ 2 \sum_{i=1}^{n} B_{xi} \ . \tag{2}$$

Here, B_{xi} and B_{yi} are the axial stiffness values of the layers, while $B = \sum_{i=1}^{n} B_i = \sum_{i=1}^{n} A_i E_i$ is that of the entire cross-section.

The deduced formulae (1) and (2) are very convenient – especially when multilayer structural elements are made of any number of rectangular layers in spite of their position with respect to each other, and their dimensions are not uniform in general, i.e. the cross-section of such multilayer structural elements is asymmetric with regard to both axes (x and y).

Whereas materials used for the production of layers have different elasticity moduli E_i and their position with regard to each other is unconstrained, in general, the resultant structure will be asymmetric both in terms of geometry and stiffness. In such case, the centre of stiffness does not match the geometrical centre. Where the configuration of the layers is irregular, the coordinates of the centre of stiffness can be calculated according to the following formulae:

$$x_E = \frac{\sum_{i=1}^{n} S_{y_i} E_i}{B} , \qquad y_E = \frac{\sum_{i=1}^{n} S_{x_i} E_i}{B} . \tag{3}$$

Thus, in order to find the position of a neutral line in a multilayer structural element, it suffices to know the elasticity moduli of the materials of each layer and their geometrical shape.

The angle between the direction of neutral line j and the direction of principal axis $x_{v,}$ can also be determined using a modified formula of the turning angle of principal axes of inertia:

$$\mathrm{tg} 2j = \frac{2 D_{xEyE}}{D_{yE} - D_{xE}} . \tag{4}$$

Here, D_{xE}, D_{yE}, D_{xEyE} is the axial and the mixed stiffness in respect of x_E, y_E axes.

The following formula has been deduced for the calculation of normal stress s_i in any point of the multilayer beam [11], [13]:

$$s_{xi} = \frac{M y_i}{D} E_{xi} . \tag{5}$$

Here, s_{xi} and E_{xi} are the normal stress of the i layer and its elasticity modulus in the direction of the x axis; y_i is the distance between the neutral line and the layer in question, which can be determined using the following equation:

$$y_i = \left| y_n - \sum_{m=1}^{i-1} d_m \right| . \tag{6}$$

When the formula of determining normal stress in any layer of the bent multilayer beam (5) is compared to the formula of stresses in isotropic material, we can see that in case of the multilayer beam, instead of the cross-section inertia moment I used in the conventional stress formula, another characteristic of the cross-section – the stiffness of the beam D is used and further multiplied by the layer elasticity modulus.

The following formula was deduced for the calculation of tangent stresses from the transverse effort:

$$t_{xy} = \frac{Q_x C_y}{D b_y} . \tag{7}$$

Here, $C_y = \sum_{i=1}^{m} E_i S_{y_i}$ is the equivalent static moment, and b_y is the width of the beam layers in a given point. The deduced equation is equivalent to the established Zhuravsky formula, which is used for the calculation of tangent stress in isotropic materials.

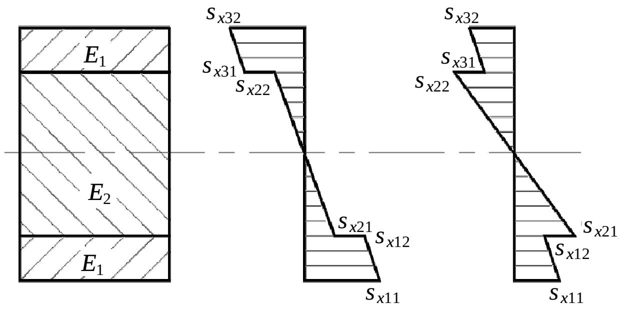

a b c

Fig. 4 Cross-section of a three-layer beam (a) and distribution of normal stresses within it (b, c), when $E_1 > E_2$ (b) and $E_1 < E_2$ (c)

When analysing the (5) equation, one can easily notice that the cross-section of the multilayer structural element shows a stress jump proportional to the ratio of elasticity moduli at the crossing from one layer of the beam to the other (Fig. 4). Therefore, the normal stresses emerging in the next layer at the layer contact area can be found from the following equation:

$$s_{i+1} = s_i \frac{E_{i+1}}{E_i}. \tag{8}$$

Distributions of normal stress shown in Fig. 4 (b and c) can be found in the cross-section of a three-layer beam (Fig. 4, a) consisting of two materials with elasticity moduli E_1 and E_2.

Cases of tangent stress distribution in the cross-section of a three-layer beam are shown in Fig. 5. Formula (7) shows that the pattern of stress distribution in the cross-section may be related to the changes of C_y and b_y values. From layer i to layer $i+1$, the layer elasticity modulus changes from E_1 to E_{i+1}, but the static moment of the layer $i+1$ is still equal to zero as the y coordinate remains the same and thus the equivalent static momentum does not change. This shows that the beam widths b_{yi} and b_{yi+1} are equal, there is no sharp tangent stress jump in stress diagram and $t_{yi} = t_{yi+1}$ (Fig. 5, a). The change of distance y only affects the intensity of change of tangent stresses depending of the elasticity modulus of the layer in question.

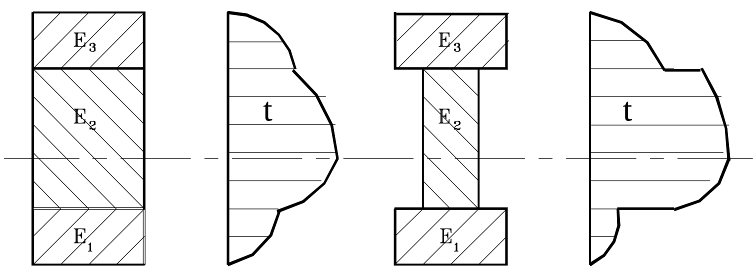

a b

Fig. 5 Distribution of tangent stresses in a three-layer beam when the beam widths are equal (a) and different (b)

When the widths of the beam are changed (Fig. 5, b) from b_{yi} to b_{yi+1}, tangent stresses of the layer contact area are calculated from the following equation:

$$t_{yi+1} = t_{yi} \frac{b_i}{b_{i+1}}. \tag{10}$$

It has to be noted, that the reduced cross-section method has been used in the design of multilayer beams until now. This method renders inaccurate pattern of tangent stress distribution or incorrect values thereof. This could result in fragmentation of the structure.

5. Design of Multilayer Columns

Multilayer columns also have their own advantages and are increasingly widely used in the construction industry. The loading of the columns is usually non-central, therefore the stresses in any point of the column can be calculated using formula [11]:

$$s_k = \frac{N}{B} E_k + \frac{M_x y_k E_k}{D} + \frac{M_y x_k E_k}{D}. \qquad (11)$$

Here, the principal axes are x and y, that cross the centre of stiffness.

For the calculation of columns, it is very important to define the boundaries of the cross-section kern. In case of multilayer columns, the coordinates of the cross-section kern have to be calculated from the following equations:

$$x_b = -\frac{D_y}{B \cdot a_x} \quad \text{and} \quad y_b = -\frac{D_x}{B \cdot a_y}. \qquad (12)$$

Here, a_x and a_y are the coordinates of the points, where the neutral line crosses the principal axes.

This is more explicitly described in a separate study [11] and science magazines in the short run.

Computer software has been prepared for the implementation of the described methodology, and the research results are constantly updated in science magazines.

References

1. **Красилщиков А.П.** Планёры СССР. Москва, 1991, 240 с. [in Russian].
2. **Работнов Ю.П.**, **Туполев А.А.** и др. Применение углепластиков в конструкции летателъных апаратов // Механика композитных материалов. 1981, с. 657–667. [in Russian].
3. **Bareišis J.**, **Kučys A.** Izoterminių kėbulų projektavimo problemos // Konferencijos “Transportas 99” pranešimų medžiaga. Kaunas, Technologija, 1999, p. 35-40. [in Lithuanian].
4. **Bulavs F.**, **Radinsh I.**, **Tirans A.** Gelžbetoninių sijų laikomosios galios padidinimas taikant dispersiškai armuotus plastiko lakštus // Journal of Civil Engineering and Management. Vilnius, Technika, 2005. T. XI, No. 3, p. 169-174. [in Lithuanian].
5. **Gurkšnys K.** Kompozitinių medienos – betono perdangų ypatumai ir skaičiavimo pagrindai // 6-osios Lietuvos jaunųjų mokslininkų konferencijos “Lietuva be mokslo **-** Lietuva be ateities“ medžiaga, Vilnius, Technika, 2003, p. 277–283. [in Lithuanian].
6. **Leung H.Y.** Plieno ir anglies pluošto polimero strypais armuotų lenkiamųjų betono sijų laikomoji galia // Journal of Civil Engineering and Management, Vilnius, Technika, 2004, Vol. 10, No. 3, p. 209-215. [in Lithuanian].
7. **Marčiukaitis G.**, **Vavilonis J.**, **Vaškevičius A.** Analysis of Behaviour of Composite Elements with Profiled Steel Sheet Loading // Proceedings of the 7th International Conference, Vilnius, 2001.
8. **Марчюкайтис Г.В.** Технологические напряжения в строительных композитах каркасной структуры. Вильнюс: Техника, 1995, 144 с. [in Russian].
9. **Bareišis J.**, **Tričys V.** Polimerų ir kompozitų mechanika. Šiaulių universitetas, 2003, 258 p. [in Lithuanian].
10. **Bareišis J.**, **Ušakov A.**, **Paulauskas V.** Investigation of operational failsafe characteristics of the sailplane LAK-12 “Lietuva” // XXI OSTIV Congress at Wiener Neudstadt, Austria, 1989. Technical soaring 1990, N3, Vol. 14, p.73-77.
11. **Bareišis J.** Plastikų, kompozitų ir daugiasluoksnių konstrukcinių elementų stiprumas. Kaunas, Technologija, 2006, 252 p. [in Lithuanian].
12. **Bareišis J.** Design and Stress State of Tension in Multilayer Bars // Journal of Composite Materials. ISSN 0191-5665. Vol. 38, No. 5, 2004, p.389-397.
13. **Bareišis J.** Stiffness and Strength of Multilayer Beams // Journal of Composite Materials. ISSN 00021-9983. Vol. 40, No. 6, 2006, p. 515-531.
14. **Bareišis J.**, **Kleiza V.** Influence of multilayer Beams Cross-section Shape on Stiffness at bending // Mechanika. ISSN 1392-1207. 2005, No. 1(47), p. 5-10.

Parallel Monte Carlo Computations in SCore Type PC Cluster

S. Bekešienė*, V. Kleiza**

* *Military Academy of Lithuania, Šilo 5A, LT-10322 Vilnius, Lithuania, E-mail: svajone.vosteriene@lka.lt*
** *Institute of Mathematics and Informatics, Akademijos st. 4, LT-08663 Vilnius, Lithuania, E-mail: vytautas.kleiza@ktl.mii.lt*

Abstract

We use the PC Cluster TAURAS [1] with the SCore cluster system software on top of Linux operating system to present the strategy for parallelizing Monte Carlo calculations. Parallel Monte Carlo (PMC) methods are successful because particles are typically independent and easily distributed to multiple processors. The PC cluster helps us to computerized parallel programs for simulating mortar firing.

In this article we present the PMC, who let us analyze how many mines and how many volleys for hitting armed target situate at a definite distance must be shot. Also we take the definition in its most general sense, and it is the random aspect of Monte Carlo that is our focus. Input data for the different trials are selected using values in prescribed distributions, using a pseudo-random number generator. An efficient algorithm is required for initializing the random number generator for each subsequence. The basic computation typically involves a significant amount of calculation, so that the pseudo-random number generation itself represents a small fraction of the total computational effort.

We present the parallel method for numerical simulation of trench-mortar tasks for SCore type cluster system. These programs, helps to calculate parameters of firing for destroy the target. Data that can be calculated are: the standard quadratic variance, number of mines for realize successful firing and destroy separate or group targets with chooses confidence probability and so on.

These programs can be used for the teaching of the future officers as well. We propose computations that are very effective because the digital experiment can substitute costly firings at the shooting range; the pollution of the environment is reduced.

KEY WORDS: *parallel Monte Carlo, SCore type cluster, trench-mortar.*

1. Introduction

The Monte Carlo method provides approximate solutions to a variety of mathematical problems by performing statistical sampling experiments on a computer. The method applies to problems with no probabilistic content as well as to those with inherent probabilistic structure.

Statistical simulation methods may be contrasted to conventional numerical methods, which typically are applied to ordinary or partial differential equations that describe some underlying physical or mathematical system. The only requirement is that the physical (or mathematical) system be described by probability density functions (pdf's). When the pdf's are known, the Monte Carlo simulation can proceed by random sampling from the pdf's. Many simulations are then performed and the desired result is taken as an average over the number of observations.

Monte Carlo is now used routinely in many diverse fields. The primary components of a Monte Carlo simulation method include the following:

- Probability distribution functions - the physical (or mathematical) system must be described by a set of pdf's.
- Random number generator - a source of random numbers uniformly distributed on the unit interval must be available.
- Sampling rule - a prescription for sampling from the specified pdf's, assuming the availability of random numbers on the unit interval, must be given.
- Scoring (or tallying) - the outcomes must be accumulated into overall tallies or scores for the quantities of interest.
- Error estimation - an estimate of the statistical error (variance) as a function of the number of trials and other quantities must be determined.
- Variance reduction techniques - methods for reducing the variance in the estimated solution to reduce the computational time for Monte Carlo simulation.
- Parallelization - algorithms to allow Monte Carlo methods to be implemented efficiently on advanced computer architectures.

We analyzed in this paper the method for numerical simulation of trench-mortar tasks. In our general focus was to present the homemade parallel program for solving the non-linear equations system, which describes the mine's moving trajectory and helps to calculate parameters of firing for destroy the target. We chose generalized results from table [2], comparing data and state the dependence of resistance coefficient upon the distance to the target. In this way we used the analytical solution and indicated the initial speed of mine v_0, the coefficient of resistance k and the influence of wind in the following manner

$$\begin{aligned} &v_0 + random[normald]\Delta v_0, \quad k + random[normald]\Delta k, \\ &F_1 + random[normald]\Delta F_1, \quad F_2 + random[normald]\Delta F_2, \end{aligned} \tag{1}$$

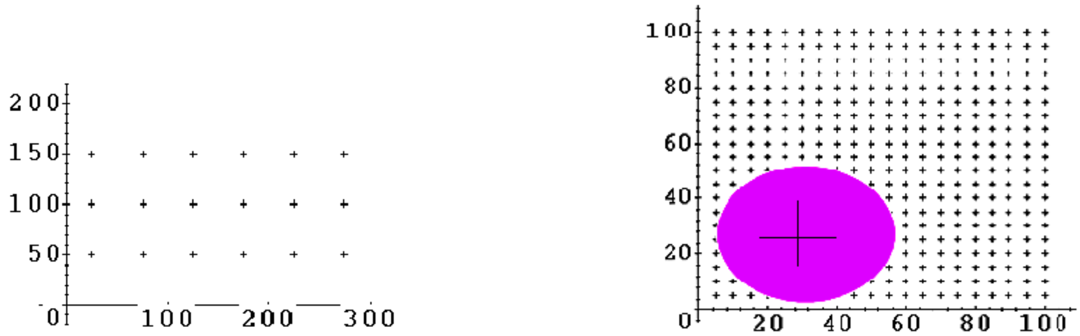

a b

Fig. 1 The schemes of: possible targets (a) and hitting power after one realization (b)

here *random*[*normald*] – generating standard normal distribution $N(0; 1)$ and Δv_0, ΔF_1, ΔF_2 – the maximal random error of initial velocity v, that of coefficient of air resistance k, the random errors of contrary wind influence F_1, or side wind influence F_2 corresponding to the concrete conditions. For example, for the 120 mm trench-mortar the decrement of initial velocity of mine is 0.5 per cent. During the shooting the gun tube wears and tears this error increase. The random fluctuation of the temperature or pressure of the atmosphere determines about one per cent of increment of coefficient k of resistance.

When we used simulation methods for trench-mortar and need to get two dependability symbols, we doing the million numerical experiences and repeating million time calculations and then do the statistical processing of data. The calculations time increase very fast of these investigations and we can get the results only after one or two ours. The analogical situation is when we solve the optimization of annihilation group target of 300 m in width and 200 m in depth. Possible scheme of targets are represented in Fig. 1.

As usually this target is hitting by battery of trench-mortar. For one volley each mortar shoots three times and each time is changing the blowpipe angle. If we know the result of destruct of mine, we can to sum up the situation. Some errors are possible shooting to the same point. We form the random variables and mean square variances s_{xi} (for x - axis) and s_{yi} (for y - axis). They may be different for distinct mortar.

$$\begin{aligned} x_i &= x_i + 3s_{xi} \times random[normald], \\ y_i &= y_i + 3s_{yi} \times random[normald]. \end{aligned} \tag{2}$$

Calculations are repeating the necessary number of times (10, 15 or 20 times), because the target must be hit with chosen confidence. Solve the task of optimization was used the Monte Carlo method, that let us to know number of mine for realize successful firing and destroy separate or group targets with choose confidence probability and so on. The programs, running 10-15 minutes, can be used for the teaching of the future officers as well. This dictate terms to calculations, so we realize all computations on PC cluster TAURAS [5] by parallel Monte Carlo method (PMC).

2. Pseudo-Random Number Generation on SCore Cluster

It is known, that the success of any Monte Carlo program depends on the quality of the pseudo-random number generators used. In this article we take the definition in its most general sense, and it is the random aspect of Monte Carlo that is our focus.

We used the PC Cluster TAURAS with the SCore cluster system software on top of Linux OS to present the strategy for parallelizing Monte Carlo calculations for our task [5]. Linux OS have some functions generate pseudo-random numbers using the linear congruent algorithm and 48-bit integer arithmetic. The *drand48()* function return non-negative double-precision floating-point values uniformly distributed between 0 and 1. The *srand48()* function is initialization function, that should be called before using *drand48(), lrand48()* or *mrand48()*. All the functions work by generating a sequence of 48-bit integers, X_i, according to the linear congruent formula:

$$X_{n+1} = \left(aX_n + c\right) \bmod m\,, \tag{3}$$

where $n \geq 0$ and in isolated case $a = 5^{17}$ and $c = 0$. The parameter $m = 2^{48}$, hence 48-bit integer arithmetic is performed. Formula (3) means, that using numbers X_n are calculating pseudo-random numbers

$$g_n = 2^{48} X_n\,. \tag{4}$$

The cluster structure let to perform for each processes the sequences of pseudo-random numbers with initialization by server’s clock time. There was written for SCore type cluster the program, which let us to perform for each process the sequences of pseudo-random numbers with initialization by server's clock time.

```
/* -------------------------------------------------------------------------------- */
/*                    initialization of random number generation                    */
/* -------------------------------------------------------------------------------- */
       rand_mas = (int*)malloc( sizeof(int)*num_of_nodes );
       if (myid==server_id) {
/* -------------------------------------------------------------------------------- */
/*                random number initialization by server's clock time                */
/* -------------------------------------------------------------------------------- */
       srand( (unsigned int)time(NULL) );
       for (i=0; i<num_of_nodes; i++) rand_mas[i] = rand();
       }
       MPI_Bcast(rand_mas, num_of_nodes, MPI_INTEGER, server_id,
       MPI_COMM_WORLD);
       init_random(rand_mas[myid]);
       free(rand_mas);
/* -------------------------------------------------------------------------------- */
       if (myid==server_id) {
              printf("\n****************************************************************\n");
              laikas_b = time(NULL);
       }

       t_b = time(NULL);
       solve_atv(m_alpha1, m_alpha2, num_of_iters, salviu_sk);
       solve_ties(m_alpha1, m_alpha2, mas_xs, mas_ys, mas_t, num_of_iters);
       t_e = time(NULL);

       for (i=0; i<num_of_iters; i++)
//            printf("node: %i, \tmx: %f\n", myid, mas_xs[i]);
              printf("node: %i, \trand: %f\n", myid, get_rand_num());

//     printf("node: %i, \tlaikas: %2is\n", myid, t_e-t_b);
```

This let us to establish a bound on the length of the subsequence required for each realization. The first subsequence is chosen to consist of the first consecutive numbers in the sequence the second subsequence to consist of the next consecutive numbers in the sequence, and so on. Each realization is assigned to the next processor that becomes free, and then it becomes feasible to undertake the identical Monte Carlo calculation on an arbitrary number of parallel processors. This holds regardless of the relative computational capacity or availability of the different processor.

1. The Optimization of Calculations for Iterations of Each Process

It is known, that the time of calculations increase very fast using the numerical experience n time, because the precision of results increase in proportional $1/\sqrt{n}$, where n means the number of experiments. When we need to get two dependability symbols, we doing the million numerical experiences and repeating million time calculations and then do the statistical processing of data.

One personal computer with 2.4 GHz CPU calculates this task about 3500 s. This time is not good for real situation, because the military decisions must be doing immediately. Also we know that to realize this simulation for teaching the military situation for students must be model in real time. On SCore type cluster TAURAS we used homemade parallel programs that generating parallel pseudo-random numbers and help to realize in real time the simulation of trench-mortar firing (Fig.2).

To solve the problem of Monte Carlo calculation continuance time we write for PC cluster the several programs in C code with MPI standard, which was used in our research work and are presented below. The calculations of iterations for each process on heterogeneous cluster let us to optimize the performance [1, 5]. SCore cluster software let us do this computations better with portion evenly the job for all CPU's:

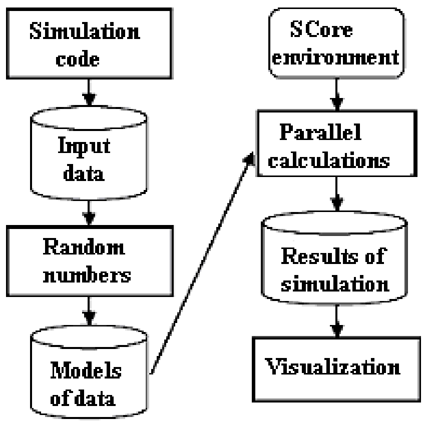

Fig. 2 The trench - mortar simulation scheme realized by parallel Monte Carlo on SCore type cluster TAURAS

```
/*      Calculations of iterations of each process for heterogeneous cluster     */

        cpu_speed_mas[server_id] = get_cpu_speed();
        for(i=server_id+1; i<num_of_nodes; i++)
                MPI_Recv(&cpu_speed_mas[i], 1, MPI_INT, i, 1, MPI_COMM_WORLD, &status);


        for(i=0; i<num_of_nodes; i++) total_MHZ+=cpu_speed_mas[i];
        MHZ_per_Iter = ceil((double)(total_MHZ)/bandymu_sk);

        for(i=0; i<num_of_nodes; i++) {
                node_iters[i] = cpu_speed_mas[i]/MHZ_per_Iter;
                tmp_total_iters+=node_iters[i];
        }
        delta_iters = bandymu_sk - tmp_total_iters;

        i=0;
        while(delta_iters>0) {
                if (i>=num_of_nodes) i=0;
                node_iters[i] += 1;
                delta_iters--;
                i++;
        }

        /*      free(cpu_speed_mas);      */
        } else {
        /*
                cpu_speed = get_cpu_speed();
                MPI_Send(&cpu_speed, 1, MPI_INT, server_id, 1, MPI_COMM_WORLD);
        */
        }

        MPI_Bcast(node_iters, num_of_nodes, MPI_INT, server_id, MPI_COMM_WORLD);
        MPI_Bcast(&salviu_sk, 1, MPI_INT, server_id, MPI_COMM_WORLD);
        num_of_iters = node_iters[myid];
```

The calculations by parallel Monte Carlo (PMC) methods were successful on PC cluster TAURAS, because wrote programs let the independent particles easily distribute to multiple processors and the cluster helps us to computerized parallel programs for simulating mortar firing.

4. The Calculation Results

The time of calculations on separate number of CPU after 15 volleys of 10000 hits show us that the heterogeneous SCore cluster is good device for such tasks and for realization simulation of trench-mortar is better the parallel Monte Carlo. For example, if the distance to the target is 3050 m and we shooting 10000 times with different number of CPU, we can get the results at the time presented below in Fig.3. Reiterating the calculus 10000 times with random errors of initial velocity of mines and that's of air resistance we get the ellipse of concentration of results shown in Fig.4.

Moreover we solve the task of optimization: how many mines must be shot to the target situated at a definite distance for hitting with the confidence probability 0.9. For this task we looking for distributed by normal distribute random values by using the formulas below

$$x = \sqrt{-2 \ln g_1}\cos(2pg_2),\; h = \sqrt{-2 \ln g_1}\sin(2pg_2)\,. \tag{5}$$

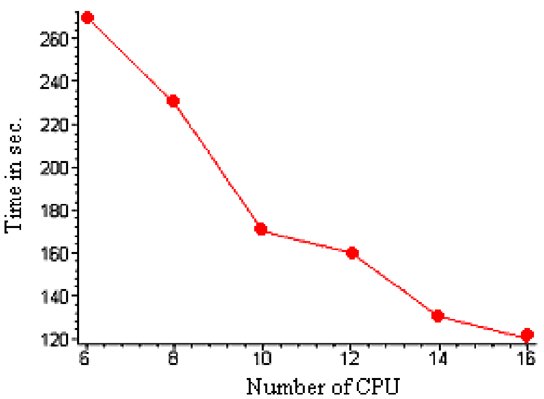

Fig. 3 The calculation time dependence from separate number of CPU

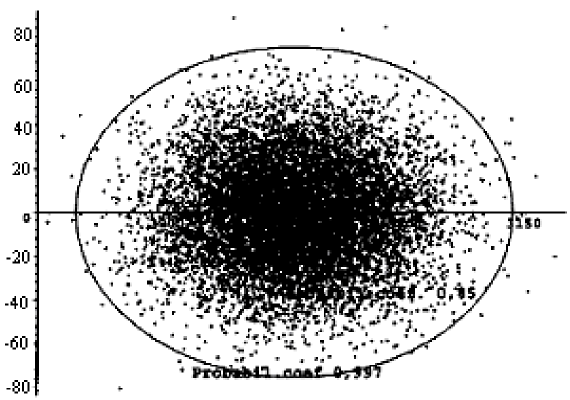

Fig. 4 The ellipse of concentration of 120 mm trench-mortar when was shoot 10000 times at the target in the distance of 3050 m

Then we calculate the quadratic variances s_x and s_y, by formulas (2) and the dispersion of hitting points. When we know the standard quadratic variances and means m_x and m_y, the probability of hitting the target equals to

$$P\{x \subset (x_1; x_2),\ y \subset (y_1; y_2)\} = \frac{1}{p s_{xx} s_{yy}} \int_{x_1}^{x_2} \int_{y_1}^{y_2} e^{-\frac{x-(L_x-m_x))^2}{2s_x^2}} e^{-\frac{(y-m_y)^2}{2s_y^2}} dxdy\ . \qquad (6)$$

Here intervals (x_1 ; x_2), (y_1 ; y_2) – signifies the size of target and (m_x ; m_y) are the coordinates of the target.

This probability is stable for determine distance, so we may find necessary number of shooting for hitting the target. In Fig.4 we present the visualization of dispersion ellipse of 10000 points hitting.

Repeating the calculus for various distances until the target and after statistical treatment of results, we get the dependence of mean square deviations on the target distance.

The dispersion of projectiles and shells is described by the normal distribution. The probability to hit the target with the chosen parameters may be calculated by the formula (6). If one falls to hit the target and one shoot again some times, then the probability of hit the target may be calculated by the formula:

$$P_n = 1 - (1 - p)^n\ , \qquad (7)$$

where $(1 - p)$ is the probability to fall to hit in every shoot separate, and that probability being constant, n is the number of shoots. For example, the probability to hit a tank (which parameters are 4×8 m) at the distance of 1 km is 0.14 (utilizing the methodology described above finding s_x and s_y). For destruction a tank with the probability of confidence 0.85 it is necessary to shoot 13 times.

5. Conclusions

An efficient algorithm is required for initializing the random number generator for each subsequence. The basic computation typically involves a significant amount of calculation, so that the pseudo-random number generation itself represents a small fraction of the total computational effort. In this article we take the definition in its most general sense, and it is the random aspect of Monte Carlo that is our center of attention. Input data for the different trials in our realization for PC cluster are selected using values in prescribed distributions, using a pseudo-random number generator of Linux OS environment.

The get results show that the parallel Monte Carlo is more better for realization our task. The presented parallel programs, helps to calculate parameters of firing for destroy the target. Data which can be calculated are: the standard quadratic variance, numbers of mines for realize successful firing and destroy separate or group targets with choose confidence probability and so on. These programs can be used for the teaching of the future officers as well, because the calculations continue shot time.

The numerical simulation of trench-mortar tasks presented by parallel Monte Carlo method was successful thanks to homemade parallel programs, and shows that both the quality of the parallel pseudo-random number generator and the statistical independence of the results calculated on each processor are important.

Also presented the parallel Monte Carlo let us analyze how many mines and how many volleys for hitting armed target situate at a definite distance must be shot.

The last and very important is that we recommend computations, which are very effective because the digital experiment can substitute costly firings at the shooting range and the pollution of the environment is reduced.

References

1. Basis of PC clusters. Available at: http://clusters.top500.org/db.
2. Table of results of shooting by trench-mortar ChM - 120. Commander-in-Chief of Lithuanian Republic. CAS "Grafema". Vilnius, Lithuania. 1997.
3. **Pincevichus A.**, **Rakauskas R. J.**, **Misevicius G.** The Numerical Simulation in Ballistics // Nonlinear analysis: Modelling and Control. ISSN 1392-5113. 2001, Vol.6, No.1, p. 89-104.
4. **Pincevicius A.**, **Rakauskas R. J.**, **Misevicius G.** The Numerical Simulation of Military Skills // Lithuanian Mathematical Journal. ISSN 0132-2818. 2001, Vol. 42, (spec. no.), p. 26-33.
5. **Janciauskas I.**, **Venskus A.** Ballistics. Lithuania Military Academy, Vilnius, Lithuania. 1999, 236 p.
6. **Ishikawa Y.**, et al. Proceedings of the 5th Annual Linux Expo. 1999, p. 55-66.
7. **Gropp W.**, **Lusk E.**, **Skjellum A.** Using MPI. The MIT Press. 1999, 371 p.
8. **Brien W. Keringhan**, **Dennis M. Ritchie.** The C programming Language (Second Edition). 2000, 286 p.

Proceedings of 3rd International Workshop. ITELMS'2008

Co_6O_m (m = 1 ... 7) Nanoparticles Geometric and Electronic Structure Changes Within Increasing of Oxygen Number

J. Tamulienė[*], R. Vaišnoras[**], G. Badenes[***], L. M. Balevičius[****]

[*] *Institute of Theoretical Physics and Astronomy of Vilnius University, Gostauto 12, LT-01108 Vilnius, Lithuania*
[**] *Vilnius Pedagogical University, Studentu 39, LT-08016 Vilnius, Lithuania*
[***] *The Institute of Photonic Sciences, Av. del Canal Ol.mpic s/n, 08860 Castelldefels, Spain*
[****] *Vilnius University, Physic Faculty, Sauletekio al. 9, LT-10222 Vilnius, Lithuania*

Abstract

For fast read-write process in recording nanophotonic devices are to be magnetic nanopaticles (NP) of smaller size where reduction of magnetic coercivity is expected thus stability of NP is an important factor. Usually metallic NP easily oxidize in air and they could loose their magnetic properties while their stability increase. In the present work theoretical investigation of Co_6O_n (n=1-7) by applying density functional approach are presented. Calculations reveal that the stability of these compounds increase when the number of O atoms increase. We have found that Co_6O_7 is the most stable particle among all investigated ones. The increase of the number of the Oxygen atoms leads to the elongation of the Co-Co bond length and dramatically changes electronic structure of NPs. The Oxygen atoms stabilize Co_6 particles due to dissolving of Co-Co bonds that possess antibonding character.
KEY WORDS: *nanoparticles, density functional, electronic and geometrical structure, electron density.*

1. Introduction

During recent years, free and deposited transition – metal clusters have been extensively studied experimentally and theoretically because of their special magnetic properties that play a key role in technology and industry, ranging from the generation and distribution of electrical power up to communication devices and the processing of information [1, 2]. It is well known, that properties of NPs depend upon symmetry and atomic composition and these processes affect even the structural parameters such as the shape of the particles or the interatomic distances. As example, by assembling cobalt nanoparticles containing up to 40 atoms, the magnetic anisotropy energy is dependent on single-atom coordination changes [3]. On the other hand, the structure affects high chemical stability of nanoparticles even if they are in contact with the ambient, in particular with Oxygen [4].

One of the most interacting and widely used nanoparticles is Co species. The Co nanocrystals display a wealth of size-dependent structural, magnetic, electronic, and catalytic properties. Pure cobalt powder samples with diameters of few nanometers are the subjects of intense research due to their properties, which make them very appealing from both the theoretical and the technological point of view. To stabilize a pure Co nanoparticles the CoO is used. Pure CoO nanoparticles in the 4.5-18 nm range have been prepared by the decomposition of Co(II) cupferronate [5]. The core-shell nanoparticles (Co-CoO) are examined. Reported results demonstrate the essential role played by shells in stabilizing the magnetism of Co-CoO nanoparticles. Few reports on the preparation and properties of pure CoO in bulk are due to difficulties to obtain the materials in pure form by simple methods [6]. The particles are often being contaminated with Co_3O_4 or Co metal. A greater stability of Co_3O_4 than that of CoO has also been established. However, reports on other Co_nO_m particle properties are not found and there is no clear data on the structure and stability of these CoO_m nanoparticles. Hence, the aim of our investigation is to find the most stable Co_6O_m particles and to exhibit how and why the electronic and geometric structures of these particles are changed.

2. Description of Method

Let us introduce briefly results that were obtained under investigation of Co_n particles [7]. These results indicate Co_6 and Co_{12} as the most stable particle. Moreover, the structure of Co_6 particle occurred in all investigated derivatives, thus this structure is called a key-element of the Co clusters. In the case of this Co_6 particle, we have three-dimensional structure with C_{2V} symmetry that was obtained after global optimization of the D_{4h} isomer of Co_6. To model Co_6O_m (m = 1 ... 7), we have used the most stable geometrical structure of the Co_6 particle (key-elements) as the starting point.

The stability and electronic structure of the Co_6O_m (m = 1 ... 7) have been investigated by using the generalized gradient approximation for the exchange-correlation potential in the density functional theory (DFT) as described by Becke's three-parameter hybrid functional using the non-local correlation provided by Lee, Yang, and Parr. The DFT methods are commonly referred to as B3LYP [8]. The 6-31G basis set for Co and O has been used as well [9]. The structures of the investigated nanoparticles have been optimized globally without any symmetry constraint and by starting with various initial geometries. The initial geometry of clusters was constructed accordingly to certain symmetry. So, the set of starting configurations was extensive enough. The GAMESS and Gaussian program suites were used for all simulations here [10-11].

3. Results

To find out how the structure of the Co nanoparticles could change due to the presence of an Oxygen atom, the different structures of the Co_6O_m (m=1-7) have been modeled and investigated applying B3LYP 6-31G approach. The most stable structures are presented in Fig.1.

Firstly, it is necessary to mention that Oxygen stabilizes the Co nanoparticle and increasing number of Oxygen atom the binding energy per atom increases also (Fig.2). The difference of the binding energy per atom of Co_6 and Co_6O is equal to 0.48 eV, while that between of Co_6O_6 and Co_6O_7 is only 0.21 eV, i.e. two times less. On the other hand, the changing of the number of Oxygen atoms from 2 to 3 leads to the largest increase of binding energy per atom (0.72 eV), while the binding energy per atom increase only up to 0.13 eV when the Oxygen atom number in a particle increases from 3 to 4. Thus, the results of our investigations allow us to predict that starting from m=7 (m is number of Oxygen) further increase of the number of Oxygen atoms will not influence the stability of these particles very strongly if the main structure *(*the key-element) will not considerably change. The explanation of such binding energy per atom changeability could be explained by the Co particle geometrical structure changes. In the case when additional Oxygen atom does not significantly increase the binding energy per atom the main part of this atom energy is used to deform the structure of the key element (Co_6). Thus, the binding energies per atom of Co_6O_3 and Co_6O_4 or Co_6O_6 and Co_6O_7 are approximately equal.

It is emphasized that the key element of the Co_6, is present in the Co_6O_m (n = 0, 1, 2, 3, 5, 6, 7) derivatives. However, the key element is slightly deformed. The changeability of the initial form is Oxygen atom depended. The largest deformation is obtained in Co_6O_7, when the distance between the planes (formed of atoms 1, 2, 3 and of 4,5,6) is increased and one plane is rotated in respect the other one by $\pi/4$ angle. Actually, another structure of the Co_6O_7 which looks like Co_6O_6 was also obtained, but the energy of formation of this particle is 1.23 eV higher than that of the particle structure described above (Fig.3).

In the Co_6O_4 particle the key element (Co_6) is deformed twice: 1. the distances between the atoms Co2-Co5 decrease; 2. Co1 and Co6 position in respect of the plane that is formed by atoms 2,3,4,5 is changed. It is emphasized, that the structure of this particle has been obtained after global geometry optimization starting with several completely different initial geometries. Thus, the geometrical structure of the Co_6O_4 particle is confirmed.

Hence, the largest particle Co_6 deformations are obtained when the number of Oxygen atoms is changed from 3 to 4 and from 6 to 7. In these cases the stabilization energy per atom is smaller than in others cases investigated. Thus, the main part of Oxygen energy is used to deform key structure of Co_6.

It is necessary to mention, that in the case of Oxygen atom 2 and 6 the structure of the Co_6O_m particle looks like the octahedron, while in the case of odd numbers of Oxygen the octahedron form is strongly deformed (except the results of Co_6O_4).

The common observation is that that the Co-Co bond lengths are marginally changed only between the atoms that are connected with O (Table 1) and as a consequence the bond enlargement leads to Co-Co bond dissolving. The attention should be paid to results of Co_6O_4. In this case, the bonds forming the Co atom connection with Oxygen are shorter than those in Co_6 particle, but the analysis of the bond order indicates that the above Co-Co bonds are weaker than those in the Co_6 particle. As example: in Co_6 particle bond order between Co1-Co5 is equal to 1.018, while that in Co_6O_4 is approximately twice smaller and equals to 0.55.

To shed some light on the observation, the analyzes of the most important orbitals of in the Co_6 particles have been investigated. In Fig. 4. the highest occupied orbital (HOMO) and the lowest unoccupied orbital (LUMO) gap dependence on the number of Oxygen atoms takes place. The HOMO-LUMO gap indicates that chemical stability of Co_6, Co_6O_3 and Co_6O_6 is very low, i.e. they tend to form new chemical bonds.

Let us remember that in the Co derivatives the number of bonding molecular orbitals that may be occupied is insufficient to locate all electrons of the system [12]. This leads to the presence of electrons on the antibonding orbital and as a consequence to the dissolution of Co-Co bonds.

Table 1

The distance between the Co atoms which are connected with the O atom.

Compound	Co-Co bond length, Å								
	1-2	1-3	1-4	1-6	2-3	2-6	4-5	4-6	3-4
Co_6	2.15	2.33	2.15	2.24	2.04	2.23	2.04	2.31	2.33
Co_6O	2.54								
Co_6O_2				3.01					
Co_6O_3				2.18	2.37	2.33	2.14		
Co_6O_4	2.27	2.27	2.27	4.72				2.27	
Co_6O_5	2.25				2.61	2.25			2.39
Co_6O_6	2.83	2.67	2.89		2.32	2.87			2.44
Co_6O_7	2.93			3.11	2.93		2.93	2.93	

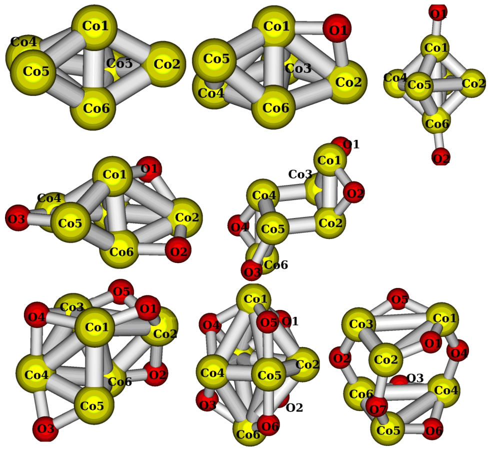

Fig. 1 The views of Co_2O_m (m = 1 ... 7) particles

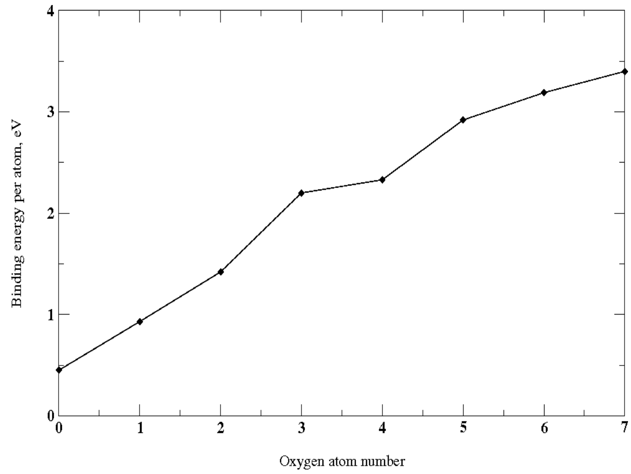

Fig. 2 The dependence of binding energy per atom on the Oxygen atom number

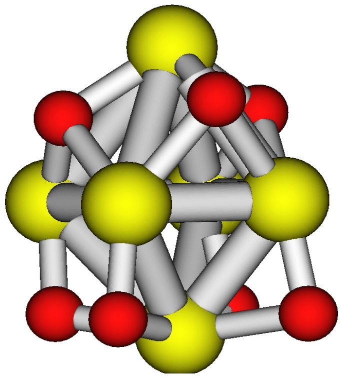

Fig. 3 Structure of the Co_6O_7 looks like Co_6O_6

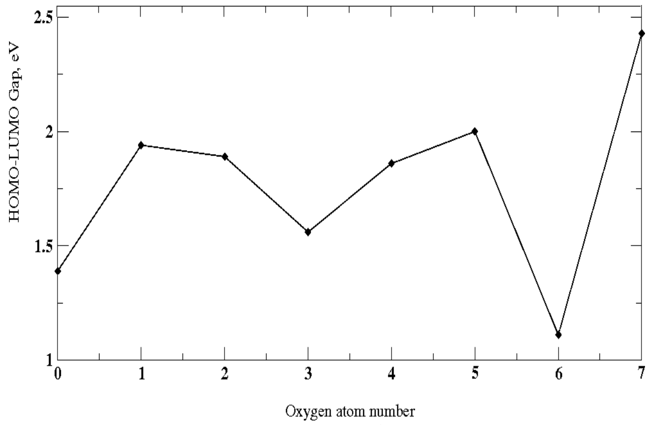

Fig. 4 The HOMO-LUMO gap of the Co_6O_m (m = 1 ... 7)

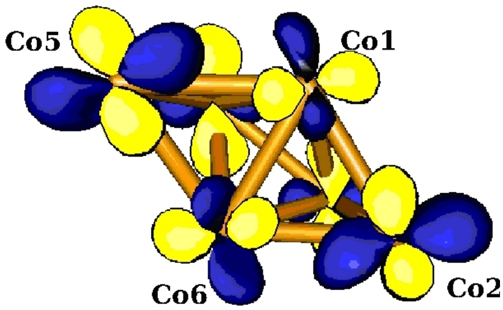

Fig. 5 The HOMO orbital antibonding character of the Co_6 particle

On the other hand, the Co electronic configuration for the ground state neutral gaseous atom is [Ar].$3d^7.4s^2$, while that of O is [He].$2s^2.2p^4$. The configuration associated with Cobalt in its compounds is not necessary the same, but it could be used to expain formally obtained results.

In Co_6 compounds all bonding orbitals are occupied and, as it hasalready been mentioned, some electrons are dispaced on the antibonding orbitals, the energy of which is higher than that of the bonding orbitals. Therefore, the stability of the pure cobalt nanoparticle is low. When Co_6 nanoparticle is joined to one or two Oxygen atoms, the number of electrons that occupy antibonding orbitals decrease because these electrons have occupied Oxygen orbitals.

To support the above explanation, the HOMO orbital character of the Co_6 particle was investigated. The antibonding atomic orbitals between Co1-Co2, Co1-Co6, Co1-Co5, Co2-Co6 and Co6-Co5 were obtained (Fig.5).

Oxygen atoms in the Co_6O_4, Co_6O_3, Co_6O_2, and Co_6O particles are joined to atoms between which the antibonding orbitals occur. Having in mind that the joining of Oxygen atoms leads to bond length increase and dissolution of Co-Co bonds, so the above mentioned prediction is confirmed. In the case of the Co_6O_3 particle, one O atom is joined to Co4-Co5 atoms. The antibonding nature of the bonds has not been observed between these atoms. In this case a stearic effect is more preferable because the other position of the Oxygen atom should complicate Co1-Co2 and Co2-Co6 elongation or leads to destruction of this particle. Hence, Oxygen atoms stabilize Co_6 particles due to dissolving of Co-Co bonds that possess antibonding character.

To be a semiconductor the solid must have at least two characteristics: 1. the bonding and antibonding orbitals must form a delocalized band; 2. the HOMO-LUMO gap in molecular species should be generally on order of 0.5eV to 3.5 eV. HOMO-LUMO gaps of investigated derivative belong to the above range. However, the number of antibonding orbitals decreases with increasing of the number of Oxygen atoms. The results allow us to predict, that Co_6O_m particles should loose their semiconductor properties if the number of Oxygen increase.

4. Conclusions

We have studied the geometrical and electronic structures of small Co_6O_m particle containing m=1-7 Oxygen atoms applying density functional theory. It has been pointed out, that the Oxygen atoms stabilize Co_6O_m (m=0-7) particles. Moreover, the geometrical structure of the key element (Co_6 particle) is insignificantly changed. The strongest deformation is obtained in the case of the Co_6O_4 and Co_6O_7 particles when all bonds with antibonding nature are dissipated.

The obtained results indicate that stabilization effect is on number of the Oxygen atom depended and allow us to predict that starting with m=7 (m is number of Oxygen atoms) further increasing of the number of atoms will not influence strongly the stability of Co_6O_m particles if the key structure will not change very strongly. On the other hand increased of the binding energy per atom is very low when the number of Oxygen atoms increase from 3 till 4 and from 6 till 7 because the main part of the added Oxygen atom energy is used to deform the key element.

The obtained results and presented explanation allow us to predict, that Oxygen atoms will stabilize Co_6 particles due to dissolution of Co-Co bonds that possess antibonding character.

Acknowledgements

Special thanks for BalticGrid, GridTechno and LitGrid project for the resources and support. Authors acknowledge the EU IST Project PHOREMOST grant no. 511616 and EU project HPC-EUROPA (RII3-CT-2003-506079).

References

1. **Chikazumi S.** Physics of Ferromagnetism, Clarendon, Oxford, ed. 2, 1997.
2. **Weller D.**, **Moser A.** Thermal Effect Limits In Ultrahigh Density Magnetic. Recording // IEEE Trans. Mag. 35, 4423, 1999.
3. **Gambardella P.**, **Rusponi S.**, **Veronese M.**, **Dhesi S.**, **Grazioli C.**, **Dallmeyer A.**, **Cabria I.**, **Zeller R.**, **Dederichs P.H.**, **Kern K.**, **Carbone C.**, **Brune H.** Giant Magnetic Anisotropy of Single Cobalt Atoms and Nanoparticles // Science 300,1130, 2003.
4. **Seifert G.**, **Tamuliene J.**, **Gemming S.** Mo_nS_{2n+x} clusters-magic numbers and platelets // Computational Material Science 35, 316, 2006.
5. **S. Tsukamoto**, **N. Koguchi**. Magic numbers in Ga clusters on GaAs (0 0 1) surface // Journal of Crystal Growth. 209 (2000), p. 258 - 262.
6. **Moumita G.**, **Sampathkumaran E. V.**, **Rao C. N. R.** Synthesis and Magnetic Properties of CoO Nanoparticles // Chem. Mater., 17 (9), 2005, p. 2348 -2352.
7. **Ghosh M.**, **Sampathkumaran V.**, **Rao C. N. R.** Synthesis and Magnetic properties of CoO nanoparticles. Chem. Mater. // 17, 2005, p. 2348-2352.
8. **Becke A. D.** Density-functional thermochemistry. The role of exact exchange // J. Chem. Phys. 98, p. 5648, 1993.
9. **Gordon M. S.**, **Binkley J. S.**, **Pople J. A.**, **Pietro W. J.** and **Hehre W. J.** Self-consistent molecular-orbital methods. 22. Small split-valence basis sets for second-row elements // J. Am. Chem. Soc. 104, 1982, p. 2797.
10. Gaussian 03, Revision C.02, **Frisch M. J.**, **Trucks G. W.**, **Schlegel H. B.**, **Scuseria G. E.**, **Robb M. A.**, **Cheeseman J. R.**, **Montgomery J. A.**, **Vreven Jr. T.**, **Kudin K. N.**, **Burant J. C.**, **Millam J. M.**, **Iyengar S. S.**, **Tomasi J.**, **Barone V.**, **Mennucci B.**, **Cossi M.**, **Scalmani G.**, **Rega N.**, **Petersson G. A.**, **Nakatsuji H.**, **Hada M.**, **Ehara M.**, **Toyota K.**, **Fukuda R.**, **Hasegawa J.**, **Ishida M.**, **Nakajima T.**, **Honda Y.**, **Kitao O.**, **Nakai H.**, **Klene M.**, **Li X.**, **Knox J. E.**, **Hratchian H. P.**, **Cross J. B.**, **Bakken V.**, **Adamo C.**, **Jaramillo J.**, **Gomperts R.**, **Stratmann R.E.**, **Yazyev O.**, **Austin A.J.**, **Cammi R.**, **Pomelli C.**, **Ochterski J.W.**, **Ayala P.Y.**, **Morokuma K.**, **Voth G. A.**, **Salvador P.**, **Dannenberg J. J.**, **Zakrzewski V. G.**, **Dapprich S.**, **Daniels A. D.**, **Strain M. C.**, **Farkas O.**, **Malick D. K.**, **Rabuck A. D.**, **Raghavachari K.**, **Foresman J. B.**, **Ortiz J. V.**, **Cui Q.**, **Baboul A. G.**, **Clifford S.**, **Cioslowski J.**, **Stefanov B.B.**, **Liu G.**, **Liashenko A.**, **Piskorz P.**, **Komaromi I.**, **Martin R.L.**, **Fox D. J.**, **Keith T.**, **Al-Laham M. A.**, **Peng C. Y.**, **Nanayakkara A.**, **Challacombe M.**, **Gill P. M. W.**, **Johnson B.**, **Chen W.**, **Wong M. W.**, **Gonzalez C.** and **Pople J. A.** Gaussian, Inc., Wallingford CT, 2004.
11. **Tamulienė J.**, **Vaišnoras R.**, **Badenes G.**, **Balevičius L. M.** "Magnetic properties of Co_2O_n (n=1-7)" to be submitted.

Proceedings of 3rd International Workshop ITELMS'2008

Control of Traffic Safety of Undergrounds' Trains

N. Hvorost

National academy of city services, Revolution str. 12, Kharkov, 61002, Kharkov, Ukraine, E-mail: Justy@fd.lg.ua

Abstract

The forecasting of reliability of the electric isolation is carried out, that is determined by capacity losses in the commutator of the converter at various types of power commutator of the converter with soft commutation in traction electric drives.

1. Investigation Results

In accordance with the State program of development of a railway transport in Ukraine, it is planned putting into production of new locomotives, passenger car for high-speed transportation, cars of electric-, diesel engines - trains and trains of the underground.

The organization of high-speed movement of railway traffic in Ukraine is considered as a necessary condition of integration of a railway transportation of the country in the all-European transport system.

In conditions when the competition in the market of transport services is becoming tougher, the increase of speed of movement of passenger trains has a special significance. Reduction of duration of trip not only promotes a sensation of psychological comfort, but also lowers its cost price for passenger in view of economy of time in transit.

The increase of competiveness of Ukrainian railways is inseparably linked with bringing of operational park of a rolling stock to a state corresponding to the norms and rules of the International Union of railways. For this purpose it is necessary to solve many problems concerning a rolling stock. In particulars, in passenger car building it is necessary to create new generations of undergrounds' cars of the higher comfortableness with a high speed of movement and more effective traction and brake systems.

At the same time the increase of movement speed predetermines necessity of the essential modernization of the rolling stock, first of all, directed on maintenance of smooth running, decrease in noise level and various kinds of vibrations, raising safety of operation and reliability of an electric equipment. Realization of such requirements is substantially connected to perfection of the characteristics of electric equipment, in particular, of traction electric motors, since about 30-35 % of breakdowns of the total number of faults of the electric equipment of a rolling stock [1] are on their share. In this connection the insurance of the safety of movement of the undergrounds' trains is an actual problem. The task of forecasting of serviceability of the traction electric motors providing the set operational reliability is actual one also. The requirements to reliability of these systems in metropolitan railways are a little bit higher than on the main line rail transport. It is caused by complexity of elimination of damages in the conditions of tunnels and also by necessity of providing with passengers' safety on the limited area of landing platforms.

The last developments in the sphere of application of power semi-conductor devices with field control in traction frequency – regulated drives have made possible the technical refitting and modernization of electric transport. It has enabled their use in new systems of frequency - regulated electric drives with the electric alternating current motors. However at the same time with a number of advantages, these devices have also serious lacks such as:

- the limited high-speed response at commutations, which is reduced in process of increase in capacity and a working voltage;
- complex manufacturing technique;
- high cost.

The elimination of restriction of speed operation at commutations is possible with application of the special expensive RLC the filters which are connected between the converter and the engine [2, 3]. They allow to limit the frequency of commutations at pulse-width modulation of powerful high-voltage semi-conductor keys at a level about 500 Hz [4] at the traditional two-zoned characteristic of the control.

The application of the raised frequency of commutations is necessary for the drives with repeatedly - short-term mode of the operation which is used in underground trains. The application of the traditional two-zoned characteristic of the control, as the investigations [5] have shown, results in not optimum copper and steel losses balance of the engine on high speeds of movement.

The elimination of the mentioned lacks is supposed due to use of the circuits of soft and one-operational commutations of power semi-conductor devices, which were generally recognized recently [6, 7]. They allow to return the energy of commutations in the power supply and to raise frequency of commutations in several times (practically without restriction of loading ability of devices on a current). Besides they allow to solve before designated actual problem, that consist in negative effect of high transconductance of the voltage fronts which is supplied on the engine and lowers the reliability of electric isolation, determined by capacity losses in the converter's commutator.

The purpose of the given work is forecasting of reliability of the electric isolation determined by the capacity losses in the converter's commutator, at application of converters with soft commutations in traction electric drives at various variants of enclosure of power commutations of the converter.

The most perspective variant of the units of soft commutation (УК) for the application in powerful converters is shown on Fig. 1. This unit is part of half-bridge (inverter arm) on IGBT-modules VT1, VD1 and VT2, VD2 and is the additional block for all converters in examined circuits of drives.

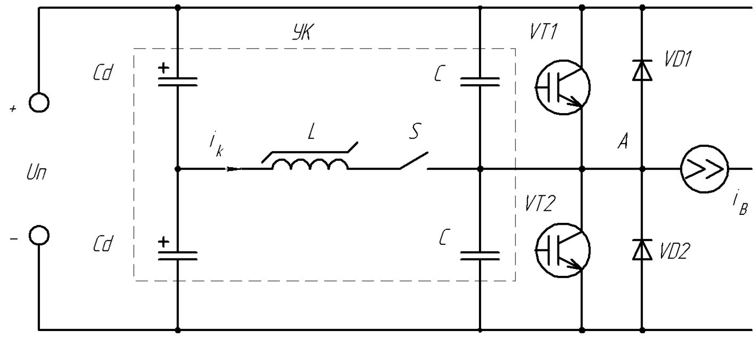

Fig. 1 The circuit of node of commutation (УК) in structure of half-bridge (inverter arm): C_d – condensers of a capacitor divider of a voltage; *L* – a commuting choke; *C* – commuting condensers; *S* – four-square auxiliary key

The feature of the unit of soft commutation lays in the fact that it demands the use of a voltage divider from two capacitors S_d enough the big capacitance, between which the voltage U_n is distributed in equal portions, but possesses the minimal established capacity of the rest of the elements.

The forecasting of reliability of electric isolation is examined for three variants of power circuits of the converters with commuting unit of the basis of the traditional three-phase circuit (the circuit 1), of two-phase one with bridge commutators in each phase (the circuit 2) and on the basis of three-phase bridge converters (the circuit 3). In these circuits the entrance capacitor divider is executed by the general one, there is one auxiliary key S for each inverter arm. In the two- phase circuit with bridge commutators the chokes of each of the bridges are tied, the commuting condensers are shunting each of transistors. Comparison of reliability of the converters is carried out on total capacity losses P in the converter commutator and in all nodes of commutation of the circuits as well as in condenser dividers. The total losses of the specified capacity for three examined circuits are given in table 1.

Table 1

Parameter	The circuit 1	The circuit 2	The circuit 3
Total capacity loss *P*, kW	9.21	6.65	8.32

The comparison of the presented results on total capacity losses shows the advantages of the two-phase circuit and confirms its reliability in comparison with other variants.

2. Conclusions

Application of converters with soft commutation in traction in frequency-regulated electric drives will allow:

1. To reduce weight of traction asynchronous engines by 30-40 % due to refusal from expensive RLC filters.
2. To raise reliability of electric isolation in 1.3…1.5 times.

References

1. **Сінчук О. М.**, **Сушко Д. Л.** Тактика підходу до створення комплексної системи діагностування тягових електродвигунів електрорухомого складу //Залізничний транспорт України. No 3/1 (48), 2005. p. 99-102.
2. **Rendusara D.**, **Engeti P.** An improved inverter output filter configuration reduces common and differential modes du/dt at the motor terminals in PWM drive systems // IEEE Trans. on Power Electronics, vol. 13, 1998, No. 6, p. 1135-1143.
3. **Бару А.Ю.**, **Шинднекс Ю.Л.** Преобразователи частоты для электроприводов большой мощности / Технічна електродинаміка, темат. Випуск „Системи електроживлення".- К.,1999, с.113.
4. IGBT-модули FZ600R65KF1. Technische information EUPEC / Москва, 2002, 7с.
5. **Хворост М.В.**, **Гончаров Ю.П.**, **Панасенко М.В.**, **Замураєв В.В.**, **Родін М.Ю.**, **Чумак В.А.**, **Нікулін В.С.** Тяговий електропривод метровагонів з однозонною характеристикою керування / Інформаційно-керуючі системи на залізничному транспорті. – К.,2005, №4 – С. 25-30. [in Ukrainian].
6. **Yuan X.**, **Barbi I.** Zero-voltage switching for three-level capacitor clamping inverter / IEEE Trans. on Power Electronics, V.14,1999, №4, p. 771-781.
7. **Гончаров Ю.П. и др**. Силовые полупроводниковые ключи с внутренней обратной связью, действующей на выключение // Вестник ХГПУ, Харьков, вып. 106, 2000. -с. 67-74. [in Russian].

Proceedings of 3rd International Workshop ITELMS'2008

Modelling the Artificial Neural Network for Heating System Choice for City Electrical Transport

I. Beinarts

Riga Technical University, Kronvalda blvd. 1, LV-1007, Riga, Latvia, E-mail: ivars.beinarts@latnet.lv

Abstract

The provided results prove that the use of Artificial Neural Networks with application of the proposed algorithm can be a very useful for solving choosing problem of HVAC system for public electric transport. Usage of created model and algorithm will raise possibility to increase efficiency of choosing task, so choosing time will be minimized with high result validity. When use artificial intellect, opportunity rises to do system self tuning and to export and change findings with some similar choosing systems. The elaborated system model can be used for different system choosing tasks, too.

Introduction

This article describes usage of Artificial Neural Network (ANN) for choice of Heating, Ventilation and Air Conditioning (HVAC) system for city electro transport passengers' interior. Neural Network is trained to analyze the parameters of the system and detect the possibility of its usage in the specific task.

There are system criteria formalized in the article. Defining of consumer's priorities and temperature control system parameters provides an optimal choice of HVAC system, taking in account effective energy consumption problem. HVAC system choosing criteria and procedure for air condition system choice are formalized in the article. Deep and detailed investigation of the behaviour of such a system, its operation and running processes requires its generalized mathematic modelling, taking into account all possible regimes of the operation of compressor and fan motors and setting an algorithm of their control in all possible regimes under any condition. When use artificial intellect, opportunity rises to do system self tuning and to export and change findings with some similar, distant choice systems.

This paper provides mathematical model of heating system choosing method for passengers' interior climate parameters control. There are main conclusions at the end of the article.

Table 1

Groups of system parameters

No	Parameter		Constructive	Environmental	Service	Costs
1.	Dimensions / mm /	d	X			
2.	Weight / kg /	m	X			
3.	Power voltage / V /	u	X			
4.	Power current / A /	i	X			
5.	Cold productivity / kW /	q_1		X		
6.	Heat productivity / kW /	q_2		X		
7.	Outside air consumption / m^3/h /	v		X		
8.	Minimal interior temperature / °C /	t_1		X		
9.	Maximal interior temperature / °C /	t_2		X		
10.	Automatic temp. regulation Y/N	s_1			X	
11.	Digital control panel Y/N	s_2			X	
12.	Outside air filtration Y/N	s_3			X	
13.	Inside air anti-virus protection Y/N	s_4			X	
14.	AI based control system Y/N	s_5			X	
15.	Energy saving control regime	s_6			X	
16.	Price EUR	c_1				X
17.	Monthly exploitation cost EUR	c_2				X
18.	Monthly service cost EUR	c_3				X

1. HVAC System Parameters

HVAC system is characterized by several parameters. They can be divided to several groups:

1. Constructive parameters;
2. Environment control parameters;

3. Service functions;
4. Costs.

Weight is adjusted to each group of parameters, which defines a degree of importance of each parameter. Each group consists of individual parameters which also are classified by their degree of importance inside each group with the respective weight.

When choosing HVAC system, individual parameters are analyzed at first and then weight category of the whole group is evaluated.

2. Problem Formulation

The purpose is to choose the optimal HVAC system for public electro transport passengers' interior, taking into account the admissible constructive parameters, the necessary interior environment parameters, as well as the necessary service functions. Costs for obtaining of system and exploitation costs are important, too. As all these parameters are defined for each product already at a factory then intellectual method for comparison of parameters of many similar devices can be used. That would give a possibility to do the choice of the most appropriate HVAC system quickly and with a high reliability.

In order to make quick and based on weights system choice, artificial intellect systems are the most appropriate, that is, usage of artificial neural network as a basis of choice system. Usage of neural networks has several advantages in comparison to other methods. Possibility to perform system training using expert's knowledge or by transferring knowledge base from similar choice systems is one of the main advantages. That is absolutely flexible and can be adjusted to any choice criteria of HVAC system. Number of parameters to be analyzed is limited only by number of neurons in input layer.

3. Artificial Neural Network

The back propagation artificial neural network (ANN) is used (Fig.1) in the decision system described in the paper.

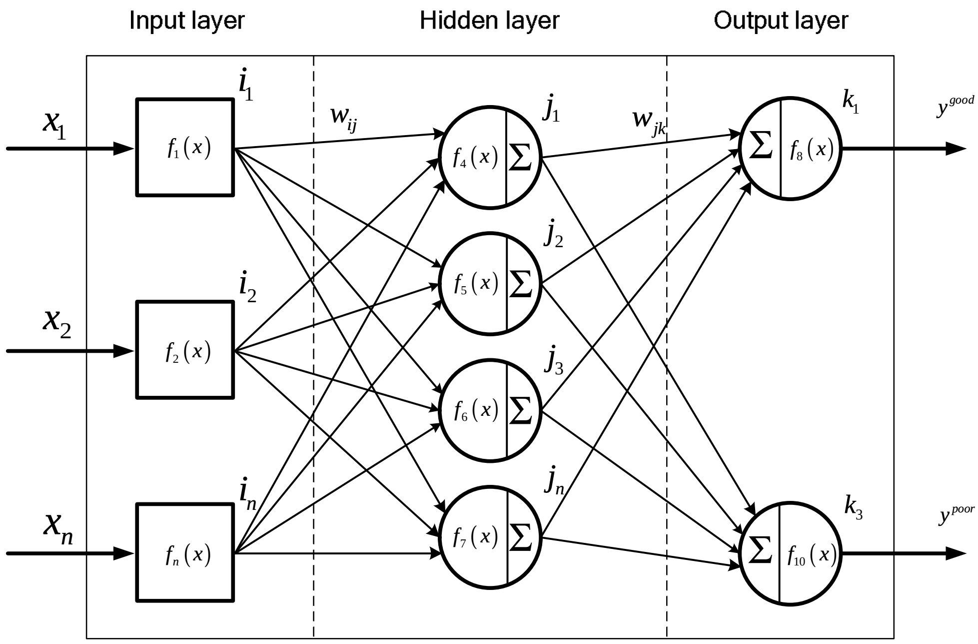

Fig. 1 Back propagation artificial neural network. Input layer elements: $\{i_1, i_2, ..., i_n\}$, hidden layer elements: $\{j_1, j_2, ..., i_n\}$, output layer elements: $\{k_1, k_2, ..., k_n\}$, input patterns: $\{x_1, x_2, ..., x_n\}$, weights: $\{w_1, w_2, ..., w_n\}$, neuron activation function: $f(x)$, outputs: $\{y^{good}, y^{poor}\}$

An ANN works as a solid massive parallel processor, which is constituted by several simple units and has a natural propensity to store experimental knowledge and use it to create non-linear relationships between inputs and outputs. In other words, an ANN is a highly interconnected network made of many simple processors. Each processor in the network maintains only one piece of dynamic information and is capable of only a few simple computations. An ANN performs computations by propagating changes in activation between the processors [2].

ANN consists of three or more layers- Input, hidden (one or more) and Output layers. The output of a neuron in a layer goes to all neurons in the following layer. Each neuron has its own input weight *w*. The weights for the input layer are assumed to be 1 for each input. The output of the ANN is reached by applying input values to the input layer, passing the output of each neuron to the following layer as input. The number of neurons in the input layer depends on the number of possible inputs, while the number of neurons in the output layer depends on the number of desired outputs. The number of hidden layers and how many neurons in each hidden layer cannot be well defined in advance, and can be changed. The addition of hidden layer could allow the network to learn more complex patterns, but at the same time decreases its performance.

The ANN could be divided into seven basic parts, as described in [3]:

- The set of individual processing units or neurons.
- The state of activation of processing unit.
- The function used to compute the output of a processing unit.
- The pattern of connectivity among the processing units.
- The rule of propagation employed.
- The activation functions for each individual processing unit.
- The rules of learning that allow the determination of the pattern of connectivity between processing units.

Step 1. Initialize system;

Step 2. Insert current (n^{th}) system parameters in ANN input layer;

Step 3. Process data with ANN. Output Good/Poor data; If Poor then delete entry (with current n);

Step 4. Save current system data in new table n_1;

Step 5. Next n;

.

Step 7. Check last entry of table;

Step 8. Repeat steps 2-7 with new table data.

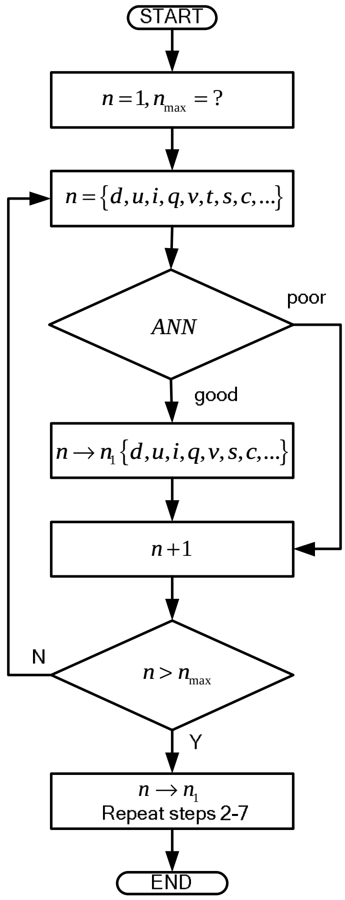

Fig. 2 Problem decision algorithm

3.1. ANN Back Propagation Algorithm

It is necessary to train a multi layer feed forward network by gradient descent to approximate an unknown function, based on some training data consisting of pairs (x, t). The vector x represents a pattern of input to the network, and the vector t- the corresponding desired output. The overall gradient with respect to the entire training set is just the sum of the gradients for each pattern.

In the paper there is used fully connected layered feed forward network- that is, each node in a given layer connects to every node in the next layer, then it is often more convenient to write the back propagation algorithm in matrix notation rather than using more general graph form. In this notation, the biases, weights, net inputs, activations and error signals for all units in a layer are combined into vectors, while all the non-bias weights from one layer to next form a matrix W which is described in [1].

4. Problem Decision Algorithm

In order to perform optimal choice of HVAC system for electro transport passengers' interior, it is necessary to define precisely an idea about admissible constructive parameters as well as about necessary interior environmental parameters and necessary service functions which has to be provided by the system. All these parameters have to be classified in groups (table 1) and weight to each of them inside the group has to be adjusted. Preparing of choice system and data is performed in the following order:

Step 1. Critical parameters groups table of systems is prepared;

Step 2. Suitable weight is assigned to each group of parameters $a_g \leq 0.5$;

Step 3. Group significance weight is assigned to each parameter in group $a_p \leq 0.5$;

Step 4. Total weight is calculated $a_g + a_p = a \leq 1$;

Step 5. ANN training is performed using expert knowledge or knowledge transferred from other choice system.

After Artificial Neural Network system training is finished, comparison procedure of aggregated system data is performed according algorithm in Fig. 2.

Data about each parameter of current system is entered in ANN input layer neurons. Value of each parameter is evaluated using the weight of neuron. If the proportion is within acceptable limits neuron becomes activated. Hidden layer neurons compare input signal values and become active according to functions assigned during training process. Hidden layer outputs are delivered to output layer neurons. Only two neurons, which indicate ANN work result, are in the output layer.

When number of system $n > n_{max}$, that means all data of HVAC systems being in the list are processed, data of not useful systems are deleted from the data base and comparison using useful systems data is performed again (Step 2-7). As well as new and stricter choice criteria are entered in ANN. Process of choice is finished when one, the most appropriate HVAC system is found.

References

1. **Beinarts I.**, **Levchenkov A.** Passengers' Interior Climate Parameters Optimization Using Intelligent Control with Neural Networks. Proceedings of 7th International Conference „Transport Systems Telematics TST 2007". Katowice, Poland, 2007.
2. **Rajasekaran S.**, **Febin M. F.**, **Ramasamy J. V.** Artifical Fuzzy neural Networks in Civil Engineering // Computers & Structures. 2002, vol. 61 ,No. 2, p. 291-302.
3. **Sriram R. D.** Intelligent Systems for Engineering: a knowledge-based approach. Springler-Verlag, 1997, 804 p.

Proceedings of 3rd International Workshop ITELMS'2008

Modeling of Scheduling Theory in Intelligent Electric Transport Systems

I. Alps[*], M. Gorobetz[**], A. Levchenkov[***], L. Ribickis[****]

[*] *Riga Technical University, Faculty of Electrical and Power Engineering, Kalku St. 1, LV-1658 Riga, Latvia, E-mail: ivarsa@com.lmt.lv*
[**] *Riga Technical University, Faculty of Electrical and Power Engineering, Kalku St. 1, LV-1658 Riga, Latvia, E-mail: mgorobetz@latnet.lv*
[***] *Riga Technical University, Faculty of Electrical and Power Engineering, Kalku St. 1, LV-1658 Riga, Latvia, E-mail: levas@latnet.lv*
[****] *Riga Technical University, Faculty of Electrical and Power Engineering, Kalku St. 1, LV-1658 Riga, Latvia, E-mail: leonids.ribickis@rtu.lv*

Abstract

In this paper authors presents modeling of neural network controller to control speed of DC drive. Main tasks of this research are to use artificial neural network for speed control of DC drive in virtual laboratory.

The feed-forward back-propagation neural network is used for controller. Levenberg-Marquardt back-propagation algorithm is proposed as a training method. Neural network is trained to maintain rotation speed of DC drive in defined interval.

Results of modeling show the possibility to use neural network controller for speed control of DC drive.

KEY WORDS: *scheduling theory, modeling, neural network.*

1. Problem Formulation

The purpose of this research is to model usage method of scheduling theory and neural network for speed control of direct current drive in virtual laboratory.

Object of research is public electric transport system.

Main tasks of research are: read up structure of public electric transport, read up methods of scheduling theory, define structure of intelligent public electric transport, research neural network application to control electric transport, read up programming and modeling facilities in Matlab environment, realize programmable model of scheduling theory method in Matlab environment, to develop GUIDE for schedule, to develop DC drive model in Simulink environment, to develop model of neural network controller, to train artificial neural network for speed control according schedule.

2. Method of Solutions

Authors propose to use following structure of neural network Fig.1.

Neural network mathematical model is based on neuron structure. Each neuron has input data set, weight for each input data, activation function and output, which usually has binary value if output neurons are perceptrons with hard limit transfer function and real value is there differentiable transfer function is used.

Neural network consists of several layers. Each layer may have definite or indefinite number of neurons. Neural networks give possibility to analyse an object by input parameter set and to detect predefined class of the object on the output. That means, neural network should be trained to detect classes and classes are predefined.

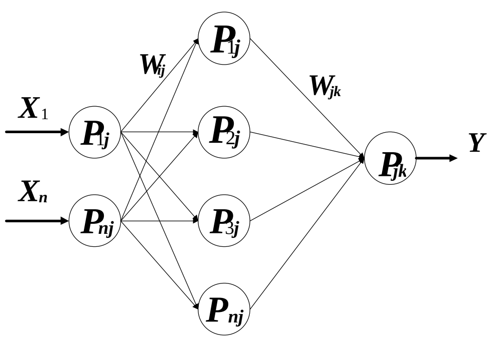

Fig. 1 Structure of neural network

3. Mathematical Model

Mathematical model for transport network. Graph (Fig.2.) – *G(N,E)*, where

1. nodes: $N = \{n_1, n_2, ..., n_v\}$;
2. edges – subset from Cartesian product of nodes: $E = \{e_1, e_2, ..., e_l\}$;

   $e_j =< n_a, n_b >, \quad j = \overline{1,l}, \quad a,b = \overline{1,v}, \quad a \neq b, \quad E \subseteq N \times N$;
3. Routes for public transport – cyclic subgraph of G:

   $Routes = \{route_1, ..., route_y\}$

   $route_k = \{< node_1, edge_1 >, ... < node_x, edge_z >, node_1\},$

   $k = \overline{1,y} \quad x \in \overline{1,v}, \quad z \in \overline{1,l},$

   $node_i \in N, \quad edge_j \in E,$
4. Each route stage – *route_stage$_r$* = < *node, edge* > *Î route$_k$* – has following parameters:
   a. *l Î* ℜ – length;
   b. *sp Î* ℜ - speed limit;
   c. *type* ∈ {"L", "X", "S", …} – type of stage – line, crossroad, stop, …;
   d. *cycle = <red_cycle, green_cycle>, red_cycle, green_cycle Î* ℜ
      additional parameter for crossroads only red light burning time, green light burning time.

Mathematical model for electric transport DC drive. DC drive and armature circuit in Simulink environment are represent at Fig.3. and Fig.4.

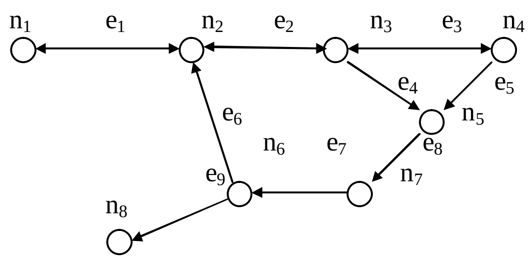

Fig. 2 An example of transport network

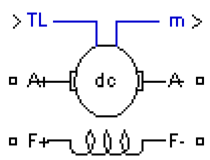

Fig. 3 DC drive in Simulink environment

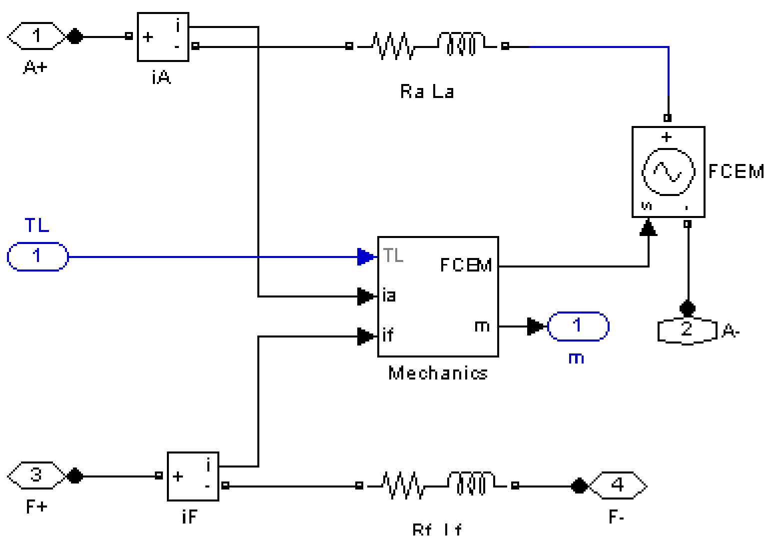

Fig. 4 Armature circuit in Simulink environment

DC drive is realized with four electric input/output (A+, A-, F+, F-), one torque signal TL and four signals containing output measurements block in following order:

1. Speed ω (rad/s)
2. Armature current I_a (A)
3. Field current I_f (A)
4. Electrical torque T (Nm)

An access is provided to the field terminals (F+, F-) so that the machine model can be used as a shunt-connected or a series-connected DC machine. The torque applied to the shaft is provided at the Simulink input TL. The armature circuit (A+, A-) consists of an inductor La and resistor Ra in series with a counter-electromotive force (CEMF) E. The CEMF is proportional to the machine speed.

$$E = K_E w.$$

where K_E is the voltage constant and ω is the machine speed.

In a separately excited DC machine model, the voltage constant KE is proportional to the field current I_f:

$$K_E = L_{af} I_f,$$

where L_{af} is the field-armature mutual inductance.

The electromechanical torque developed by the DC machine is proportional to the armature current I_a:

$$T_e = K_T I_a,$$

where K_T is the torque constant. The sign convention for T_e and T_L is

$$T_e T_L > 0\text{: motor mode}$$

$$T_e T_L < 0\text{: generator mode}$$

The torque constant is equal to the voltage constant:

$$K_T = K_E.$$

The armature circuit is connected between the A+ and A- ports of the DC Machine block. It is represented by a series Ra La branch in series with a Controlled Voltage Source and a Current Measurement block.

The mechanical part is represented by Simulink blocks that implement the equation

$$J\frac{\mathrm{d}w}{\mathrm{d}t} = T_e - \mathrm{sgn}(w)T_L - B_m w - T_f,$$

where J is inertia, B_m is viscous friction coefficient, and T_f is Coulomb friction torque.

Mathematical model for schedule:

1. A set of processors P – stops and crossroads, where $P = \{P^1, P^2\}$, $P \in N$, Stops: $P^1 = \{p_1^1, p_2^1, ..., p_s^1\} \subset P$, Crossroads: $P^2 = \{p_1^2, p_2^2, ..., p_c^2\} \subset P$
2. A set of jobs U – vehicles, where $U = \{u_1, u_2, ..., u_m\}$
3. Each vehicle has the schedule: $\forall u \in U, \quad s_u : P^1 \to \{t_{u1}, t_{u2}, ..., t_{us}\} \subset \Re$
4. Each stop has the schedule: $\forall p \in P^1, \quad s_p : U \to \{t_{p1}, t_{p2}, ..., t_{pm}\} \subset \Re$

Mathematical model for neural network

1. Input data set for neural network: $X = \{x_1, x_2, ..., x_n\}$
2. Set of artificial neural network hidden layers: $L = \{l_1, l_2, ..., l_k\}$
3. Set of neurons for each *j*-th hidden layer: $P^j = \{p_1, p_2, ..., p_r\}$
4. Set of neural network outputs: $Y = \{y_1, y_2, ..., y_m\}$
5. Weights for each input of *i*-th neuron of *j*-th layer: $W_i^j = \{w_{i1}, w_{i2}, ..., w_{in}\}$
6. Bias for each *i*-th neuron of *j*-th layer: b_i^j
7. Input summation function for each *i*-th neuron of *j*-th layer: $s_i^j = \Sigma\left(W_i^j \cdot X\right) + b_i^j$
8. Transfer function for all neurons of *j*-th layer : $F^j(s^j)$

4. Problem solution algorithm

Schedule correcting algorithm. Schedule correcting block diagram is presented in Fig.5.

Algorithm for neural network controller training. Authors propose to use *Levenberg-Marquardt (LM)* back-propagation algorithm. This network training function that updates weight and bias values corresponding to *Levenberg-Marquardt* optimization.

Levenberg-Marquardt algorithm usually use with:

1. Feed forward network.
2. *Cascade-forward* network.
3. *Elman* network etc.

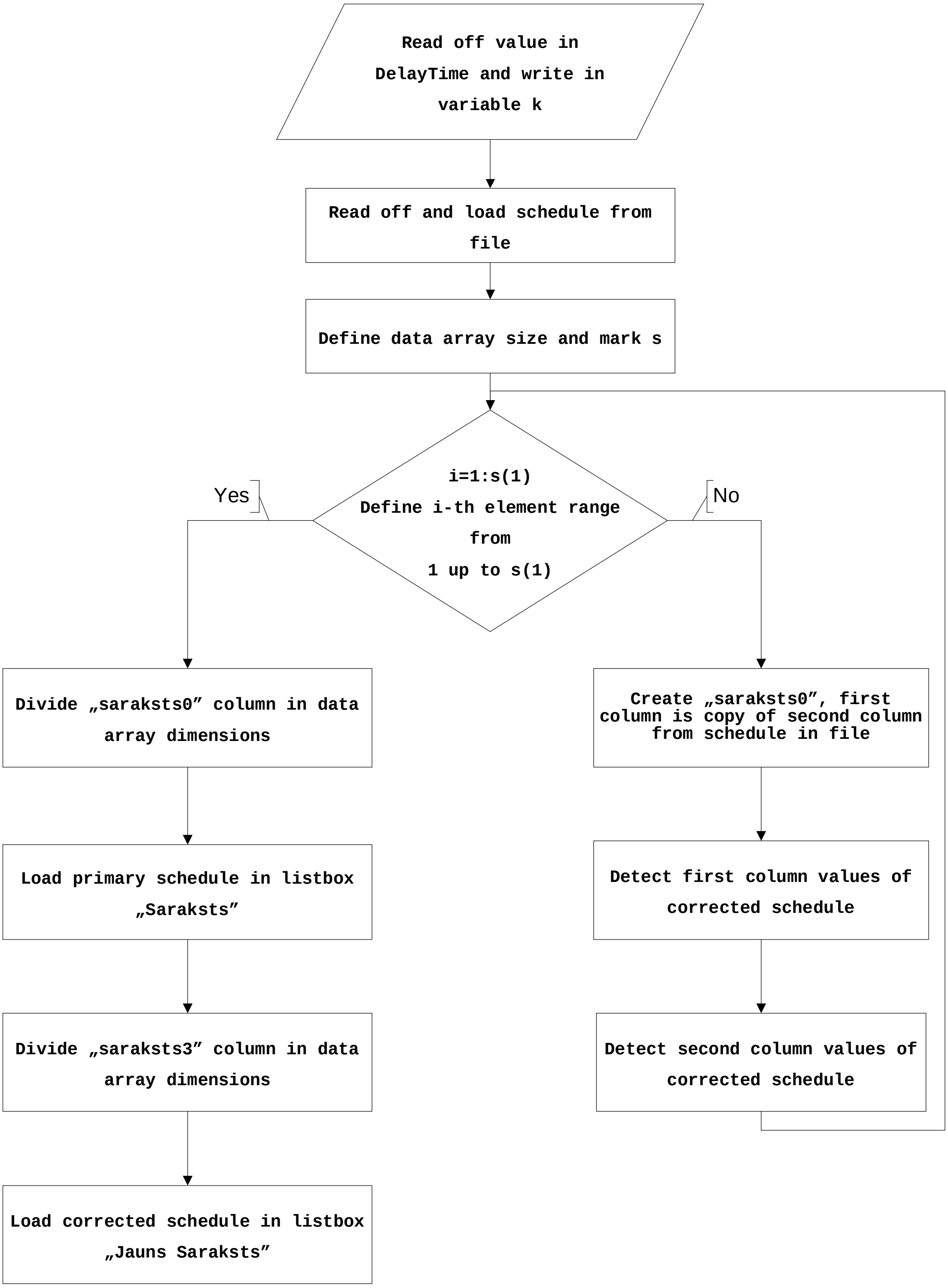

Fig. 5 Schedule correcting block diagram

Levenberg-Marquardt can train any network as long as its weight, net input and transfer functions have derivative functions.

Back-propagation is used to calculate the Jacobian *jX* of performance with respect to the weight and bias variables *X*. Each variable is adjusted according to *Levenberg-Marquardt*:

$$jj = jX \cdot jX,$$

$$je = jX \cdot E,$$

$$dX = -(jj + I \cdot mu) / je,$$

where *E* is all errors and *I* is the identity matrix.

The adaptive value *mu* is increased until the change above results in a reduce performance value. The change is then made to the network and *mu* is decreased.

Algorithm stops when any of these conditions occur:

1. The maximum number of epochs (repetitions) is reached
2. The maximum amount of time has been exceeded.
3. Performance has been minimized to the goal.
4. The performance gradient falls below minimum.
5. Value of *mu* exceeds maximal value.

Computer experiment

Modelling of DC drive. General schema of DC drive with artificial neural network controller in Matlab environment is presented in Fig.6. Result of modeling is presented in Fig.7.

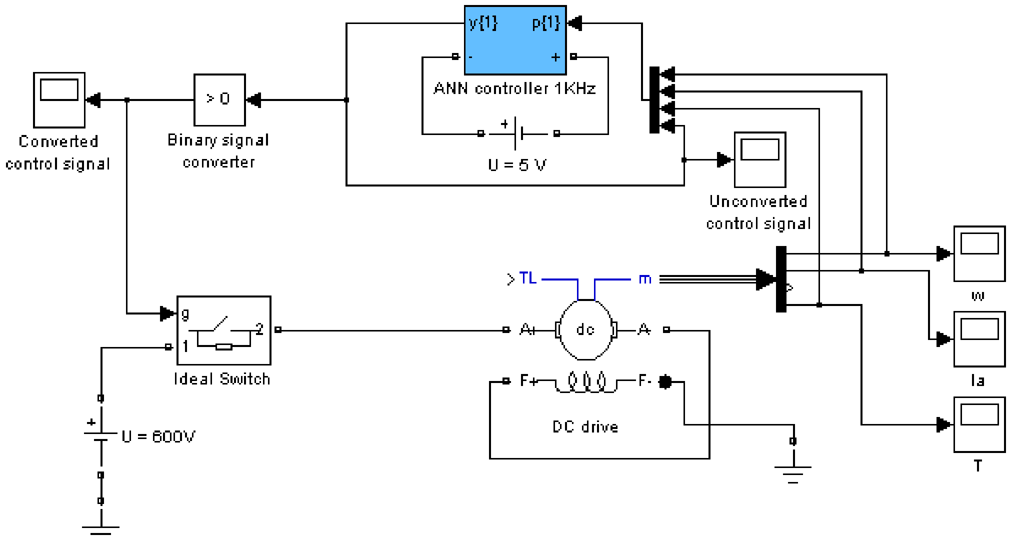

Fig. 6 Model of DC drive with ANN controller

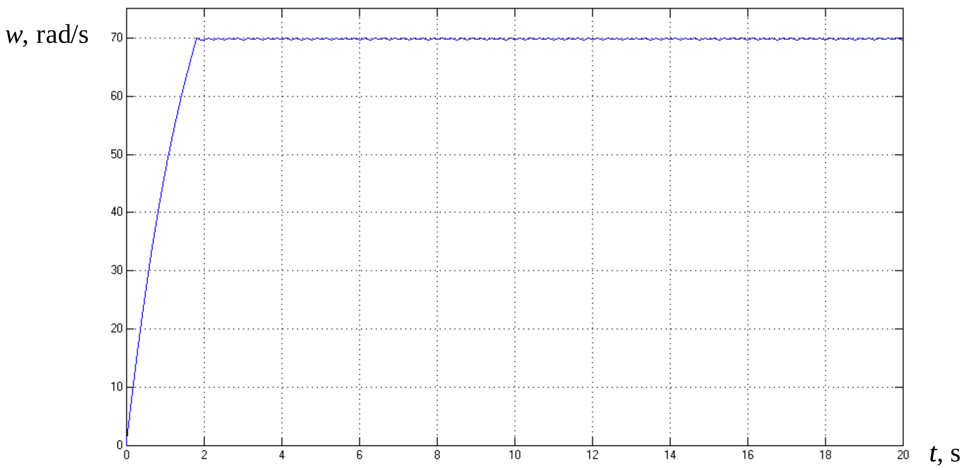

Fig. 7 Rotation speed controlled by trained neural network with clock rate 1kHz

Model allow to use any value clock rate, but in real life this parameter should be appropriate corresponding to sensors, switches, quantity of data, size of neural network. That is why it is necessary to find out an optimal time interval for process digitizing and monitoring. Too short time interval may need a lot of CPU resources for analysis, but too long time interval may be dangerous. Time interval has minimum and maximum limits. Minimum is limited by response time of all electric devices, but maximum is limited by safety level criterion.

Schedule modeling. Arriving time in stops after starting: 1 stop – after 15 min, 2 stop – after 45 min, 3 stop – after 1h and 10min (70 min), 4 stop – after 1h and 40 min (100 min).

Creating a program in Matlab environment we obtain a solution of problem, which is presented in Fig.8.

Graphical User Interface development environment (GUIDE) in Matlab for neural network training is presented in Fig.9.

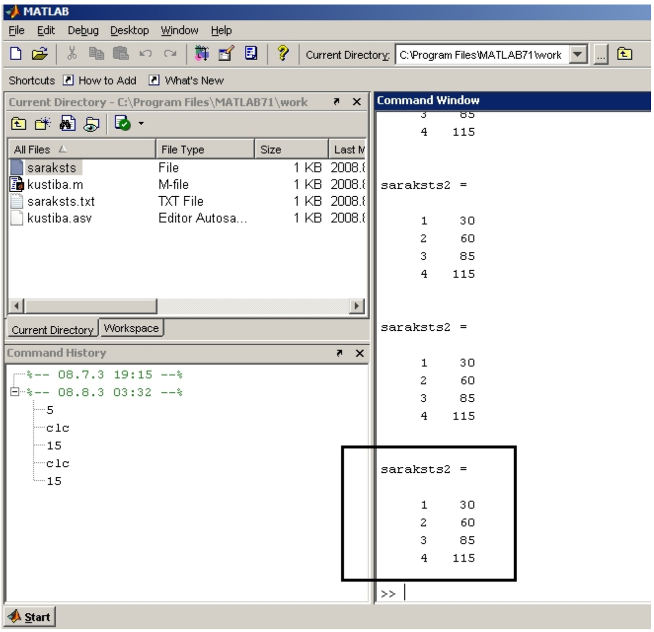

Fig. 8 Creating corrected schedule in Matlab environment

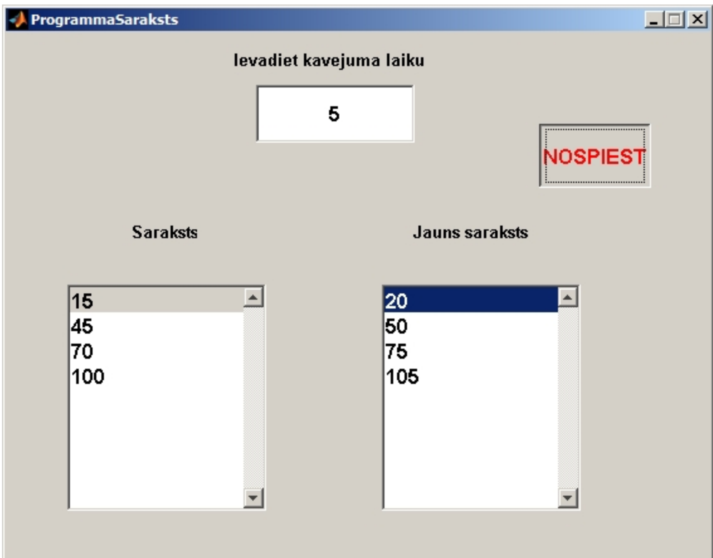

Fig. 9 GUIDE in Matlab for neural network training

Conclusions

Results show the possibility to create corrected schedules for pulic electric transport with programs in Matlab environment. Computer experiments show that program in Matlab environment could be use for public transport.

Results of modeling show the possibility to use neural network controller for speed control of DC drive. Neural network allow producing not only signal but set of control signals.

Neural network controller may be used as for control as for forecasting and warning about dangerous situation. It may prevent breakdowns and accidents and may be used for optimal speed control of public transport.

Refereces

1. **Luger G. F.** Artificial Intelligence. Structures and Strategies for Complex Problem Solving, Williams, 2003, 863 p.
2. **Russel S. J.**, **Norvig P.** Artificial Intelligence. A Modern Approach, 2nd edition. Prentice Hall, 2006, 1408 p.
3. **Rankis I.**, **Gorobetz M.**, **Levchenkov A.** Optimal Electric Vehicle Speed Control by Intelligent Devices. Rīgas Tehniskās universitātes raksti. Enerģētika un Elektrotehnika. Sērija 4, sējums 16. 2006. p. 127-137.
4. **Gorobetz M.**, **Levchenkov A.** Modelling Of Artificial Neural Network Controller For Electric Drive // In Proceedings of 10th International Conference on Computer Modelling and Simulation (UKSIM), Cambridge, UK, 1-3 April, 2008.

Proceedings of 3rd International Workshop ITELMS'2008

Effect of Long-Term Thermal Influence on Mechanical Properties of Welded Joints for Carbon Steels Used in Power Engineering

Ž. Bazaras*, B. Timofeev**

* *Kaunas University of Technology, Daukanto 12, LT – 35212, Panevėžys, Lithuania, E-mail: zilvinas.bazaras@ktu.lt*
** *St. Petersburg State Polytechnic Institute, St. Petersburg, Russia*

Abstract

For the manufacture of separate power equipment components (steam generators, separators, collectors, pressurizes and so on) it is wide used carbon steel of the type 22K. As these elements are very responsible for pressure vessels having a thickness above 80 mm it is therefore best to apply steel of improved metallurgical quality, obtained by means of electroslag or vacuum-arc re-melting. As a rule, 22K steel of standard quality (open-hearth furnace melting) is usually used for multiple forced circulation circuit (MFCC) piping of RBMK reactors and special melting methods – for steam generator case. The application of special method of melting for this type of steel provides a higher quality level. High requirements are imposed also on the level of welded joints mechanical properties at 20°C (ultimate tensile stress $UTS = s_B = 420$ MPa, yield stress $YS = s_{0.2} = 220$ MPa, elongation $A_5 = 20\%$, reduction of area $Z = 50\%$), which practically coincides with the minimum level of base metal properties, specified in TY24-3-449-74.

KEY WORDS: *carbon steels, power engineering, ultimate tensile stress.*

1. Investigated materials

Melting of steel of the given mark (22K) from metallic change is a task of open hearth process. The composition of metallic charge may vary from 100% pig iron to 100% steel return, in this case the pig iron component may be in liquid and solid state. Materials: ore, pitch, oxygen and fuel. Melted metal is cast. The low part of ingot (zone with negative chemical heterogeneity) and sink head (zone of positive segregation with increased content of sulphur, phosphorus and carbon) are removed and we have open-hearth furnace steel.

Metal of electroslag melting is obtained by melting of bars (rods) of open- hearth melting in the electrical conductive slag. Electroslag process takes place in copper mould cooled by water. Slag is formed at the expense of melting of the flux AHF-6 ($CaF_2 + Al_2O_3$). Metal is obtained of more pure especially on the content of gases because the process of rod metal melting takes place in the protective slag system. Metal of vacuum arc melting is practically formed under the same conditions like the electroslag process. Vacuum is used instead of slag protection and the process itself – electric arc. This makes possible to obtain more pure metal.

Steel of special melting methods has more dense uniform oriented structure, containing minimum number of non-metallic inclusions. It is well known that with using melting it is possible to obtain more refined metal containing sulphides less by 40 ... 50%, the number of oxide inclusions and silicates less by 1.5 times as compared with the steel of the same type of open-hearth melting. Ductility and fatigue strength of steel (of these melting methods) is higher considerably than for steel of open-hearth melting.

In NPP material used for products manufacture the macrostructure of zone with increased etching ability must be limited in sizes and mainly depends on metal crystallization and sulphur content in it. It is necessary to take into account the fact that in ingots from 22K steel of usual melting the off-axis inhomogeneity take place. In some ingots the sources of this inhomogeneity are sulphides “whiskers” which reach considerable sizes. In the process of operation the presence of such defects may result in metal delaminating or plate cracking.

In VAR and ESR due to the oriented crystallization and uniform sulphur distribution across the whole section the “whiskers” are absent, therefore the production of components and welded joints of pressure vessels with wall thickness equal to 120 mm and more is carried out only from steel of special melting method. The content of gas in metal of special procedures of melting is considerably lower than by the open hearth melting.

As concerns density, homogeneity and absence of internal defects the vacuum-arc steel exceeds greatly electroslag, open-hearth and electric furnace steels. Structure and properties of steel depend not only on metallurgical effect of melting but also on a possible variation of its chemical composition within the limits of values permissible in Specification.

2. Requirements for stability of properties during operation

In accordance with item 7.6.3 of “Rules of arrangement and safe operation of equipment and piping of NPP”, PNAE G-7-008-89 [1] the inspection of equipment mechanicalproperties is carried out using destructive and non-destructive techniques. It shall be performed out not rarely than at interval of 100000 hrs of operation for NPP with water-cooled and water-moderated reactors (WWER) and water-graphite reactors (RBMK), and at intervals of 50000 hrs for fast reactors with liquid metal coolant (BN). This order of assessment of actual properties of material in the process of operation was introduced in the regulations of NPP works for the purpose of safety provision. This requirement was associated with the necessity to obtain valid information about material ageing in the NPP equipment operation and on the base of this information to estimate the change of strength margin coefficient used in design with regard to variations of initial mechanical properties of materials. It is possible to assess various methods using surveillance specimens, part of materials removed from the inner surface of equipment (RPV, SG and other large cases) or a part of the piping [2]. For RPV as a rule the variation of mechanical properties are examined with the use of surveillance specimens which are tested not less than six times during the calculated design lifetime of reactor.

By the development of the first normative documents for NPP arrangement and safe operation of other equipment and piping of NPP PNAE G-7-008-89 [1] the regulation about a periodical inspection of steel mechanical properties on the base of test results of specimens removed from pipe-lines was introduced. It makes possible to follow the actual state of pipe-lines and variation of mechanical properties of base metal and welded joints under the influence of real operating conditions (elevated temperature, pressure, corrosive medium) by all regimes. It is natural to suggest that due to the operation influence (static and cyclic loads, a prolonged effect of elevated temperatures and coolant) the degradation of material mechanical properties is possible. Of course in accordance with “Strength Calculations Norms” these factors should be taken into consideration in the condition by calculations. The values of the mechanical properties of NPP materials during the whole designed lifetime is estimated by definite requirements which are presented in Table 1.

At a present time a great experience has been accumulated on the determination of ageing processes under conditions of NPP pipe-lines operation which has shown that the steel mechanical properties variations of pipe-lines are small and are within the limits of measurement accuracy. Such results might be expected for operation conditions of pipe-lines in light water pressurized reactors thanks to:

- steady structure equilibrium of structural steels used for pipe-lines which should provide a relative stability of steel structure and properties during operation;
- a low level of membrane stresses (margins $n_{0.2}$ = 1.5 and n_B = 2.6) assuring the operation of the main metal mass in the elastic area;
- in principle the steels considered are cyclically stable and this makes the processes of cyclic hardening insignificant.

The aim of this presentation is as follows:

- generalization of experimental results and analysis their stability;
- determination of a possible decrease of inspection scope of mechanical properties under NPP conditions up to a complete or partial cancellation, decrease or cancellation of metal removal from real pipe-lines considering the fact that the removal of specimens from real pipe-lines did not promote the increase of pipe-lines quality and reliability because the repair process results in the increase of defective pipe-lines welds which are performed under assembling conditions with radiation influence.

Based on the operation conditions by the conduction of strength calculations of equipment it is necessary to take into account the variation of properties due to the action of the main damaging factors during the designed service life (30 years). They are:

- structural changes and degradation of material properties caused by a prolonged influence of elevated temperatures;
- generation of cracks caused by low cycle loads by a combined action of cyclic (including thermal cycles) and static loads;
- embrittlement of material and welded joints due to the influence of static and cyclic loads;
- corrosion damage due to a prolonged effect of coolant.

Table 1

Requirements of mechanical properties for NPP equipment materials

Base material	Part of welded joint	At 20°C				At 350°C				TKO, °C
		UTS, MPa	*YS*, MPa	A_5, %	*Z*, %	*UTS*, MPa	*YS*, MPa	A_5, %	*Z*, %	
22K	Base metal	430	215	18	40	392	177	18	40	+40
	SAW Sv-08A	353	196	20	55	314	176	13	50	0
	MAW YONII-13/45 YONII-13/55	 353 431	 216 255	 20 20	 55 50	 314 372	 176 216	 20 18	 55 50	 +20 +30

Ageing is defined as the metal state variations which may take place in the course of time under external influences or without them. The ageing by heat treatment, a prolonged temperature influence, by strain aging, under operational and thermo-mechanical influences, etc. are distinguished. As ageing occurs, as a rule, mechanical properties of metal are degraded. Taking into account an obligatory execution of the item 7.6.3 PNAE G-7-008-89 a lot of tests of specimens removed from piping after operation 100000 hrs were carried out in our country and also other countries and large number of data were accumulated. Nevertheless the published information about the effect of operational factors on material mechanical properties is quite limited. The first publication was devoted to the investigations performed for the main circulating piping from stainless steel intended for units 3 and 4 of Novo-Voronezh NPP [3]. Such results for piping made from carbon steels appeared later and are presented in Ref. [4]. The information accumulated for the last 15 years on the investigation of the state of base metal and welded joints after a prolonged operation (100000 hrs and more) makes possible to analyze the variation of strength and ductility characteristics. Besides there are some publications [5, 6] about thermal ageing of RPV steels and their welded joints. This paper presents the analysis for carbon steel and their welded joints mainly as applied to operation conditions of NPP.

3. Thermal Ageing

The first results for piping made from carbon steels appeared later and they are presented in Refs. [5, 6]. The information accumulated for the last 15 years on the investigation of the state of base metal and welded joints after a prolonged operation (100000 hrs and more) makes possible to analyze the variation of strength and ductility characteristics. The mechanical properties of carbon steels of the type 20 and 22K and their welded joints produced using manual arc welding (MAW) with covered electrode after a prolonged (100000 hours) influence of operation temperatures up to 290°C practically do not change. This tendency for base metal is confirmed up to 200000 hours, i.e. to the designed service life of piping (30 years) makes possible to correct item 7.6.3 “Rules of arrangement and safe operation of equipment and piping of NPP” as concerns the inspection periodicity of mechanical properties with destructive techniques at the NPP in the period of planned maintenance repair. As the degradation of mechanical properties of carbon steel is practically absent during the designed service life was recommends to carry out inspection after 200000 hrs of operation and not 100000 hrs and the basis for this conclusion was presented. On the base of earlier performed investigations [5, 6] we can mention a high stability of strength and ductile properties of this steel at 20°C independent of temperature and a prolonged thermal exposure. In this case the level of mechanical properties after thermal exposures does not decrease below the normative requirements for the initial period of operation. At the same time it should be noted the insignificant decrease of impact strength of steel by Ménage specimens tests after the exposure during 10000 hrs at the thermal temperature 450°C if we compare with value according to the normative requirements. The critical transition temperature of 22K steel is also nearly stable after thermal ageing at studied temperatures (except 340°C) on the duration 100000 hrs.

A section of Du-800 piping was cut out from Sosnovyj Bor NPP, operated under the influence of elevated temperatures and pressure for nearly 30 years, in order to assess the mechanical properties variation of piping material after a prolonged operation. Specimens were made from base metal (22K steel) of the removed from piping (∅828×38 mm) element and tested by one-fold tension.

Fig.1 presents the summarized results which make possible to judge about the relation between actual properties of materials with the requirements on the values of characteristics specified by the technical normative documentation and it was accepted to conduct strength calculations by the chief designer of the power plant. In this case the actual values in as-produced condition are accepted with regard for their distribution according to the investigation data in Ref. [7] after 100000 hours of operation – data of NPP reports for various power units and after 30-year period of operation – test results of specimens removed from the piping of unit 1 Sosnovyj Bor NPP [7, 8].

As follows from Fig.1 the variations of mechanical properties of both base metal and weld metal during the designed operation time of pipe-lines made from carbon steels as related to these materials in as-produced condition (before operation) practically do not occur and thus margins of static strength accepted at the project stage are retained. This conclusion may be drawn for margins of cyclic strength because the values of material reduction of area independent of the thermal ageing duration is actually at the same level as in as-produced condition.

The obtained experimental data for 22K steel show those after the operation time (30 years) the mechanical properties are appreciably higher than required by the documentation Tu-24-3-449-74. And this is the evidence for the fact that a prolonged heating of 22K steel within the range of operation temperatures and operating pressure does not result in an appreciable degradation of properties.

4. Strain Ageing

The equipment and pipe-lines of NPP manufactured in carbon steel are operated at elevated temperatures up to 360°C that lay within the temperature range of dynamic strain ageing which manifests itself in strength properties improvement and plastic properties deterioration under single loading [7]. The variation of mechanical and fatigue properties of steels in the temperature range from 20 to 400°C can be attributed to different reasons, including carbon and nitrogen atomic hardening around screw dislocations, strain ageing due to internodes carbon and nitrogen atoms, and also to dislocation precipitation of carbide and nitride particles. From these assumptions it is noted in Ref. [9] that the effect of mechanical and fatigue properties variation must be most evident in welded joints since high heating temperatures in welding and subsequent fast cooling enhance super saturation and ageing. Some investigations carried out in our country during 1970 are devoted to this problem. The variation of mechanical properties in the temperature range from 20°C up to 400°C was investigated for different materials (base metal and welds) under single tension at the strain rate of $150 \cdot 10^{-4}\ s^{-1}$ (the rate applied in low-cycle fatigue tests). It has been established that strain ageing shows up most vividly in reduction of area Z [9-11].

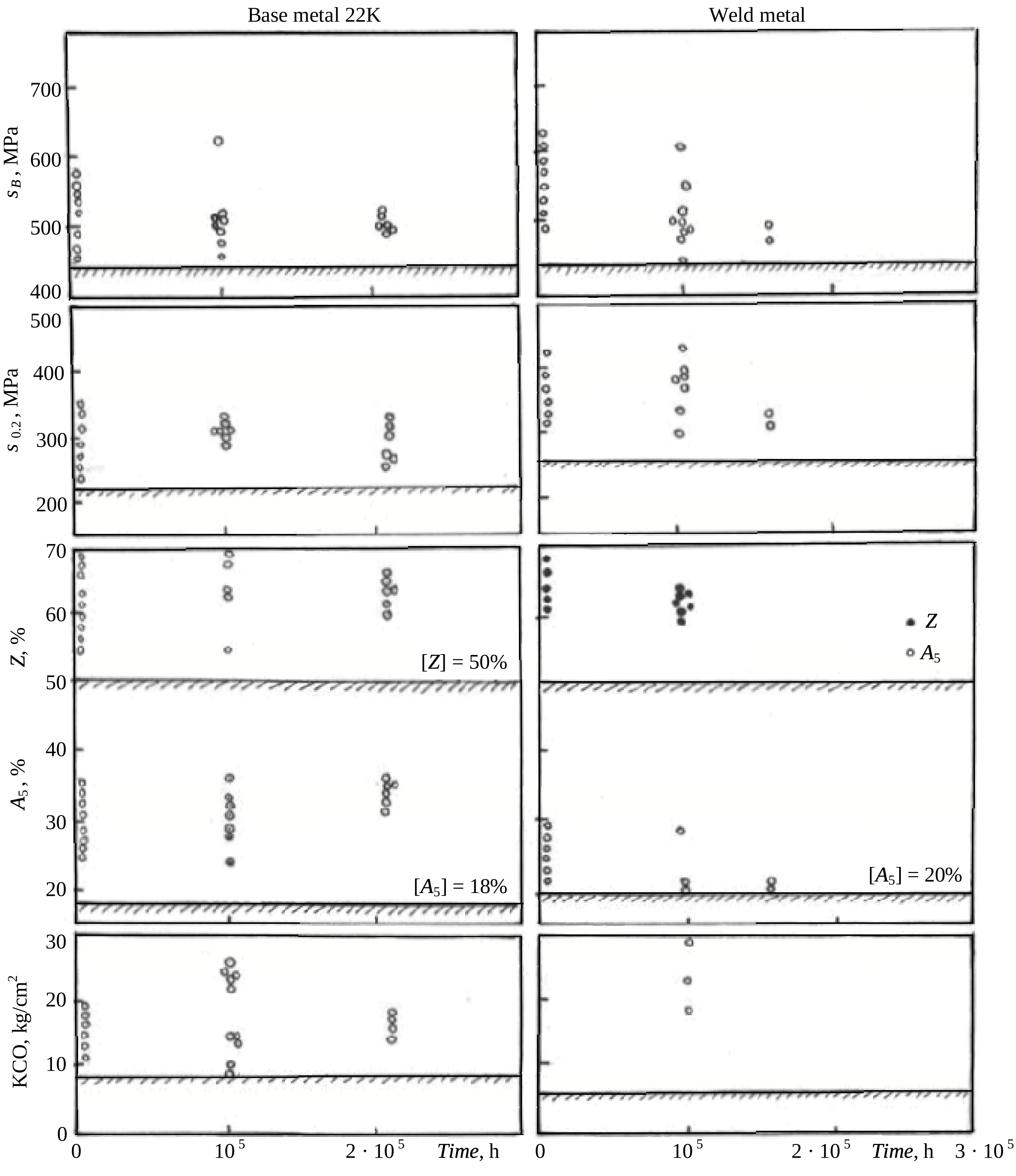

Fig. 1 Summarized data of effect of thermal ageing on mechanical properties of welded joints for carbon steel type 22K

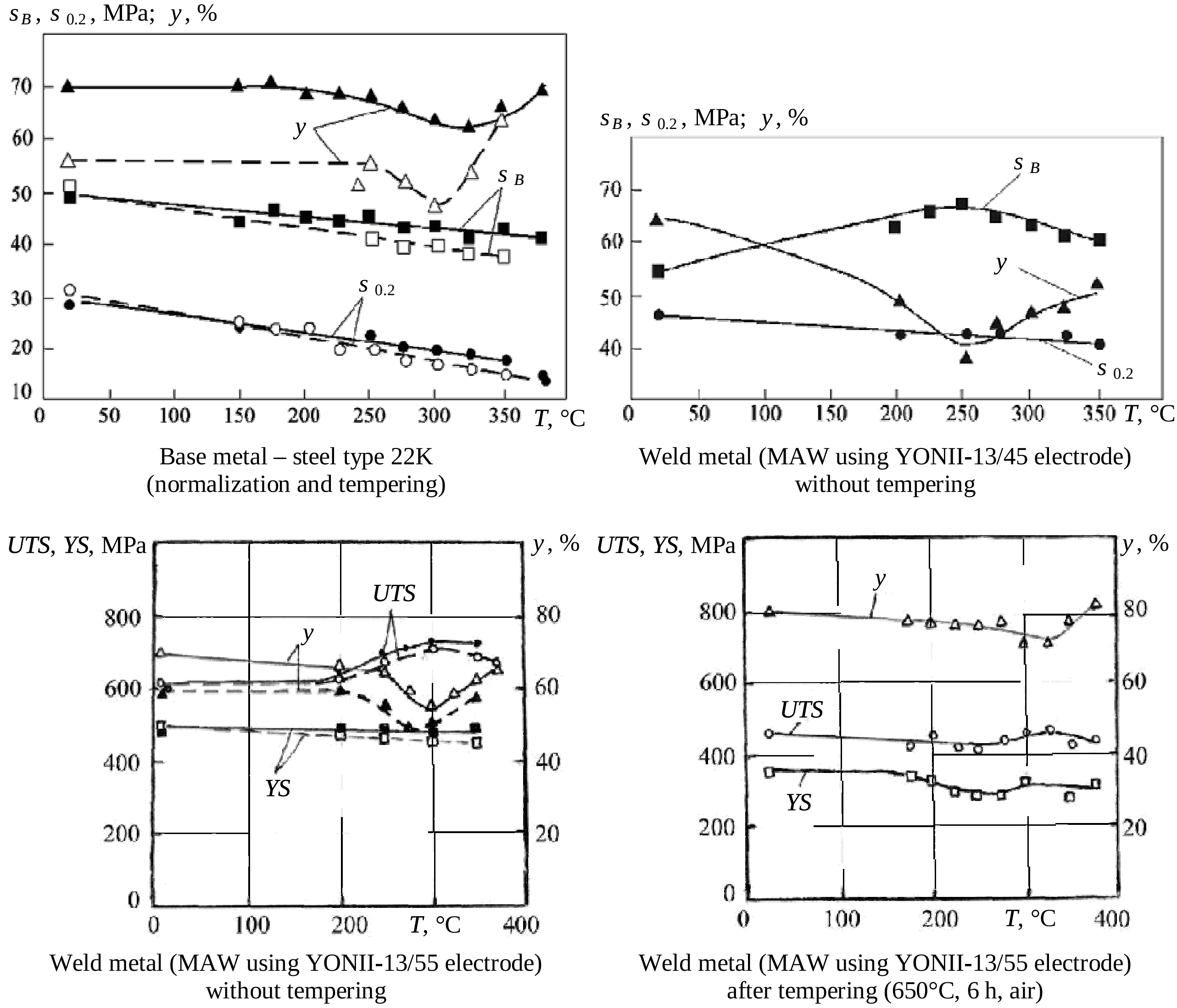

Base metal – steel type 22K (normalization and tempering)

Weld metal (MAW using YONII-13/45 electrode) without tempering

Weld metal (MAW using YONII-13/55 electrode) without tempering

Weld metal (MAW using YONII-13/55 electrode) after tempering (650°C, 6 h, air)

Fig. 2 Variation of mechanical properties for base and weld metal of 22K welded joints in BOL ($t = 0$) and EOL ($t = 30$ years)

4. Conclusion

The generalization of experimental investigation results performed in our country and devoted to the effect of thermal ageing at 250-350°C on mechanical properties of carbon steel and its welds has shown that variation of structure, strength and ductility characteristics, practically, does not occur during the 30-years service life. There are only some deviations from the general tendency, however they are small and always within the limits of the accuracy of characteristic measurement on the accepted determination procedure.

A prolonged operation experience of carbon steels in the composition of equipment of the LWR confirmed the absence of variation of mechanical characteristics of the carbon steel. Some decreasing of reduction of area materials is observed because some of them (weld metal without tempering) have sensitivity to strain ageing.

References

1. PNAE G-7-008-89. Regulations of the NPP Equipment Installation and Piping Safe Operation. Energoatomizdat, Moscow, 1990, 168 p.
2. PNAE G-7-002-86. Strength Calculations Norms for Nuclear Power Plasnt Equipment and Piping. Energoatomizdat, Moscow, 1989, 525 p.
3. **Gaponov A. A.** The State of the Du-500 piping of the WWER Main Circulating Circuit after 100000 hrs Operation. Teploenergetika, No.1, 1989, p. 43-44.
4. **Beznosikov S. A.**, **Mjasnjankin A. I.**, **Veselovsky V. F.**, **Timofeev B. T.**, **Filchagin Yu. G.** Assessment of State of Properties for Base Metal and Welds of NPP Pipe-Lines after Prolonged Operation. Proceedings of Workshop “Ageing of NPP Component Materials”, St- Petersburg, 28 February-2 March 1995, p. 221-232.

5. **Karzov G. P.**, **Timofeev B. T.**, **Filchagin Yu. G.** The Influence of Prolonged Exposure to Operating Temperatures and Strain Aging on the Material Properties of Nuclear Power Plant Reactor Vessels and Piping. International Journal of Pressure Vessel and Piping. Volume 53, No.2, 1993, p. 195-216.
6. **Karzov G. P.**, **Timofeev B. T.** Assessment of Degradation of Mechanical Properties of Steels and Weldments for Pressure Vessels and Piping. Proceedings of the Joint EC – IAEA Specialists Meeting on NDT "Methods for Monitoring Degradation". 10-12 March 1999, Petten, p. 94-103.
7. **Timofeev B. T.**, **Shalygin A. S.** Assessment of Variation of Properties for Welded Joints of Piping from Carbon Steels during Design Lifetime. Voprosy Materialovedenija, No. 3(39), 2004, p. 54-61.
8. **Petrov V. A.**, **Timofeev B. T.**, **Shalygin A. S.** Influence of Prolonged Operation Time on Mechanical Properties of NPP Piping Welded Joints from Carbon Steels. Proceedings of the Tenth Workshop "Provision on Safety and Economy of Power Engineering Equipment". 23-26 November 2004, St. Petersburg
9. **Daunene S.A.**, **Karzov G.P.**, **Timofeev B. T.**, **Timofeeva A. I.** Experimental Assessment of Sensitivity of Weld Metal to Strain Ageing. Sudostroitelnaja Promyshlennost, serja "Svarka", issue 20, 1975, p.17-21.
10. **Daunys M. A.**, **Daunene S. A.**, **Timofeev B. T.** Properties of Welded Joints at Strain Ageing during Low Cycle Fatigue. Svarochnoe Proizvodstvo, No.12, 1982, p.12-14.
11. **Timofeev B.**, **Bazaras Z.** Cyclic Strength of the Equipment of Nuclear power Plants Made of 22K Steel. Cyclic Strength of the Equipment of Nuclear power Plants Made of 22K Steel. International Journal Materials Science, 2005, vol.41, No.5, p. 680-685.

Proceedings of 3rd International Workshop ITELMS'2008

Application of Multicriteria Analysis in Assessment of Social Benefits of Transport Corridors

D. Micevičienė[*], A.Tautkus[**]

[*] *Kaunas University of Technology Panevėžys Institute, Klaipėdos str. 1, LT-35209, Panevėžys, Lithuania, E-mail: diazvik@ktu.lt*
[**] *Kaunas University of Technology Panevėžys Institute, Klaipėdos str. 1, LT-35209, Panevėžys, Lithuania, E-mail: arunas.tautkusi@ktu.lt*

Abstract

Multicriteria analysis (MCA) describes any structured approach used to determine overall preferences among alternative options, where the options accomplish several objectives. MCA allows decision makers to include a full range of social, environmental, technical, economic, and financial criteria. It is usually used to synthesise the opinions expressed, in order to determine the priority structures, to analyse conflictual situations, or to formulate recommendations or operational advice. This was the reason of using the tool for evaluation of so ambitious projects of transport corridors generating both direct and the indirect effects which generally are not well understood and are not included in so popular among decision makers cost-benefit analysis of transport projects. For the reason the authors do conclude that there is a need to improve the decision making process in transport corridor planning and maintainance and present a practical tool for the assesment of transport corridors' projects impact on ennvironment employing the issues of multicriterial analysis.

KEY WORDS: *multicriteria analysis, transport corridors, social, benefits, assessment.*

1. Introduction

Transport is one of the main branches of economy without which the functioning of a modern economy is impossible in general. It ensures the necessary economic links, joins all industrial units of a country into one whole thus establishing the conditions for economy to function coherently and efficiently. Efficient work of transport is significant not only for economy, but also for other spheres of activity. Thus, transport is an important branch of economy, however, its infrastructure expansion needs much investment. That is why investment projects for the development of the transport structure have to be thoroughly selected, and their implementation has to ensure sufficient efficiency. Taking into account that transport generates a number of adverse effects from transport infrastructure and vehicles, the indirect ones - environmental influences might be included into the group - may have even greater consequences on society than direct effects. Unfortunatelly the indirect effects are not generally well understood and are not included in so popular among decision makers cost-benefit analysis of transport projects. For the reason the authors do conclude that there is a need to improve the decision making process employing the issues of multicriterial analysis. The aim of the paper is to demonstrate the ability to substantiate the project's validity (in social terms) supplementing the cost – benefit analysis with fundamentals of multicriteria analysis.

2. The Concept of a Transport Corridor

There is no basis in scientific theory for the corridor approach. In contrast, there are numerous examples of, as well as practical experience with, the use of a corridor approach in, admittedly, widely varying contexts where in most cases the aim is to resolve a specific problem of co-operation between partners developing links along a given corridor in which they have a shared interest; a certain pragmatism always lies behind the original decision to promote a corridor. With the enlargement of the European area, this practical experience with corridors developed into more formal arrangements as well as agreements between national and international institutions. The outcome is that experience with a given corridor has not always proved beneficial in the development of subsequent corridors, given the degree to which the particular context, objectives and partners involved can vary from one project to another [1] . However, the concept of transport corridor is directly connected with the processes of transport planning. If to take an example from the more recent past, one of the first projects to leave a mark on transport planning was the development of the North-Eastern corridor in the U S during the 1960 - ies. The North-Eastern corridor, which runs from North of Boston to South of Washington D.C., was designed to address resolve major congestion problems arising from high rates of traffic growth that were a major source of concern for the future of the U S; the aim was to adopt a long-term approach to infrastructure development, traffic allocation and modal split [1]. The "strip" of national territory analysed was relatively wide and provided a framework in which to simulate possible transfers and allocation of traffic between routes, particularly passenger traffic. In this particular case, the concept of "corridor" was defined in particularly broad terms in that it was used to refer to the general alignment of international traffic flows within the European area. These projects were not of an overtly political nature and mainly involved national research agencies and study centres, even though the long-term objective was indeed to help bring countries closer together, strengthen co-operation, facilitate trade and provide better co-ordination of policies and investment. Finally, the most important initiative involving a corridor approach was set against the highly politicised background of the early stages in the process of opening-up to Eastern Europe in Prague in the framework of the first and following Pan-European Transport Conferences (1991, 1994, 1997). At present the most actual discussions on the corridors concept are hold in the developing countries seeking to substanciate the expediency of huge investment into the poor infrastructure. Such questions as link between transport corridors and economic development issues, environmental and social impacts are the key point of the discussion on the topic. Anyway, in very general terms the corridor approach can be said to be a product first of a need to globalise, to have a more general approach to transport more closely aligned to not only economic activity but also the need to be operational, to take practical action; there is a "decision-making aspect" to the corridor approach and because of this what might even be termed an institutional dimension. The corridor concept occupies a slightly intermediate and more operational position between evaluation of a project whose framework is too restricted and evaluation of policy towards transport networks where the interactions are too complex to understand and use as a basis for deriving an operational approach. The corridor concept therefore becomes a kind of bridge between local and global constraints in the communications area, between individual and collective decisions, between modal and intermodal approaches, between short-term and long-term decisions, all different facets of the diversity of experiences [2].

3. The Practice of Assessing Transport Projects: Problem Formulation

Taking into accout the compexity of transport corridors and the range of effects – environmental ones her are included as well - generated it must be concluded that the question of corridor project assesment still remains one the most complicated ones. Practice shows that at presents the macroeconomic evaluation of transport infrastructure projects - even such large-sclaled as a corridors- is performed using almost the most popular tool – cost – benefit analysis. The process of judging whether or not a project should be accepted is called project evaluation. Cost – benefit analsys is is the examination of a decision in terms of its consequences or costs and benefits. In the context of project evaluation a cost – benefit analsyis *test* is a simple decision rule which consists of accepting only those projects which make a positive profit. In order to evaluate a project from the point of view of its consequences, it is crucial to have a model which predicts the total effect on the state of the economy of undertaking a particular project. This total effect involves a comparison of the economy "with" the project and the economy "without" it. Formally, we embody the relation between a project and its consequences in the notion of a "policy", i.e. a rule which associates a state of the economy with each public production plan [4], [5]. Assesment, quaalification and determination of single factor is subsequently divided in two cases. In first case the project will be implemented and in second case will not. The difference lies in evaluation of operating costs and ifrastructure service costs. Some of presented variants will drop out after the implementation of basic evaluation. So we do not take them into account in next step. But this analysis does not assess just monetary impacts from contribution and costs perspective. It also takes non-monetary impacts into account. These impacts are estimated either by conversion to financial units (conversion on the basis of chosen key) or on the basis of evaluation by beforehand set scale, which must be used again for all rated alternatives by the same procedure. Stressing that despite the efforts to limit the impact of transport on environment – this is one of the reason the corridors are formed – the fleet in the corridors generate traffic, at the same time impacts on the environment through pollution from engine exhaust gases, particularly in urban areas.Plants, animals and habitats are sensitive to the pollutants. For example, nitrogen oxides from exhausts form acid rain in the atmosphere that can damage the trees and soil. Vehicles also release greenhouse gases to the atmosphere that contribute to climate change. Although air transport is growing rapidly and may impact air quality in the future. Transport also affects the environment in other ways. Land and habitats are lost when new roads are built. Oil slicks from wrecked tanker ships can damage the marine environment and a sustainable transport policy means automatically an overall all-mode transport & energy policy. A sustainable transport policy is always related to the broader policy of general sustainability. Accordingly, the shared effects of transport policy measures in other areas, i.e. 'secondary benefits' and trade-offs, must be taken into consideration. Since any sustainability policy has the risk of being misguided for an environmental policy under a fashionable new title, it is important to continually highlight the importance of the socio-economic dimension, not forgetting to involve citizens and business community in an early stage. The new credo must become ‘creating instead of compensating’, meaning that companies should invest in innovations (jobs) in front of their own door, instead of trading with CO2 rights by ‘planting trees’ in third countries only.

So these examples let us conclude, that cost-benefit analisys might be considered to be too smal – scaled tool for decision making in the planing and / or maintaining such large infratsructure objects as transport corridors. Ignorance of the issues enables the decision makers to dismiss most important effects and to take maybe not the best solution (for the society) in solving most economic, social or environmental prolems. The recourse here could be application of multicriteria analysis Multi-Criteria Analysis that could be used for exploiting the preferences of decision-makers, stakeholders, or environmental experts (in the following simply referred to as “stakeholders”) to derive monetary values for impacts whose monetization has remained problematic. The ultimate goal is to integrate multi-criteria methodology into the wider frame of cost-benefit analysis (CBA) for supporting policy and decision-making, especially in the context of sustainable development [6].

4. Principal Issues on Multi-Criteria Analysis

Multicriteria analysis (MCA, also known as multi-attribute analysis, multi-goal analysis and multi criteria decision making) is a two stage decision procedure. The first stage identifies a set of goals or objectives and then seeks to identify the trade-offs between those objectives for different policies or for different ways of achieving a given policy. The second stage seeks to identify the 'best' policy by attaching weights (scores) to the various objectives [6], [7], [8]. As most authors do conclude that MCA is especially widely used in the Netherlands. Multicriteria analysis appeared in the 1960s as a decision-making tool. It is used to make a comparative assessment of alternative projects or heterogeneous measures. With this technique, several criteria can be taken into account simultaneously in a complex situation. The method is designed to help decision-makers to integrate the different options, reflecting the opinions of the actors concerned, into a prospective or retrospective framework. Participation of the decision-makers in the process is a central part of the approach. The results are usually directed at providing operational advice or recommendations for future activities.

MCA has undergone an impressive development during the last 30 years, in part because it is amenable to handling today's complex problems, in which the level of conflict between multiple evaluation axes is such that intuitive solutions are not satisfactory. MCA is not a tool providing the 'right' solution in a decision problem, since no such solution exists. The solution provided might be considered best only for the stakeholders who provided their values in the form of weighting factors, while other stakeholders' values may indicate another alternative solution. Instead, it is an aid to decision-making that helps stakeholders organize available information, think on the consequences, explore their own wishes and tolerances and minimize the possibility for a post-decision disappointment. The purpose of the tool is to structure and combine the different assessments to be taken into account in decision-making, whereby decision-making is made up of multiple choices and the treatment given to each of the choices condition the final decision to a large extent. Importantly, multi-criteria analysis is used to highlight the reasoning and subjective convictions of the different stakeholders on each particular question. It is usually used to synthesise the opinions expressed, in order to determine the priority structures, to analyse conflictual situations, or to formulate recommendations or operational advice.

Multiple MCA methods are available, suitable for a wide variety of decision situations. Furthermore, several weighting techniques have been developed to help stakeholders involved in a MCA procedure become aware and articulate their preferences. However, certain structural elements are common to all decision situations, independent of the MCA method used.

The main steps involved in multicriteria analysis can be broken down into several phases described chronologically below. It is possible to repeat the phases and thus to make corrections.
Projects or actions definition to be clearefied (Phase 1). This will involve an inventory of the planned or implemented actions, or the elements on which the comparative judgement will be made. Definition of judgement criteria **(**Phase 2).

Particular attention must be given to the definition of criteria, in order to be as exhaustive as possible and to define the question properly. The criteria must reflect the preferences of the decision-makers or the different points of view, so as to summarise and group together diverse characteristic dimensions used to evaluate an action. In the case of European Union socio-economic programmes, the success of a measure is normally judged in terms of its contribution to the achievement of the intermediate objectives stated in the programming documents. The main European Union policy priorities (XE "policy priority") (e.g. environment, equal opportunities) are also judgement criteria. A variant consists of relying instead on the implicit objectives (XE "implicit objective") of the programme, reconstructed by the steering group (XE "steering group") or extended work groups, e.g. with the aid of the concept mapping of impacts. If the evaluation was intended to focus primarily on the relevance of the programme to the regional economy rather than the impacts, the multicriteria analysis would concentrate on the main strengths and weaknesses of the regional economy and the way in which the different measures build on strengths or offset weaknesses.

The synergy between the impacts of the different measures could also be considered, and if so 'synergy' would become a judgement criterion in its own right. It is possible to use a matrix of cross impacts and, in particular, coefficients of synergy for taking this criterion into account in the formulation of a synthesised judgement on the measures. In the case of European Union socio-economic programmes, the success of a measure is normally judged in terms of it contribution to the achievement of the intermediate objectives stated in the programming documents. The main European Union policy priorities (XE "policy priority") (e.g. environment, equal opportunities) are also judgement criteria. A variant consists of relying instead on the implicit objectives (XE "implicit objective") of the programme, reconstructed by the steering group (XE "steering group") or extended work groups, e.g. with the aid of the concept mapping of impacts [9].

The synergy between the impacts of the different measures could also be considered, and if so 'synergy' would become a judgement criterion in its own right. It is possible to use a matrix of cross impacts and, in particular, coefficients of synergy for taking this criterion into account in the formulation of a synthesised judgement on the measures. Unlike the number of measures to be compared, which can be very large, the number of criteria must not exceed a reasonable limit. Experience has shown that the maximum number of criteria for an effective evaluation is eight criteria.

The compensation method is the best-known variant and consists of attributing a weight (XE "weighting") to each criterion and then of calculating a global score for each measure, in the form of a weighted arithmetic average of the scores attributed to that measure for the different criteria. This variant is called "compensatory" because the calculation of the weighted average makes it possible to compensate between criteria. For example, a measure which had a very bad impact on the environment could still obtain a good global weighted score if its impact on employability were considered excellent. MAVT aim to associate a unique number (‘value’) representing the overall strength of each alternative taking all criteria into account. If there is substantial uncertainty about the performances of alternatives, the term ‘utility’ is used to denote that the preferences of stakeholders against risk are formally included in the analytical procedure. To begin, partial value (or utility) functions are defined for each criterion for reducing performances, in the [0-1] interval. Partial values are then aggregated for deriving total values and for preordering examined alternatives. The transition from partial to global value functions (taking into account the whole set of criteria) implies the use of an aggregation formula together with the inter-criterion preferences provided by the decision maker.

In MAVT methods, weights play the role of scaling factors in the sense that they relate scores among the different critieria. By assigning weights denoting relative importance, stakeholders implicitly express what portion of one criterion they are willing to give up in order improving the performance of another criterion by one unit. So, if the weight of criterion *i* is double the weight of criterion *j*, then the stakeholder values 10 units on criterion *i*, the same as 20 units on criterion *j*. In order for the stakeholders to more clearly express preferences in terms of the necessary trade-offs between criteria, weights are defined on initial natural scales and then taking into account the absolute level of performances and absolute differences in scores.

The outranking variant is used where the criteria are not all considered commensurable, and therefore no global score can be produced. The analysis is based on multiple comparisons of the type: "does Measure A outrank Measure B from the point of view of the environment criterion?", "does Measure A outrank Measure B from the point of view of the employability criterion?" and etc. These questions can be answered yes or no or be qualified, in which case the notions of a weak preference and a threshold criterion are introduced. The analysis makes all possible comparisons and presents a synthesis of the type: "Measure A is at least as good as Measure B, in relation to a majority of criteria (case of agreement), without being altogether too bad in relation to the other criteria (case of disagreement)". The analysis could include protection against a favourable judgement for a measure that would be disastrous from the point of view of the given criterion, by setting a ‘veto threshold’ for each criterion. The introduction of a veto threshold strongly differentiates the logic of outranking from the logic of compensation. If there were a veto threshold, a very bad impact on the environment would make it impossible to consider the measure good, even if its impact on employability were considered excellent.

Outranking has the advantage of reflecting the nature of relations between public institutions better, since there is often a correspondence between evaluation criteria and evaluation stakeholders. In cases where the steering group (XE "steering group") is extended to about ten partners, it is not unusual for participants to identify themselves strongly with the "environment" or "employment" criteria. In this situation the outranking variant will probably better reflect the collective process of formulating a judgement within the steering group.

Creating a decision matrix (Phase 3). It's critical to rate solutions based on a ***ratio scale*** and not on a ***point scale***. For instance, the ratio scale could be 0-5, 0-10, or 0-100. Should you feel you must use a point scale (for instance, maximum speed, temperatures, etc.), you must then convert rating values on a ratio scale by assigning the maximum ratio to the estimated maximum value, which could be, for instance, 5 (for a 0-5 scale), 10 (0-10), or 100 (0-100). Indeed, a point scale with high values introduces a bias even if it's of less importance in the final decision. The demonstration how the process of evaluation goes might be illustrated by the example as follws presented by [10]. The information was included into a 2-dimension, L-shaped decision matrix as shown below, and then compute the scores for each solution regarding the criteria with the formulas:

$$W_i = R_i P_i ,$$

$$\sum_{i=1}^{j} W_i = \sum_{i=1}^{j} R_i P_i ,$$

where W_i is score, R_i is ratind, P_i is weight. The result is the following:

Scenario #1 Table 1

CRITERIA	Weight	Alternatives					
		Option A		**Option B**		**Option C**	
		Rating	Score(1)	Rating	Score(1)	Rating	Score(1)
Criterion C1	1	3	**3**	3	**3**	3	**3**
Criterion C2	2	2	**4**	1	**2**	2	**4**
Criterion C3	3	1	**3**	3	**9**	2	**6**
Total	6	4	**10**	7	**14**	7	**13**

(1) Score = Rating * Weight

For a better interpretation, we can visualize the data in histograms. To do so, let's consider, as the data source, the ***ratings*** and ***scores*** of evaluated solutions. Here is the result:

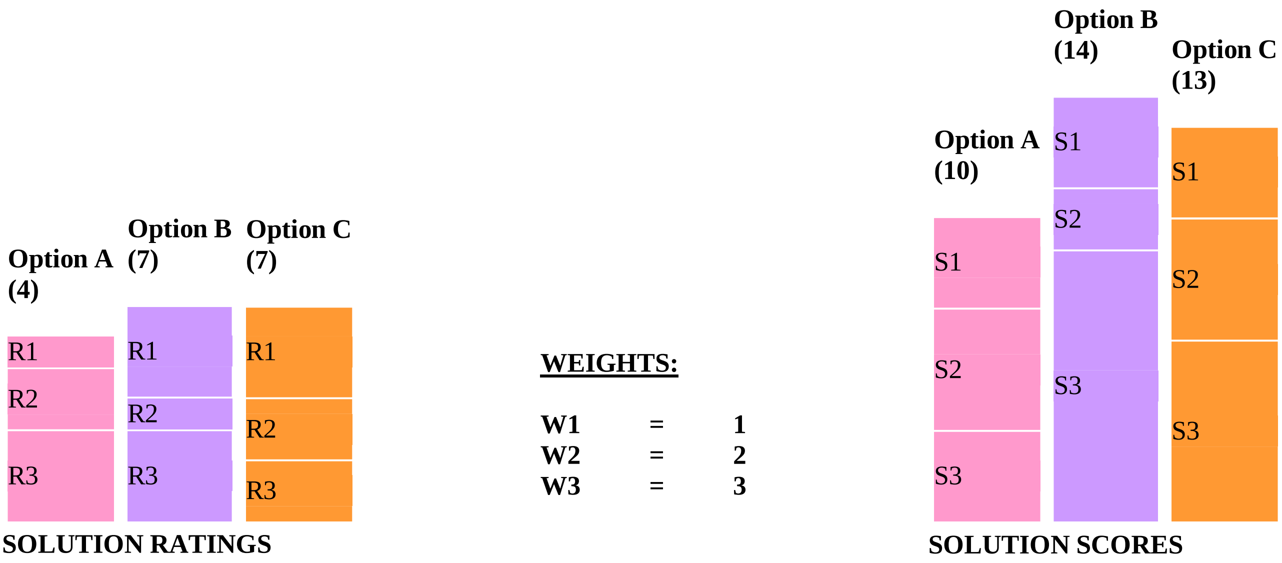

Fig. 1 Visualization of decision matrix

When we sum up the ratings, both solutions B and C are equivalent and outperforming solution A. While similar globally, options B and C present different intrinsic strengths and weaknesses. Indeed, option B is better than option C for the criterion C3, but weaker on C2, while option C distribute more evenly its forces.
Therefore, Option B is usually called a ***best-of-breed solution***, while Option C is a typical ***suite*** or ***integrated solution***.

6. Strengths and Limitations: Conclusive Remarks

As mentioned already, multicriteria analysis provides a framework in which all the actors can take part in decision-making and in problem solving. Through negotiation between stakeholders and explicit treatment of judgment criteria, the technique serves to give form to an unstructured reality. The strength of multicriteria analysis therefore, lies in the fact that it allows the values and individual opinions of several actors to be taken into consideration, and the processing of functional relations within a complex network, in a quantitative way.
The intervention of an expert, the margin of manoeuvre enjoyed by decision-makers and similarities with vote-based methods makes this a suitable tool for a partnership approach.
The technique is well suited to the way in which partnerships function in so far as it outlines areas of consensus in which the partners agree on the ranking (XE "ranking") of measures, and areas of dissension which reveal the measures considered successful for some and unsuccessful for others. Experience has shown that consensual conclusions are generally in the majority. This can be explained by the fact that the different weightings apply to the same impact scoring matrix. Thus, a measure which has a low score for all the criteria will never have a high weighted global score, irrespective of the differences of priorities between partners. The different points of view of the partners cannot strongly contradict the conclusions resulting from empirical observation if these conclusions show that certain measures are really part of best practice (XE "best practice") and that others pose real problems of effectiveness [11], [12].

Furthermore, the technique may help to reach a compromise or define a coalition of views, but it does not dictate the individual or collective judgment of the partners. Decision makers often prefer approaches of this type because since they are involved in the process through a relatively simple technical framework.

Despite these factors, in the domain of evaluation in the strict sense of the term, multicriteria analysis is seldom used for purposes other than those closely resembling decision-making aid and, in particular, the ex ante evaluation of transport infrastructure projects of such importance and scope as transport corridors.

References

1. **Bouyssou, D.** Some remarks on the notion of compensation in MCDM // European Journal of Operational Research. Vol. 26, 1996, p. 150-160.
2. **Dietz, T. and Stern, P.** Toward a theory of choice: Socially embeddedpreference construction // The Journal of Socio – Economics. 1995, vol. 24 (2), p. 261-279.
3. **Keeney, R.** Value - Focused Thinking: A path to Creative Decision Making, Harvard University Press. Cambridge, Massachusetts. 1992.
4. **Keeney, R. and Raiffa, H.** Decisions with Multiple Objectives. J. Wiley &Sons, New York. 1996.

5. **Bruinsma, F. R., S. A. Rienstra and P. Rietveld.** Economic Impacts of the Construction of a Transport Corridor; A Multi-Level and Multi-Approach Case Study for the Construction of the Highway in the Netherlands // Regional Studies. 1997, vol. 31, no. 4, p. 391-402.
6. **Nijkamp P., P. Rietveld and H. Voogd.** Multicriteria Evaluation in Physical Planning , North Holland, Amsterdam. 1997.
7. **Vickerman, R.** Restructuring of Transport Networks // EUREG. 1996, vol. 3, p. 16-25.
8. Evaluating Socio Economic Development, SOURCEBOOK 2: Methods & Techniques: Multicriteria analysis http://www.sciencedirect.com/science
9. file:///C:/Documents%20and%20Settings/Diana/My%20Documents/Maltos/INTRODUCTION%20TO%20COST%20BENEFIT%20ANALYSIS.htm
10. http://ec.europa.eu/regional_policy/sources/docgener/evaluation/evalsed/downloads/sb2_swot.doc
11. Macro-Economic Evaluation of Transport Infrastructure Investments. Evaluation Guidelines for the Federal Transport Investment Plan. Final Report to EE-Project No. 90372/92 of the Federal Minister of Transport. Essen Bonn.
12. Cost Benefit Analysis of Transport Infrastructure Projects. Economic Commission for Europe. United Nations. ISBN 92-1-116837-6.

Proceedings of International Workshop ITELMS'2008

Testing the Capacitive Micromachined Transducers Produced with Wafer Bonding Process

G. Vanagas*, D. Viržonis, M. Mikolajūnas*****

* *Kaunas University of Technology, Institute of Physical Electronics, Savanorių 271, LT-50131 Kaunas, Lithuania, E-mail: nkontora@zebra.lt*
** *Kaunas University of Technology, Panevėžys Instute, Daukanto 12, LT-35212, Panevėžys, Lithuania, E-mail: darius.virzonis@ktu.lt*
*** *Kaunas University of Technology, Panevėžys Instute, Daukanto 12, LT-35212, Panevėžys, Lithuania, E-mail: marius.mikolajunas@ktu.lt*

Abstract

Static and dynamic parameters of capacitive micromachined ultrasound transducers (cMUT) arrays, produced with wafer bonding were investigated experimentally. 36, 40 μm square and 39, 40 μm circular membranes were tested. Thickness of insulation layer was 0.3 μm, vacuum gap height 0.15 μm, thickness of silicon membrane 1.5 μm. Measurements of capacitance – bias voltage characteristic show that device tends to accumulate electrical charge due the good dielectric characteristics of insulation layers. Experimental setup and electronic circuits for pulse-echo experiments was developed. Pulse-echo experiments were performed with cMUT's immersed in transformer oil. Fractional bandwidth was calculated from the received echo signal using fast Fourier transform. Central frequency of tested arrays was at 7 MHz as an average. The increase of the bias voltage caused the fractional bandwidth to increase, preferably to the higher frequency range. Tests show that array of 0.3×0.5 mm cMUT elements is sufficient to be used in conventional ultrasound scanners without any essential changes in the hardware.
KEY WORDS: *Capacitive micromachined ultrasound transducer, wafer bonding, pulse-echo characteristics.*

1. Introduction

Ultrasound is widely used in medical imaging and nondestructive evaluation. Currently most of ultrasound transducers are fabricated using piezoelectric crystals and composites. In medical analysis are domains such partially invasive analysis or three dimensional (3D) imaging where using conventional piezoelectric transducers is complicated or impossible. Piezoelectric transducers require special matching layers in order to couple ultrasound into liquid or gas medium and these layers need to be manufactured to tight mechanical tolerances [1]. Designs of complex arrays (for example, two dimensional arrays for 3D imaging) are limited to technically possible configurations, and the cost of manufacturing can be unacceptable. The drawbacks and limitations of conventional transducers are the main motives to search for alternative ultrasound techniques. cMUT's may be adjusted in many applications not overtaken and micromechatronics systems.

Significant contribution is made here during the last two decades by the Stanford University, which developed the cMUT concept [2]. Surface micromachined versions of capacitive ultrasonic transducers were introduced in 1994 [3]. Now cMUTs were reported to be successfully used in several medicine applications [4, 5]. cMUT concept is expected to make a strong impact on imaging technologies, especially volumetric imaging, and is expected to appear in commercial products in the near future [6]. Generaly, two methods of cMUT fabrication are widely known today: the surface micromachining with sacrificial release [2] and wafer bonding method [2].

Wafer bonding method is widely used in micromachining, and it is older than surface micromachining techniques [6]. There are three basic wafer bonding techniques: anodic bonding, fusion bonding and adhesive bonding. Physical process of each techniques is different but result is the same: the permanent bonding of two similar or two different substrates. In cMUT's fabrication silicon fusion process is used [2]. Silicon fusion bonding is a direct bond between two silicon surfaces that takes place at high temperatures, forming strong covalent bonds between two silicon wafers The bond is hermetic , and exceptionally stable both mechanically and electrically. Yield of bonds is close to the yield strength of single-crystal silicon [6]. The bond is equally stable, even when one of the wafers is thermally oxidized.

The wafer-bonding technique of fabrications the cMUT's begins with two wafers: a prime quality silicon wafer and a SOI wafer. The prime quality silicon wafer is thermally oxidized. Then by a photolithography step are formed the cavity. The photo resist is removed and additional layer of silicon dioxide is thermally grown. This layer protect from shorting as membrane material is conductive silicon. Main operation is bonding SOI and prime wafers in vacuum. After bonding and annealing auxiliary layers of SOI wafer is removed to release the membranes. At the finish step the top electrodes are evaporating. The elements of cMUT array are defined by etching isolating trenches. Main steps sacrificial release process and wafer bonding method are presented in Fig. 1.

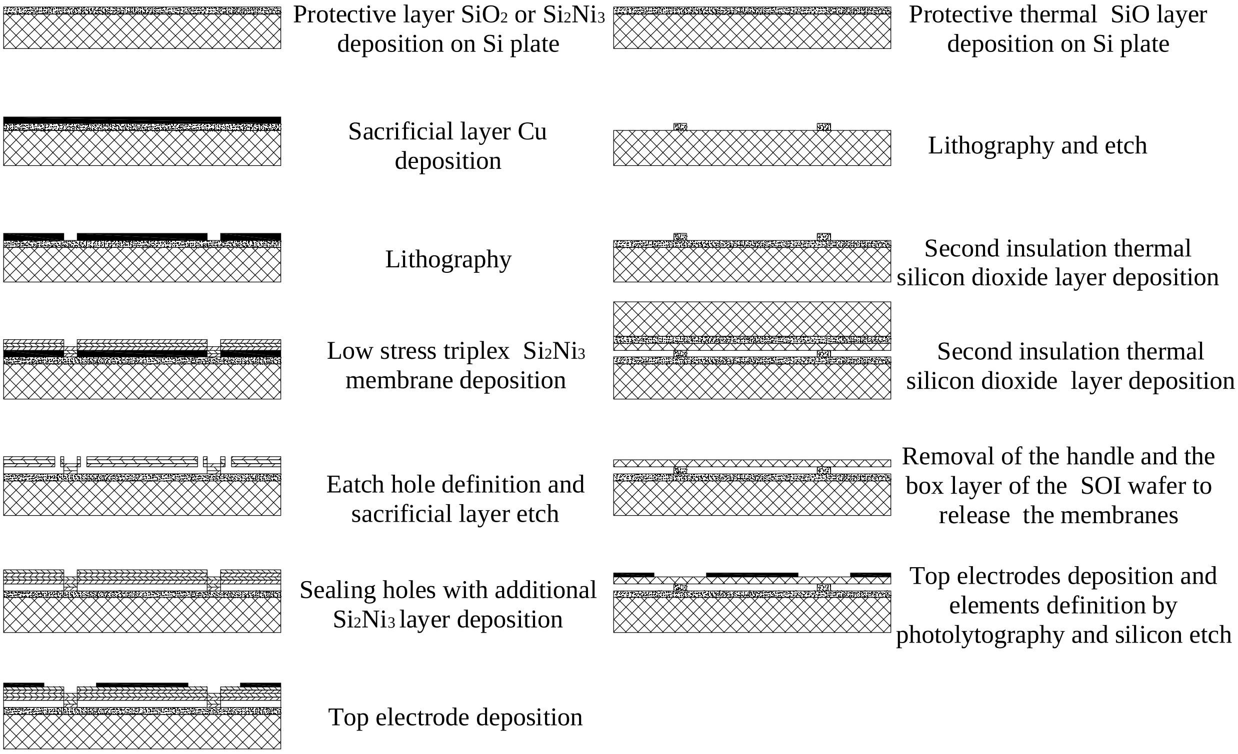

Fig. 1 Main steps sacrificial release process and wafer bonding method.

2. Description of devices

The test devices were manufactured by Khuri-Yakub group (Stanford University) by the wafer bonding technology. The layouts and photographs of the devices are shown on Fig. 2. The cMUT arrays were wire bonded to printed cirquit boards to have the convenience of testing. Next in this paper we are reporting about testing results.

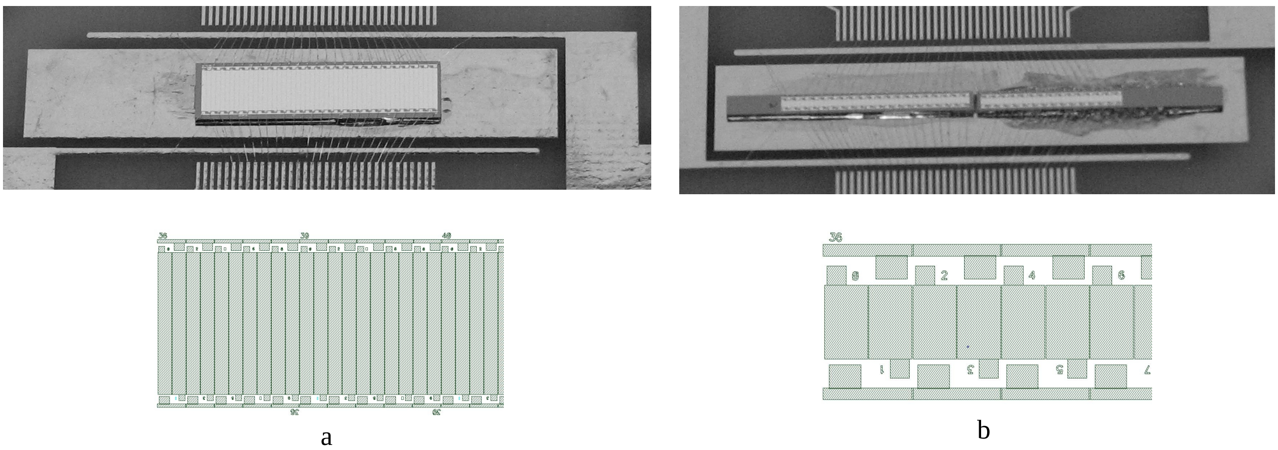

Fig. 2 Boards with cMUT arrays being tested: a – fragment of cMUT array of 300 μm by 3 mm elements; b – cMUT array of 300 μm by 500 μm elements. Above the photographs of wirebonded arrays is given

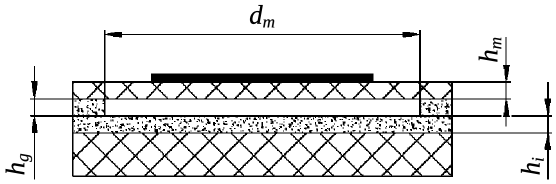

Fig. 3 Cross section of cMUT cell. There h_i – thickness of insulation silicon dioxide layer, h_g – vacuum gap height, h_m – thickness of silicon membrane, d_m – diameter for circular cells membranes or length of side for square cells membranes

We tested two boards with cMUT arrays whose have the elements with different cell dimensions. The variety of the cells is described in Table 1. Each of cMUT array elements contains from tens to hundreds of membrane cells. Cross section of one cMUT cell is shown in Fig. 3.

For all tested cMUT's cells arrays $h_i = 0.3$ µm, $h_g = 0.15$ µm, $h_m = 1.5$ µm. There are difference between dimensions d_m and forms of transducers cell: circular or squared. Also were tested arrays of membranes with mixture circular and squared membranes. Structural data of membranes arrays are presented in Table 1.

Table 1

Structural data of membranes arrays

Definition of cMUT arrays	d_m , µm	Type	Element pitch, µm	Element length, mm
36_3	36	square membranes	300	3
39_3	39	circular membranes	300	3
40_3	40	square membranes	300	3
43_3	43	circular membranes	300	3
364050_3	36,40,50	mixture of 36 µm, 40 µm and 50 µm square membranes	300	3
36_05	36	square membranes	300	0.5
39_05	39	circular membranes	300	0.5
40_05	40	square membranes	300	0.5

3. Experimental results

Static parameters. The most important static parameters of cMUT are the membrane displacement performance (static electromechanical transfer function for transmission) and the capacitance performance (static electromechanical transfer function for receiving). To characterize static characteristics of transducers the capacitance – bias voltage test were performed. The electrical circuit shown in Fig. 4 was used for static characterization.

Capacitance – voltage response was measured in the air. The results of cMUT array having element length 3 mm and element pitch 0.3 mm is shown in the Fig. 5. The applied voltage was followed by the increase of cell capacitance. Capacitance – bias voltage characteristic were measured twice: when increasing and when decreasing the bias voltage. Results are shown in Fig. 5. The single cMUT elements with 39 and 43 µm circular membranes, 36 and 40 square membranes and mixture of 36 µm, 40 µm, 50 µm square membranes were characterized. The capacitance response pattern during increase of the bias voltage does not fit the pattern when the bias voltage is decreasing. We attribute this to the charging of cMUT cells. The charging problems are reported previously as caused by the charges trapped in the thin dielectric layer used to insulate the electrodes [8]. Two sources of these trapped charges were described: the fabrication process and the strong electric field within the transducer cavities during operation. Trapped charge creates electrostatic forces that prevent the membrane from snapping back after collapse. Therefore, in capacitance – voltage response characteristics shown in Fig. 5 the clear collapse/snapback behavior can not be observed. It was found the collapse voltage for 36 µm square membranes to be 115 V, for 40 µm square membranes it was 95 V, for 39 µm circular membranes it was 120 V, for 43 µm circular membranes it was 100 V and mixture of 36 µm, 40 µm, 50 µm square membranes – about 125 V.

Intensity of electric field of 260 ... 350 kV/mm was reached during the described tests. No electrical disruptions were observed. This demonstrates the good dielectric properties of thermal silicon dioxide. From the other hand, good insulation within the cavities caused the trapped charges to be accumulated. This can be the cause of unstable operation parameters. The additional constructional solutions like featuring isolation posts [8] for improving devices reliability are required.

Pulse-echo response test. To characterize the actual operation of transducers the pulse-echo experiments in immersion were performed. The experimental setup for pulse-echo test is consisted form transmit/receive block, connected to the cMUT, pulse generator and oscilloscope (Fig. 6). The transmit/receive block supplies the rectangular pulses of 60 V with adjustable due, which can be optimized for maximum transmit/receive reliability. During the

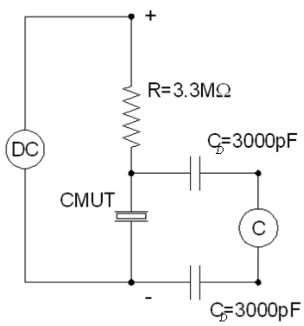

Fig. 4 Circuit diagram for capacitance-bias voltage test. There DC controlled positive high DC voltage source, CMUT tested cMUT transducer. Resistance and capacitors have a auxiliary function

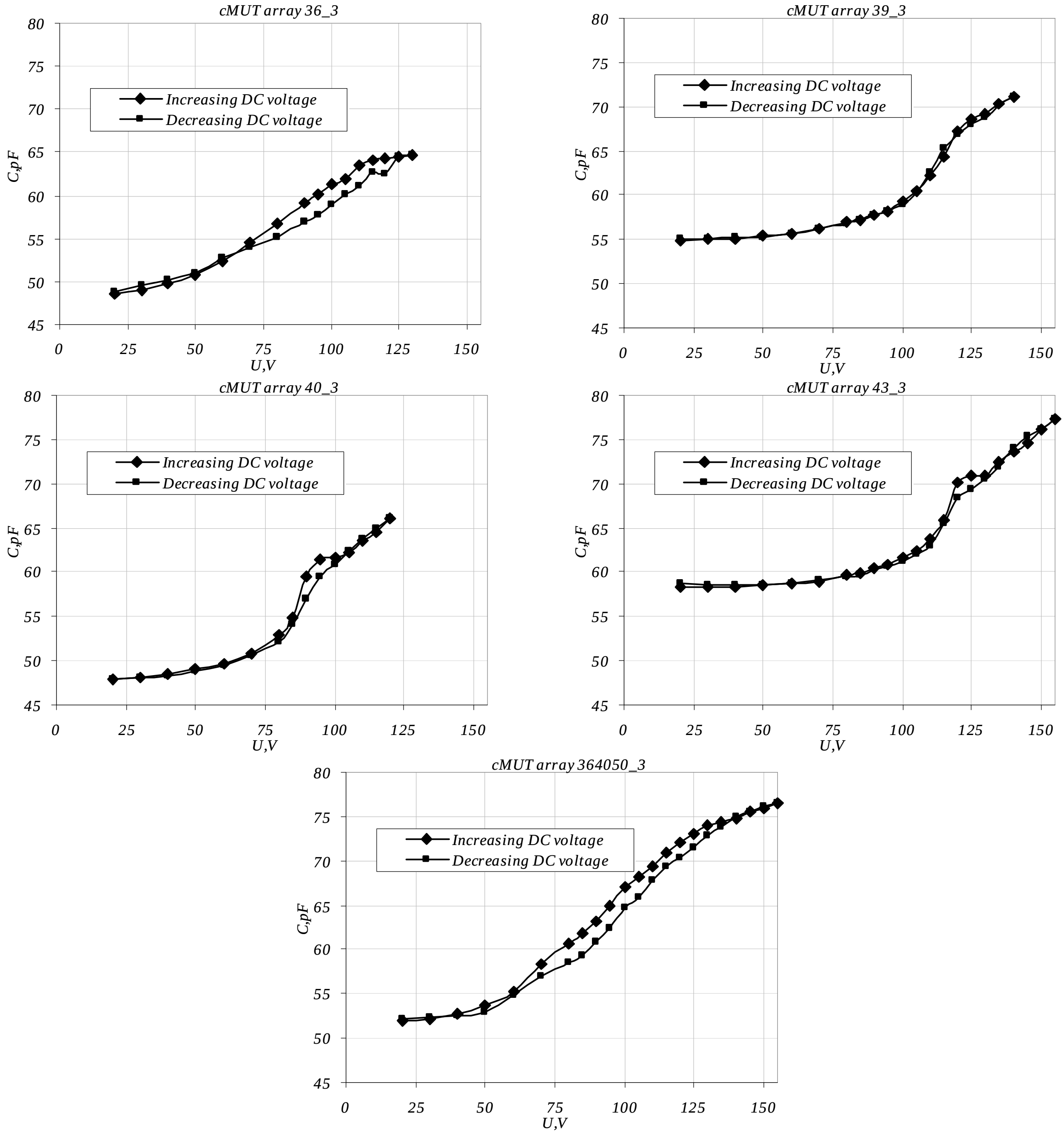

Fig. 5 Capacitance – bias voltage characteristics.

transmit cycle the pulse is directed to cMUT via the signal separation circuit. During the receive cycle the same signal separation circuit directs the pulse from cMUT to the amplifier. The array was immersed in high quality transformer oil NESTE TRAFO 10X. Density of the oil is 895 kg/m^3 and the disruption voltage of it is 52 kV. The interface between the upper side of the oil container bottom and the oil was used as an acoustical mirror to reflect the pulse back to the transducer. This interface was 5 mm away from the transducer surface. The thickness of the plexiglas container bottom was made to be 10 mm in order to have the clear separation between the pulses reflected from the oil – plexiglas interface and the bottom surface of the container. The different types of cMUT's arrays were tested one-by-one. Most of the measurements were performed in near-to-collapse regime, because it gave the best results as described in [9]. The reference [9] teaches the efficiency of cMUT's to be determined as the product of the device capacitance and the applied electric field strength. Reduced gap (which is the case of near-to-collapse operation) increases both parameters, resulting in an improved electromechanical transformer ratio.

Unipolar pulse excitation was used to obtain the frequency response of cMUT. The pulse-echo performance can be optimized using different pulse widths [9]. Fig. 7 shows received pulses, reflected from the oil-plexiglas interface. Excitation pulse due was adjusted from 40 ns to 100 ns. The amplitude of received pulse dropped if the transmitted pulse due was decreased to less than 40 ns (Fig. 7, a). The pulses longer than 100 ns resulted in reflected pulses with narrowed bandwidth. We found optimum pulse due to be 80 ns. All the rest of the pulse-echo tests were performed at said optimal pulse width. Frequency response diagrams were obtained using Fast Fourier Transform (FFT).

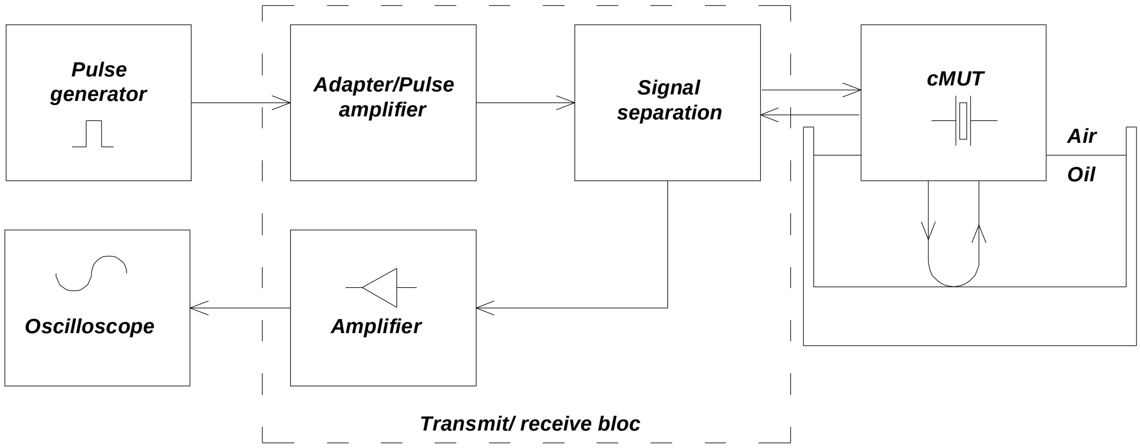

Fig. 6 Pulse-echo experiment schematic

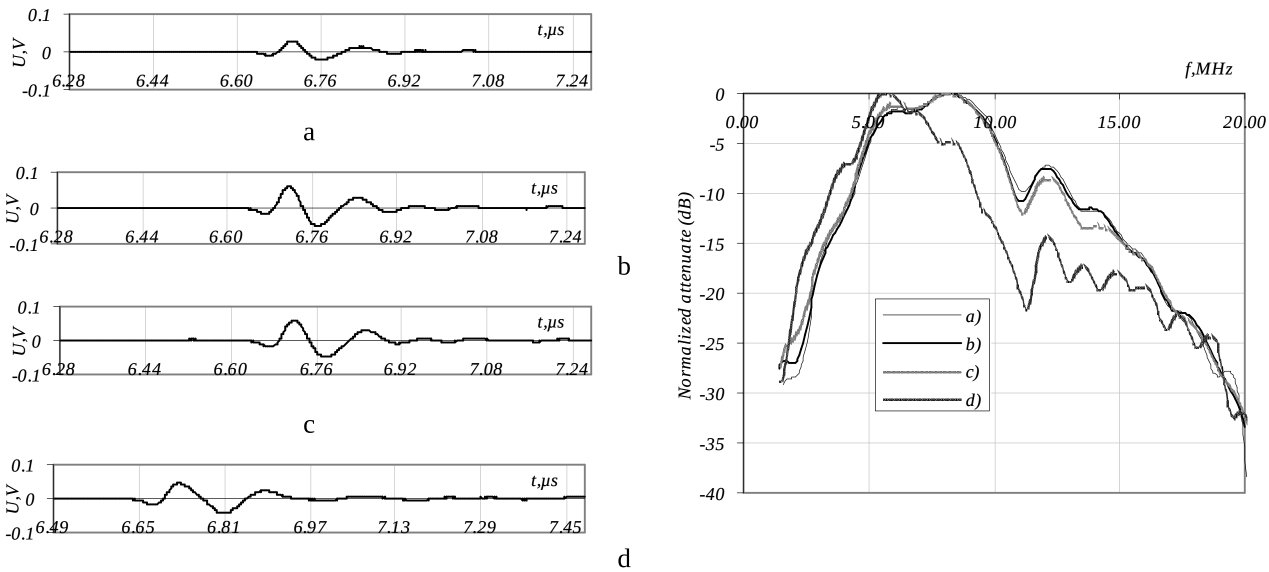

Fig. 7 Pulse-echo results. Example 36_05. V_{bias} = 125. V_{pulse} = 60 V. a – t_{pulse} = 40 ns, b – t_{pulse} = 60 ns, c – t_{pulse} = 80 ns, d – t_{pulse} = 100 ns

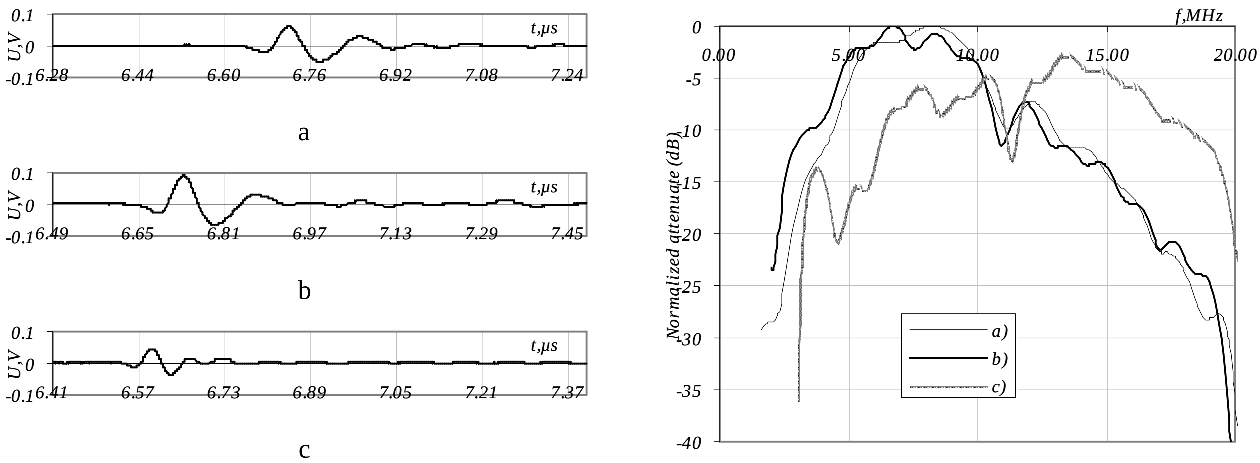

Fig. 8 Pulse-echo results. Received signals parameters as function of cMUT membrane construction. V_{pulse} = 60 V. a – Example 36_05. V_{bias} = 125. t_{pulse} = 80 ns, b – Example 39_05. V_{bias} = 125. t_{pulse} = 60 ns,. c – Example 40_05. V_{bias} = 125. t_{pulse} = 50 ns

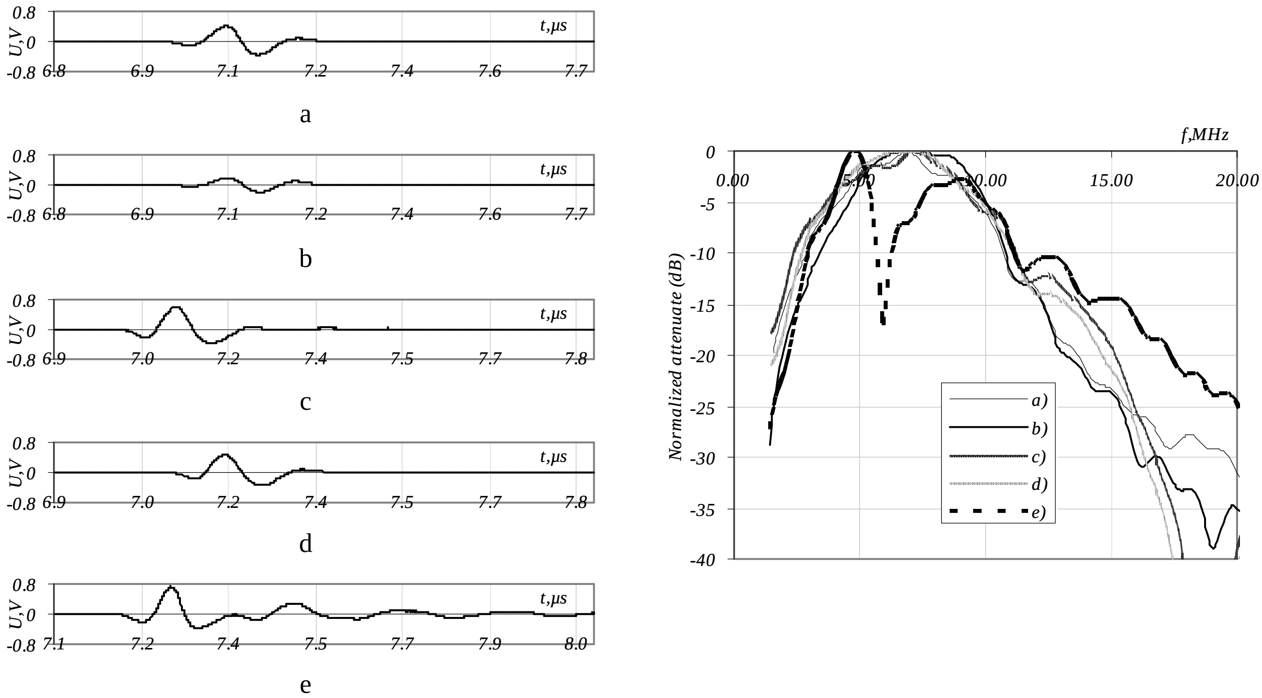

Fig. 9 Pulse-echo results. Received signals parameters as function of cMUT membrane construction. $V_{pulse} = 60$ V. a – Example 36_3. $V_{bias} = 125$ V. $t_{pulse} = 90$ ns, b – Example 39_3. $V_{bias} = 100$ V. $t_{pulse} = 90$ ns, c – Example 40_3. $V_{bias} = 120$ V. $t_{pulse} = 80$ ns, d – Example 43_3. $V_{bias} = 125$ V. $t_{pulse} = 80$ ns, e – Example 364050_3. $V_{bias} = 120$ V. $t_{pulse} = 70$ ns

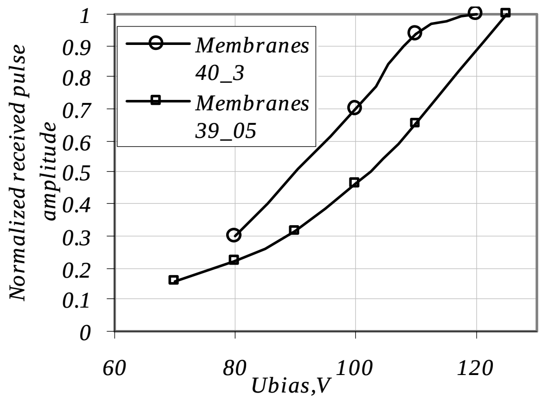

Fig. 10 Received pulse amplitude as function of bias voltage. For 40_3 design pulse length 80 ns, for 39_05 – pulse length 60 ns

As written above, we carried the experiments with different types of transducer cells design with different dimensions d_m and patterns of the cells. Frequency response and the shapes of received for different configurations of membrane cells are presented in Fig. 8 for 0.3×0.5 mm element array and in Fig. 9 for 0.3×3 mm element array. Central frequency for designs 36_05, 36_05, 36_3, 39_3, 40_3, 43_3 is in the region of 7 MHz. As a result of change of membrane shape, the frequency shift is observable for design 40_05 [9]. cMUT elements with mixture of 36 µm, 40 µm, and 50 µm square membranes have drawn out shape of response signal without clear resonant frequency.

The amplitude of received signal has strong positive dependence on the bias voltage: it increases with increase of DC voltage (Fig 10). Change rise of graph pulse amplitude – bias voltage escarpment begin then membrane collapsed (Fig. 10, design 40_3).

The central frequency has no remarkable shift with changing bias voltage in all the cases, except design 40_05 (Fig. 11). The increase of the bias voltage caused the frequency band to widen, especially at the range of higher frequencies. For design 40_3 fractional bandwidth at -3 dB increase from 4.1 MHz to 4.5 Mhz when bias voltage change from 80 V to 120 V. For design 39_05 fractional bandwidth increase from 4.5 MHz to 5.0 Mhz when bias voltage change from 70 V to 125 V. This is attributable to the increase of the cells capacity in receiving mode and, possibly, increased impact to the overall performance of small regions of the membranes, which are considerably less involved, when the bias voltages are lower.

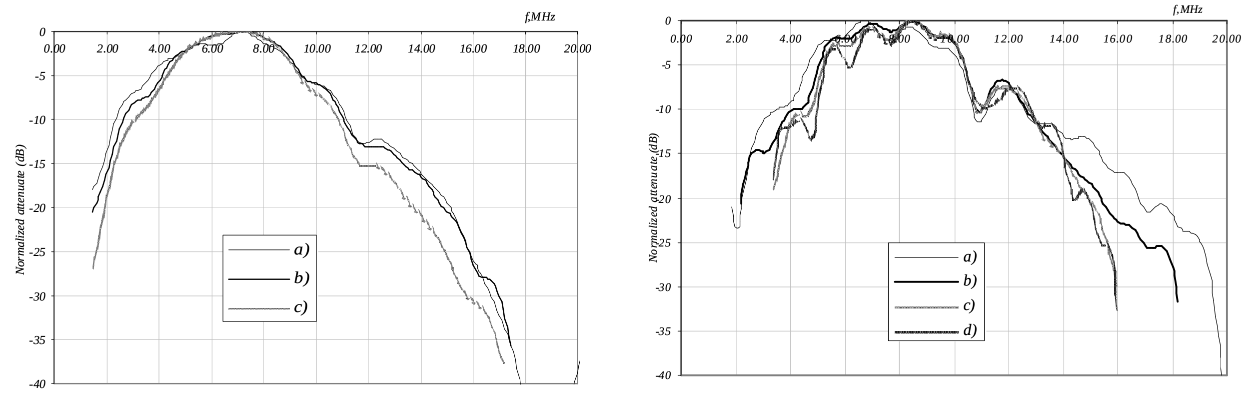

Fig. 11 Pulse-echo results. Received signal frequency band as function of bias voltage. In right side design of 40_3 transducer. Pulse length 80 ns: a – V_{bias} = 120 V, b – V_{bias} = 100 V, c – V_{bias} = 80 V. In left side design of 39_05 transducer. Pulse length 60 ns: a – V_{bias} = 125 V, b – V_{bias} = 110 V, c – V_{bias} = 90 V, d – V_{bias} = 70 V

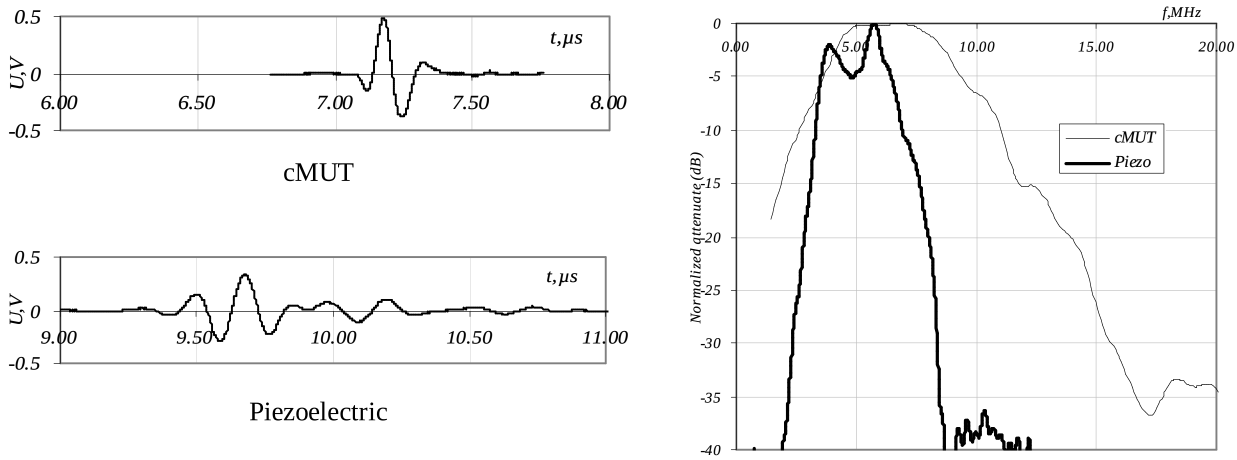

Fig. 12 Equalization piezoelectric and cMUT transducers

4. Conclusions

Measurements of static capacitance – bias voltage characteristic show that charging problems is actual for this device design. We state the dielectric properties of the devices to be fine.

Consecutive tests of cMUT elements having different membrane types (though designed for the same central frequency) show no significant differences in static and dynamic properties of the transducers, except of design No 40_05, which has a mix of different cells.

Higher bias voltages improve the overall pulse-echo performance of the transducers: the amplitude of received pulses is higher, and the bandwidth tends to widen towards the higher frequencies.

When simultaneous cMUT and piezoelectric transducers pulse-echo exeriments were carried, it was found cMUTs having shorter response signal and wider fractional frequency band than piezoelectric transducers (Fig. 12) Tests show what 0.3×0.5 mm cMUT array can be used in conventional ultrasound scanners without any essential hardware changes.

Acknowledgements

This research was supported by the Lithuanian State Science and Study foundation. It is also the part of the research under the grant from EU structural funds, contract No BPD2004-ERPF-3.1.7-06-06/0029. The test arrays were fabricated by Ph.D. candidate Xuefeng (Steve) Zhuang (Stanford University). Authors also thank him for valuable collaboration and support during the tests preparation.

References

1. **Soh H.T.**, **Ladabaum I.**, **Atalar A.**, **Quate C.F.**, **Khuri-Yakub B.T.** Silicon micromachined ultrasonic immersion transducers. Ultrasonic Symposium 1998. Proceedings, 1998 IEEE Page(s): 985 - 991 vol.2

2. **Ergun A.S.**, **Huang Y.**, **Zhuang X.**, **Oralkan O.**, **Yaralıoglu G.G.**, **Khuri-Yakub B.T.** Capacitive Micromachined Ultrasonic Transducers: Fabrication Technology. IEEE Transactions on Ultrasonic, Ferroelectrics, and Frequency Control, vol. 52, no. 12, December 2005.
3. **Haller M.I.**, **Khuri-Yakub B.T.** A Surface micromachined electrostatic ultrasonic air transducer, Proceedings Ultrasonics Symposium 1994 pp. 1241-1244.
4. **Mills D.M.**, **Smith L.S.** Real-Time In-Vivo Imaging With Capacitive Micromachined Ultrasound Transducer (cMUT) Linear Arrays. IEEE Ultras. Symp., Honululu, USA 2003.
5. **Panda S.**, **Daft C.**, **Wagner P.**, **Ladabaum I.**, **Pellegretti P.**, **Bertora F.** Microfabricated Ultrasonic Transducer (cMUT) Probes: Imaging Advantages over PZT Probes. In WFUMB (hosted by AIUM) Conference, Montreal, Canada 2003.
6. **Ergun A.S.**, **Huang Y.**, **Zhuang X.**, **Orlkan O.**, **Yarahoglu G.**, **Khuri-Yakub B.T.** Capacitive Micromachined Ultrasonic Transducers: Fabrication Technology Transactions on ultrasonic, ferroelectrics and frequency control, vol. 52, 2005.
7. **Mikolajūnas M.** et al. Study of stacked PECVD silicon nitride films used for surface micromachined membranes. Thin Solid Films 2008; Submitted.
8. **Huang Y.**, **Haggstrom E.O.**, **Zhuang X.**, **Ergun A.S.**, **Khuri-Yakub B.T.** A solution to the Charging Problems in Capacitive Micromashined Ultrasonic Ttransducers. Transactions on ultrasonic, ferroelectrics and frequency control, vol. 52, No. 4, april 2005.
9. **Oralkan O.**, **Bayram B.**, **Zhuang X.**, **Yarahoglu G.**, **Ergun A.S.**, **Kupnik M.**, **Yeh D.T.**, **Wygant I.O.**, **Khuri-Yakub B.T.** Experimental characterization collapse-mode CMUT operation. Transactions on ultrasonic, ferroelectrics and frequency control, vol. 53, No. 8, august 2006.

Authors' index

INTELLIGENT TECHNOLOGIES IN LOGISTICS AND MECHATRONICS SYSTEMS (ITELMS'08). Proceedings of the 3rd International Workshop.
(Held on May 22-23, 2008, Panevezys, Lithuania).

INTELEKTUALIOS TECHNOLOGIJOS LOGISTIKOJE IR MECHATRONINĖSE SISTEMOSE (ITELMS'08). 3 - čio tarptautinio seminaro, įvykusio Panevėžyje 2008 m. gegužės 22-23 d., pranešimų medžiaga (anglų kalba).

Maketavo D. Vaičiulis